Probabilistic Contamination Risk Assessment with Application to PFOS in Aquifers under Single-lined Landfills

Linxue Zhao

Doctor of Philosophy

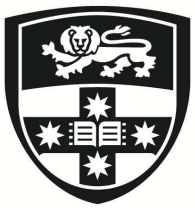

THE UNIVERSITY OF SYDNEY

Supervisor: Prof. Abbas El-Zein

Associate Supervisor: Asoc. Prof. Yixiang Gan

A thesis submitted in fulfilment of

the requirements for the degree of

Doctor of Philosophy

School of Civil Engineering

Faculty of Engineering

The University of Sydney

Australia

2026

Statement of originality

I confirm that this thesis is my original work, not submitted elsewhere. All sources are acknowledged, and collaborations are disclosed. I understand and uphold academic integrity in this submission.

Student Name: Linxue Zhao

Signature:

Date: 5 September 2025

Authorship attribution statement

During the course of this thesis, two papers have already been published.

1. Chapter 4 Section 4.3 of this thesis is part of the publication: Rowe, R.K., & Zhao, L. (2023). Implications of double composite liner behaviour for PFAS containment. *ISSMGE*. https://doi.org/10.53243/ICEG2023-64
2. Part of Chapter 5 of this thesis is published as: Zhao, L., Rowe, R. K., & El-Zein, A. (2024). Evaluation of PFOS contamination in aquifers under single lined landfills. *ECSMGE 2024*. https://doi.org/10.1201/9781003431749-684

Two manuscripts, derived respectively from Chapters 6 and 7, are being finalised and are expected to be submitted shortly.

For each of the above publications, I (Linxue Zhao) was responsible for performing the numerical simulations, processing the data, and drafting the original manuscripts. My supervisor, Prof. Abbas El-Zein, contributed to the study design, interpretation of results, and revision of the drafts.

Signature:

Date: 5 September 2025

As supervisor for the candidature upon which this thesis is based, I can confirm that the authorship attribution statements above are correct.

Supervisor Name: Abbas El-Zein

Signature:

Date: 5 September 2025

Abstract

Per- and polyfluoroalkyl substances (PFAS) have emerged over the past two decades as contaminants of concern because of their persistence and mobility in the environment and their toxicity to humans. This is especially true for perfluorooctane sulfonic acid (PFOS), one of the most concerning PFAS compounds, detected globally in biota and found to be the most dominant PFAS in human tissues. Municipal solid waste landfills (MSWLs) are a major potential source of PFAS contamination, with high levels of PFOS found in landfill leachates. To protect nearby aquifers, landfills are typically equipped with a single composite liner system (SCLS) including a geomembrane (GMB) placed over either a Geosynthetics Clay Liner (GCL) or a Compacted Clay Liner (CCL) above a natural attenuation layer (AL). In some cases, the natural clay is of sufficiently low permeability to serve as the primary barrier (Natural Clay Liner or NCL). However, SCLSs have not been designed to contain PFAS contaminants, including PFOS, and the risk to groundwater remains poorly understood.

PFOS transport into aquifers below landfills can be numerically modelled using the coupled water flow and reactive diffusion-advection equation but only one such attempt has been made in the literature and only under simplified assumptions that do not capture spatial variability of concentration in the aquifer. In addition, a range of landfill configurations are used around the world, and significant variability and/or uncertainty in material properties, environmental conditions and construction quality are present. As a result, deterministic predictions cannot be made with reasonable confidence, and a probabilistic approach is necessary. Monte Carlo simulations (MCS) can be used to generate probability distributions of PFOS concentrations in aquifers. However, conducting such simulations can be computationally prohibitive. Surrogate modelling techniques such as Polynomial Chaos Expansion (PCE) can reduce the computational cost significantly, but they have only been applied to problems with a relatively small number of uncertain parameters and are yet to be validated for a larger number, such as encountered in PFOS transport through liner systems.

The goal of this thesis is to address the above knowledge gaps in view of conducting a probabilistic assessment of the risk of PFOS contamination in aquifers underlying single-lined municipal waste landfill, based on best available experimental evidence. The following objectives are pursued:

1) To establish, based on best available experimental evidence and expert knowledge, probability distributions of uncertain parameters required for modelling PFOS transport through liner systems.
2) To conduct a preliminary assessment of PFOS risk to groundwater under landfills by running deterministic simulations based on the geometric mean values identified under objective 1).
3) To develop a PCE surrogate of the MCS, in the context of PFOS transport through landfill liners, with up to 12 uncertain parameters, and evaluate its ability to reproduce MCS predictions and reduce computational cost.
4) Building on developments in 1), 2), and 3),
    a) To perform a probabilistic PFOS risk assessment by conducting PCE-enhanced MCS for three types of SCLS (with GMB+GCL+AL, GMB+CCL+AL, or GMB+NCL) under different scenarios of construction quality.
    b) To identify key variables with most influence on PFOS groundwater concentration.
5) Based on the above, to discuss options for improving the management of PFOS in MSWLs and make recommendations.

Key findings from the study include:

1) PCE surrogate model is found to be accurate when 12 uncertain variables are considered, while reducing the computational cost of MCS by more than one order of magnitude.
2) The probability of PFOS aquifer contamination exceeding drinking water guidelines/standards under GMB+GCL+AL liner systems is found to range between 57% and 99%, depending on the specific construction scenario and guideline/standard used. The corresponding probabilities for the GMB+CCL+AL and GMB+NCL systems are 58~99% and 49~92%, respectively.
3) PFOS concentrations in the aquifer may not reach their peaks until more than 150 years after PFOS is first accepted into the waste landfill.
4) Better construction quality reduces peak PFOS concentrations in the aquifer but even under best-case scenario of construction quality, the risk of exceeding drinking water guidelines/standards remains high.

5) Mass of PFOS accepted into the landfill, PFOS concentration in the leachate, hydraulic conductivity of functional clay liners, and construction quality are the variables with most impact on PFOS aquifer concentrations.

Findings of this study have several practical implications. First, for new landfills expected to receive PFOS-polluted waste, double composite base liners, often used in hazardous waste landfills, may be required. Second, reducing PFOS content of waste upstream of the waste management chain, strictly limiting the amount of PFOS-polluted waste accepted into the landfill, and/or enhancing the quality of materials and construction of the liner systems appear to be the most effective measures to mitigate the impact of PFOS on aquifers beneath landfills.

Future research directions include consideration of PFAS other than PFOS, experimental investigations that reduce the range of uncertainty of key variables for key PFAS compounds, probability risk assessments of PFAS transport in double composite liners, and site-specific studies of PFAS contamination, combining site measurements and numerical modelling.

Acknowledgements

This PhD journey has been both intellectually challenging and personally transformative. It would not have been possible without the guidance, support, and encouragement I have received from many people along the way, to whom I owe my sincerest thanks.

I would like to begin by expressing my highest appreciation to my principal supervisor, Professor Abbas El-Zein. Throughout my candidature, his role has been truly pivotal. From shaping the initial research plan to establishing methodologies, analysing results, and refining this thesis, his guidance has been fundamental to every stage of this work. Beyond academic mentorship, he has also shown exceptional patience and understanding, offering encouragement and helping me navigate numerous challenges. I am profoundly grateful for his continuous support and invaluable advice, both academically and personally.

I am also deeply grateful to Professor R. Kerry Rowe from Queen's University, Kingston and his team. As one of the leading authorities in my research field, he generously dedicated his time despite his demanding schedule, offering critical insights on research ideas, key data, and methodological rigor, and supporting comparative analyses conducted by his students. Their help was indispensable to the success of this project. My sincere thanks also go to Professor Abdelmalek Bouazza from Monash University and his team for their contribution to certain experimental work, as well as to my auxiliary supervisor, Associate Professor Yixiang Gan, whose advice and guidance were helpful during my candidature. I also wish to acknowledge my panel members, Professor David Airey and Associate Professor Daniel Dias-da-Costa, for their constructive comments and feedback.

My appreciation further goes to the School of Civil Engineering at the University of Sydney for providing a supportive academic environment. I am thankful to the lecturers of the courses I attended, the administrative and technical staff, and my colleagues and peers, both within my research group and across the broader faculty, for their assistance, collaboration, and companionship.

I would also like to thank those who supported me personally throughout this journey. My heartfelt appreciation goes to my flatmates, friends, landlord, and even online

companions, whose encouragement and kindness have helped me stay resilient through the ups and downs of PhD life.

This research would not have been possible without the financial support of the Australian Research Council (ARC) Linkage grant (LP180101178), which funded my scholarship and provided essential support throughout the majority of my candidature.

Finally, and most importantly, I owe my deepest gratitude to my parents, Zhao, Hongquan and Feng, Kaimei. Your dedication to my education, along with your unconditional love, patience, and unwavering support, has been the foundation of all my achievements. To my mother, Ms. Feng, thank you for your constant encouragement and for always pushing me forward. To my father, Mr. Zhao, your quiet devotion and thoughtful care have meant more to me than words can convey. I am truly blessed to have you both by my side.

Completing this thesis has been one of the most significant milestones of my life, and it would not have been possible without the generous guidance, help, and love I have received. To each of you, I extend my heartfelt thanks.

Contents

List of Abbreviations

AL: attenuation layer

AM: arithmetic mean

AQ: aquifer

BC: boundary condition

BCS: Bayesian compressive sensing

CCL: compacted clay liner

CDF: cumulative distribution function

CONFEM: core engine underpinning SPAS

CQA: construction quality assurance

CT-BC: contaminant transport boundary condition

DAE: diffusion-advection equation

ED: experimental design

ELL: electrical leak location

EurEau: European Federation of National Associations of Water Services

FCL: functional clay liner

FD: frequency distribution

FEM: finite element method

FLM: finite layer method

GCL: geosynthetic clay liner

GM: geometric mean

GMB: geomembrane

GSA: global sensitivity analysis

GSD: geometric standard deviation

HDPE: high-density polyethylene

HEPA: Heads of Environmental Protection Agencies Australia and New Zealand

IC: initial condition

KDE: kernel density estimation

LARS: least angle regression

LHS: Latin Hypercube Sampling

LHSMDU: Latin Hypercube Sampling with Multidimensional Uniformity

LLDPE: linear low-density polyethylene

MAPE: mean absolute percentage error

MCL: maximum contaminant level

MCS: Monte Carlo simulations

MSWL: municipal solid waste landfill

NCL: natural clay liner

ND: not detected

NHMRC: National Health and Medical Research Council

OMP: orthogonal matching pursuit

PCE: polynomial chaos expansion

PD: probability density

PDE: partial differential equation

PDF: probability density function

PE: polyethylene

PFAA: perfluoroalkyl acid

PFAS: per- and polyfluoroalkyl substances

PFC: perfluorinated compound

PFCA: perfluoroalkyl carboxylic acid

PFOA: perfluorooctanoic acid

PFOS: perfluorooctane sulfonic acid

PFSA: perfluoroalkyl sulfonic acid

PoE: probability of exceedance

POLLUTE: a numerical solver based on FLM

PrD: prediction design

QoI: quantity of interest

RDAE: reactive diffusion-advection equation

RSc: reference scenario, assuming good CQA with ELL

RSc0: theoretical reference scenario, assuming no leakage

RVE: representative volume element

Sc-: scenario with lower CQA, assuming good CQA but no ELL

Sc+: scenario with higher CQA, assuming excellent CQA with ELL

SCLS: single composite liner system

SD: standard deviation

SI: Sobol' index

SP: subspace pursuit

SPAS: Soil Pollution Analysis System, a numerical solver based on FEM

TL: transmissive layer

UQLab: a MATLAB-based uncertainty quantification framework

USEPA: US Environmental Protection Agency

WF: water flow

WF-BC: water flow boundary condition

WFE: water flow equation

WWTP: wastewater treatment plant

List of Symbols

$2a_0$: wetted distance

2b: width of leaks on GMB

C: concentration of PFOS dissolved in pore water

$C_{aq\text{-}max}$: maximum PFOS concentration in the aquifer

$C_{aq\text{-}max\text{-}95\%}$: 95% percentile of $C_{aq\text{-}max}$

$C_{aq\text{-}max\text{-}xy}$: maximum concentration in the aquifer as a function of time

C_b: PFOS concentration at the boundary

C_{b0}: initial PFOS concentration in leachate

$C_{GMB\text{-}bs}$: PFOS concentration at the lowermost point in the GMB

$C_{GMB\text{-}ts}$: PFOS concentration at the topmost point in the GMB

C_{PFOS}: PFOS concentration

C_{ref}: drinking water guidelines/standards for PFOS concentration

C_{soil}: PFOS concentration in the layer below the GMB and in contact with its bottom surface

C_{waste}: PFOS concentration in the leachate in contact with the top surface of the GMB

D: molecular diffusion coefficient

D_{AL}: diffusion coefficient of attenuation layer

D_{AQ}: diffusion coefficient of aquifer

D_{CCL}: diffusion coefficient of CCL

D_g: diffusion coefficient of GMB

D_{GCL}: diffusion coefficient of GCL

D_{NCL}: diffusion coefficient of NCL

d_s: mass of waste per surface area in landfill

d_{TL}: thickness of the TL

D_{xx}: coefficient of hydrodynamic dispersion in the x direction

D_{xy}, D_{yx}: cross-terms of hydrodynamic dispersion

D_{yy}: coefficient of hydrodynamic dispersion in the y direction

f_{nb}: PFOS flux normal to the boundary

f_x: x component of the mass flux of PFOS through the porous medium

f_y: y component of the mass flux of PFOS through the porous medium

G: computational gain obtained by using PCE relative to MCS

h: pressure head acting between the GMB and underlying clay liner

H: total hydraulic head

H_b: total hydraulic head at the boundary

H_{bot}: total hydraulic head at the bottom of the aquifer

H_f: equivalent height of leachate

$h_{p\text{-}bot}$: pressure head at the bottom of the aquifer

$h_{p\text{-}top}$: pressure head on top of liner

H_{top}: total hydraulic head on top of liner

k_a: hydraulic conductivity of GCL in contact with GMB

k_{AL}: hydraulic conductivity of attenuation layer

k_{AQ}: hydraulic conductivity of aquifer

k_b: hydraulic conductivity of GCL below wrinkles

k_{CCL}: hydraulic conductivity of CCL

K_d: sorption coefficient of layers

k_{FCL}: hydraulic conductivity of functional clay liner

k_{GCL}: hydraulic conductivity of GCL

k_{NCL}: hydraulic conductivity of NCL

k_{sa}: harmonic mean of hydraulic conductivity in the liner under the intact parts of the GMB

k_{sb}: harmonic mean of hydraulic conductivity in the liner under the wrinkled parts of the GMB

k_x: saturated hydraulic conductivity in the x direction

k_{xTL}: x component of the hydraulic conductivity of the TL

k_y: saturated hydraulic conductivity in the y direction

L_w: length of holed wrinkles per hectare

L_x: landfill dimension in the x direction

L_z: landfill dimension in the z direction

n: porosity

n_{AL}: porosity of attenuation layer

n_{AQ}: porosity of aquifer

n_{CCL}: porosity of CCL

n_{GCL}: porosity of GCL

n_{NCL}: porosity of NCL

N_u: number of uncertain input parameters

p: degree of PCE function

p_0: PFOS waste content

P_g: permeation coefficient of GMB

$PrD_{ref\text{-}CCL}$: reference set of MCS realisations for CCL-case for PCE validation

$PrD_{ref\text{-}GCL\text{-}1}$, $PrD_{ref\text{-}GCL\text{-}2}$, $PrD_{ref\text{-}GCL\text{-}3}$: three reference sets of MCS realisations for GCL-case for PCE validation

$PrD_{ref\text{-}GCL\text{-}2D}$: reference set of MCS realisations for GCL-case with 2D uncertainty for PCE validation

$PrD_{ref\text{-}NCL}$: reference set of MCS realisations for NCL-case for PCE validation

q: hyperbolic truncation norm for PCE function

q_0: percolation rate into the landfill

q_a: leakage rate through the liner system

q_c: leachate collection rate by the drainage system

R_{MCS}: number of realisations for MCS

$R_{MCS\text{-}PCE}$: number of MCS realisations for training the PCE model

$R_{MCS\text{-}PCE\text{-}opt}$: optimal number of MCS realisations for training the PCE model

R_{PCE}: number of realisations for PCE-enhanced MCS

R_{stable}: number of MCS realisations required to achieve stable Monte-Carlo predictions

S_g: partitioning coefficient of GMB

t: time dimension

t_0: calculation time of one realisation by the PCE model

$t_{1/2}$: half-life of PFOS in layers

T_{AL}: thickness of attenuation layer

T_{AQ}: thickness of aquifer

T_{CCL}: thickness of CCL

T_{CLAL}: total thickness of the clay and attenuation layer

T_{GCL}: thickness of GCL

T_{GMB}: thickness of GMB

$T_{LHS\text{-}ED}$: time needed to generate high-dimensional input samples by LHSMDU for the ED

$T_{LHS\text{-}stable}$: time needed to generate high-dimensional input samples by LHSMDU for the large number (R_{stable}) of realisations

t_{max}: time to reach $C_{aq\text{-}max}$

T_{MCS}: computational time required to conduct MCS

T_{NCL}: thickness of NCL

T_{PCE}: computational time required to conduct PCE-enhanced MCS

t_{SPAS}: calculation time of one simulation in SPAS

T_{train}: time needed to establish PCE model by UQLab based on the ED

v: magnitude of seepage velocity

$V_{ax\text{-}in}$: inward horizontal Darcy velocity in aquifer

$V_{ax\text{-}out}$: outward horizontal Darcy velocity in aquifer

v_{ay}: downward Darcy velocity

v_{nb}: component of the seepage velocity normal to the boundary

v_x: x component of the seepage velocity vector

v_y: y component of the seepage velocity vector

x: horizontal dimension of the 2D landfill model

x_{max}: horizontal position to reach $C_{aq\text{-}max}$

y: vertical dimension of the 2D landfill model

z: dimension perpendicular to the 2D landfill model

α_{AL}: dispersivity of attenuation layer

α_L: longitudinal dispersivity

$\alpha_{L\text{-}AL}$: longitudinal dispersivity of attenuation layer

$\alpha_{L\text{-}AQ}$: longitudinal dispersivity of aquifer

$\alpha_{L\text{-}CCL}$: longitudinal dispersivity of CCL

$\alpha_{L\text{-}GCL}$: longitudinal dispersivity of GCL

$\alpha_{L\text{-}NCL}$: longitudinal dispersivity of NCL

α_T: transverse dispersivity

$\alpha_{T\text{-}AL}$: transverse dispersivity of attenuation layer

$\alpha_{T\text{-}AQ}$: transverse dispersivity of aquifer

$\alpha_{T\text{-}CCL}$: transverse dispersivity of CCL

$\alpha_{T\text{-}GCL}$: transverse dispersivity of GCL

$\alpha_{T\text{-}NCL}$: transverse dispersivity of NCL

δ: shift for a shifted lognormal distribution

ΔH: difference in total hydraulic head between top of GMB and aquifer

ϵ: absolute error

θ: transmissivity

$\theta_{GMB\text{-}CCL}$: transmissivity of the contact region between GMB and CCL

$\theta_{GMB\text{-}GCL}$: transmissivity of the contact region between GMB and GCL

$\theta_{GMB\text{-}NCL}$: transmissivity of the contact region between GMB and CCL

θ_{xTL}: transmissivity of the TL in the x direction

μ: mean

ρ_{AL}: dry density of attenuation layer

ρ_{AQ}: dry density of aquifer

ρ_{CCL}: dry density of CCL

ρ_{GCL}: dry density of GCL

ρ_{NCL}: dry density of NCL

σ: standard deviation

Note: The symbols used in Appendix 3.3 form an independent notation system that is separate from the symbols listed above. Therefore, they are not included in the above list. Their definitions are provided within Appendix 3.3 itself.

List of Figures

List of Tables

Chapter 1
Introduction

1.1 Background and Research Gaps

1.1.1 PFOS in landfills with single-liner systems

Per- and polyfluoroalkyl substances (PFAS) (aka "forever" chemicals) are a diverse group of synthetic organic compounds composed of a carbon chain wherein some or all of the hydrogen atoms are replaced by fluorine atoms. As such, they contain at least a perfluorinated methyl group ($-CF_3$) or a perfluorinated methylene group ($-CF_2-$) (Wang et al., 2021), as well as other functional groups which contribute to their specific properties. The thermodynamically strong C-F bond enhances their thermal and chemical stabilities even under harsh environmental conditions (Renner, 2001). In addition, PFAS substances have surfactant properties due to their hydrophilic functional end groups and hydrophobic fluorinated tail (3M Company, 1999b).

Since the 1950s, PFAS have been widely used in both consumer products (e.g., non-stick cookware, cleaning agents, soil- and stain-resistant coatings for textiles, carpets, and leather, and grease- and oil-resistant coatings for paper products) and industrial applications (e.g., metal plating, fire-fighting foams, electronics production, photography, mining and oil well surfactants, alkaline cleaners, floor polishes, denture cleaners, shampoos, and ant insecticide) (Arvaniti et al., 2014; Renner, 2001). A notable and typical application related to the surfactant properties of PFAS is the dominant presence of long-carbon-chain PFASs in aqueous film forming foams (AFFFs) (Milley et al., 2018). As a result, they have been detected extensively in the environment, including the biota (Buck et al., 2011). Their use has now been slashed in many fields, and the production of some specific PFAS compounds has even been phased out. Nevertheless, over the past two decades or so, PFAS have been increasingly identified as contaminants of concern due to their persistence and mobility in the environment, as

well as their bioaccumulation and toxicity to humans (Ravindiran et al., 2023; Liu et al., 2019; Simon et al., 2019).

Perfluorooctane sulfonic acid (PFOS, C_8F_{17}-SO_3H) is one of the most concerning PFAS compounds because it has been detected globally in biota (Giesy and Kannan, 2001) and found to be the most dominant PFAS in human tissues (Hansen et al., 2001; ATSDR, 2021; Benskin et al., 2012). Furthermore, evidence has shown that PFOS is carcinogenic and impacts human reproduction, development, and cell function (ATSDR, 2021; Eriksen et al., 2013; Wee and Aris, 2023). The production of PFOS and its precursors was phased out by major manufacturers starting in the early twenty-first century (USEPA, 2000). However, it continues to be of concern because of its widespread and persistent presence from past emissions (Brooke et al., 2004; Paul et al., 2009), its ongoing generation from the environmental transformations of other PFAS compounds and the degradation of other precursors (Bouazza, 2021), and the severity of its health and environmental effects. Hence, further study is necessary to fully understand the environmental risk it poses and to develop effective strategies to mitigate its impact.

Municipal solid waste landfills (MSWLs) around the world are usually the destination for most consumer products and industrial wastes containing PFAS and hence a major potential source of PFAS contamination, including PFOS. The potential risk is especially significant for the surrounding bio- and hydro-spheres. Perfluoroalkyl acids (PFAA), a large category of PFAS that includes PFOS, are widely detected at ng/l to ug/l levels in landfill leachates (the toxic liquid found in buried landfill waste, which constitutes its most mobile component). Specifically, leachates have been found to contain PFOS, up to concentrations of 2700 ng/l (Australia), 4840 ng/l (Canada), 1000 ng/l (USA), 7400 ng/l (Ireland), 2920 ng/l (Norway), and 6020 ng/l (China) (for full reviews see Zhang et al., 2023). These values are up to three orders of magnitude higher than health-based drinking water guidelines/standards which range from 4 ng/l (US Environmental Protection Agency, USEPA) and 70 ng/l (Australia's National Health and Medical Research Council, NHMRC) to 100 ng/l (European Federation of National Associations of Water Services, EurEau) and 600 ng/l (Health Canada). It is also noteworthy that Australia has recently adopted a newly revised guideline, and Canada is in the process of revising its own, with both developments expected to lead to more

stringent guideline values. However, the newly published Australian guideline is so recent that it has not been included as a reference in this study.

MSWLs are typically equipped with a single composite liner system (SCLS), placed below the waste, to separate it from the surrounding environment and ensure containment of pollutants by minimising leachate transport into the subsurface. An SCLS usually contains four core components, presented here in the order in which they are located below the waste, from top to bottom (see Figure 1.1):

a) a synthetic or soil-based leachate drainage system to minimise hydraulic pressures on underlying layers,

b) a 1-2.5mm thick, low-permeability, chemically resistant geomembrane (GMB) usually made of high-density polyethylene (HDPE) or linear low-density polyethylene (LLDPE), which forms an advective barrier to contaminants,

c) a low-permeability geosynthetic clay liner (GCL) made of sodium bentonite, or a low-permeability compacted clay liner (CCL), that constitutes a barrier against further migration of any contaminant transmitted from above,

d) an additional buffer zone of soil found on site, known as an attenuation layer (AL), separating the above components from the underlying aquifer (AQ).

Component c) can be omitted in some sites that naturally have low-permeability and a thick AL, which is then called natural clay liner (NCL). In summary, three designs of SCLS between the drainage system and the aquifer are commonly adopted and thus considered in this study, which are GMB+GCL+AL, GMB+CCL+AL, and GMB+NCL. Since SCLSs have not been designed to address persistent PFAS contaminants, including PFOS, an urgent question is whether current state-of-the-art engineering of landfills can protect groundwater from PFAS contamination and, if not, what measures can be taken to address the problem.

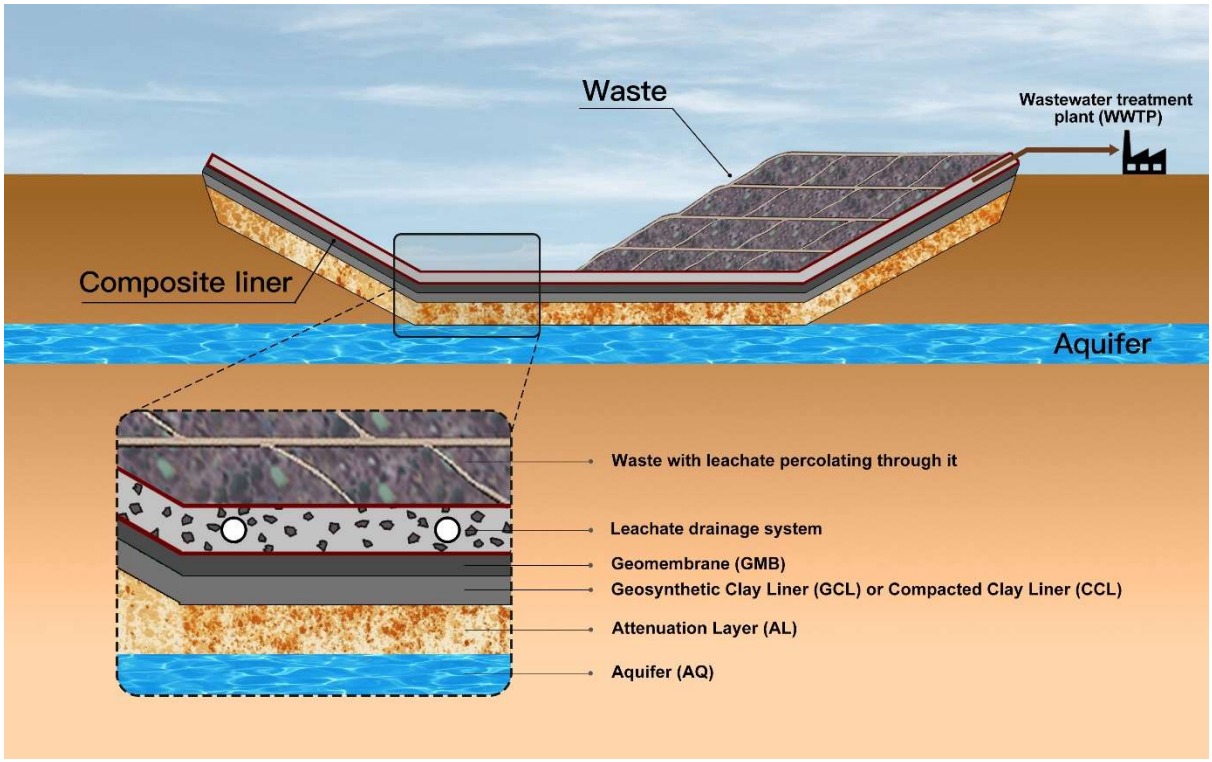

Figure 1.1. Single composite liner system at the base of a municipal solid waste landfill.

PFOS present in leachate undergoes multiple processes governing its fate and transport, including advection, mechanical dispersion, molecular diffusion, biological decay, and partitioning. Current knowledge of the fate and transport of PFOS in liner systems stems from two inter-connected sources. First, over the past fifty years or so, knowledge on the performance of liner systems, including potential and actual failures in their ability to protect groundwater, has accrued in the literature based on a body of experimental, theoretical, and computational research. This research has broadly confirmed that the coupled water flow (WF) and reactive diffusion-advection equation (RDAE), within the framework of continuum soil hydrology and soil mechanics, can predict observed behaviour of these systems for a range of organic and inorganic contaminants. This source of knowledge is non-PFAS specific but provides a pertinent framework for understanding PFAS fate in liner systems. Second, over the past decade or so, some experimental knowledge relevant to PFAS interactions with different components of liner systems has accrued, including knowledge on diffusion, partitioning and decay of PFAS in different media (Di Battista et al., 2020; Rowe et al., 2023; Barakat et al., 2024; etc), and hydraulic conductivity of clay material to PFAS-rich permeants (Bouazza, 2021; Barakat et al., 2024; etc). However, significant

uncertainties persist and do not allow deterministic predictions to be made with reasonable confidence, hence necessitating a probabilistic approach.

To the best of the author's knowledge, only two attempts at modelling PFAS transport through liner systems have been made before this study (Rowe and Barakat, 2021; Barakat and Rowe, 2025). One of them numerically analysed the transport of PFOS in an MSWL with GCL-SCLS using a 1½-D model finite-layer method. This study has yielded important preliminary findings and raised concerns about the ability of SLCS to protect groundwater against PFOS in landfills. However, it was essentially deterministic in nature based on a small number of input data sets, only considered GCL-SCLS, and required simplifying assumptions to allow lower spatial dimensionality especially in representing the aquifer, all of which limited the scope of its findings. No study to date has attempted to systematically incorporate uncertainties in prediction of the risk of PFAS contamination from landfills. Without such assessment, given the wide variety of contexts and the variability in key parameters in liner systems, no judgment can be made on the risk to groundwater from tens of thousands of landfills around the world. This includes uncertainty about physical processes, material properties, liner dimensions, environmental conditions, as well as variability in the construction quality of liner systems, all of which can have significant effects on their environmental performance, including hydraulic leakage rates and contaminant concentrations in the underlying aquifers. Furthermore, no numerical simulations, deterministic or probabilistic, aiming at assessing the ability of SLCS containing GMB+CCL+AL or only GMB+NCL to protect underlying groundwater from PFOS have been conducted.

1.1.2 Probabilistic analyses of subsurface contaminant transport

Extensive studies over the past three decades have focused on conducting probabilistic analyses of subsurface contaminant transport. Some early attempts include the Random Walk method (Roco et al., 1989), the first-order reliability method (FORM) (Piggott and Cawlfield, 1996), and a Markovian analysis approach (Patrick Wang and Zheng, 2005). The classical Monte Carlo simulation (MCS) method is commonly used to incorporate uncertainty because it is conceptually simple, easy to implement, and often statistically accurate (Harter, 2000; Rajabi and Ataie-Ashtiani, 2014).

However, MCS can be computationally expensive since its accuracy depends on the number of realizations used. This is particularly the case for some 2D or 3D simulations of coupled problems, such as the WF-RDAE considered here. To address this problem, meta-modelling (surrogate modelling) approaches have been developed which build data-driven, physics-free, and computationally efficient approximations of the original model response (Rajabi et al., 2015a; Razavi et al., 2012). This approach can reduce the computational cost of MCS by several orders of magnitude (Jin et al., 2001). The polynomial chaos expansion (PCE) is a powerful meta-modelling approach originally introduced by Wiener (1938), which carries the following two advantages (Wiener, 1938). It provides a computationally efficient functional approximation based on a suitably built orthonormal polynomial basis (Marelli et al., 2024a), and it allows an easy realization of global sensitivity analysis (GSA) which is valuable for understanding the effect of uncertainty on system behaviour (Marelli et al., 2024b).

The PCE has been used successfully in modelling hydrogeological problems, including the stochastic simulation of coupled water flow and contaminant transport equations (Xiu and Karniadakis, 2002; Wan and Karniadakis, 2005; Lin and Tartakovsky, 2010; Fajraoui et al., 2011; Ciriello et al., 2013; Rajabi et al., 2015b; Geetha Manjari and Sivakumar Babu, 2018; Koohbor et al., 2019; Ciriello and De Barros, 2020; Focaccia et al., 2021; Botti et al., 2023).

On the other hand, none of the PCE studies mentioned above have considered more than six uncertain variables in their simulations. As the number of uncertain variables increases, the complexity of the surrogate orthonormal polynomials underlying PCE increases which may affect the accuracy and computational efficiency of the method. Hence, the ability of the PCE to address higher dimensions of uncertainty in water flow and contaminant transport problems, such as the one considered in this thesis, remains unexplored. In addition, no study has used PCE to probabilistically investigate the fate and transport of contaminants in liner systems. The unique complexity of this problem lies in its a) combination of natural and engineered materials, b) highly contrasting geometrical scales (from millimetres for the thicknesses for geomembranes and geosynthetic clay liners to up to several kilometres for the length of the aquifer), and c) the multiple processes (advection, molecular diffusion, mechanical dispersion, sorption, degradation, etc) occurring simultaneously in different parts of the model domain.

1.1.3 Summary of research gaps

The thesis will hence address the above-identified research gaps:

1. No quantification of the uncertainty of key parameters required to model PFOS transport in liner systems has been attempted on the basis of available experimental evidence.
2. Only one attempt at modelling PFOS transport in liner systems containing GCL has been made; the study was deterministic in nature, with simplifying assumptions required for reduced spatial dimensions, and did not consider CCL or NCL. A very recent study focusing on PFOA improved the modelling assumptions and the numerical solver and considered different liner designs, yet it also remained deterministic.
3. No attempt at a probabilistic risk assessment of PFAS, including PFOS, in aquifers under landfills has been made.
4. PCE surrogate models have been successful in reducing the computational cost of MCS of coupled water flow and contaminant migration equations, but they were only studied for up to six uncertain variables, and PCE has never been applied to solute transport problems in liner systems. By contrast, the problem of PFOS transport in liner systems is likely to entail up to a dozen uncertain parameters.

1.2 Research Objectives and Research Questions

The overall goal of this study is to assess the ability of three commonly encountered types of single-liner systems in municipal solid waste landfills to protect underlying aquifers from PFOS contamination. The following objectives will be pursued to achieve this goal:

1) Conducting a survey of the literature in order to establish, based on best experimental evidence and expert knowledge, probability distributions of uncertain parameters required for the numerical modelling of PFOS migration through SCLS containing GMB+GCL+AL, GMB+CCL+AL, or GMB+NCL.
2) Conducting a preliminary assessment of PFOS impact on groundwater under landfills by running deterministic simulations in full two-dimensional space for

SCLSs containing GMB+GCL+AL, GMB+CCL+AL, or GMB+NCL, based on the geometric mean values identified in 1.

3) Developing a PCE surrogate for the original modelling of WF-RDAE and evaluating its ability to reduce computational cost (referring to computational time in this thesis) of MCS while maintaining accuracy in the context of PFOS transport in liner systems with up to 12 uncertain parameters.
4) Building on developments in 1, 2, and 3,
    a) performing a probabilistic risk assessment of PFOS contamination in groundwater underlying landfills by conducting PCE-enhanced MCS for the three types of SCLS considered here.
    b) evaluating the sensitivity of PFOS groundwater concentration to different uncertain parameters to help prioritise future research and identify risk management options.
5) Discussing options for improving the management of PFOS in MSWLs and making recommendations.

The following research questions will be addressed:

1) What forms of probability distribution best describe uncertain parameters required for modelling the fate of PFOS in liner systems?
2) How high is the PFOS risk to groundwater under different liner systems considered here, based on the mean values of uncertain parameters?
3) How accurate and computationally efficient is PCE when applied to PFOS transport in liner systems with up to 12 uncertain parameters considered?
4) How high is the probability of exceeding PFOS drinking water guidelines/standards in aquifers underlying municipal waste landfills with different types of single-liner systems?
5) How important is the quality of construction in reducing PFOS contamination and, more generally, which variables provide most leverage in managing PFOS contamination risk?

1.3 Originality and Significance

This study makes the following novel contributions:

1. Uncertainties in the transport of PFOS in SCLSs are systematically quantified for the first time by estimating the probability distributions of key parameters, based on available experimental data and expert knowledge. This is critical for conducting risk assessments of PFOS contamination under landfills. Estimation of relevant parameters not only supports numerical modelling in this study, but also provides a valuable reference for later research.
2. Full 2D finite element method (FEM) modelling of PFOS migration in liner systems is conducted for the first time in a way that allows more realistic assumptions to be made than hitherto achieved and for migration downgradient in the aquifer under the landfill to be examined.
3. The first attempt is made to apply PCE surrogate models to problems of water flow and contaminant transport with 12 uncertain variables, in the context of PFOS transport through landfill liners characterised by multiple spatial scales. This is critical for conducting computationally cost-effective probabilistic analyses of a range of hydrogeological contamination problems, including the above-mentioned one.
4. PFOS migration in liner systems of three commonly encountered designs is conducted probabilistically for the first time, with various uncertainties considered. The risk assessment thus made can contribute to better decision-making in managing PFAS contaminants in landfills. It is worth noting that the models used are not site-specific but rather based on generic designs commonly encountered around the world. In addition, the probabilistic analyses are used to conduct sensitivity analyses that enhance our understanding of key factors of controlling PFOS contamination in aquifers under landfills.

1.4 Thesis Layout

The thesis is structured around the five objectives described above. Chapter 2 presents a literature review, expanding on the information presented in the Introduction, grounding it in the existing literature, and providing a detailed rationale for the research questions studied and methodological choices made in the thesis.

Chapter 3 describes the methodology used in this study, including the theory and governing equations underlying the models used, the types of uncertainty considered, the uncertainty framework used for both MCS and PCE, the computer programs developed and/or used, both deterministic and probabilistic, and the different liner systems modelled.

Chapters 4 to 8 present and discuss the results of the investigations described in the methodology chapter. Chapter 4 presents the determined probability distributions of input parameters for the three different liner designs considered in the thesis.

Chapter 5 discusses the results of the deterministic simulation of PFOS transport through SCLSs with three different designs of clay liner, i.e., GMB+GCL+AL, GMB+CCL+AL, and GMB+NCL. The spatial distribution and temporal change of PFOS concentration in the underlying aquifer are computed, and the maximum concentration is compared to various published PFOS drinking water guidelines/standards.

Chapter 6 evaluates the predictive accuracy and computational efficiency of PCE surrogate model in simulating PFOS transport through the three studied liner designs, with up to 12 uncertainties considered.

Chapter 7 presents and processes results of the probabilistic simulation of PFOS transport through SCLS, including comparisons of maximum PFOS concentrations in the aquifer to drinking water guidelines/standards and a global sensitivity analysis (GSA) to assess the relative importance of various uncertain parameters. Three different SCLS designs are investigated: with GMB+GCL+AL (12 uncertainties considered), with GMB+CCL+AL (10 uncertainties considered), and with GMB+NCL (9 uncertainties considered), respectively. The temporal evolution of risk and sensitivity is also investigated for one scenario under the GMB+GCL+AL design.

Finally, Chapter 8 summarizes the conclusions of this study, including the strengths and limitations of applied methods, the contamination risk of PFOS in SCLSs with different clay liners, recommendations for controlling PFOS contamination in MSWL, and directions for future work.

Chapter 2
Literature Review

2.1 PFAS

2.1.1 Fundamentals of PFAS

Per- and polyfluoroalkyl substances (PFAS) are a group of over 4000 chemicals containing one or more perfluoroalkyl moieties (C_nF_{2n+1}-) and other functional groups attaching to the fluorinated carbon chain. As mentioned earlier, due to PFAS's unique surface-active properties and high chemical and thermal stability, they are used extensively in both consumer products and industrial applications (Buck et al., 2011; Arvaniti et al., 2014; Renner, 2001).

Two main production technologies for PFAS are electrochemical fluorination and telomerization (Buck et al., 2011). Since the 1950s, PFAS's wide use in commercial and industrial applications has resulted in numerous emissions of related contaminants (Kissa, 2001). Consequently, a broad range of these substances have been detected in the environment, wildlife, and humans in Australia and overseas (Buck et al., 2011; Bouazza, 2021). Although the use of PFAS has been reduced significantly and even banned in some contexts, environmental researchers and regulators are still racing to answer questions about prevalence in the environment, exposure risks, transport, and toxicity, in various contexts.

McDougall and Kalinovich (2021) conducted hazard rating calculations to assess the contamination risk of 11 PFAS, which is based on human health, environmental fate, deleterious quantity, and release and impact modifier. Lee (2013) investigated multiple environmental and biological processes that occur in the post-application fate of fluorinated surfactants and emphasized the exposure to PFAS of wildlife and humans through plant and livestock consumption. Zhao et al. (2022) provided a synthesis of research on the environmental occurrence, migration, and risk associated with both legacy and novel PFAS compounds in groundwater. Rasmusson and Fagerlund (2024) comprehensively reviewed existing knowledge on the multiple processes governing

subsurface fate and transport of PFAS and presented a compilation of fundamental parameters of 21 PFAS. Simon et al. (2019) summarized the limitations of existing research and the new challenges brought by PFAS. They emphasized that the effects of PFAS on human and ecosystem health remain poorly explored and that more research was needed to better characterise PFAS's physico-chemical properties and fate in the environment. They also argued that PFAS presented more serious challenges than traditional contaminants, considering the complexities of their persistence, mobility in soil, including at the air-water interface, toxicology, and difficulties of mitigation and remediation.

2.1.2 Classification of PFAS and the importance of PFOS

A general classification of PFAS is shown in Figure 2.1 (Buck et al., 2011). A primary distinction between non-polymers and polymers is followed by a division between perfluoroalkyl and polyfluoroalkyl ones, both encompassing numerous families. PFAS is such a broad concept that for each family, there are many individual homologous members and isomers. Among all branches, perfluoroalkyl acids (PFAAs) have attracted the greatest attention due to their high persistence and extensive industrial and consumer applications. The family of PFAAs includes perfluoroalkyl carboxylic, sulfonic, sulfinic, phosphonic, and phosphinic acids.

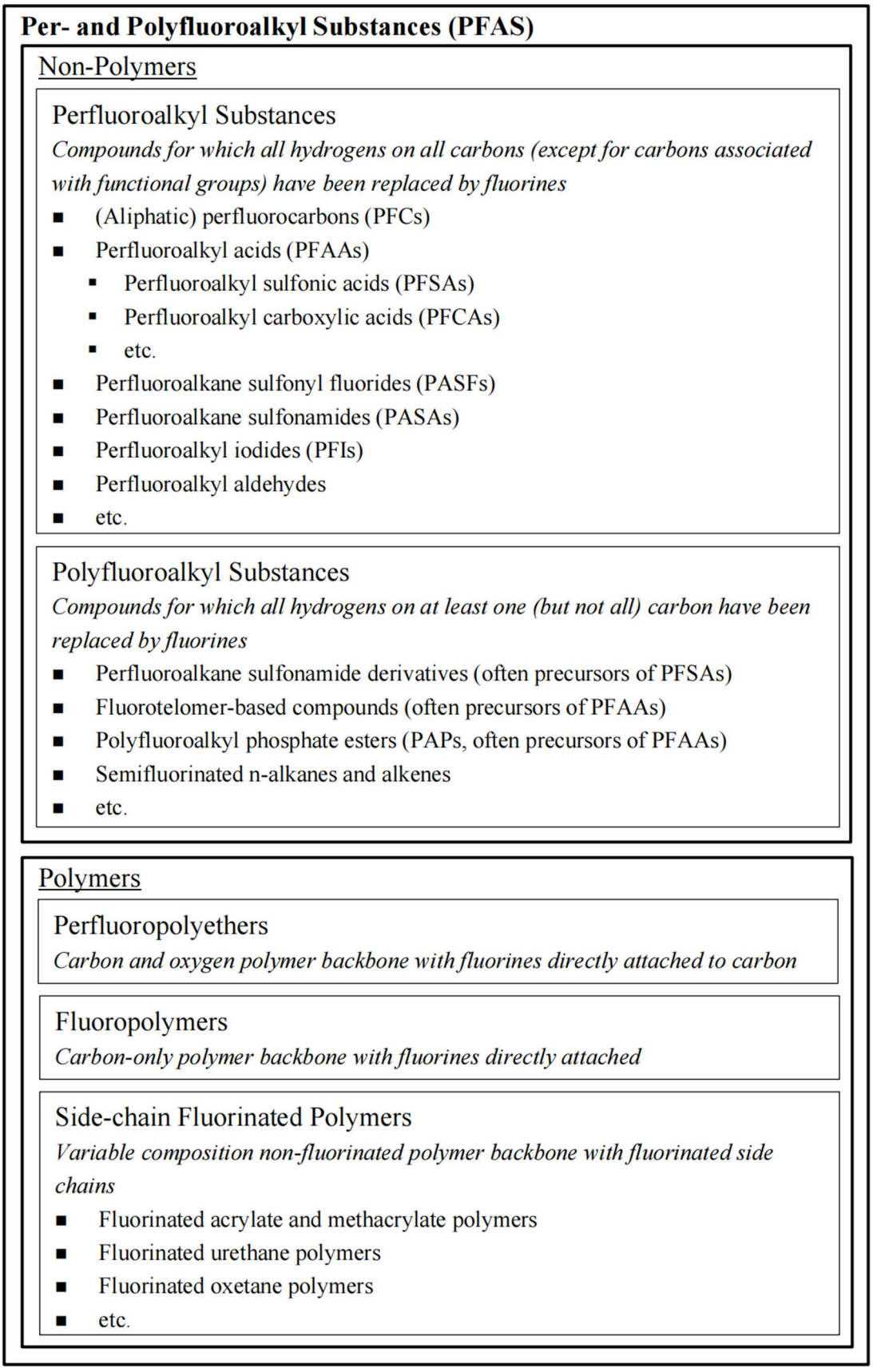

Figure 2.1. Classification hierarchy of environmentally relevant PFAS. Adapted from Buck et al. (2011)

Perfluoroalkyl sulfonic acids (PFSAs), with the general chemical formula $C_nF_{2n+1}SO_3H$, are a major PFAA family. PFSAs with 6 or more carbons are defined as long-chain ones, while those with fewer than 6 carbons are considered short-chain (OECD, 2020). Perfluorooctane sulfonic acid (PFOS, n=8) is the most concerning type of PFSA since it has been detected globally in biota (Giesy and Kannan, 2001) and humans (Hansen et al., 2001). The production of long-chain PFSAs, such as PFOS, PFHxS (n=6), and PFDS (n=10), and their precursors, was phased out by a major manufacturer (3M) in the United States in 2002 (USEPA, 2000), although broader regulatory restrictions were introduced later. In other regions, timelines and scopes of the phase-out varied. For example, Australia began implementing national measures in the mid-2010s, with a particular focus on PFOS-based firefighting foams (Queensland Government, 2021; NSW EPA, 2022). PFSAs with shorter perfluoroalkyl chain length, such as PFBS (n=4), have been adopted as alternatives due to their lower bioaccumulation (Olsen et al., 2009). However, the important role of long-chain PFSAs, especially PFOS, in PFAS contamination still demands significant attention considering that a) they were used in large quantities (Brooke et al., 2004; Paul et al., 2009), b) they are often identified as end products of environmental transformation of PFAS contamination (Bouazza, 2021), and c) their non-PFAS precursor substances can also transform into them (3M Company, 1999a, 2000; Boulanger et al., 2005; Rhoads et al., 2008).

In this study, PFOS is the focus substance, and its chemical structure is depicted in Figure 2.2. Finally, the full forms of PFAS acronyms appearing in this chapter are presented in Table 2.1 for reference.

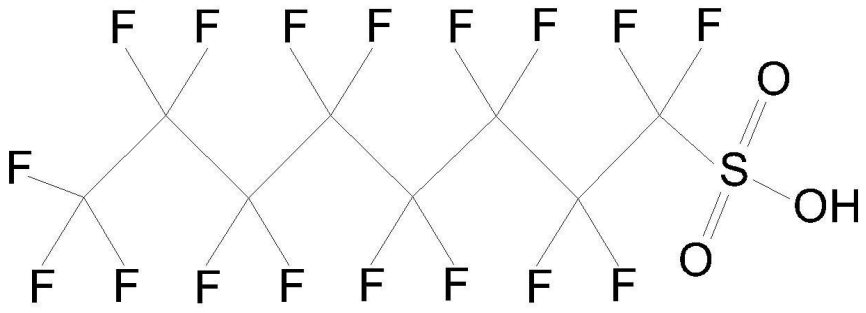

Figure 2.2. Chemical structure of PFOS

Table 2.1. Full name list for PFAS acronyms appearing in this chapter. (Note: This table is provided for reference purposes only and does not constitute an exhaustive list.)

Acronym	Full name of substance	Group (see Figure 2.1)	Chain length
PFHxA	Perfluorohexanoic acid	PFCAs	Short chain
PFHpA	Perfluoroheptanoic acid	PFCAs	Short chain
PFOA	Perfluorooctanoic acid	PFCAs	Long chain
PFBS	Perfluorobutane sulfonic acid	PFSAs	Short chain
PFHxS	Perfluorohexane sulfonic acid	PFSAs	Long chain
PFOS	Perfluorooctane sulfonic acid	PFSAs	Long chain
PFDS	Perfluorodecane sulfonic acid	PFSAs	Long chain
FTOH	Fluorotelomer alcohols	Fluorotelomer-based compounds	n/a
FTCA	Fluorotelomer carboxylic acid	Fluorotelomer-based compounds	n/a
FTUCA	Fluorotelomer unsaturated carboxylic acid	Fluorotelomer-based compounds	n/a
FTSA	Fluorotelomer sulfonic acid	Fluorotelomer-based compounds	n/a

2.2 PFAS in Landfills and Geosynthetic Liner Systems

2.2.1 PFAS occurrence in landfills

One of the most widely used disposal methods for waste consumer products is landfilling (Renou et al., 2008). Municipal solid waste landfills (MSWLs) are built to contain waste and leachate, as well as minimize the migration of contaminants into the aqueous environment. Because of the ubiquitous use of PFAS in industry and consumer products, they have drawn a relatively high, though recent, research attention as emerging contaminants in landfill leachate (Houde et al., 2011).

2.2.1.1 PFAS families in landfill leachates and their dominances

PFAAs have been widely detected in landfill leachates at ng/l to µg/l level, including PFCAs and PFSAs. The carbon chain length of PFCAs is mostly within 4-14, compared

to 4-10 for PFSAs. Common sources of PFAAs include consumer products, building materials, electronics, and impurities from by-products of manufacture (Bečanová et al., 2016; Kotthoff et al., 2015). In addition, PFAAs may originate from the degradation of their precursors, such as FTOH, n:2 FTCA, n:2 PTUCA, n:3 FTCA, n:2 FTSA, which are also known as Fluorotelomer-based substances. These compounds are present in landfill leachates (Benskin et al., 2012; Allred et al., 2014; Lang et al., 2017) and can degrade to PFAAs before and after product disposal in landfills (Allred et al., 2015; Lang et al., 2016). Furthermore, other families of PFAS are also found in leachates, such as Perfluoroalkyl sulfonamide derivatives (Huset et al., 2011; Allred et al., 2014; Lang et al., 2017) and Polyfluoroalkyl phosphate esters (PAPs) (Lee, 2013; Liu and Liu, 2016). However, PFAS substances other than PFAAs are much less dominant in landfill contexts.

Although there are some differences in PFAA profiles and concentrations in leachates from various countries, as demonstrated by Hamid et al. (2018), a few general trends do exist. First, PFCAs are generally the most dominant types of PFAS (Huset et al., 2011; Li et al., 2012; Allred et al., 2014; Fuertes et al., 2017). Second, the concentrations of short-chain (C4-C7) PFAAs tend to be higher than long-chain (≥C8) ones (Busch et al., 2010; Li et al., 2012; Fuertes et al., 2017). This trend generally results from three factors: a) a shift in PFAS production from long- to short-carbon chain starting from the early 2000s when many countries began restricting or phasing out long-chain PFAS (Canada. Environment Canada, 2010; Vierke et al., 2012); b) the preferential leaching of short-chain PFAS due to their higher solubility and sensitivity to hydrophilic groups (Yan et al., 2015), and c) the fact that some short-chain PFAS are by-products of the degradation of long-chain ones or other precursors. Third, PFOA tends to dominate over C4-C6 PFCAs in leachates, exhibiting both higher frequency and higher concentrations. This is due to its historically high level of usage in consumer products and the surface treatment industry (Vestergren et al., 2015; Wang et al., 2014). Fourth, while PFOS is typically dominant among PFSAs in solid wastes and sediments, it is still significant in landfill leachate, even if it is not the most abundant one. (Venkatesan and Halden, 2013; Knutsen et al., 2019; Zhao et al., 2022).

In the USA, the concentrations of PFCAs in landfill leachates vary from 10 to 8900 ng/l, and the medians for C4-C8 PFCAs are from a few hundred to more than 1000 ng/l. PFCAs accounts for 20-90% of total PFAS (Huset et al., 2011; Allred et al., 2014; Lang

et al., 2017). For PFSAs, the concentrations range from 50 to 3200 ng/l with median concentrations of several hundred ng/l for PFBS (C4), PFHxS (C6), and PFOS (C8). However, despite extensive use of PFOS, its concentration in leachates is not always higher than that of PFBS and PFHxS, although exceptions were reported by Allred et al. (2014), Huset et al. (2011), and Lang et al. (2017). In Australia, Gallen et al. (2017) carried out a comprehensive leachate study on 27 operating or closed landfill sites and identified 5 dominant PFAS: PFHxA, PFHpA, PFOA, PFHxS, and PFOS. The same dominant group, with an addition of PFBS, was reported by Simmons (2019), who studied 20 landfills across the state of Victoria. According to Gallen et al. (2016), the peak concentrations of PFCA and PFSA were found to be 5700 ng/l and 1900 ng/l, respectively, and for most PFAA types, the medians were less than 550 ng/l. These values are smaller than those typically reported in the USA.

2.2.1.2 PFOS concentrations in leachates

MSWLs around the world are usually the destination for most consumer products and industrial wastes containing PFOS, and hence a major potential source of PFOS contamination. Since landfill leachates are the toxic liquid found in buried landfill waste and constitute its most mobile component, they serve as the primary medium for PFOS migration in MSWLs. For Australia, an overall PFOS concentration range of 1.3~4800 ng/l can be drawn from four nationwide landfill studies. An investigation on 27 Canadian landfills (Li, 2011) gave a mean of 279 ng/l and a maximum of 4840 ng/l for PFOS concentration in leachates. PFOS was also widely detected in landfill leachates of the United States at a level from ND (not detected) to 1000 ng/l. In Asia, the highest reported PFOS concentration in landfill leachate was 6020 ng/l in China, while in Europe, a maximum concentration of 7400 ng/l was reported in Ireland. Table 2.2 presents a summary of PFOS concentrations in untreated leachates from landfills across 9 major countries (mostly MSWLs).

Table 2.2. PFOS concentrations in untreated landfill leachates (C&I: Commercial and Industrial waste landfills; C&D: Construction and Demolition waste landfills). Adapted from Zhang et al. (2023)

Country	Number of landfills	Primary waste type	Years of waste disposal	Number of PFAS analyzed	PFOS concentration (ng/l)	Reference
Australia	19	Mixed putrescible waste, solid inert waste, and prescribed industrial waste (hazardous)	1964 ~ current	15	20 ~ 1200	Simmons (2019)
	27	MSW, C&I, C&D	1969 ~ current	9	13 ~ 2700	Gallen et al. (2017)
	13	MSW, C&I, C&D, green waste	Closed; 1995 ~ current	14	34 ~ 1100	Gallen et al. (2016)
	7	Municipal and/or industrial waste	1930s ~ 1990s	14	1.3 ~ 4800	Hepburn et al. (2019)
Canada	27	-	-	13	279 (mean) 4840 (max)	Li (2011)
	10	MSW, construction waste, industrial waste, and sewage sludge	-	2	<9.5 ~ 744	Gewurtz et al. (2013)
USA	5	MSW	-	2	26 ~ 92	Clarke et al. (2015)
	18	MSW	1966 ~ current	70	ND ~ 801	Lang et al. (2017)
	4	MSW with some non-municipal solid waste (e.g., industrial, construction, and demolition)	1982 ~ current	24	56 ~ 160	Huset et al. (2011)
	5	MSW, C&D, MSW ash, MSWA/MSW-gas condensate	1981 ~ current	11	120 ~ 1000	Solo-Gabriele et al. (2020)
China	5	MSW	-	14	1150 ~ 6020	Yan et al. (2015)

Country	Number of landfills	Primary waste type	Years of waste disposal	Number of PFAS analyzed	PFOS concentration (ng/l)	Reference
Finland	1	-	-	4	87 ~ 140	PerKola and Sainio (2013)
Ireland	40	MSW	-	10	<0.1 ~ 7400	Harrad et al. (2019)
Japan	2	MSW	1974 ~ current	17	5.5 ~ 100	Kameoka et al. (2022)
	3	Industrial	1994 ~ current	17	99 ~ 380	
Norway	2	MSW	1972 ~ 2006	16	455 ~ 2920	Eggen et al. (2010)
	10	Primarily MSW, in some cases industrial waste, and contaminated soil & sewage sludge	1960 ~ current	28	15 ~ 160	Knutsen et al. (2019)
Spain	4	MSW	-	16	ND ~ 43	Fuertes et al. (2017)

2.2.1.3 Regulations of PFOS concentrations

The widespread prevalence and potential environmental and human-health hazards of PFAS, including PFOS, highlight the importance of establishing a sound regulatory system based on evidence-based standards for protecting human health. Unfortunately, until 2018, not only were PFAS not included in regulated monitoring in most countries, but their presence in waste streams was not sufficiently emphasised (Bouazza, 2021). However, since 2018, partly in response to media attention and mounting public concern about PFAS contamination, several American states and USEPA have initiated regulation programs, including the setting up of low lifetime health advisory levels for PFAS in drinking water, the listing of new Superfund sites specially for PFAS, the application of more stringent state standards, and the implementation of new detection and remediation programs (Simon et al., 2019). Later, Heads of Environmental Protection Agencies Australia and New Zealand (HEPA, 2023) have provided a set of acceptance criteria of PFOS+PFHxS and PFOA in landfill or on-site repositories, referring to the international guidelines agreed under Stockholm Convention (UNEP, 2019a) and Basel Convention (UNEP, 2019b).

As for the health advisory considering long-term effects of contamination in drinking water, the standards vary by country, reflecting differences in the tolerance of risks and uncertainties in the risk assessments. There is also a trend towards the tightening of relevant regulatory limits. Key regulatory guidelines or standards for PFOS concentrations in drinking water are summarized below, some of which will be used as a reference in the risk evaluation presented in this thesis. In Australia, a health-based drinking water guideline for PFOS+PFHxS is set at 70 ng/l (NHMRC, 2022), while the latest published revision specifies a guideline of 8 ng/l for PFOS (NHMRC, 2025), which is so recent that it has not been considered as a reference in this study. In the USA, the newest Maximum Contaminant Level (MCL) for PFOS in drinking water set by the USEPA is 4 ng/l (USEPA, 2023), which will take time to be fully implemented, while five other different regulations from the states of New Jersey (13 ng/l), Texas (290 ng/l), California (40 ng/l), Michigan (16 ng/l), and New York (10 ng/l) are also available (NJDEP, 2019; CalEPA, 2020; EGLE, 2020; NYSDOH, 2020). In Canada, a guideline for the maximum acceptable concentration of PFOS for drinking water set by Health Canada (2018) is 600 ng/l. However, although a new Canadian guideline is still in development, an interim document (Health Canada, 2024) has been released, setting a target of 30 ng/l for the sum of 25 PFAS. Several European drinking water limits apply to the sum of multiple PFAS compounds (including PFOS), which can also be referenced as indicative thresholds for PFOS. For example, a limit of 100 ng/l for total PFAS has been proposed by the European industry association EurEau (2018) during discussions around the revision of relevant EU regulations. The European Parliament & Council of the European Union (2020) has presented two group requirements, i.e., 100 ng/l for a sum of 20 PFAS and 500 ng/l for total PFAS. In Sweden, an action limit for the sum of 11 PFAS is 90 ng/l (Banzhaf et al., 2017). Among these, the 100 ng/l limit is adopted in this thesis as a representative benchmark of PFOS drinking water standard for European regulatory practices.

2.2.2 PFAS fate in landfills

The total mass of PFAS present with landfill leachate is a function of their concentrations and the leachate volume. The former factor is complex and highly variable, depending on multiple landfill- and waste-related conditions (Hamid et al., 2018). The latter is weather-dependent and thus highly time-varying (Gallen et al., 2017). PFAS present in landfill leachates undergo multiple processes affecting their fate.

These processes are closely related to the physico-chemical properties of PFAS and leachate, which will change as the waste goes through successive stages of aerobic, acetogenic, and methanogenic biodegradation (Renou et al., 2008; Yan et al., 2015).

The positive correlation between PFAAs' mobility and pH is reported by a few papers (Benskin et al., 2012; Yan et al., 2015; Gallen et al., 2017), possibly due to the altered electrostatic behavior of the sorbents (Higgins and Luthy 2006). This phenomenon is in line with the negative correlation between sorption of PFOS/ PFOA and the solution pH, which is due to fewer positive sites on sorbents with higher pH (Yu et al., 2009; Wang and Shih, 2011). In a study of multiple media around a landfill in China, it has been concluded that the partitioning behavior of PFCAs in water-sediment system is positively correlated with carbon-chain length for long-chain PFCAs, and negatively so for short-chain ones (Xu et al., 2021). Higgins and Luthy (2006) have discussed how sorption behavior is affected by carbon-chain length and the functional head group. Hepburn et al. (2019) have analysed PFAS contamination in groundwater surrounding legacy landfills in an Australian urban redevelopment precinct. They have observed positive correlations between PFCAs and typical leachate indicators (ammonia-N, bicarbonate), and found that PFCAs tend to migrate further in subsurface environments than PFSAs, likely due to their lower sorption affinity, greater chemical and biological persistence, and hence higher mobility in groundwater. Total organic carbon (TOC) is reported to be weakly correlated with PFAA concentration (Benskin et al., 2012; Gallen et al., 2017). With higher PFAA concentration in leachate, both higher (Benskin et al., 2012) and lower (Yan et al., 2015) electrical conductivities have been observed. Some recent studies (Kim et al., 2015; Du et al., 2014) suggest that the effects of ionic strength on PFAS mobility and sorption, as well as the underlying mechanism, are complex and often ion-type and concentration dependent.

Biological processes also influence PFAS fate. By using anaerobic landfill reactors to study PFAS fate through both biological and abiotic processes, it has been found that the total PFAS concentration in leachates from live bioreactors is much higher than from biologically inactive reactors (Allred et al., 2015; Lang et al., 2016). After the start of methanogenic stage, concentrations of a few biodegradation intermediates of PFAA precursors increase (e.g., n:2 and n:3 FTCAs) (Allred et al., 2015). Benskin et al. (2012) has suggested that leachate recirculation can accelerate the biodegradation of PFAA

precursors, leading to the dominance of PFAAs over their precursors and a lower total PFAS concentration. A similar trend has been observed by Huset et al. (2011).

Rainfall can result in lower PFAS concentrations by dilution within a short period, while the subsequent infiltration will affect the bioactivity and hydrolysis in landfills over a longer time frame (Benskin et al., 2012; Gallen et al., 2017). However, Lang et al. (2017) have observed that the concentrations of some PFAS in leachates are higher when the climate is wetter, based on a study of 18 landfills with different climatic conditions. Yin et al. (2017) have concluded that the release of short-chain PFAAs is highly related to precipitation, while concentrations of some other PFAS are strongly affected by partitioning. Landfill age is another important factor. Increasing landfill age usually means significant decreases in PFAS concentration, due to biodegradation (Gallen et al., 2017; Busch et al., 2010). Meanwhile, higher concentrations of short-chain PFAS have been detected in leachates from younger wastes, which can be attributed to the shift of PFAS used in consumer products (Lang et al., 2017). The waste type (e.g., municipal, commercial, construction, and demolition) also plays an important role in determining the PFAS profile and concentration in landfill leachates (Lang et al., 2016, 2017; Gallen et al., 2017).

2.2.3 Composite liner systems in landfills

MSWLs are commonly equipped with barrier systems to provide containment of pollutants and environmental protection. They are composite liner systems, made of different combinations of a GMB, a low-permeability clay liner (CCL or/and GCL), and an attenuation layer (AL) that is usually natural clay (Jones and Dixon, 2011; Rowe, 1998; Touze-Foltz et al., 2006). In the past, CCL was frequently employed beneath GMB. However, in many regions, the complexities and costs associated with CCL installation have led to increased use of GCL as an alternative, particularly where suitable clay materials are limited or construction quality control is challenging. Furthermore, the GMB/GCL combination does not always achieve containment, and the addition of an AL enhances its barrier performance. Generally, the combined GMB/GCL/AL system has proven to be an effective liner system (Li et al., 2022a). As shown in Figure 2.3, however, since 2000, published studies on composite liner systems as integrated systems have been considerably fewer than those focusing on individual components.

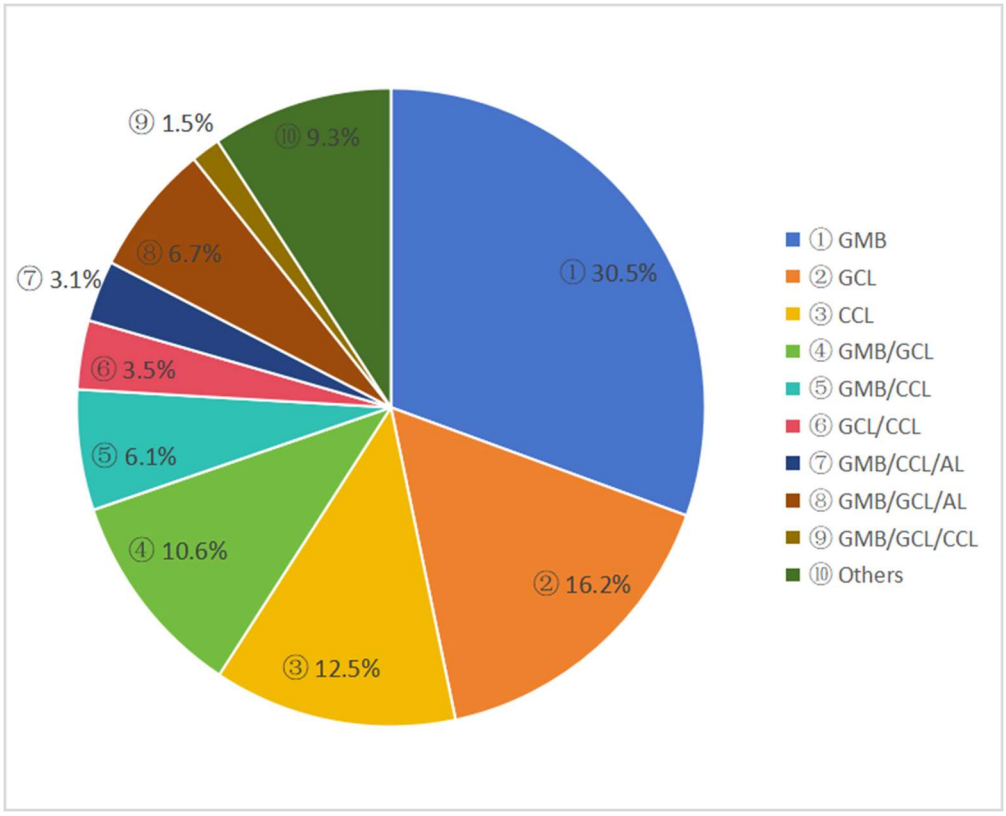

Figure 2.3. Percentage of published studies addressing composite liner systems or their individual components (2000~2022). Adapted from Li et al. (2022a)

A comparison between GCL and CCL is summarised in Table 2.3. Although both are low-permeability materials, GCL has much lower hydraulic conductivity than CCL and is usually set by a much lower thickness. Generally, GCL is considered a more advanced liner than CCL, since GCL is more convenient for production and installation and is less space-occupying while achieving similar or better containment performance. It also has good recovery capacity when damaged during handling and installation (Vishnupriya and Rajagopalan, 2022). Nevertheless, CCL carries some advantages over GCL, such as no requirements for hydration before acceptance of waste, higher resistance to chemical degradation, greater structural integrity under various water quality conditions, and less vulnerability to physical damage and external pressure. Liner design, including choice of clay material, depends on site-specific & environmental conditions and the targeted contaminants.

Note, however, that PFAS are newly emerged contaminants and comparisons between CCL and GCL based on both research and practices in liner systems, such as the one provided here, do not consider their respective effectiveness in containing PFAS specifically.

Table 2.3. Comparison between GCL and CCL. Adapted from Uma Shankar and Muthukumar (2017)

Characteristic	GCL	CCL
Composition	Bentonite and adhesives geotextiles	Native soils or blend of soil and bentonite
Thickness	5~12 mm	Typically 300 to 1000 mm
Hydraulic conductivity	Less than 10^{-10} m/s	Less than 10^{-9} m/s
Speed and ease of construction	Rapid and simple installation	Slow and complicated construction
Vulnerability to damage during construction from desiccation and freeze-thaw	GCLs are essentially dry; GCLs cannot desiccate during construction; not particularly vulnerable to damage from freeze-thaw	CCLs are nearly saturated; can desiccate during construction; vulnerable to damage from freeze-thaw.
Vulnerability to damage from differential settlement	Can withstand much greater differential settlement than compacted clay liner	Cannot withstand much differential settlement without cracking
Materials	Materials easily shipped to any site	Suitable materials not available at all sites
Cost	Reasonably low, highly predictable cost that does not vary much from project to project	Highly variable, depends greatly on characteristics of localy soils
Ease of repair	Ease of repair with patch placed over problem area	Very difficult to repair, must mobilize heavy earth-moving equipment if large area requires repair
Experience	Limited to novelty	Has been used for many years
Regulatory approval	Equivalence in meeting performance objects	Usually required by regulatory
Fissures	Cannot develop fissures if moisture available	May develop fissures
Weight	Light	Heavy

2.2.4 Data availability: PFAS fate in composite liner systems

In order to assess risk to aquifers beneath landfills, it is necessary to quantitatively predict the migration of PFAS through the liner systems. This requires a thorough understanding of processes governing PFAS mobility in these systems, as well as the material properties and environmental conditions determining the relative importance of these processes. Processes governing PFAS fate include advection, mechanical dispersion, molecular diffusion, biological decay, and partitioning. Knowledge on parameters quantifying these processes is limited and reviewed herein.

2.2.4.1 PFAS fate in GMBs

Polyethylene (PE) sheets of 1.0-2.0 mm thickness are commonly applied as geomembranes (GMBs) in liner systems. Ideally, a GMB layer devoid of defects can provide a complete barrier for advection transport of contaminants so that molecular diffusion is the most dominant transport mechanism (Rowe et al., 2004).

Multiple factors affect the diffusive characteristics of a GMB, which essentially depend on properties of the contaminant and the GMB. Generally speaking, these factors include the structure of the polymer (i.e., density, thickness, crystallinity, degree of cross-linking, polarity, etc.), as well as the concentration of the contaminant and its molecular characteristics (Bouazza, 2021). As a semi-crystalline polymer, PE has both crystalline and amorphous zones, which exhibit low and high susceptibility to diffusion of contaminants, respectively (Naylor, 1989). In other words, diffusion is a function of the degree of crystallization of the polymer. Another relevant property of PE is its non-polarity since it has no functional polar group capable of hydrogen bonding (Bouazza, 2021). As a result, PE is less resistant to non-polar organic substances and vice versa (Sangam and Rowe, 2005). PFAS have a head group that is usually hydrophilic and oleophobic, and a fluorocarbon tail that is hydrophobic and oleophilic. This partial polarity of PFAS makes it harder to predict the migration behavior of PFAS through GMBs.

High-density polyethylene (HDPE) geomembranes are the most widely used type in liner systems due to their extraordinary chemical resistance and durability. However, under long-term exposure to high-concentration PFAS solutions, HDPE is considered insufficiently resistant (Orion, 2020), and the use of high-density cross-linked polyethylene (XLPE) has been recommended due to its better mechanical and chemical performance (ACRP, 2017). In addition, it has been suggested that the use of more polar-based GMBs, such as PVC-EIA (PVC: polyvinyl chloride; EIA: ethylene interpolymer alloy) and HDPE-EVOH (EVOH: ethylene vinyl alcohol), may be a better option for on-site repositories. EVOH, a co-polymer of ethylene and vinyl alcohol, is of high hydrophilic nature, which leads to its lower diffusion and partitioning coefficients of non-polar organic contaminants compared to PE (Di Battista et al., 2020).

An experimental investigation of the diffusion and partitioning of PFOA and PFOS in GMBs and GCLs has been in progress in recent years, and is still ongoing, conducted by R. Kerry Rowe's team in Queen's University, Kingston, Canada, with findings

reported by Di Battista et al. (2020) and Rowe et al. (2023), as described next. Diffusion of PFOA and PFOS through linear low-density polyethylene (LLDPE) and LLDPE coextruded with EVOH of 0.1 mm and 0.75 mm at 23 °C, 35 °C, and 50 °C was examined by Di Battista et al. (2020). Corresponding best estimates of diffusion D_g, permeation P_g, and partitioning S_g coefficients for PFOS are shown in Table 2.2. Although LLDPE is less commonly used in landfills than HDPE, it can provide a conservative estimate for the diffusion coefficients of HDPE because LLDPE has a lower crystallinity than HDPE, which generally results in a higher diffusion coefficient due to a smaller tortuosity of the diffusive path (Islam and Rowe, 2009). Rowe et al. (2023) reported results of tests on the diffusion of five PFAS through thermoplastic polyurethane (TPU) and three types of PVC-EIA of about 0.3 mm, still under the above-mentioned three temperatures, and higher diffusion through TPU was observed compared to PVC-EIA and LLDPE. Corresponding best estimate values of permeation and diffusion coefficients for PFOS are also shown in Table 2.2, noting that S_g is always assumed to be 1 in Rowe et al. (2023).

When considering the barrier function of liner systems, however, it's impractical to assume that the GMB will always stay intact. Due to exposure to solar radiation, the GMB will expand and develop wrinkles. Also, during the construction of a landfill, the GMB will develop holes even if the quality assurance is good. Some defects (at least 3-5 defects per hectare) are usually inevitable, and they act as pathways for leachate leaking into underlying liner components. The number and size of defects need to be taken into account when modelling the PFAS-GMB interaction. The extent of leakage through the GMB into the underlying clay layer (usually GCL or CCL) depends largely on the transmissivity (θ), which defines the resistance to lateral leachate flow in the interface between the GMB and the lower layer, and reflects the quality of the contact region between the GMB and the lower layer. Transmissivity of the interface between GMB and GCL was estimated to be 0.0002~0.5 m^2/year for an applied stress of 100 kPa or higher, with the most likely value being 0.001 m^2/year (Rowe and Jabin, 2021, 2022). Furthermore, according to Barakat et al. (2024), the existence of PFAS in MSWL leachate can have a small to negligible positive impact on the magnitude of the GMB-GCL transmissivity.

Table 2.4. Best-estimate of coefficients describing diffusion of PFOS through LLDPE, LLDPE coextruded with EVOH, TPU, and PVC-EIAs. Adapted from Di Battista et al. (2020) and Rowe et al. (2023)

Material	Thickness (mm)	Temp. (°C)	PFOS		
			D_g ($\times 10^{-16}$ m^2/s)	S_g (-)	P_g ($\times 10^{-16}$ m^2/s)[a]
LLDPE	0.1	23	≤0.40	2.8-5.3	≤1.6; ≤0.33
	0.75	23	≤6.5-6.7	2.8-5.3	≤19-34; ≤13
	0.75	35	≤7.6-7.8	2.8-5.3	≤22-40; ≤17
	0.75	50	≤9.8-9.9	2.8-5.3	≤27-52; ≤16
LLDPE coextruded with EVOH	0.1	23	-	-	≤0.55; ≤0.13
	0.75	23	-	-	≤6.8; ≤3.3
	0.75	35	-	-	≤8.3; ≤3.3
	0.75	50	-	-	≤8.2; ≤3.5
TPU	0.3	23	760 ± 310	1	760 ± 310
	0.3	35	2000 ± 7500	1	2000 ± 7500
	0.3	50	2400 ± 8900	1	2400 ± 8900
EIA1	0.29	23	≤1.0	1	≤1.0
	0.29	35	≤1.3	1	≤1.3
	0.29	50	11 ± 1.7	1	11 ± 1.7
EIA2	0.33	23	≤1.2	1	≤1.2
	0.33	35	1.7 ± 0.2	1	1.7 ± 0.2
	0.33	50	180 ± 56	1	180 ± 56
EIA3	0.26	23	≤0.8	1	≤0.8
	0.26	35	≤0.8	1	≤0.8
	0.26	50	1.8 ± 0.6	1	1.8 ± 0.6

[a] For P_g of LLDPE and CoEx LLDPE, the two values are tested on 483/509/399/399 days and 1331/1331/1246/1246 days, respectively.

2.2.4.2 PFAS fate in GCL and CCL

Geosynthetic clay liners (GCL) are often another important component in composite liners of landfills. When used as part of a composite liner system, a GCL forms the principal insulating material preventing contaminant migration into the subsurface, owing to its very low hydraulic conductivity. It is usually laid under the GMB because the latter has higher chemical resistance to aggressive leachate in the waste and can

help protect the GCL from chemical damage. The GCL is made of bentonite clay encased between two geotextiles. The low hydraulic conductivity of GCL is attributed to the bentonite, which swells in the presence of water to form a tight, gel-like sealing layer (Gates et al., 2009; Bouazza and Gates, 2014; Mcaulou and Huling, 1999). The hydrophilicity of bentonite also results in its relatively low sorption capacity to organic pollutants (Li and Denham, 2000; Richards and Bouazza, 2007). GCL development has evolved mostly empirically, and although they are used worldwide, many gaps remain in our understanding of their behaviour.

Past research has generated considerable data about the hydraulic performance of GCLs for containing non-standard liquids and various chemical solutions and fluids (Bouazza and Gates, 2014), such as leachate or gas (Bradshaw et al., 2016; Bouazza et al., 2017), saline solutions (AbdelRazek and Rowe, 2019b), and non-neutral pH solutions (Benson et al., 2010; Gates and Bouazza, 2010). However, very little research on GCL interaction with PFAS compounds in aqueous solutions has been conducted to date. If an existing GCL is considered inadequate for attenuating the transport of organic contaminants, such as PFAS, a further reduction in transport can be achieved by increasing the number and capacity of contaminant sinks (Bouazza, 2021). Contaminant sinks refer to any process reducing the concentration of mobile contaminants, including radioactive or biological decay and transfer of contaminants into a less mobile phase. Another effective way of mitigating the migration of organic contaminants through GCLs is by increasing the sorption capacity of the bentonite component. For example, Bouazza (2021) has shown that this can be achieved for PFAS substances through the application of activated carbon amended GCL (ACA-GCL).

A limited amount of data exists on parameters characterising the fate of PFAS in GCL. Li et al. (2015) have conducted batch tests showing that perfluorinated compounds (PFCs) in landfill leachate hardly ever bind to bentonite. Meanwhile, the hydraulic conductivity of a sand-bentonite mixture with PFC-spiked landfill leachate has been found to be around 10^{-12}~10^{-11} m/s. Sörengård et al. (2020) has reported the solid-aqueous partitioning coefficient (K_d) of 17 PFAS onto 44 inorganic/organic sorbents including 5 types of bentonites, and log(K_d) for bentonite has been found to be mostly between 0~1. Jeon et al. (2011) has measured sorption distribution coefficients (K_d) on montmorillonite (the key constituent of bentonite) of about 8.5 l/kg and 1.3 l/kg for PFOS and PFOA, respectively. It is possible to derive an estimate of the molecular

diffusion coefficient of PFAS into GCLs as the product of GCL's apparent tortuosity factor and PFAS's aqueous diffusivity. Based on estimates of the tortuosity factor presented by Nguyen et al. (2011) and aqueous diffusivity for 9 PFAAs given by Schaefer et al. (2019), the coefficient of molecular diffusion of PFAS in GCLs is estimated a range between 3.33×10^{-11} m^2/s and 1.85×10^{-10} m^2/s.

Measurements of the hydraulic conductivity to PFAS solution of a standard thermally treated and needle punched GCL and an ACA-GCL have been reported in Bouazza (2021). The hydrating solution is a cocktail of PFAS compounds, and some early-stage results indicate that the hydraulic conductivity is 4.4×10^{-11} m/s for the normal GCL and 1.6×10^{-10} m/s for the ACA-GCL. This marks a slight increase in hydraulic conductivity compared to those measured with deionized water as permeant (2.8×10^{-11} m/s and 6.5×10^{-11} m/s, respectively). In addition, adsorption of PFAS onto the GCL has been estimated by monitoring PFAS concentration in the effluent (Bouazza, 2021). The study has found that ACA-GCL has a higher adsorption capacity than the normal GCL, and long-chain PFAS are more prone to be adsorbed than short-chain ones (Bouazza, 2021).

Barakat et al. (2024) has provided a comprehensive examination of the material properties of GCL, relevant to PFOS and PFOA transport, under different applied stresses, and results from this paper for PFOS are summarized in Table 2.5. The diffusion coefficients deduced from GCL diffusion tests for PFOA and PFOS decrease linearly with increasing applied stresses. The different components of GCL are tested for PFOA and PFOS sorption. No significant sorption of PFOA is observed for any of the components of the GCL, while some sorption of PFOS onto the geotextiles of the GCL is observed. At last, tests for hydraulic conductivity have revealed very little impact of PFAS on the hydraulic conductivity of GCLs under high stresses, but a small increase is seen on the GCLs under relatively low stresses.

Table 2.5. Material properties of GCL estimated for PFOS at different applied loads. Adapted from Barakat et al. (2024)

Applied load (kPa)	K_d (l/kg)	D ($10^{-11}m^2/s$)	k (10^{-11}m/s) (estimated from graph)
20	2.2	3.5	10
60	2.2	2.6	4.1
150	2.2	1.8	0.5

Mikhael et al. (2024) has conducted an experimental study examining the sorption behaviors of four PFAAs on polypropylene cover and carrier geotextiles typically

utilized in GCL. The study explores the effects of several operational variables. They report that the adsorption kinetics for all tested PFAAs can be represented by a bi-exponential adsorption model. Additionally, the sorption of PFAAs is found to be significantly influenced by the terminal functional groups and the length of the perfluorinated carbon chains of the PFAAs.

As for CCL, only one study can be found in the literature on parameters characterising the fate of PFAS. Yu Tan et al. (2022) performed hydraulic conductivity tests on three CCL materials using synthetic MSWL leachate, either with or without PFAS (PFHxA or PFOS at 1000 ng/l), under an average effective stress of 20 kPa. The tests related to PFOS yielded values of 1.4×10^{-10} m/s, 3.8×10^{-11} m/s, and 2.4×10^{-11} m/s for a low plasticity clay, a high plasticity clay, and a moderately plastic organic clay, respectively, which are comparable to those from tests using leachate without PFOS.

2.2.4.3 PFAS fate in buffer soil

Compared with GMB and GCL, studies on the interaction between PFAS and various soils are much more abundant. Schaefer et al. (2021) has measured coefficients of diffusion of 6 PFAAs through a saturated soil column with a sand/silt/clay percentage of 6.6%/28%/65%. For PFOS and PFOA, the reported values are 3.2×10^{-11} m^2/s and 7.8×10^{-11} m^2/s, respectively. Some investigations have been carried out on a site in central Canada (Carey et al., 2019; McGregor, 2018), where the shallow overburden aquifer is composed of medium sand with some silt. The hydraulic conductivity for a PFAS solution measured at that site is reported to be 3.0×10^{-5} m/s. In another case of a silty sand unconfined aquifer, measurements of the horizontal hydraulic conductivity for a PFAS and trichloroethylene (TCE) cocktail have yielded values in the range of $4.8\times10^{-6} \sim 6.3\times10^{-4}$ m/s (McGregor and Zhao, 2021). Some papers suggested informed guesses of certain parameters based on earlier sources and expert advice. For example, Schrefler and Delage (2010), evaluating the containment properties of composite liners, suggest using a non-PFAS specific hydraulic conductivity of 1.0×10^{-7} m/s and a diffusion coefficient of 9.5×10^{-10} m^2/s for the attenuation layer. Rowe and Barakat (2021) have assumed a value of 6.3×10^{-10} m^2/s for the diffusion coefficient of PFOS in the attenuation layer.

There have been a large number of studies on the adsorption of PFAS onto a variety of soils. Schaefer et al. (2021) reported linear adsorption coefficients for PFOS and PFOA of 1.8 l/kg and 0.6 l/kg. Through measurements on the sandy aquifer sediments from

beneath a landfill, the adsorption coefficient averaged 1.2 l/kg for PFOS and 0.27 l/kg for PFOA at the early stage of the experiment, albeit declining with time and becoming undetectable after 740 days (Ferrey et al., 2012). The sorption coefficients of an Ottawa sand were tested by single- and multi-solute experiments, and the values were reported to be 0.085 l/kg, 0.175 l/kg for PFOS and 0.035 l/kg, 0.005 l/kg for PFOA (Chaudhuri, 2019). Van Glubt (2020) calculated the equivalent K_d using an isotherm regression, and the values for a quartz sand were 0.23 l/kg (PFOS) and 0.13 l/kg (PFOA), while the values for Accusand quartz sand were 0.4 l/kg (PFOS) and 0.2 l/kg (PFOA). Nguyen et al. (2020) assessed the soil-water partitioning behavior of 29 PFAS onto 10 diverse soils to explore the influences of chemical properties, soil properties, and solution pH on the partitioning coefficients. Corresponding $\log(K_d)$ ranges from less than 0 to approximately 3. The adsorption behavior of PFAS, especially PFOS and PFOA, were also investigated considering many other pools of sorbents, such as various natural and anthropogenic carbonaceous sorbents (Zhi, 2017), sludge from 16 different sewage treatment plants (Campo et al., 2014), 19 coastal sediments collected from the east coast of Australia (Oliver et al., 2020a), 114 temperate and tropical soils from Australia and Fiji (Umeh et al., 2021), 96 soil samples from agricultural and forest sites across North Rhine-Westphalia (Martz et al., 2019), Eustis soil and Vinton soil (Brusseau et al., 2019), ten soils with different organic carbon contents and composition of soil minerals (Miao et al., 2017), and 28 tropical soils with different physicochemical properties (Oliver et al., 2020b). Generally speaking, the sorption of PFAS is highly influenced by the clay fraction, the carbon content, and the organic matter of the soil, as well as the pH. Meanwhile, the adsorption coefficients of PFAS onto different sorbents are highly variable. Hence, given the uncertainty attached to the sorption behavior of PFAS, zero sorption is a reasonable assumption to make in risk assessments of PFOS in landfills, especially considering that this will provide a conservative assessment.

As for degradation of PFAS, no study appears to have reported specific degradation half-lives of PFAS compounds in landfills. In an early study modelling global-scale fate and transport of PFOA (Armitage et al., 2006), its degradation half-life in soil and water was nominally taken as 6900 years (equivalent to 1% degradation per 100 years) to characterize its extreme stability. Later, photochemical half-lives for PFOA of more than 256 years, 5120 years, and 25,600 years at zero depth of ocean, at mixing layer of open ocean, and at coastal ocean, respectively, were suggested by Vaalgamaa et al.

(2011). Li et al. (2017) assumed a degradation half-life for 9 PFCAs of >5120 years in wastewater treatment plants (WWTP) and water (following the photolytic half-life of PFOA in open ocean in Vaalgamaa et al. (2011)), and 6900 years in landfills, dumping, soil, and sediment (following the nominal value in Armitage et al. (2006)). Furthermore, given the lack of landfill-specific data, assuming no degradation (half-life of infinity) in the waste and the subsurface beneath landfills is sound and conservative.

Numerical modelling of the fate of PFAS in liner systems and underlying soils is necessary to generate assessments of risk to groundwater from PFAS present in waste landfills. It is clear from the above literature review that such modelling must be based on a combination of existing experimental knowledge, both PFAS and non-PFAS specific, and expert judgment and informed guesses. This means that large uncertainties are bound to be present in such assessments. The next section discusses numerical modelling approaches and how best to incorporate such uncertainties.

2.3 Modelling of PFAS Fate in Liner Systems

This part of the literature will proceed as follows. First, the vast literature on the modelling of contaminant fate in porous media is briefly reviewed, including both analytical and numerical solutions to governing differential equations (e.g., RDAE). Following from this, water flow and contaminant fate in liner systems are specifically discussed to better understand the state-of-the-art in this area, including available simulation software. Finally, the small number of studies on the simulation of PFAS in liner systems are discussed, and gaps in the literature are identified. Note that the discussion in this section is restricted to deterministic studies, with probabilistic approaches reviewed in Section 2.4.

2.3.1 Modelling of contaminant fate in porous media

A vast body of theoretical and experimental research has built up over the past century and generated a theoretical framework for quantifying and predicting the transport of contaminants through porous media including both natural soils and engineering materials such as GMBs, GCLs, and CCLs. The framework is phenomenological in nature and grounded in the continuum assumptions of soil hydromechanics, but broadly consistent with first principles of thermo- and fluid-dynamics (Bear and Cheng, 2010).

Over the past few decades, it has been found to be successful in accounting for observed laboratory and site data and has been extensively validated in the context of several soil contamination problems. Examples of validation include, amongst others, problems of organic and inorganic contamination in the subsurface (e.g., Kia, 1991; Dhanraj and Ganesha, 2023), nuclear waste repositories (e.g., Kelkar et al., 2010), and, especially relevant for this thesis, transport of contaminants in landfill leachate into the surrounding environment (e.g., Praveen Kumar and Dodagoudar, 2010; Markhali and Ehteshami, 2016; Srivastava and Ramanathan, 2018; Divya et al., 2020). The set of equations generated by the framework (and used here for simulating PFOS transport through liner systems) has been presented in numerous publications (Rowe and Booker, 1985; El-Zein and Rowe, 2008; El-Zein and Balaam, 2012). It consists of two core and coupled equations: the water flow equation (WFE) simulating transport of water and the reaction diffusion-advection equation (RDAE) representing transport of solute dissolved in the water. While, in some contexts, mechanical, electro-chemical and/or biological processes may also play a part and may require additional equations to be included in simulation models (Mendoza-Sanchez & Cunningham, 2012; Masi et al., 2019; Wu & Wang, 2020), the WFE and RDAE, are often sufficient to capture changes in contaminant concentrations in space and time at the continuum and field scales. In this thesis, the saturated version of semi-coupled steady-state WFE and time-dependent RDAE is used to depict the behaviour of PFOS in liner systems. An extensive discussion of the rationale for adopting this version of the equations and the assumptions behind the adopted equations is presented in the methodology chapter.

Analytical solutions to the WFE and RDAE have been developed since the 1960s. One of the earliest and most cited analytical solutions was the Ogata-Banks equation (Ogata and Banks, 1961), which described 1D advection-dispersion in a semi-infinite saturated porous medium under constant boundary conditions. This foundational model laid the groundwork for many subsequent developments. Baetsle (1969) extended the formulation to 3D transport under the assumption of an instantaneous point source injection. Bear (1972) considered first-order decay in multi-dimensional advection-dispersion formulations, providing a basis for reactive transport modelling. Van Genuchten (1981) incorporated adsorption, zero-order production, and first-order decay into analytical solutions, enabling broader treatment of reactive solute transport. Domenico and Robbins (1985) derived closed-form solutions for plume migration in

2D and 3D under constant source concentration, accounting for anisotropic dispersion and finite-width sources. Rowe and Booker (1985) provided 1D layered-system solutions tailored to landfill applications under specified mass input, explicitly modelling contaminant transport through clay liners. Leij et al. (1993) further advanced the framework by developing analytical solutions for multi-dimensional non-equilibrium transport using Laplace and Fourier transform techniques.

In recent decades, analytical solutions have been extended to accommodate more realistic and complex field conditions. Selvadurai (2008) proposed nonclassical formulations that allow time-dependent boundary concentrations and flow velocities, enhancing applicability to transient systems. Pérez Guerrero et al. (2009) developed solutions for multi-species transport involving sequential first-order decay reactions in finite domains. Jaiswal et al. (2011) addressed variable environmental conditions by deriving solutions with time-dependent transport coefficients. Hwang (2021) derived exact solutions for 2D advection-dispersion equations on polygonal domains with nonhomogeneous boundary conditions using the unified transform method. Yadav and Roy (2022) developed analytical solutions for 1D solute transport in finite heterogeneous media with scale-dependent dispersion and spatially varying flow. Singh et al. (2024) further extended analytical solutions to 3D domains with Cauchy-type boundary conditions.

While desirable, analytical solutions are often limited to overly simplified conditions. Consequently, numerical solutions are required under more complex and realistic conditions. Numerical solutions to the saturated, steady-state WFE are reasonably straightforward, and accurate results can be generated at low computational cost using well-established numerical methods such as the finite-difference method (FDM) and the finite-element method (FEM). Given the extensive literature on numerical solutions of the RDAE, only a concise review is presented in the following, focusing on four representative classes: finite-difference method (FDM), finite-element method (FEM), finite-volume method (FVM), and other relevant approaches. A description of the mathematical foundations and historical emergence of the FDM, FEM, and FVM is beyond the scope of this thesis, and the reader is referred to Kolditz (2002), who discussed these methods in the context of solute transport, as part of an overview of numerical modelling in environmental fluid mechanics. The review here will focus instead on more specific developments in solute transport and the RDAE.

The finite difference method (FDM) has historically served as a fundamental tool for solving advection-dispersion-reaction equations in porous media. Douglas and Russell (1982) developed numerical methods based on FDM or FEM for solving convection-dominated diffusion problems. Cheng et al. (1984) presented an advancement in FDM for reducing numerical dispersion and improving solution accuracy for convection-dispersion equation. Zheng and Bennett (1995) systematically introduced the application of FDM in solving such problems and established the basis for the widely used MT3D code. Ferraresi and Marinelli (1996) proposed an extended formulation of FDM that permits a more accurate approximation of the governing equations in heterogeneous anisotropic media. Natarajan and Suresh Kumar (2010) extended this approach to multispecies reactive transport by coupling advection, dispersion, and reaction processes in a finite-difference framework. Hulagabali et al. (2014) developed a MATLAB-based 2D FDM model for simulating contaminant migration in saturated porous media and validated it against FEM results. Djordjevich et al. (2017) applied an explicit FDM scheme to simulate 2D transport under periodic flow, capturing the cyclic variation of solute concentrations. Gharehbaghi (2021) proposed a 1D FDM formulation for multi-species transport and demonstrated its accuracy by comparison with analytical solutions.

Finite element methods (FEM) have gained prominence for their capability to handle complex geometries, heterogeneous material properties, and coupled processes in subsurface transport modelling. Neuman (1984) introduced an adaptive Eulerian-Lagrangian FEM, exploring both convection-dominated and advection-dominated situations. Yeh and Tripathi (1991) developed a comprehensive FEM-based model for multispecies reactive transport, capable of representing spatially variable flow and chemical reactions. Gambolati et al. (1993) presented a broad overview of FEM applications in groundwater contaminant modelling, including the treatment of nonlinearity. Abdulle and Huber (2014) proposed a discontinuous Galerkin FEM with multiscale capabilities for simulating advection-diffusion in heterogeneous systems. Diersch (2014) elaborated on the FEM-based FEFLOW software, encompassing flow, mass, and heat transport, outlining advanced FEM formulations for coupled, non-isothermal, and reactive transport processes under variable-density condition. Berrone et al. (2018) improved FEM robustness through a stabilized virtual element method (VEM), particularly for high Peclet number problems. Brenner et al. (2023) applied an

algebraic flux correction (AFC) FEM with semi-implicit time integration to simulate solute transport in fractured porous media.

Finite-volume methods (FVM) are widely valued for their local conservation properties and adaptability to unstructured meshes. Balaguer et al. (1995) applied a 2D FVM scheme for simulating pollutant transport in groundwater, validating the results against analytical solutions. Bertolazzi and Manzini (2004) proposed a cell-centered FVM with slope-limited gradient reconstruction, ensuring non-negativity and compliance with the maximum principle in reactive solute transport simulations. Wu et al. (2023) developed a second-order implicit FVM framework and applied it to model the spread of heavy metals in farmland soil and the transport of PFAS in unsaturated porous media.

Other numerical approaches have also contributed to solving the RDAE, often in conjunction with the primary methods discussed above. The method of lines (MOL) has been used to transform partial differential equations (PDEs) into ordinary differential equation (ODE) systems, which are amenable to standard time integration schemes (Kanney et al., 2003; Fahs et al., 2011). The finite increment calculus (FIC) method, though frequently embedded within FEM formulations, introduces a distinct stabilization strategy for advection-diffusion-adsorption problems. Notable developments include a nonlinear high-resolution Petrov-Galerkin FIC scheme (Nadukandi et al., 2012) and an accurate FIC-FEM formulation for the transport equations in the exponential and propagation regimes (Oñate et al., 2017). More recently, machine learning methods, such as the physics-informed neural networks (PINNs), have been successfully applied to solve the RDAE (He and Tartakovsky, 2021; Faroughi et al., 2023; Kamil et al., 2025).

2.3.2 Modelling of water flow and contaminant fate in composite liners and underlying aquifers

Two key aspects of liner system behaviour have received significant attention in the literature, namely quantification of leakage rates caused by defects in the GMBs and transport of contaminants through the liner system, into the underlying aquifer.

The pioneering work of Giroud and Bonaparte (1989) and Giroud et al. (1989) proposed early equations for calculating leakage through composite liners, and has since been further developed by the same research group to address different scenarios (Giroud et al., 1992; Giroud, 1997; Touze-Foltz et al., 1999; Giroud and Touze-Foltz, 2005). An

analytical equation estimating leakage rate through GMB with defects, placed over a CCL, has been proposed by Rowe (1998) and later modified by Rowe and Abdel Razek (2019) and Yu et al. (2025) to accommodate liners with GCL, and other applications. Rowe (1998) presented two versions of this equation under different assumptions regarding leachate transmission at the GMB-clay interface and the spacing of defects. Touze-Foltz et al. (2008) has presented a summary of analytical and empirical equations for predicting flow rates in liner systems.

The literature on analytical solutions of contaminant transport in liner systems has been reviewed by Touze-Foltz et al. (2021). Key developments reported by Touze-Foltz et al. (2021) include: a) the early formulation of analytical solutions for contaminant transport in multi-layered liners (Chen et al., 2009), which were progressively extended to incorporate degradation (Xie et al., 2013), consolidation (Xie et al., 2016), unsaturated soil properties beneath landfill barriers (Chen et al., 2019), and a triple-layer liner system (Pu et al., 2020a); b) to address the effects of GMB defects, the analytical solutions developed by Xie et al. (2010) accounting for leakage through damaged wrinkles, which were later complexified to incorporate leachate head, wrinkle length, and interface transmissivity (Xie et al., 2015), a triple-layer liner system (Xie et al., 2018), and transient transport behaviours (Feng et al., 2019).

More recent developments on analytical solutions for contaminant transport in composite liners have placed emphasis on different aspects of the problem, such as adsorption, diffusion and thermo-diffusion for a GMB/CCL liner (Peng et al., 2021), non-isothermal diffusion under unsaturated conditions (Yan et al., 2021b), a crack in CCL (Xie et al., 2022), temperature-dependent distribution coefficient and effective diffusion coefficient in a triple-layer liner (Qiu et al., 2023a), CCL effective porosity, GMB defects, and thermo-diffusion in a GMB/CCL liner (Qiu et al., 2023b), soil heterogeneity and non-uniform contaminant distribution in the leachate (Shi et al., 2025), longevity of liner components (Xie et al., 2025).

Numerical solutions, while requiring significant computational resources and expertise, offer higher flexibility and applicability than analytical and empirical equations, enabling the effective modelling of contaminant transport in composite liners.

The finite difference method (FDM) is conceptually more straightforward than other numerical approaches, and has been occasionally applied to solve contaminant

transport in composite liners. Most relevant developments were within 1D scope, such as the coupled modelling for consolidation and contaminant transport considering nonlinear compressibility and permeability (Pu et al., 2020b) and under non-isothermal distribution condition (Li et al., 2022b), as well as an extension of the solution to non-isothermal transport in a three-layer liner with defective GMB (Jiang et al., 2025).

Based on the finite layer method (FLM) initially presented by Rowe and Booker (1984), POLLUTE v7 (Rowe and Booker, 2004) was developed to realize the so-called 1½-D modelling of solute transport, which incorporates only vertical 1D advective-dispersive-diffusive transport through laterally continuous horizontal layers as well as horizontal advective transport in an aquifer layer. By combining POLLUTE v7 and the analytical equations of leakage rate mentioned above, the modelling of contaminant migration through composite liners with holed wrinkles was carried out by Rowe and Abdelrazek (2019) and Rowe and Barakat (2021). Rowe and Abdelrazek (2019) also compared their approach to FEM results and discussed the advantages and disadvantages of the two approaches.

Pu and Fox (2016) developed Consolidation and Solute Transport 3 (CST3), a numerical model based on the CS2 method within a Lagrangian framework (Fox and Berles, 1997; Fox and Pu, 2012), to simulate coupled large-strain consolidation and solute transport in saturated multi-layered soils. Using CST3, Pu et al. (2018) performed numerical simulations to explore the effects of liner consolidation on the migration of a volatile organic compound (VOC) in a composite liner system containing both GCL and CCL.

Rupali and Sawant (2016) developed a 1D model of contaminant transport through GMB overlying soil layers by employing the Element-Free Galerkin Method (EFGM).

Several FEM software, such as GeoStudio (Geo-Slope International, 2018a, 2018b) and COMSOL Multiphysics, can also be used to estimate the leakage and simulate the migration of contaminants through a composite liner into the underlying aquifer. For example, Bannour (2023) simulated organic contaminant migration through a composite liner with holed GMB by Geo Studio; Peng et al. (2023) applied COMSOL Multiphysics for 1D simulations in a typical composite liner emphasizing thermo-diffusion. However, in 2D and 3D, they require significant computational power when addressing simulations in composite liner due to the multiple scales involved (from mm

for the thickness of the GMB and that of the transmissive layer between GMB and underlying layer to several 100m, up to kilometres, for the length of the landfill and the aquifer).

The Soil Pollution Analysis System (SPAS) is an FEM-based program, tailored for modelling leachate flow and contaminant migration in landfill liner systems, and has been extensively validated over the past two decades (El-Zein and Balaam, 2012; El-Zein et al., 2016; Hanna and El-Zein, 2023). SPAS, which can handle both 2D and 3D problems, is made of a finite element engine (COMFEM) combined with a graphic user interface (pre- and post-processing tool) that makes it easier to simulate different components of a liner system, including GMBs with defects, as well as a range of boundary conditions. For example, El-Zein et al. (2012) used SPAS-3D to simulate the movement of dichloromethane through a standard composite liner. SPAS is adopted in this thesis to conduct all simulations. The rationale for its adoption here is provided in the methodology chapter.

Within the above review, the spatial distribution of contaminant concentrations has been widely examined as a key aspect of contaminant fate. Many analytical solutions explicitly describe vertical concentration profiles across liner components (e.g., Peng et al., 2021; Yan et al., 2021b; Qiu et al., 2023a). Such profiles are also a primary focus of numerical studies and are commonly used for verification through comparison with analytical solutions, for example using FDM (Li et al., 2022b; Jiang et al., 2025), CST3 (Pu et al., 2018), and EFGM (Rupali and Sawant, 2016). In addition, lateral concentration profiles within the underlying aquifer have been reported using FLM (Rowe and Abdelrazek, 2019). While full 2D or 3D concentration fields are in principle attainable using FEM-based software, their application is often constrained by the strong multi-scale nature of the problem. SPAS, as an FEM-based tool specifically developed for liner systems, provides a practical framework for resolving 2D spatial distributions of contaminant concentrations (El-Zein and Balaam, 2012).

2.3.3 Numerical modelling of PFAS transport in composite liners

To the best of the author's knowledge, only two studies have reported simulations of PFAS transport in liner systems. The first focused on PFOS (Rowe and Barakat, 2021), while the second simulated the transport of PFOA (Barakat and Rowe, 2025). These two studies, including their key findings and limitations, are discussed below.

Rowe and Barakat (2021) simulated the transport of PFOS in a municipal solid waste landfill lined by a single GCL composite liner. They solved the RDAE using the above-mentioned 1½-D finite layer method (POLLUTE v7). Both the pure diffusion case and the case considering advection through GMB were investigated to evaluate the effect of leakage of leachate through the GMB. Furthermore, sensitivity analyses were conducted to assess the influence of size of holed wrinkles, GMB-GCL interface transmissivity, hydraulic conductivity of GCL, and initial concentration in source leachate. The paper concluded that, although the theoretical pure-diffusion case can guarantee safe PFOS concentrations based on common water-quality standards, when leakage is taken into account and transport is governed by both advection and diffusion, the single-liner system is not adequate for PFOS containment, and a double-layer design is more prudent. The paper's scope was limited, however, in that it did not conduct probabilistic simulations and therefore did not account for various sources of uncertainty surrounding the fate of PFOS in liners. In addition, two key assumptions that are inherent for the approach used in the paper, i.e., advective-dispersive-diffusive flux only migrates vertically downward and only horizontally advective flux exists in the aquifer, may also compromise the reliability of results.

Barakat and Rowe (2025) simulated PFOA transport through various single and double composite liners using the FEM software GeoStudio (SEEP/W and CTRAN/W). The study incorporated experimentally derived parameters for PFOA diffusion, partitioning, and interface transmissivity, and investigated both diffusion-only and advection-diffusion scenarios. Several parametric analyses were performed to quantify the impact of key factors on the peak PFOA concentration in the aquifer, which was then compared to various regulatory standards. The results concluded that a) particularly influential factors on aquifer PFOA peak concentration include initial concentration in leachate, the leakage passing through the liner, and the flow in the aquifer, b) single composite liners are unlikely to effectively contain PFOA in most cases, and c) double liners offer much better performance, and among the secondary liner configurations, the combination of GCL and CCL provides the greatest reduction in leakage and the best control of concentration, followed by the use of GCL alone, and then CCL alone. Despite improvements over the abovementioned study based on 1½-D FLM, this study remained deterministic in nature and did not address uncertainty arising from variability in input parameters or site conditions.

2.4 Probabilistic Analysis Methods

Uncertainties pervade physical, chemical, and biological processes in geoenvironmental engineering and hydrogeologic contexts. On this ground, probabilistic contamination analysis is warranted due to the high heterogeneity of hydraulic and transport properties of liner-subsoil systems and widespread uncertainties existing throughout the contamination process. With a rational quantification of uncertainties, by assuming input conditions to be stochastic, probabilistic analysis can provide statistical results about contaminant migration, leading to risk-based assessment of contamination, as well as enhancing the generalisability of the findings of relevant research.

2.4.1 Probabilistic subsurface contamination analysis

Probabilistic models of water flow in the subsurface have been developed since the early 1960s (Warren and Price, 1961; Tang and Pinder, 1977; Bakr et al., 1978; Smith and Freeze, 1979). Then, building on these developments, significant efforts have been made to conduct probabilistic analyses of contaminant transport in groundwater and apply them to contamination risk assessments, especially from the late 1980s onwards. In an early attempt, Roco et al. (1989) conducted a set of comprehensive analyses of 1D contaminant transport in porous media by Gaussian field approach and Random-walk method, considering various kinds of randomness. Piggott and Cawlfield (1996) adopted the first-order reliability method (FORM) to carry out probabilistic sensitivity analyses, unravelling the relative importance of various uncertain parameters for the probabilistic outcome. Later on, Patrick Wang and Zheng (2005) investigated the effects of randomness in contamination sources, such as their timing, location, and magnitude. Two types of sources were studied by a stochastic PDE and a Markovian analysis approach, respectively. Tartakovsky (2007) and Winter and Tartakovsky (2008) proposed a reduced-complexity model for probabilistic risk assessment of groundwater contamination, which treated the contamination progress as a sequence of components or sub-states and assumed transitions between states as Markov jump processes. Zhang (2009) developed a fuzzy-stochastic partial differential equation (FSPDE) model to differentiate random and non-random uncertainties that are involved in groundwater flow and solute transport. De Barros and Nowak (2010) explored the dependency of statistical results about contaminant plume migration on the uncertainty in the source release condition, which is characterized by a parameter named effective source width,

incorporating both the source flux and the geometric source width. An extended study was carried out later to quantify the effects of the hydraulic conductivity's heterogeneity and the mass release rate on the uncertainty in solute mass discharge, whose analytical and semi-analytical solutions were derived for a 3D problem based on the perturbation theory, and the output parameter can be propagated to contamination risk assessment (De Barros 2018). De Barros et al. (2011) came up with a new form of stochastic fault tree accounting for uncertainties in both hydrological and human health components to assess contaminants' health risk. Chang and Boateng (2012) adopted an adaptive Kalman filter (AKF) as a stochastic data assimilation scheme to simulate subsurface Benzene transport in a simulated true field undergoing random noise injection, verifying its superiority over the conventional Kalman filter and a finite-difference scheme. Dogan et al. (2014) introduced a new fractal method for generating stochastic heterogeneous fields of hydraulic conductivity with adequate connectivity based on high-resolution data, which can be used in non-deterministic water flow and solute transport calculations. Guo et al. (2019) compared the performance of MT3DMS and RWhet (advanced random-walk particle method) in simulating a pump-and-treat (PAT) operation conducted at a large, contaminated site, which was modeled heterogeneously conditioned on high-resolution data.

More frequently, probabilistic analyses of contaminant transport in groundwater were conducted within the framework of Monte Carlo simulation (MCS). MCS gained popularity because it is conceptually simple, easy to implement, and often statistically accurate (Harter, 2000; Rajabi and Ataie-Ashtiani, 2014). Cadini et al. (2013) applied MCS to the problem of radionuclide migration in fractured rock to assess the performance of radioactive waste repositories, which is based on Kolmogorov-Dmitriev (K-D) theory and the use of a dual-permeability. Napa-Garcia et al. (2014) carried out sensitivity analyses on the probability of exceedance for various related parameters including hydraulic properties, initial concentration, and source conditions, via MCS. Bong and Son (2019) analyzed the impact of the probability distribution function and the spatial variability of hydraulic conductivity on contaminant transport by generating non-Gaussian random fields and analytically solving the governing equations. In Mumford et al. (2016), 3D numerical simulations were performed to evaluate the contamination risk to groundwater after source remediation by using a

finite difference technique along with MCS, while uncertainties exist in hydraulic conductivity, fraction of organic carbon, and biodegradation rate constant.

2.4.2 Probabilistic analysis of leakage or solute transport in landfill contexts

Among all probabilistic studies of subsurface contamination, the analysis of contaminant transport in composite liners has experienced certain advancements, although they are still relatively limited in number and research scope. Most of them have utilized MCS or methods based on MCS. In Abbaspour et al. (1998), the Bayesian Uncertainty Development Algorithm (BUDA) was applied to account for the uncertain features in the evolution of a chloride plume around an aged landfill. Plimmer et al. (1999) introduced a probabilistic risk assessment for landfills using the LandSim model, which employs MCS to consider parameter uncertainties, focusing on a case study of chemical containment of ammonia. Liu et al. (2004) proposed an integrated approach combining an analytical groundwater solute transport model, an exposure dose model, and a fuzzy risk assessment model to assess groundwater risks from landfill leachate contamination, with MCS used to address associated uncertainties. Chaudhuri and Sekhar (2005) used a stochastic finite element method (SFEM), based on the perturbation theory, to evaluate 1D pollutant migration in landfill soil liners, treating key parameters such as hydraulic conductivity and porosity as random fields to capture inherent uncertainties and revealing the significant influence of correlations between parameters and correlation lengths of parameters. Bieda (2013) carried out MCS to statistically calculate the transit time of contaminants through a simplified landfill model, while the uncertainty of input parameters was also simplified, and the calculation was under 1D transport assumptions. Mahjouri and Shamsoddinpour (2016) introduced an advanced method for early leakage detection at landfill sites using fuzzy transformation techniques and probabilistic artificial neural networks. This method optimally determines monitoring well placements by addressing uncertainties with fuzzy set theory. Mishra et al. (2017) evaluated the health risk of heavy metals from Navi Mumbai's Turbhe landfill by using LandSim 2.5 to simulate the fate and transport of heavy metals and a MCS framework to consider the uncertainties, followed by univariate and multivariate sensitivity analyses. Santhosh et al. (2017) presented a reliability-based method to predict leachate head in MSWLs using the Hydrologic Evaluation of Landfill Performance (HELP) model. It focused on the effects of uncertainties in the hydraulic properties of layers and defects and the placement

conditions of GMB. Zhan et al. (2017) conducted a failure probability assessment based on the transit time of the target contaminant through CCL using MCS. Parameter sensitivity analysis showed that the uncertainties in adsorption parameters, longitudinal dispersivity, and hydraulic conductivity have the most significant effects on failure probability. Zhan et al. (2018) developed an algorithm for hydraulic connectivity analysis and evaluated leakage rates through composite liners in landfills, considering random hole distributions in a GMB wrinkle network and their impact on liner integrity, which offers improved predictions of leakage probabilities. Yin et al. (2018) modelled the transport of 12 organic compounds through five different reactive media under diffusion and advection using deterministic and MCS to evaluate their effectiveness for sediment capping and liners. Chaudhary et al. (2024) analysed sustainable landfill liners made from local soils and wastes mixed with bentonite, assessing how stochastic variations in hydraulic conductivity affect performance. The performance was evaluated by conducting a series of numerical experiments in HYDRUS 2D/3D in terms of breakthrough time, peak concentration, and solute mass distribution in the liner. Yu and Zhao (2024) examined the performance of CCL in MSWLs using both deterministic and probabilistic approaches, using the time when the contaminant concentration in the aquifer exceeds the acceptable level as the index.

2.4.3 Polynomial chaos expansion and its application in solute transport analysis

As presented above, the classical Monte Carlo simulation (MCS) method is commonly used to incorporate uncertainty due to its robustness and conceptual simplicity. However, MCS is usually computationally expensive since its accuracy depends on the number of realizations used. To enhance the efficiency, meta-modelling (surrogate modelling) approaches were developed to build data-driven, physics-free, and computationally cheap approximations of the original model response (Rajabi et al., 2015a; Razavi et al., 2012), reducing the computational cost of MCS by several orders of magnitude (Jin et al., 2001). Polynomial chaos expansions (PCE) are a powerful meta-modelling approach providing a functional approximation based on a suitably built orthonormal polynomial basis (Marelli et al., 2024a), which was originally introduced by Wiener (1938). PCE has been extended to the generalized polynomial chaos (gPC) (Xiu and Karniadakis, 2002; Wan and Karniadakis, 2006) and the arbitrary polynomial chaos (aPC) (Oladyshkin and Nowak, 2012) to handle more varied types of data distribution. Another advantage of PCE is that it allows an easy realization of

global sensitivity analysis (GSA). GSA aims to quantify the relative contribution of the variability of each input variable or combinations thereof to the variability of the model response (Marelli et al., 2024b). Various approaches have been proposed to perform GSA, such as derivative-based, variance-based, regression-based, and moment-independent techniques (Bianchi Janetti et al., 2019; Iooss and Lemaitre, 2015). Within variance-based GSA, which treats variance as the sole metric to quantify the contribution, the Sobol' indices are commonly used as sensitivity metrics (Sobol', 1993), because they do not need to assume monotonicity or linearity in the adopted interpretive model (Ciriello et al., 2013). The Sobol' indices are traditionally estimated by MCS (Sobol', 2001), and hence at high computational cost. To overcome this difficulty, Sudret (2008) presented a method of calculating Sobol' indices from coefficients of the PCE surrogate model without substantial extra computational effort.

The application of PCE to solute transport problems with uncertainty has seen certain developments over the past two decades, most of which involve GSA to explore the relative contributions in uncertainty propagation. Some early works validated the feasibility and efficiency of PCE in approximating stochastic water flow and solute transport equations. Xiu and Karniadakis (2003) presented the application of generalized polynomial chaos (gPC) to two incompressible flow simulations, and the efficiency and convergence were examined by comparison with MCS. Then gPC was further developed to deal with stochastic differential equations including the advection–diffusion equation (Wan and Karniadakis, 2005). Lin and Tartakovsky (2010) used a probabilistic collocation method (PCM) approach, which is an extension of PCE with a collocation projection, to solve three-dimensional (3D) stochastic flow and transport equations.

To investigate the sensitivity of outputs of interest to multiple input uncertainties, the variance-based GSA using Sobol' indices, which is in conjunction with PCE, is widely used in coupled water flow and contaminant transport problems. This framework has been adopted in various scenarios with uncertainty, including nonreactive transport experiments in laboratory-scale porous media (Fajraoui et al., 2011), the radionuclide transport in a randomly heterogeneous aquifer (Ciriello et al., 2013), the radionuclide migration in near surface disposal facilities (NSDFs) (Geetha Manjari and Sivakumar Babu, 2018), the seawater intrusion (SWI) simulation for a fractured coastal aquifer (Koohbor et al., 2019), semi-analytical solutions for the first two moments of solute

discharge in groundwater (Ciriello and De Barros, 2020), the groundwater nitrate response to uncertainties including climate change in an Italian groundwater body (Focaccia et al., 2021), and the reactive transport in fractured porous media using a mixed-dimensional approximation (Botti et al., 2023). In addition, Rajabi et al. (2015b) conducted uncertainty analysis within SWI simulations for a real-world aquifer by estimating moment-independent sensitivity indices. The basic information of the above PCE applications is summarized in Table 2.6. It is clear from the table that PCE models have never been verified and employed to address contaminant transport problems either with more than six uncertain inputs or in landfill contexts with composite liners.

Table 2.6. PCE applications in probabilistic analysis of solute transport

Reference	Studied context	Number of Uncertain Parameters	Spatial dimension	GSA index
Lin and Tartakovsky (2010)	flow and transport in a 3D randomly heterogeneous porous cubic domain	1	3D	-
Fajraoui et al. (2011)	nonreactive transport experiments in laboratory-scale porous media	4	2D	Sobol' indices
Ciriello et al. (2013)	radionuclide transport in a randomly heterogeneous aquifer	3	2D	Sobol' indices
Geetha Manjari and Sivakumar Babu (2018)	radionuclide migration in near surface disposal facilities	5	3D	Sobol' indices
Koohbor et al. (2019)	seawater intrusion in a fractured coastal aquifer	5	2D	Sobol' indices
Ciriello and De Barros (2020)	solute discharge through a control plane	3	2D	Sobol' indices
Focaccia et al. (2021)	groundwater nitrate response to uncertainties including climate change in an Italian groundwater body	5	3D	Sobol' indices
Botti et al. (2023)	reactive transport in fractured porous media	3	2D	Sobol' indices
Rajabi et al. (2015b)	seawater intrusion in a real-world aquifer: the Henry problem & the small island problem	2, 6	2D, 3D	Moment-independent indices

2.5 Summary

The environmental persistence, mobility, and toxicity of PFAS, particularly PFOS, are cause for concern regarding their widespread occurrence in landfills and surrounding environments. Engineered barriers, widely adopted in modern landfills, rely on composite liner systems to prevent or mitigate PFAS migration into groundwater. This chapter has provided a comprehensive review of existing studies relevant to PFAS fate in landfill-related contexts, including the occurrence and environmental behaviour of PFAS in landfills, a survey of available data related to liner components, and numerical modelling strategies, both deterministic and probabilistic.

Some studies have investigated the occurrence and general behaviour of PFAS in landfills, as well as material properties related to PFAS fate in liner systems. While such studies provide valuable insights into PFAS mobility and persistence, the availability and consistency of transport-relevant parameter data, such as hydraulic conductivities, diffusion coefficients, sorption coefficients, and interface transmissivity, remain limited, particularly in the case of PFOS. These limitations hinder the reliability of subsequent modelling efforts and contamination assessments and necessitate a probabilistic approach to better quantify inherent uncertainty.

In parallel, significant advances have been made in the development of analytical and numerical methods for modelling contaminant transport in porous media. In particular, several numerical solvers have been developed to capture the complexities of contaminant transport in liner systems. On the other hand, other than the work reported in this thesis, only two attempts have been made to model PFAS transport in liner systems. Both of these attempts are deterministic in nature, which further highlights the need for probabilistic analysis that takes into account different liner designs, quality of construction and monitoring, inherent uncertainties in material properties, and variabilities of environmental conditions encountered across diverse landfill contexts.

Probabilistic methods have been increasingly applied in environmental modelling, including in landfill contexts, mostly through Monte Carlo simulations (MCS). Surrogate modelling techniques such as Polynomial Chaos Expansion (PCE) have also been occasionally employed to enhance computational efficiency. However, no prior study has applied PCE to probabilistic modelling of contaminant transport problems with high-dimensional uncertainty (e.g., involving more than six uncertain parameters),

as is required when modelling PFOS migration through composite liners, attempted in this thesis.

This thesis hence addresses the above gaps by pursuing the objectives outlined in Chapter 1. The methodology adopted to fulfil these objectives is presented in the next chapter.

Chapter 3
Methodology

3.1 Introduction

The goal of this thesis is to conduct a probabilistic analysis of PFOS transport in liner systems (GCL, CCL and NCL). This is achieved in multiple steps (see Figure 3.1):

1) build numerical model of liner systems including means and probability distributions of input variables under three different scenarios of construction quality.
2) conduct deterministic analyses, using mean values of input variables, as a reference against which probabilistic results can be assessed.
3) develop a surrogate modelling technique for the simulation model, based on PCE, to enhance the computational performance of Monte Carlo simulations.
4) Conduct PCE-enhanced MCS to develop probabilistic assessment of risk to groundwater from PFOS in landfill waste.

In this chapter, a detailed description of the overall methodology is presented, including the underlying theory of water flow and contaminant transport in porous media, details of the simulation models and software used, and the development and implementation of deterministic and probabilistic analyses, including PCE surrogate models. Finally, in the last section of this chapter, assumptions and validity of the theory and models used in this thesis, as well as different forms of validation of these models, are discussed.

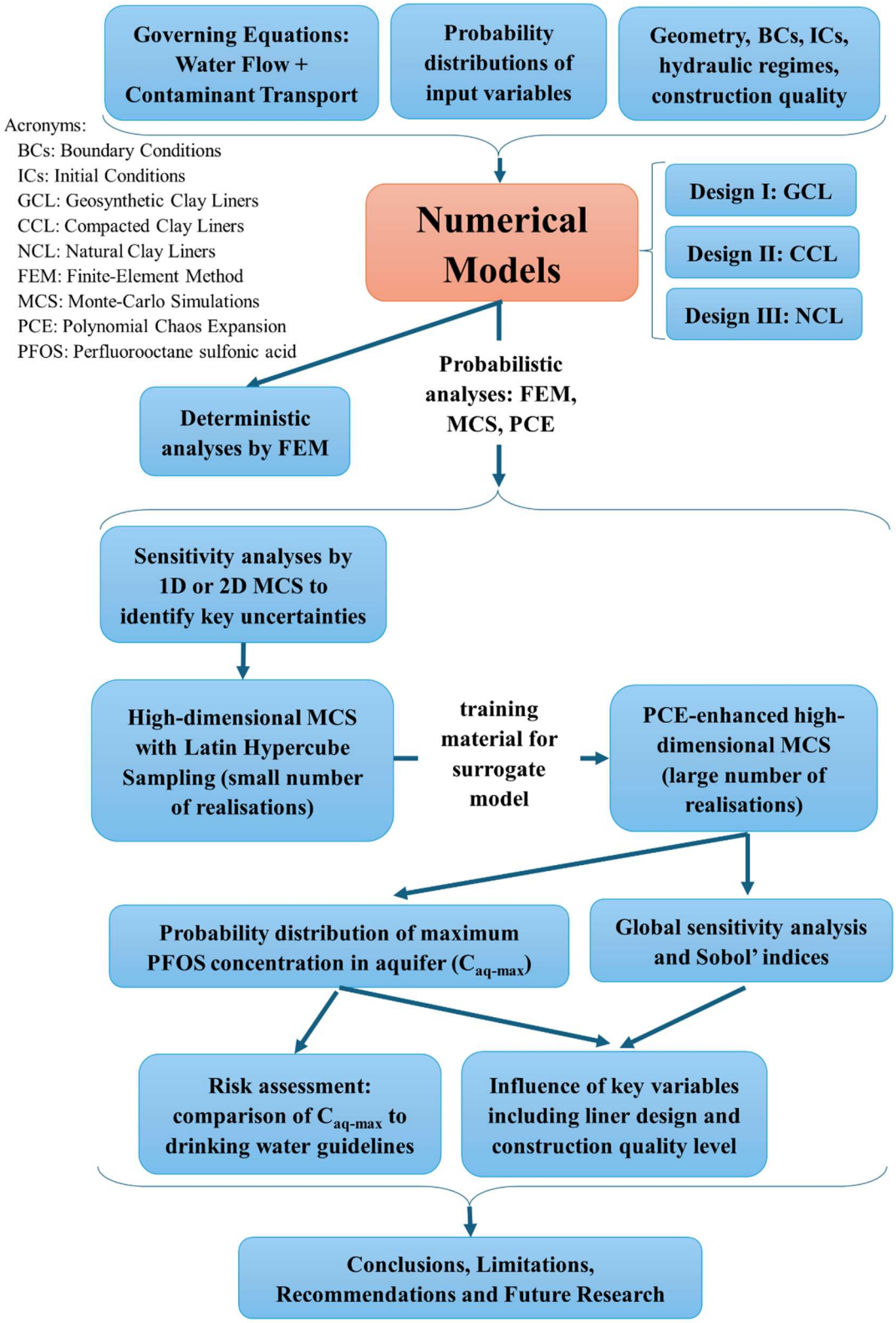

Figure 3.1. Overall Research Design ('high-dimensional' and '1D or 2D' refer to the number of parameters that are treated as uncertain in probabilistic analyses, and not to spatial dimension; all core numerical analyses in this thesis are conducted in two spatial dimensions)

3.2 Transport of PFOS in Porous Media: Governing Equations

As noted in Chapter 2, the theoretical framework employed in this study for simulating PFOS transport through landfill liner systems is well established and grounded in the continuum principles of soil hydromechanics. The coupled governing equations, i.e., the water flow equation (WFE) and the reaction diffusion-advection equation (RDAE), have been validated across various scenarios, including subsurface pollution (Kia, 1991; Dhanraj and Ganesha, 2023), nuclear waste repositories (Kelkar et al., 2010), and landfill leachate transport (Praveen Kumar and Dodagoudar, 2010; Markhali and Ehteshami, 2016; Srivastava and Ramanathan, 2018; Divya et al., 2020). These equations have been presented in studies by Rowe and Booker (1985), El-Zein and Rowe (2008), and El-Zein and Balaam (2012).

In this thesis, a specific version of the equations is employed to generate assessments of risk to groundwater beneath PFOS-containing landfills, i.e., WFE denotes the saturated, steady-state water flow equation, under Darcian flow regimes, and the RDAE denotes the time-dependent version of the equation under saturated conditions of non-deformable porous media. While the topmost parts of the clay liners may sometimes be partially saturated, assumption of full saturation captures a worst-case scenario while reducing the complexities and non-linearities of the equations, an important consideration especially in the context of numerically intensive probabilistic simulations. The assumption of steady-state water flow is also justified on account of the long-time scale (decades to centuries) over which aquifer contamination typically develops beneath landfills, with usually little long-term effect from transient (diurnal or seasonal) hydrological processes. A summary of the adopted version of equations is reproduced herein.

3.2.1 Water flow and migration of non-reactive contaminants in liner systems: reactive diffusion-advection equation

The following assumptions are made:

1) All parts of the porous medium are saturated, and the problem is two-phase: water and soil particle,
2) The flow is laminar, and a linear version of Darcy's law applies (hydraulic conductivity is independent of water pressure),

3) The porous medium is incompressible and isothermal,

4) Molecular diffusion and mechanical dispersion can be described by a Fickian process.

In addition, in the case of PFOS transport in liner systems and underlying soil, it can be conservatively assumed that:

1) Given the dimensions of liner systems and provided region of interest is away from the landfill's slopes, flow and contaminant transport through liner systems can be reduced from 3D to 2D space.

2) Hydraulic equilibrium is reached much faster (hours to weeks) than solute equilibrium (decades and centuries) and flow is hence approximated by its steady-state version,

3) Sorption and biological decay are negligible, and contaminant transport is hence non-reactive (i.e., mass balance of PFOS is retained in the liquid phase).

Based on the above assumptions, momentum- and mass-conservation principles can be applied at a representative volume element (RVE) scale, to derive the following partial differential equations:

$$v_x = -\frac{k_x}{n}\frac{\partial H}{\partial x} \tag{3.2.1}$$

$$v_y = -\frac{k_y}{n}\frac{\partial H}{\partial y} \tag{3.2.2}$$

$$\frac{\partial}{\partial x}\left(k_x \frac{\partial H}{\partial x}\right) + \frac{\partial}{\partial y}\left(k_y \frac{\partial H}{\partial y}\right) = 0 \tag{3.2.3}$$

$$f_x = -nD_{xx}\frac{\partial c}{\partial x} + nv_x c \tag{3.2.4}$$

$$f_y = -nD_{yy}\frac{\partial c}{\partial y} + nv_y c \tag{3.2.5}$$

$$\frac{\partial}{\partial x}\left(D_{xx}\frac{\partial c}{\partial x}\right) + \frac{\partial}{\partial y}\left(D_{yy}\frac{\partial c}{\partial y}\right) - v_x\frac{\partial c}{\partial x} - v_y\frac{\partial c}{\partial y} = \frac{\partial c}{\partial t} \tag{3.2.6}$$

where x [L] and y [L] are Cartesian coordinates,

H(x,y) [L] is the total hydraulic head,

n [$L^3.L^{-3}$] is the porosity of porous medium,

k_x [$L.T^{-1}$] and k_y [$L.T^{-1}$] are the coefficients of saturated hydraulic conductivity in the x and y direction, respectively,

v_x [$L.T^{-1}$] and v_y [$L.T^{-1}$] are the x and y components of the seepage velocity vector,

t [T] is time,

C(x,y,t) [$M.L^{-3}$] is the concentration of PFOS dissolved in pore water,

D_{xx} [$L^2.T^{-1}$] and D_{yy} [$L^2.T^{-1}$] are the coefficients of hydrodynamic dispersion in the x and y directions, which incorporate both molecular diffusion and mechanical dispersion,

f_x [$M.L^{-2}.T^{-1}$] and f_y [$M.L^{-2}.T^{-1}$] are the x and y components of the mass flux of PFOS through the porous medium.

The coefficients of hydrodynamic dispersion account for both molecular diffusion and mechanical dispersion and are calculated from the following equations:

$$D_{xx} = D + \alpha_L \frac{v_x^2}{v} + \alpha_T \frac{v_y^2}{v} \quad (3.2.7)$$

$$D_{yy} = D + \alpha_T \frac{v_x^2}{v} + \alpha_L \frac{v_y^2}{v} \quad (3.2.8)$$

where D [$L^2.T^{-1}$] is the molecular diffusion coefficient,

α_L [L] and α_T [L] are the longitudinal dispersivity and the transverse dispersivity,

$v = \sqrt{v_x^2 + v_y^2}$ [$L.T^{-1}$] is the magnitude of seepage velocity.

Note that the cross-terms of hydrodynamic dispersion, corresponding to coefficients D_{xy} and D_{yx}, have been omitted from Eq. (3.2.6) for simplicity.

Eq. (3.2.3) is the steady-state version of the flow equation which, when combined with Darcy's law (Eqs. (3.2.1) and (3.2.2)) and a suitable set of boundary conditions, can be used to calculate the seepage velocity field in the porous medium. Eqs. (3.2.4) and (3.2.5) are expressions of contaminant flux based on Fickian diffusion/dispersion and advective transport. Finally, Eq. (3.2.6) is a 2D version of the non-reactive diffusion-advection equation (DAE) which, when combined with Eqs. (3.2.1) -(3.2.5) and a suitable set of boundary and initial conditions (BCs and ICs), can be used to estimate contaminant concentrations and fluxes in the porous medium. The following equation, applied at each boundary point b, is used in solving the flow equations:

$$a_1 H_b + b_1 v_{nb} = g_1 \quad (3.2.9)$$

where H_b [L] is the total hydraulic head at the boundary, v_{nb} [$L.T^{-1}$] is the component of the seepage velocity normal to the boundary, and a_1, b_1 and g_1 are known BC parameters. Eq. (3.2.9) can represent both Dirichlet (b_1=0) and Neumann (a_1=0) hydraulic BCs. For the contaminant transport problem, a similar equation is used:

$$a_2 C_b + b_2 f_{nb} = g_2 \qquad (3.2.10)$$

where C_b [$M.L^{-3}$] is the PFOS concentration at the boundary, f_{nb} [$M.L^{-2}.T^{-1}$] is the PFOS flux normal to the boundary, and a_2, b_2 and g_2 are known BC parameters. Similarly to hydraulic BCs (3.2.9), Eq. (3.2.10) can represent both Dirichlet (b_2=0) and Neumann (a_2=0) hydraulic BCs. In addition, a mass-conserving BC is used to capture time-changing concentration of PFOS in the landfill leachate:

$$C_b = C_{b0} - \frac{1}{H_f}\int_0^t f_{nb}\, d\tau - \frac{q_c}{H_f}\int_0^t C_b\, d\tau \qquad (3.2.11)$$

where C_{b0} [$M.L^{-3}$] is the initial PFOS concentration at the boundary, H_f [L] is the equivalent height of leachate, q_c [$L^3.L^{-2}.T^{-1}$] is the leachate collection rate per unit area of landfill by the drainage system, and t [T] is a time integration variable. The following equation can be used to evaluate H_f:

$$H_f = \frac{d_s p_0}{C_{b0}} \qquad (3.2.12)$$

where d_s [$M.L^{-2}$] is the mass of waste per unit area and p_0 [$M.M^{-1}$] is the PFOS content of the waste.

3.2.2 Special treatment of geomembrane and leakage

While Eqs. (3.2.1) to (3.2.12) are used to describe water flow and transport in all layers of the models, additional treatment is required to better capture conditions in the geomembrane (GMB), in two ways. First, sorption of contaminants in GMB has been shown to be best described as a process of partitioning occurring at the top and bottom surfaces of the GMB, using the following equations:

$$C_{waste} = S_g C_{GMB-} \qquad (3.2.13)$$

$$C_{soil} = S_g C_{GMB-bs} \qquad (3.2.14)$$

where C_{waste} [$M.L^{-3}$] is the PFOS concentration in the leachate in contact with the top surface of the GMB, C_{soil} [$M.L^{-3}$] is the PFOS concentration in the layer below the GMB and in contact with its bottom surface, $C_{GMB\text{-}ts}$ [$M.L^{-3}$] and $C_{GMB\text{-}bs}$ [$M.L^{-3}$] are the PFOS

concentrations at the topmost and lowermost points in the GMB, respectively, and S_g is a partitioning coefficient.

Second, extensive evidence exists that leakage through liner systems often occurs because of the formation of wrinkles on the GMBs which makes them more susceptible to damage and puncturing (Rowe, 2012). Leakage through holed wrinkles can be reduced by improved quality of construction and monitoring but is very difficult to prevent completely (Giroud, 2016) and hence needs to be accounted for in any realistic assessment of the performance of the system.

Research has also shown that extent of leakage depends on several factors, including the length of holed wrinkles per surface area of landfill L_w [$L.L^{-2}$], the shape and size 2b [L] of each hole, and the hydraulic conductivity of the part of the GCL below the wrinkle k_b [$L.T^{-1}$] (Rowe, 1998).

In addition, the quality of contact between the GMB and underlying GCL has been shown to be a significant factor (Rowe et al., 2004). This effect can be captured by including a transmissive layer (TL) between the GMB and GCL in the simulation model (El-Zein and Rowe, 2008) whereby:

$$k_{xTL} = \frac{\theta_{xTL}}{d_{TL}} \qquad (3.2.15)$$

where d_{TL} [L] is the thickness of the TL, k_{xTL} [$L.T^{-1}$] is the x component of the hydraulic conductivity of the TL and θ_{xTL} [$L^2.T^{-1}$] is the transmissivity of the TL in the x direction. It has been shown previously that simulation results are insensitive to d_{TL}, provided it is at least one order of magnitude smaller than the thickness of GMB (El-Zein and Rowe, 2008).

Finally, a useful indicator of extent of leakage is the leakage rate q_a, defined as the vertical seepage at the base of the clay liner, averaged over its length (L [L]) and expressed by:

$$q_a = \frac{1}{L}\int_0^L n v_y \, dx \qquad (3.2.16)$$

3.3 Models of Liner Systems

3.3.1 Overview

In this section, various aspects of the models of different liner systems built for this thesis are presented, including geometry and design configurations, boundary and initial conditions for flow and contaminant transport equations, simulation of the effect of leachate drainage system in the landfill, treatment of hydraulic flow and mass transport associated with leaks, hydraulic regime in the aquifer, and simulation of the effect of construction quality.

3.3.2 Liner design configurations

This typical design of SCLS contains four core components separating the solid waste from the aquifer: a synthetic or soil-based leachate drainage system, a GMB, a GCL or CCL, and an additional buffer zone of onsite soil, or attenuation layer (AL). In some cases, natural clay is present onsite and can be used as both a clay liner and an attenuation layer. Hence, three different design configurations of SCLSs, commonly encountered in MSWLs, are investigated in this study to evaluate their abilities to mitigate the risk of PFOS contamination in underlying aquifers. All three designs include a 1.5mm-thick GMB at the top of the liner. As shown in Figure 3.2, the first two designs include a GCL and a CCL, respectively, below the GMB, all sitting above an AL. In the third design, also shown in Figure 3.2, a natural clay layer (NCL) separates the GMB from the aquifer. Hence, models of the 3 designs include the following layers, ordered from top to bottom:

a) Design I: GMB+GCL+AL+AQ
b) Design II: GMB+CCL+AL+AQ and
c) Design III: GMB+NCL+AQ.

Note that, while the thickness of the GCL (Design I) is usually known with reasonable certainty (6~10mm & set as 7mm herein), there is far more variability in the thickness of the CCL (Design II) and NCL (Design III) and hence these will be captured with probability distributions. In addition, the average levels of total thickness of GCL+AL and CCL+AL are assumed to be similar, and the average level of the thickness of NCL is larger. In the remainder of this thesis, the above three designs (a, b, and c) will be referred to as Design I, Design II, and Design III, or equivalently as “GCL+AL”, “CCL+AL”, and “NCL”, respectively.

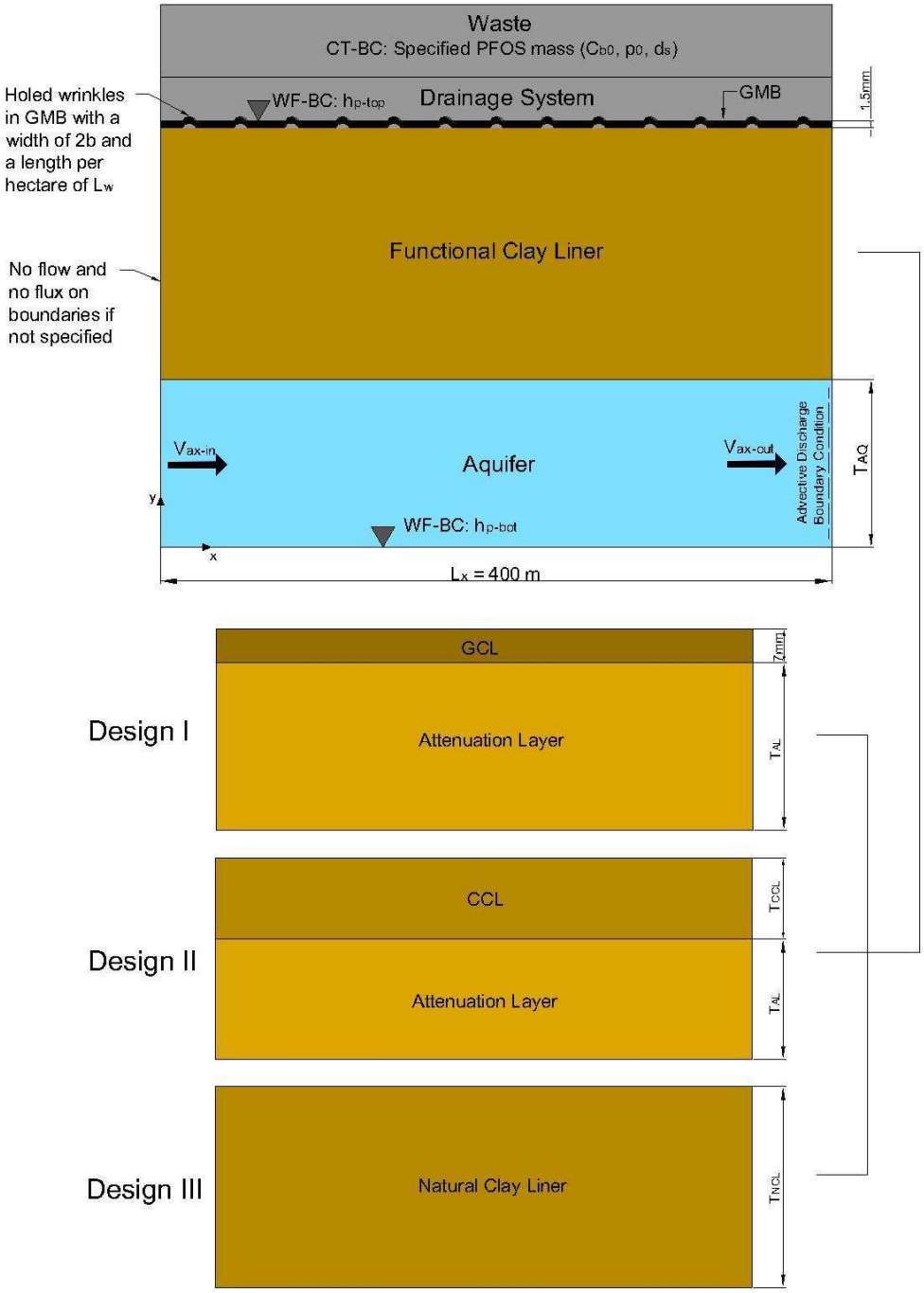

Figure 3.2. Model dimensions and boundary conditions for RSc for the 3 designs (100 m in the z direction; WF-BC: water flow boundary condition; CT-BC: contaminant transport boundary condition; not to scale).

3.3.3 Boundary and initial conditions

Hydraulic Boundary Conditions

The pressure head on top of the liner is specified as $h_{p\text{-}top}$=0.3m, which is a maximum pressure head legally required in many parts of the world and is usually achieved

through a leachate drainage system (Rowe, 1998; 2020b). In this thesis, $h_{p\text{-}top}$ is considered as a known constant with no uncertainty associated with it. Bernoulli equation can be used to derive an estimate of the pressure head at the base of the aquifer, $h_{p\text{-}bot}$ [L]. Taking the datum to be at the bottom of the aquifer, Bernoulli equation can be written at the top of the GMB and the bottom of the AQ as follows:

$$H_{bot}=h_{p\text{-}bot} \tag{3.3.1}$$

$$H_{top}=h_{p\text{-}top}+T_{AQ}+T_{CLAL}+T_{GMB} \tag{3.3.2}$$

where H_{bot} [L] and H_{top} [L] are the total hydraulic head at the bottom of the aquifer and the top of the GMB, respectively, T_{AQ} [L] and T_{GMB} [L] are the thicknesses of the aquifer and the GMB, and T_{CLAL} [L] is the total thickness of the clay and attenuation layer. Hence, in Design I, $T_{CLAL}=T_{GCL}+T_{AL}$. In Design II, $T_{CLAL}=T_{CCL}+T_{AL}$ and in Design III, $T_{CLAL}=T_{NCL}$. The difference between total hydraulic heads ΔH [L] can be calculated from Eqs. (3.3.1) and (3.3.2):

$$\Delta H = H_{top}-H_{bot} = h_{p\text{-}top} + T_{AQ} + T_{CLAL} + T_{GMB} - h_{p\text{-}bot} \tag{3.3.3}$$

Rearranging:

$$h_{p\text{-}bot} = h_{p\text{-}top} + T_{AQ} + T_{CLAL} + T_{GMB} - \Delta H \tag{3.3.4}$$

While $h_{p\text{-}top}$ and T_{GMB} are assumed to be known constants, variability of the other items on the right-hand side of Eq. (3.3.4) will be captured by probability distributions as discussed in Chapter 4. Finally, all other hydraulic BCs are no flow.

Mass Transport Boundary and Initial Conditions

The PFOS pollution load in the leachate is represented by a specified-mass boundary condition on top of the GMB and the drainage system as described by Eqs. (3.2.11) and (3.2.12). This type of BC takes into account the initial concentration of PFOS in the leachate C_{b0} [$M.L^{-3}$], the mass of PFOS per mass of waste accepted into the landfill p_0 [$M.M^{-1}$], and the mass of waste per surface area in landfill d_s [$M.L^{-2}$]. A conservative assumption is made that the full PFOS pollution load is available from t=0, i.e., from the time the landfill starts receiving waste. An additional factor that needs to be considered is the leachate drainage system that removes leachate indefinitely from the waste at a rate of q_c [$L^3.L^{-2}.T^{-1}$] and typically transports it to a wastewater treatment plant. As a result, the PFOS mass present in the removed leachate is no longer part of the pollutant load. This is reflected by the third term on the right-hand side of Eq.

(3.2.11). q_c can be calculated as the difference between the rate of percolation into the landfill q_0 [$L^3.L^{-2}.T^{-1}$] and the rate of leakage through the defects in the GMB q_a [$L^3.L^{-2}.T^{-1}$]. q_a is estimated from the solution to the flow equation. A value of q_0=0.15 m/year is adopted based on regulatory minimum permitted (MoE, 2011).

At the downstream end of the aquifer, it is assumed conservatively that PFOS leaves the vertical boundary by advection alone (advective discharge BC). All other contaminant transport BCs are assumed to be zero-flux. Finally, a zero initial PFOS concentration is assumed to prevail everywhere except in the waste.

3.3.4 Hydraulic regimes in aquifer and leaking GMB

Hydraulic Regime in Aquifer

To capture the hydraulic regime in the aquifer, the entire watershed would normally need to be simulated requiring a much larger simulation domain, which would add significant computational cost. To avoid this, a seepage velocity in the aquifer is directly specified, allowing the simulation domain to be restricted to the aquifer immediately below the landfill, as seen in Figure 3.2 (El-Zein and Rowe, 2008). The specified horizontal seepage velocity is taken based on the average of the inflow Darcy velocity $V_{ax\text{-}in}$, upstream of the aquifer, which is specified as a probability distribution, and the outflow Darcy velocity $V_{ax\text{-}out}$, downstream of the aquifer, which can be obtained based on hydraulic mass conservation.

Hydraulic Regime in Leaking GMB

As discussed in 3.2.2, leakage through the GMB is an important, and largely unavoidable, process affecting environmental outcomes in liner systems. This process is taken explicitly into account in this thesis by introducing into the model a set of leaks (holed wrinkles) in the GMB. In past work on leakage in liner systems, three key factors have been shown to influence the leakage rate, namely number of leaking wrinkles per surface area, width of holes in the wrinkles 2b [L] and horizontal hydraulic transmissivity θ [$L^2.T^{-1}$] at the interface between the GMB and underlying clay layer (GCL, CCL or NCL) (Rowe, 2012; Zhan et al., 2018; Rowe and AbdelRazek, 2019). The latter is a reflection of the quality of contact between the GMB and underlying layer, whereby poor contact creates more space for the leachate to spread horizontally, come into contact with the underlying clay layer, and yield higher leakage rates.

Under assumptions of 2D transport, each wrinkle is assumed to extend across the full length of the third dimension, i.e., axis z normal to the page in Figure 3.2, and density of wrinkles can hence be expressed as length of wrinkles per surface area L_w [$L.L^{-2}$]. For example, assuming a landfill width of 100m along the z direction, the 13 defects shown in Figure 3.2 represent a wrinkle length of 1300 m over an area of 4 hectares (400m×100m), i.e., L_w of 325 m/ha. Therefore, the three parameters needed to estimate the seepage velocity field, and leakage rates, caused by defects in the GMB are L_w, 2b and θ. All of these parameters are treated as probability distributions in the probabilistic analyses in this thesis.

3.3.5 Effects of variable construction quality

Of all the variables affecting leakage rate, L_w is most susceptible to improvement via construction quality assurance (CQA) and the use of electrical leak location (ELL) technologies (Gilson-Beck, 2019). Hence, four scenarios are considered:

1) Theoretical reference scenario (RSc0): no leakage.
2) Scenario with lower CQA (Sc-): good CQA but no ELL
3) Reference Scenario (RSc): good CQA with ELL.
4) Scenario with higher CQA (Sc+): excellent CQA with ELL.

Under RSc0, the GMB is assumed to be free of defects and no leakage occurs. In this case, advective transport is expected to be negligible and PFOS transport through the liner is essentially by molecular diffusion alone. This case is extremely unlikely to occur, but it is of theoretical interest because, by comparing its results with those of other scenarios, especially RSc, insights can be gained into the contribution of leakage, relative to diffusion, to the overall mobility of PFOS. On the other hand, differences in maximum PFOS concentration in the aquifer between Sc-, RSc and Sc+ will provide insights into the extent to which construction quality and ELL can mitigate risk of PFOS contamination. L_w is assumed to be the only parameter affected by improvements in CQA+ELL, with different L_w probability distributions used to simulate different scenarios for any given liner design. In deterministic analyses, all four scenarios are considered for each of the three liner systems. However, in probabilistic analyses, only the three scenarios of RSc, Sc- and Sc+ are simulated for all three liner systems. The diffusion-only scenario (RSc0), given that it is of purely theoretical interest, is only simulated for the GCL-liner design.

3.3.6 Input variables

Table 3.1 shows a summary of all input variables required for modelling. It is clear from the above discussion that input parameters for the numerical models, including geometry, material properties, boundary and initial conditions, can be divided into two categories, depending on whether they are treated as a) known with reasonable certainty or b) uncertain and described with probability distributions. The choices made are also shown in Table 3.1. The rationale for including variables in one category or the other will be discussed in Chapter 4.

Note that the presence of wrinkles in the GMB has a well-known effect on the hydraulic conductivity of GCL, k_{GCL}, as follows (Rowe, 2020a). Under a wrinkle in the GMB, bentonite in the GCL is subject to lower overburden stress, and hence lower effective stress, than bentonite lying under, and in contact with, intact parts of the GMB. Consequently, a lower k_{GCL} is expected under the intact part of the GMB than under the wrinkles (Rowe, 1998; Rowe and Abdelrazek, 2019). The two variables, denoted by k_a and k_b, respectively, will be used in calculating the hydraulic regime in the liner system. Note that though distinct, k_a and k_b are related and the relationship between them will be discussed in Chapter 4 when developing probability distributions of variables. Note that no such effect is expected to be present in CCL (Design II) and NCL (Design III) because the difference in overburden pressure is not large enough to generate significant differences in hydraulic conductivity. Hence, only one hydraulic conductivity variable for the clay will be used in these cases.

3.3.7 Expected transport patterns

Based on the above and the BCs applied in the model, the overall outline of PFOS transport from the landfill leachate into the aquifer is expected to be as follows (see Figure 3.3):

1) through GMB:
    a) downwards by leakage through the damaged parts of the GMB and,
    b) simultaneously downward, by molecular diffusion through its intact part, into the GCL, then
2) through GCL/CCL+AL or NCL:
    a) further downwards by vertical diffusion and laterally by horizontal diffusion, and

b) further downwards by vertical advection into the aquifer, and

3) through AQ:

a) horizontally and vertically in the aquifer by mechanical dispersion,

b) horizontally along the aquifer's length in the direction of water flow by advection, and

c) exiting the downstream boundary of the aquifer (located under the edge of the landfill) by advection alone.

Table 3.1. Input Variables of Models (values and probability distributions of variables are provided and discussed in Chapter 4).

TYPE		VARIABLE	DESIGN	SYMBOL	UNITS	F or P*
Geometry		GMB thickness	All	T_{GMB}	m	F
		GCL thickness	I	T_{GCL}	m	F
		CCL thickness	II	T_{CCL}	m	P
		NCL thickness	III	T_{NCL}	m	P
		AL thickness	I & II	T_{AL}	m	P
		AQ thickness	All	T_{AQ}	m	P
		Landfill dimension in the x direction	All	L_x	m	F
		Landfill dimension in the z direction	All	L_z	m	F
Boundary and Initial Conditions	Hydraulic	Hydraulic pressure head on top of GMB	All	$h_{p\text{-}top}$	m	F
		Infiltration rate into the landfill	All	q_0	$m.year^{-1}$	F
		Difference in total hydraulic head between top of GMB and AQ	All	ΔH	m	P
		Density of wrinkles	All	L_w	$m.hectare^{-1}$	P
		Width of leak	All	2b	m	P
		Inward horizontal Darcy velocity in AQ	All	$V_{ax\text{-}in}$	$m.year^{-1}$	P
	Contaminant Transport	Mass of waste per surface area in landfill	All	d_s	$kg.m^{-2}$	F
		Initial PFOS content in waste	All	p_0	$ng.kg^{-1}$	P

		Initial PFOS concentration in leachate	All	C_{b0}	$ng.litre^{-1}$	P
Material Properties	Both	GCL porosity	I	n_{GCL}	1	F
		CCL porosity	II	n_{CCL}	1	F
		NCL porosity	III	n_{NCL}	1	F
		AL porosity	I & II	n_{AL}	1	F
		AQ porosity	All	n_{AQ}	1	F
		GCL dry density	I	ρ_{GCL}	$kg.m^{-3}$	F
		CCL dry density	II	ρ_{CCL}	$kg.m^{-3}$	F
		NCL dry density	III	ρ_{NCL}	$kg.m^{-3}$	F
		AL dry density	I & II	ρ_{AL}	$kg.m^{-3}$	F
		AQ dry density	All	ρ_{AQ}	$kg.m^{-3}$	F
	Hydraulic	GCL hydraulic conductivity in contact with GMB	I	k_a	$m.year^{-1}$	P
		GCL hydraulic conductivity below wrinkles	I	k_b	$m.year^{-1}$	P
		CCL hydraulic Conductivity	II	k_{CCL}	$m.year^{-1}$	P
		NCL hydraulic conductivity	III	k_{NCL}	$m.year^{-1}$	P
		AL hydraulic conductivity	I & II	k_{AL}	$m.sec^{-1}$	P
		AQ hydraulic conductivity	All	k_{AQ}	$m.sec^{-1}$	F
		GMB-GCL transmissivity	I	$\theta_{GMB-GCL}$	$m^2.year^{-1}$	P
		GMB-CCL transmissivity	II	$\theta_{GMB-CCL}$	$m^2.year^{-1}$	P
		GMB-NCL transmissivity	III	$\theta_{GMB-NCL}$	$m^2.year^{-1}$	P
	Contaminant Transport	GMB diffusion coefficient	All	D_g	$m^2.sec^{-1}$	F
		GMB partitioning coefficient	All	S_g	1	F
		GCL diffusion coefficient	I	D_{GCL}	$m^2.year^{-1}$	F
		CCL diffusion coefficient	II	D_{CCL}	$m^2.year^{-1}$	F
		NCL diffusion coefficient	III	D_{NCL}	$m^2.year^{-1}$	F
		AL diffusion coefficient	I & II	D_{AL}	$m^2.year^{-1}$	F

		AQ diffusion coefficient	All	D_{AQ}	$m^2.year^{-1}$	F
		Longitudinal dispersivity in GCL	I	$\alpha_{L\text{-}GCL}$	m	F
		Transverse dispersivity in GCL	I	$\alpha_{T\text{-}GCL}$	m	F
		Longitudinal dispersivity in CCL	II	$\alpha_{L\text{-}CCL}$	m	F
		Transverse dispersivity in CCL	II	$\alpha_{T\text{-}CCL}$	m	F
		Longitudinal dispersivity in NCL	III	$\alpha_{L\text{-}NCL}$	m	F
		Transverse dispersivity in NCL	III	$\alpha_{T\text{-}NCL}$	m	F
		Longitudinal dispersivity in AL	I & II	$\alpha_{L\text{-}AL}$	m	P
		Transverse dispersivity in AL	I & II	$\alpha_{T\text{-}AL}$	m	P
		Longitudinal dispersivity in AQ	All	$\alpha_{L\text{-}AQ}$	m	P
		Transverse dispersivity in AQ	All	$\alpha_{T\text{-}AQ}$	m	P
		Sorption coefficients of layers	All	K_d	$litre.kg^{-1}$	F
		Half-life of PFOS in layers	All	$t_{1/2}$	year	F

*****Is the variable assumed fixed (F) or probabilistic (P) in probabilistic analyses, i.e., is it described by a single value or a probability distribution function (PDF)? In deterministic analyses, the geometric mean of the PDF is used in simulations.

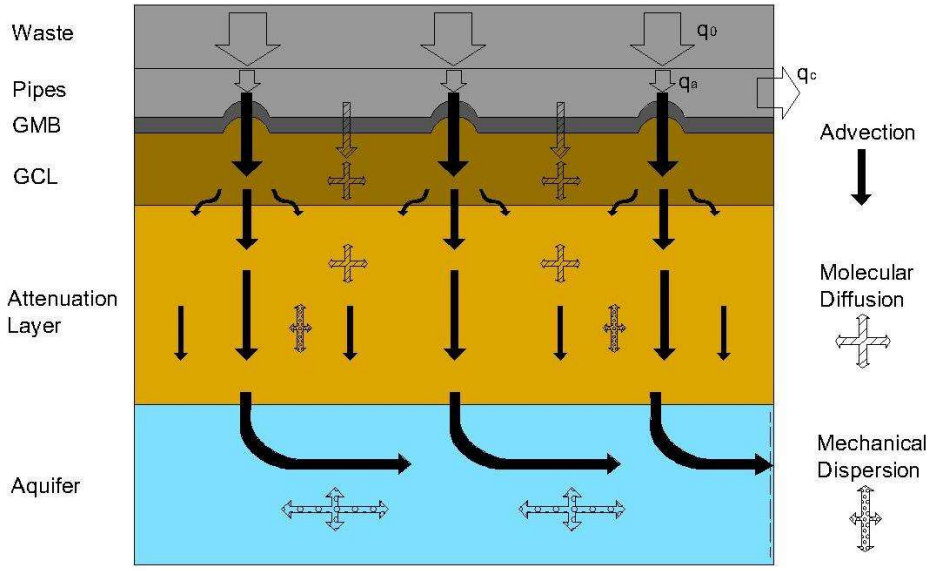

Figure 3.3. Expected transport patterns under landfill waste. Not to scale.

3.4 Deterministic Analyses

3.4.1 Overview

Deterministic analyses, although limited in scope because they do not consider uncertainty in data, are useful in providing an estimate of the average level of peak concentration, as well as a useful reference for interpretation of probabilistic results. In this section, the numerical method and software used to simulate the models described earlier are presented. In addition, two different approaches to the coupling of the water flow and contaminant transport parts of the model are presented, and the rationale for their use is also presented. Note that since the simulation of every single realisation in MCS is deterministic in nature, the information and discussion provided in this section also apply to the probabilistic analyses described in Sections 3.5 and 3.6.

3.4.2 SPAS/CONFEM software

Numerical simulations of PFOS transport through the liner system and into the aquifer for three designs in question shown in Figure 3.2 are conducted using the Soil Pollution Analysis System (SPAS) and its FEM engine CONFEM. SPAS/CONFEM was developed specifically for modelling landfill liner systems by El-Zein and Balaam (2012) by incorporating landfill liner features into its input and coding data structures. Over the past decade, it has been extensively validated (El-Zein and Balaam, 2012; El-

Zein et al., 2016; Hanna and El-Zein, 2023) and applied to various problems of organic and inorganic contaminant transport in liner systems (El-Zein and Rowe, 2008; El-Zein et al., 2012). Numerical validation of the software was performed by comparison to analytical, semi-analytical and numerical approaches, for both water-flow predictions including leakage rates and contaminant concentrations. Several key advantages of SPAS/CONFEM, compared to other FEM solvers of the WFE-RDAE, warrant its adoption in this thesis, including

a) its graphics user interface (pre- and post-processors) and data structures and automated features designed specifically for liner systems.
b) stream-lined and user-friendly ability to incorporate regularly spaced leaks in the GMB and explicitly simulate their effects on the hydraulic regime and pollution plume evolution, without the need for further simplifying assumptions usually required by analytical or semi-analytical approaches.
c) ability to incorporate, in addition to conventional Dirichlet and Neumann-type BC, a specified-mass BC (Eq. (3.2.11)) which also accounts for contaminant removal by the leachate drainage system; this BC is critical for accurate modelling of contaminants leaching from landfill waste.
d) optimised routines that achieve computationally efficient solutions, an important consideration in the context of this thesis because of the computational cost of probabilistic simulations.

CONFEM is based on a weighted-residual Galerkin formulation of the governing equations spatial discretization with linear, quadratic or exponential shape elements (El-Zein et al., 2005; El-Zein, 2005). For time discretization, two approaches are available: a time-marching scheme (TMFEM) and a Laplace transform scheme (LTFEM) (El-Zein and Booker, 1999; El-Zein et al., 2005). In this thesis, quadratic spatial discretization (8-noded rectangular elements) combined with LTFEM are employed due to their computational efficiency.

Under saturated conditions, SPAS/CONFEM contains two core solvers that can be used individually or in coupled mode: Water-Flow Solver (Poisson equation) and Contaminant-Transport solver (diffusion-advection equation). Coupling is discussed next.

3.4.3 Coupling of flow and transport equations: two approaches

In the most straightforward approach to solving the steady-state flow equation coupled with the reactive diffusion-advection equation, SPAS/CONFEM is used to run both simulations successively in fully automated mode (Approach 1), summarized in Figure 3.4(a). In this approach, hydraulic input data (see Table 3.1) are used by SPAS/CONFEM's Water-Flow Solver to solve the flow equation over the entire liner-system model (see Figure 3.2) and generate the total hydraulic head field H(x,y) and seepage velocity fields $v_x(x,y)$ and $v_y(x,y)$, as well as estimates of the leakage rate q_a. Next, contaminant transport input data (see Table 3.1), as well as calculated seepage velocities are used by the Contaminant-Transport Solver to generate PFOS concentration C(x,y,t) and fluxes $f_x(x,y,t)$ and $f_y(x,y,t)$. A post-processing search of C(x,y,t) can then be conducted next to identify the maximum concentration of PFOS anywhere in the aquifer at any time. This approach is highly streamlined and hence especially convenient for multiple simulations by MCS and PCE. However, it suffers from one drawback when applied to Designs II and III, as described next.

As mentioned earlier in this chapter, when leachate migrates through leaks in the GMB, it can spread laterally in the gap between the GMB and the underlying clay layer. The extent of spread, called wetted distance ($2a_0$), depends on the quality of contact between the GMB and underlying layer, which is captured by the interface transmissivity, also discussed earlier. As a result, leachate comes into direct contact with the clay, with no protection from the GMB, over the extent of the wetted distance. However, in the coupling approach (Approach 1) described above, while SPAS/CONFEM accurately calculates the leakage rate and seepage velocities around the leaks, it assumes, for the purpose of diffusion/advection, that the contaminant is in contact with the clay only over the width of leak (2b), not the wetted distance. Numerical tests conducted as part of the thesis showed that this assumption has small effect in Design I because the transmissivity of GMB-GCL is usually small enough for $2a_0$ to be only slightly larger than 2b. However, this is not necessarily the case with Designs II and III where both transmissivities and wetted distances are larger, compared to Design I. Hence, an alternative approach (Approach 2b) is used for all simulations for Designs II and III as follows (see Figure 3.4(b)).

First, the wetted distance $2a_0$ is calculated analytically using an analytical approximation developed by Rowe (1998):

$$a_0 = b - \frac{1}{\sqrt{\left[\frac{T_{CCL}+T_{AL}}{\theta(T_{CCL}+T_{AL})\left(\frac{T_{CCL}}{k_{CCL}}+\frac{T_{AL}}{k_{AL}}\right)}\right]}} \ln\left(\frac{T_{CCL}+T_{AL}+T_{AQ}-h_{p-bot}}{T_{CCL}+T_{AL}+T_{AQ}+h_{p-top}-h_{p-bot}}\right) \quad (3.4.1)$$

All definitions of variables appearing in Eq. (3.4.1) are given in Table 3.1. Note that the term within the natural logarithm (ln) bracket is always less than 1 and hence the second term on the right-hand side of the equation is always negative, which yields a_0>b, as expected. Note that the equation above is shown for Design II (CCL+AL); for Design III, simply replace T_{CCL} with T_{NCL} and k_{CCL} with k_{NCL} while setting T_{AL} to zero. (A fuller description of the Rowe equations is given in Appendix 3.1.)

Second, CONFEM Water-Flow Solver is run to generate an estimate of the overall leakage rate q_a.

Finally, the Contaminant-Transport Solver is run separately under the following conditions:

a) leaks are specified as $2a_0$ in width, hence ensuring contact with the underlying clay over the entire width of the wetted distance.
b) the seepage velocity is directly input into the solver under the leaks in CCL/NCL and AL, as an idealised step-function that recovers the overall leakage rate q_a calculated by the Water-Flow Solver (see Figure 3.5).

While the idealisation described in b) will incur some inaccuracy, numerical tests comparing predictions from the two approaches, as well as predictions of CONFEM to those of finite-layer software POLLUTE v7 (Rowe and Booker, 2004), widely used for landfill contamination problems (Rowe and Abdelrazek, 2019; Rowe and Barakat, 2021), have confirmed the viability of this approach (see Section 5.1). Note that during the finalisation of the framework for Approach 2b, an intermediate version (Approach 2a) was developed. Its only difference from Approach 2b lies in the calculation of q_a, which is based on the Rowe equation (Eq. (A3.1.1)) rather than the CONFEM Water-Flow Solver. Since, ultimately, Approach 2a has not been adopted, it is not further elaborated here. It will, however, be revisited in the comparative analysis in Section 5.1.

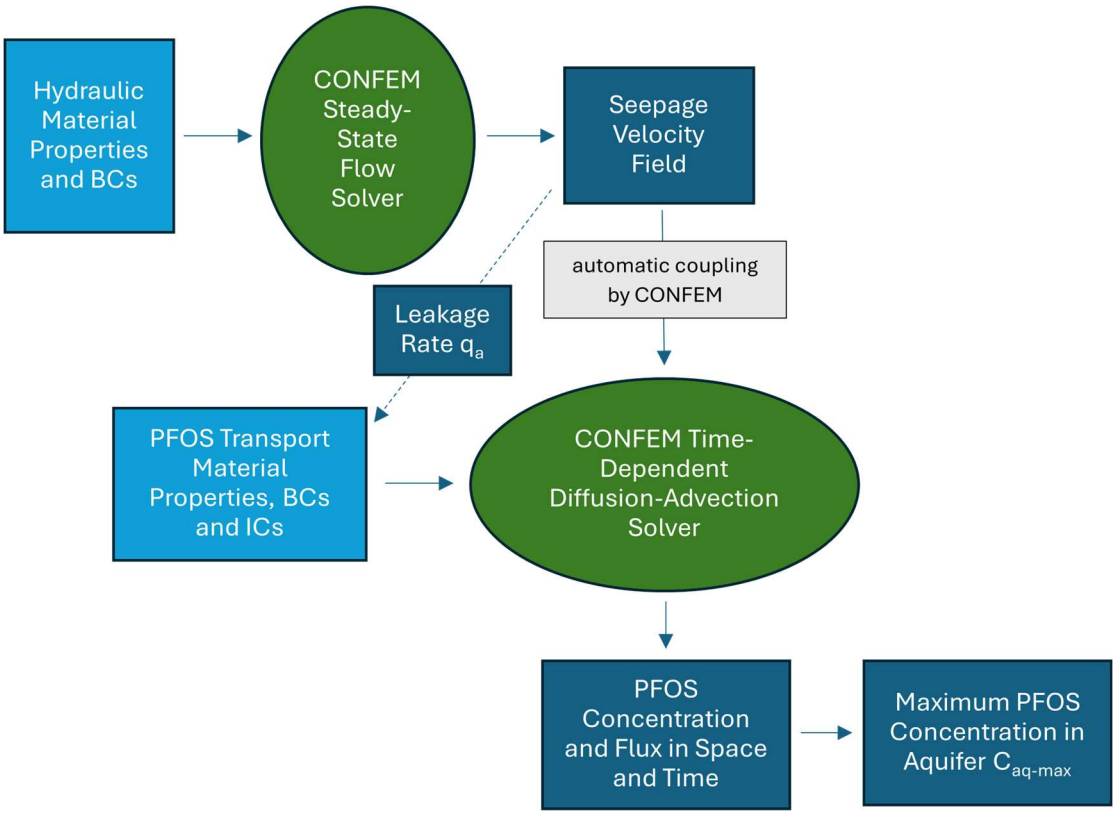

(a) Approach 1 (applied to Design I with GCL): automatic coupling

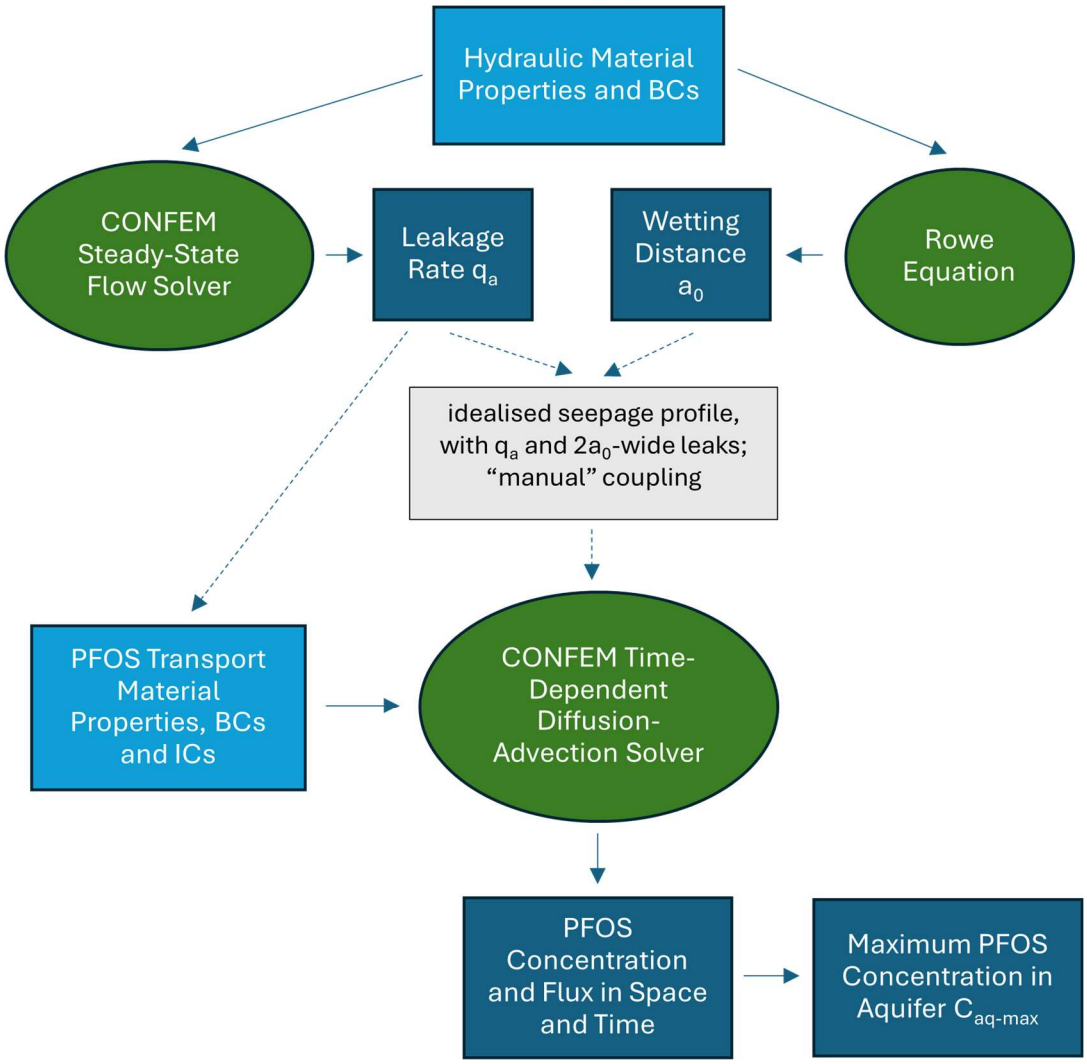

(b) Approach 2b (applied to Designs II & III with CCL & NCL): "manual" coupling (see Figure 3.5 for more details)

Figure 3.4. Two approaches to coupling flow and contaminant transport equations.

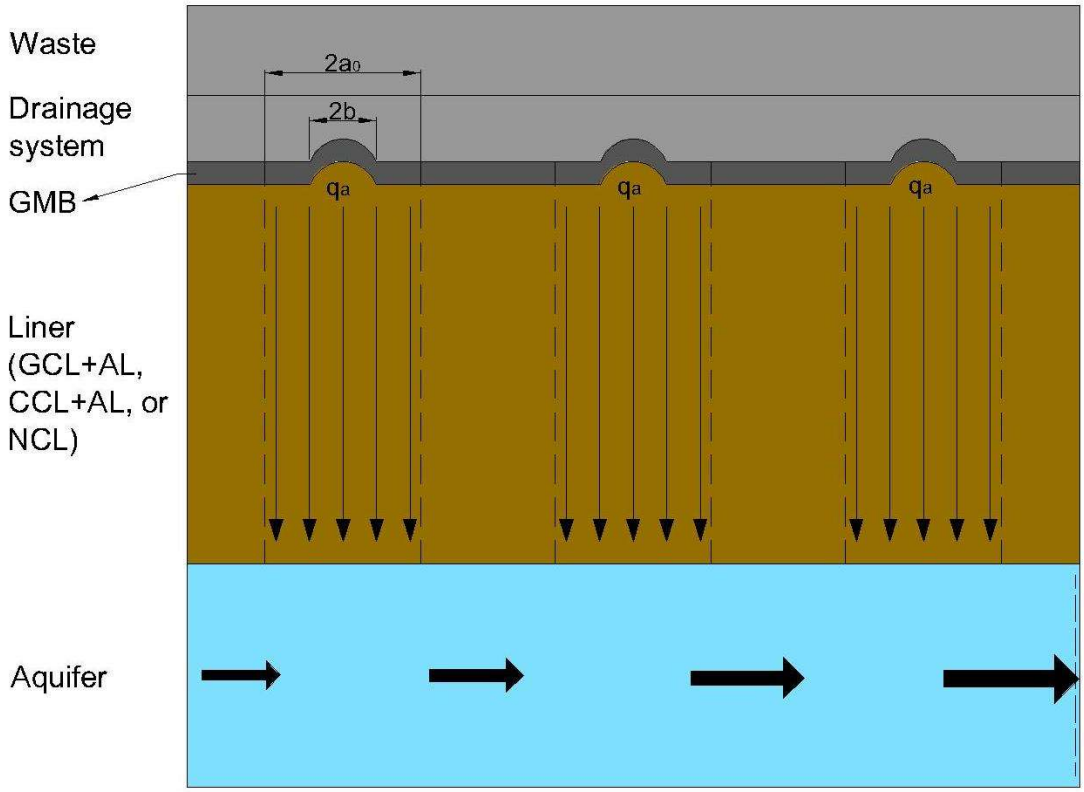

Figure 3.5. Approximation of seepage field in contaminant transport modelling under Approach 2b: idealised wetted profile based on leakage rate q_a (calculated by CONFEM) and wetted distance $2a_0$ (estimated by the Rowe equation).

3.5 Probabilistic Analyses

3.5.1 Overview

The final probabilistic analyses in this project are conducted by the method of Monte Carlo simulation (MCS), based on a surrogate model of polynomial chaos expansion (PCE) (this PCE-enhanced MCS is henceforth referred to as PCE for brevity). The use of PCE is necessary because conducting the analyses using conventional MCS (henceforth referred to as MCS) is computationally prohibitive, given the high dimensionality of the involved uncertainty (i.e., the large number of uncertain variables) which requires in turn a very large number of Monte Carlo realisations. While an individual SPAS simulation is conducted in two-dimensional space and can run in a matter of a few minutes, the cumulative cost (i.e., computational time) of multiple MCS becomes very high. On the other hand, as mentioned earlier, in the field of contaminant transport, PCE has not been applied to problems with more than six uncertain

parameters, i.e., half the number of uncertain parameters needed for the GCL design in this thesis; nor has it been specifically applied to problems of contaminant transport in liner systems.

Hence, the aim of PCE developments in this thesis is twofold. First, the accuracy and computational performance of PCE when modelling water flow and contaminant transport in liner systems, with a relatively large number of uncertain parameters, are examined. In particular, the extent to which PCE reduces the computational cost of MCS is evaluated. Second, the PCE is used to achieve the project's overall goal, namely assessing the risk of PFOS contamination in aquifers under landfills.

The starting point for the establishment of a PCE surrogate model is a set of MCS derived from the original model, i.e., the numerical simulation by SPAS, to generate pairs of input parameters, sampled from their probability distributions, and the desired output ($C_{aq\text{-}max}$). Hence, the development is conducted in two stages: a) MCS is conducted with a relatively small number of realisations to generate training data, also known as the experimental design (ED) and b) the PCE surrogate model is built based on this training data, and then run with a much larger number of realisations (referred to as the prediction design, PrD), at much lower computational cost than MCS, to generate probability distributions of the desired output. Each of these stages is discussed next.

3.5.2 Monte Carlo simulations

3.5.2.1 Procedure for MCS

MCS is conducted by repetitive simulations using SPAS/CONFEM, which is the software introduced in Section 3.4. To support the simulation, probability distributions of uncertain parameters are sampled through a stratified sampling technique called Latin hypercube sampling (LHS).

An original MATLAB program has been written as part of this thesis to implement the MCS scheme through the following steps: reading input information, generating input samples, then, for each realisation, updating the SPAS data file, calling CONFEM to conduct simulation, extracting desired outcomes (e.g., peak concentration in the aquifer), then moving to the next realisation.

The core MATLAB script for the above procedure, along with its supporting subscripts, is presented in Appendix 3.2.

3.5.2.2 Sampling technique for MCS: LHSMDU

Sampling is a key starting point for both MCS and PCE. The liner-system models studied in this thesis (Figure 3.2) involve high-dimensional uncertainty. Hence, the traditional purely random sampling method requires a large number of realisations to achieve convergence, incurring significant computational cost. To address this challenge, a multivariate sampling technique is needed to efficiently generate high-dimensional input samples.

Assuming a model containing N uncertain input variables that need to be realized L times, purely random sampling generates L samples from each of the N distributions and combines them randomly into N-dimensional samples. On the other hand, the Latin hypercube sampling (LHS), developed by McKay et al. (1979), is a form of stratified sampling that can be used to reduce the number necessary for an MCS to achieve a reasonably accurate output distribution. One-dimensional LHS is realized by evenly stratifying a given cumulative distribution function (CDF) into L different strata and randomly choosing one value from each stratum to obtain L samples (see Figure 3.6). Hence, LHS avoids nearly identical values which can be accidentally generated by purely random sampling and may cause wasted computing power. It emphasizes uniform sampling of the univariate distribution and thus produces samples better reflecting the true underlying distribution (Deutsch and Deutsch, 2012).

However, the stratification of the univariate CDFs with LHS can't effectively support multivariate uniformity through random combination into N-dimensional samples. Deutsch and Deutsch (2012) proposed a modified LHS method, which extends the idea of univariate uniformity used by LHS to a multivariate situation, named Latin hypercube sampling with multidimensional uniformity (LHSMDU). It is achieved by generating a greater number of samples than needed and then eliminating samples that are too close to others in the multidimensional parameter space. Still aiming at the N×L sampling task, LHSMDU first introduces a small redundancy coefficient, M, which is greater than 1 (M=5 is used herein), so that ML N-dimensional samples are required in this step. N×ML uniform random values in [0,1] are generated to form the original sample pool of size ML. Secondly, the most redundant samples, defined by the smallest Euclidean distance to neighbours, are eliminated iteratively, until the pool size is equal to L. Finally, the resulting L N-dimensional samples in [0,1] provide a ranking reference, based on which the N univariate sample sets generated by one-dimensional LHS are re-

ordered. In summary, LHSMDU enables a more uniform and representative coverage of the entire parameter space by the generated sample points.

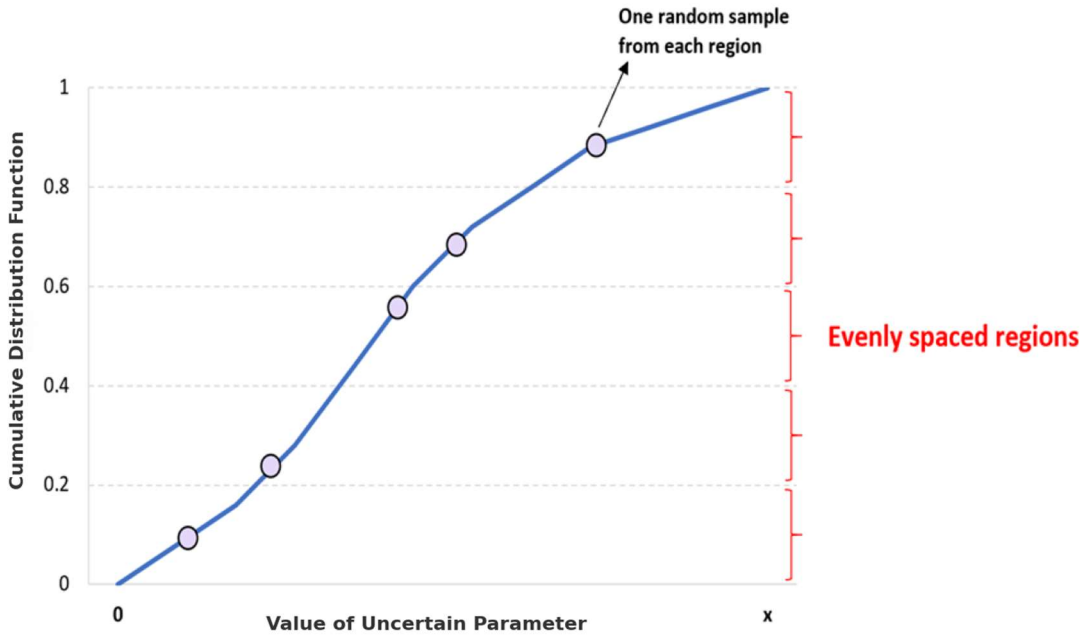

Figure 3.6. Illustration of one-dimensional Latin hypercube sampling.

The higher efficiency of LHS compared to random sampling has been demonstrated for some applications (McKay et al., 1979; McKay, 1992). LHSMDU has also been shown to perform better than LHS and another alternative technique called maximinLHS, in a case involving five uncertain parameters (Deutsch and Deutsch, 2012).

3.5.2.3 Application of MCS

Prior to building a PCE surrogate model, the conventional MCS is used for two applications: a) to conduct a set of preliminary sensitivity analyses to ALL parameters identified as probabilistic in Table 3.1 (with either 1 or 2 uncertain parameters in each analysis) and b) to generate training data (experimental design, ED) for building the PCE model.

MCS for preliminary sensitivity analyses

The aim of preliminary sensitivity analyses is to assess the extent to which each uncertain variable influences $C_{aq\text{-}max}$, as well as the direction of the relationship. To keep the computational cost low and use MCS (rather than PCE), only one or two variables are treated as uncertain at any one time, while the remaining variables are given their mean values. As will be discussed in Chapter 4, in two cases, parameters are co-variates

(k_a and k_b; C_{b0} and p_0) and must be treated as such, hence the need for two uncertain variables instead of one in these particular cases.

To this end, multiple sets of MCS with 1D uncertainty are conducted with 200 realizations for each set. Meanwhile, those with 2D uncertainty are conducted with 700 realizations. All individual-parameter MCS are implemented for RSc only. The MCS at this stage serves to identify uncertain variables with low influence on results (i.e., those whose variance produces a narrow range of $C_{aq\text{-}max}$ values); these variables are then treated as known, rather than uncertain, in later high-dimensional MCS and PCE, with all remaining uncertainties incorporated.

Full-parameter MCS for Experimental Design

Based on each of the three designs of the liner system, full parameter MCS is conducted for different scenarios of CQA. In the full-parameter MCS, all uncertain variables whose influences have been found to be non-negligible in preliminary sensitivity analyses are incorporated simultaneously. In this study, one set of full-parameter conventional MCS is conducted with 2000 realisations simulated. The $C_{aq\text{-}max}$ results of all 2000 realisations are collated along with corresponding input samples and serve as the experimental design (ED) for training a PCE functional approximation.

Note that following examination of results from multiple simulations, the location along the horizontal axis corresponding to $C_{aq\text{-}max}$ has been found to always match that of the rightmost leak or a point in its immediate vicinity (see Figure 3.2). Along the vertical axis, $C_{aq\text{-}max}$ is found to be always at the top of the aquifer. Therefore, for the probabilistic analysis, the search of $C_{aq\text{-}max}$ is simplified by recording the maximum concentration over time at that location in the aquifer (the top of the aquifer, directly below the rightmost leak).

3.5.3 PCE-enhanced MCS

3.5.3.1 Introduction

The mathematical formulation for PCE is presented in Appendix 3.3, based on the works of Deman et al. (2016), Marelli et al. (2024a, 2024b), Sudret (2008), Blatman and Sudret (2010), and Gratiet et al. (2016). In this subsection, the procedure of PCE-enhanced MCS is described as follows: a) development of the PCE model and subsequent MCS based on the surrogate, b) processing of the simulation results for

assessing the risk of PFOS contamination in the aquifer, and c) global sensitivity analysis (GSA) based on the constructed PCE model.

3.5.3.2 Development of PCE-enhanced MCS

The development and optimisation of the PCE model based on the experimental design (ED) generated in Section 3.5.2, as well as the subsequent MCS performed on the prediction design (PrD), are carried out using UQLab, a MATLAB-based uncertainty quantification framework (Marelli and Sudret, 2014). The UQLab surrogate modelling tools provide an efficient, flexible and easy-to-use PCE module that allows one to apply state-of-the-art algorithms for non-intrusive, sparse and adaptive PCE on a variety of applications. The establishment and application of the PCE model in our MCS are greatly facilitated by this mature MATLAB-based PCE module. The following steps are pursued to develop a PCE surrogate model and implement the subsequent MCS.

Step 1. Using LHSMDU described earlier, a set of input parameters for a sufficiently large number of realisations (PrD), to be ultimately simulated with PCE, is generated. A conservative value of the size of PrD is examined to be 60,000 realisations for the investigated problem with 12 uncertain parameters.

Step 2. Based on the ED generated through the conventional MCS in Section 3.5.2, the PCE model is developed. Details of the implementation are provided below.

The input data for both ED and PrD need simple transformations to ensure that each input variable obeys classic types of distribution, i.e., lognormal, normal, or triangular, so that classic families of polynomials can be adopted. It's also notable that in the calculation by the PCE model, $C_{aq\text{-}max}$ needs to be transformed into $\ln(C_{aq\text{-}max})$ because the distribution of $C_{aq\text{-}max}$ exhibits strong lognormal characteristics and using $\ln(C_{aq\text{-}max})$ as the output quantity can significantly enhance the quality of the model.

The following information or options need to be specified when using UQLab's PCE module: a) the input and output data of ED, b) the types and statistics of each input distribution, c) the configuration of the PCE model (see Appendix 3.3 for definitions), including the type of polynomial family for each input parameter, the degree of PCE model (p), the value of q-norm (q), and the adopted sparse regression technique. The process of optimising the PCE model by determining the optimal values of p and q, the best regression technique, and an adequate ED size, will be detailed in Chapter 6. The

criterion for optimisation is minimising the differences between MCS and PCE predictions.

Step 3. Based on the functional approximation of PCE, the PrD set can now be simulated in a computationally highly efficient manner, and results are recorded in an Excel file. The computational gains achieved by PCE, relative to conventional MCS, for the problems at hand, are also evaluated.

Step 4. Following the theory introduced in Appendix 3.3, the Sobol' indices of input parameters can also be conveniently calculated by the UQLab's PCE module.

Relevant MATLAB scripts are shown in Appendix 3.4, with Step 1 implemented by Script 3-11 and Steps 2-4 by Script 3-12.

3.5.3.3 Application of PCE-enhanced MCS: risk assessment and GSA

The ultimate objective of this study is to assess the contamination risk of PFOS in the aquifer underlying the landfill equipped with different liner systems. This is achieved through the following steps:

Step 1. The histogram of $C_{aq\text{-}max}$ calculated by PCE can be drawn as frequency distribution (FD) for visual inspection.

Step 2. The basis statistics of $C_{aq\text{-}max}$ are calculated, including arithmetic mean (AM), standard deviation (SD), geometric mean (GM), geometric standard deviation (GSD), and median.

Step 3. Two alternative approaches are followed to generate a probability density function (PDF) from the FD. The first approach is the kernel density estimation (KDE), which does not require a predefined closed-form distribution and thus does not yield an explicit formula of PDF. The second approach assumes that $C_{aq\text{-}max}$ obeys a lognormal distribution, and the PDF formula can be obtained accordingly.

Step 4. Based on the PDF generated by KDE, the probability of exceedance (PoE) function (Jones, 1993) can also be derived. The PoE can then be compared to drinking water guidelines/standards (C_{ref}) from different statutes in Australia (NHMRC, 2022), USA (USEPA, 2023), Canada (Health Canada, 2018), and the European Union (EurEau, 2018), as the main benchmark of contamination risk.

Step 5. By using Sobol' indices as the sensitivity metrics, a variance-based GSA is conducted for $C_{aq\text{-}max}$ to explore the attribution of its variation to different input

uncertainties. The mechanisms through which these influences emerge are also discussed.

Step 6. Beyond focusing on the peak concentration over time, the set of concentration at every time node can be extracted to reflect the change of contamination risk over time. The temporal evolution of concentration's statistics, PoE, and Sobol' indices, can all be investigated. Note that Step 6 is implemented only for RSc of the GCL-liner design.

Step 7. For all the three liner-system designs (I, II and III), the scenarios under different levels of construction quality assurance (CQA), i.e., Sc+, RSc, and Sc-, are compared to evaluate the effects of this factor on PFOS contamination risk.

Step 8. The risks associated with the three liner-system designs are compared to explore their respective effectiveness in mitigating PFOS contamination to the underlying aquifer.

3.6 Models Validity: Assumptions and Validation

3.6.1 Introduction

Hassan (2004) defines model validation as "the process of evaluating and testing the different aspects of the model for the purpose of refining, enhancing and building confidence in the model predictions in such a way that allows for sound decision making." A key obstacle to validation encountered in this thesis is the lack of specific landfill site data involving both the occurrence of PFOS and relevant contextual parameters, or laboratory data based on physical models of liner systems. While some studies do report PFAS occurrence at real landfill sites, the available information is generally insufficient to support validation of the type of numerical modelling undertaken in this thesis, although the underlying validation approach itself is sound. This is the basis for an ultimate form of validation that increases confidence in the model. The project described in this thesis was part of a larger multi-university investigation with laboratory experiments planned as part of another PhD project, at a partnering University. These experiments would have provided validation data for the models in this thesis. Unfortunately, for reasons outside the scope of this thesis, this experimental data was not received by the author.

Nevertheless, recognising that models are made of several components (e.g., theory and partial differential equations, geometrical and material property assumptions and approximations, probability distributions of uncertain data, numerical solvers), the purpose of this section is to discuss and clarify which parts of the models built in this thesis have been validated and in what way.

3.6.2 Key assumptions underlying numerical models

Table 3.2 summarizes key assumptions in the models and the rationale behind them. Four types of rationales for assumptions are used:

a) Evidence: indicates that evidence exists to support the assumption, in the context of PFOS transport in landfill liner systems.
b) Feasibility: indicates that deviations from this assumption would lead to increased cost and complexity of probabilistic modelling which significantly reduces its feasibility.
c) Conservative nature of assumption: the assumption is conservative, i.e., predicted contamination is likely to be worse than in reality, all other things being equal.
d) Lack of sufficient data: there is no sufficient data, in the context of PFOS transport in landfill liner systems, to allow evidence-based deviation from this assumption.

…

Table 3.2. Key Assumptions and their Rationale

Assumption	Reality	Rationale for assumption	Is assumption conservative?	Type of rationale	Landfill liner studies that have considered alternative assumptions
Saturated media	Topsoil is often unsaturated	a) dearth of data on unsaturated properties; b) conservative predictions because i. PFOS is retained along air-water interface in unsaturated soil to form a source of contamination (Costanza et al., 2019) so the assumption of saturation causing the neglect of air-water partitioning is conservative, and ii. PFOS has low volatility and transport of non-volatile contaminants in unsaturated media is likely slower than in saturated ones; c) simpler numerical modelling.	Yes	Feasibility, conservative nature, and lack of sufficient data	Liu and Hu (2014), Reddy et al. (2017), Khan et al. (2022)
Laminar Darcian flow in steady-state	Flow can be turbulent and time-dependent	a) low water velocities in the subsurface; b) time scale of contaminant transport in liner systems is much larger than that of water flow.	Unknown	Strong evidence	Zhang et al. (2012), Yan et al. (2021a)
Incompressible, isothermal media	Deformation and thermal gradients are present in liner systems and can have an impact on contamination	a) Compressibility and thermal gradients can have an impact on contaminant transport but these are difficult to model generically; b) simpler numerical modelling	Can be either	Evidence and feasibility	Zhang et al. (2012), Yan et al. (2021a), Yan et al. (2021b), Qiu et al. (2023a)
Two-Dimensional Transport	All transport is 3D in reality and 3D features exist in landfills (e.g., slopes)	a) Landfills are typically much larger in horizontal directions than vertical ones; b) Focus of model is central part of landfill away from slopes; c) 2D approximations are generally conservative; d) simpler numerical modelling.	Likely Yes	Evidence and feasibility	El-Zein et al. (2012), Masum et al. (2023), Zerenduoji and Yu (2024)

Assumption	Reality	Rationale for assumption	Is assumption conservative?	Type of rationale	Landfill liner studies that have considered alternative assumptions
Single-species transport with no sorption, biodegradation or chemical reactions	A certain degree of PFOS adsorption occurs within the components of the liner system; Leachate contain multiple contaminants that may compete for sorption sites; PFOS biodegrades albeit very slowly; PFOS can be produced from chemical transformation of precursors	a) As introduced in Chapter 2, the available literature data about the sorption coefficient of PFOS onto buffer soils lacks consistency and cannot offer solid references; b) Ignoring sorption gives conservative predictions because the sorption of PFOS onto liner systems leads to less reaching of PFOS into the aquifer; meanwhile, since no sorption is considered, the impact of the competition for sorption sites is also ignored; c) The few estimates on the half-life of PFAS in the literature are around several millenniums, and ignoring the biodegradation gives conservative predictions	Likely Yes	Feasibility, conservative nature, and lack of sufficient data	Varank et al. (2011), Xie et al. (2016), Zhao et al. (2024)
No deterioration of liner system over time	Evidence exists of deterioration of GMB over a time scale of decades	a) Lack of data on long-term deterioration b) Different components likely deteriorate at different rates, making modelling difficult	No	Feasibility and lack of sufficient data	Qiu et al. (2024), Xie et al. (2025)
A horizontal seepage velocity in the aquifer is directly specified	The flow field in the aquifer is multidirectional and spatially non-uniform, formed under the influence of the entire watershed	a) The simulation of the entire watershed can be avoided, allowing the simulation domain to be restricted to the aquifer immediately below the landfill and thus bringing much lower computational cost.	Unknown	Feasibility	Aliewi et al. (2021), Hu and Yu (2024)
PFOS leaves the aquifer at the downstream by advective discharge only	PFOS is likely to be transported by diffusion and dispersion as well at that position	a) conservative predictions; b) simpler numerical modelling	Yes	Feasibility and conservative nature	

Assumption	Reality	Rationale for assumption	Is assumption conservative?	Type of rationale	Landfill liner studies that have considered alternative assumptions
Full PFOS pollution load is available at time t=0	PFOS will be received over the lifetime of the landfill	a) The time-dependent arrivals of PFOS into the landfill are hard to track in reality and inconvenient to simulate in the modelling; b) simpler numerical modelling by setting a specified-mass BC on top of the liner at t=0; c) conservative predictions because all later-arriving PFOS is assumed to be present from the outset	Yes	Feasibility, conservative nature, and lack of sufficient data	Ding et al. (2021), Ding and Feng (2022)
Wrinkles are straight, equidistantly parallel, and normal to the page, forming the leaks in 2D, and the leaks are equal in size	Wrinkles are randomly shaped, directed, distributed and sized	a) No existing studies on the distribution pattern of wrinkles in GMB; b) simpler numerical modelling	Unknown	Feasibility and lack of sufficient data	Zhan et al. (2018), Chen et al. (2020)
Rate of exfiltration of leachate from the waste is assumed constant, which is the sum of the rate of collection by the drainage system and the rate of infiltration into the liner.	The leachate exfiltrates downward from the waste at a relatively stable but not an absolutely constant rate	a) a rational and convenient way to consider the leachate transport from the waste into the liner system and the underlying mass conservation of leachate	Unknown	Feasibility	

3.6.3 Models validity

The validity of numerical models is not a yes/no question but rather a matter of degrees, depending on the model's intended purpose and the level of uncertainty that can be tolerated in decision-making. As emphasised by Hassan (2004), model validation should be viewed as a continuous and evolving process, rather than a final check. Referring to the perspective of Oreskes et al. (1994), cited in Hassan (2004), a valid model is not one that is "true" in an absolute sense, but one that "does not contain known or detectable flaws and is internally consistent." In this sense, the validation work presented in this thesis may not be exhaustive, but it is sufficiently robust for its intended use, i.e., to provide probabilistic insight into the fate and transport of PFOS through different landfill liner systems. This also justifies the adoption of a probabilistic framework, which allows the incorporation of various uncertainties.

Some of the common sources of error discussed by Hassan (2004), such as simplification of system conditions, parameter uncertainty, and reliability of numerical solver, have been encountered in this work. As shown in Table 3.3, efforts have been made to address them within the constraints of available information. In this context, the validation in this thesis is considered acceptable and useful. As stated in Grant (2002), "...rejecting what can be learned from [modelling] because of its messy uncertainties... is treating a problem of blurred vision by putting out one eye. The result will be that we will see like a cyclops, with no depth of field." This thesis takes the position that even imperfect models can provide valuable insights, as long as their limitations are clearly understood.

Table 3.3. Validation Matrix

Object of Validation	Question	Potential Sources of Error	Sources of Validity in this Thesis	Ideal Forms of Validation
Fundamental Processes and Equations	Does the adopted set of PDEs* capture all key processes of water flow and contaminant transport relevant to PFOS in liner systems?	- Key assumptions (see Table 3.2) - Choice of BCs and ICs (no flow, specified head, specified mass of PFOS)	- Refer to extensive validation of this approach found in the literature including validation based on site measurements (Kia, 1991; Dhanraj and Ganesha, 2023; Kelkar et al., 2010; Praveen Kumar and Dodagoudar, 2010; Markhali and Ehteshami, 2016; Srivastava and Ramanathan, 2018; Divya et al., 2020).	-PFOS-specific laboratory experiments to identify key transport, partitioning and decay processes - Models validated against PFOS data from landfill sites
Model Construction	Does the simulation model reflect real conditions on landfill sites?	- Variability of geometry, material parameter, and environmental conditions - Assumption of long-term durability of liner is unlikely to be true.	- Use a probabilistic approach to capture variability and uncertainty. - Make conservative assumptions, if possible, when knowledge is scarce (e.g., saturated conditions, no sorption, no decay) - Key non-conservative assumption is non-deterioration of liner - implications discussed in results section.	- Models validated against a) PFOS data from landfill sites and/or b) PFOS laboratory experiments
Uncertainty Characterisation and Probability Distributions	Does the choice of probability distribution accurately reflect variability of key parameters?	- Some variables adopted as known (e.g., q_0, T_{GCL}, $h_{p\text{-}top}$) may turn out to have more variability in real life. - For uncertain variables, probability distributions adopted here may not reflect actual variability.	- Extensive review of the literature to build and confirm probability distributions used in modelling. See Chapter 4. - Multiplicity of scenarios considered and wide range of sources for data allows a range of landfill designs, construction quality, soils and materials properties to be considered.	- Extensive survey of landfills from around the world to quantify variability of key parameters - Detailed surveys of single landfill sites.
Numerical Solver	Does the software used accurately solve the set of PDEs?	- Poor accuracy of the numerical method. - Coding error in method implementation.	- Refer to extensive numerical validation of SPAS/CONFEM in the literature (El-Zein and Balaam, 2012; El-Zein et al., 2016; Hanna and El-Zein, 2023).	

		- Inadequate discretisation of spatial and temporal domains	- Conduct extensive convergence analyses to establish optimal discretisation and mesh-independent models. - Compare predictions of Approaches 1, 2a, and 2b to each other and to POLLUTE software when coupling water flow and contaminant transport components. - Compare predictions of PCE-enhanced MCS to MCS only, to validate PCE.	

* PDEs: partial differential equations, namely Laplace Equation for Steady-State Saturated Flow and Reactive Diffusion/Dispersion Advection Equation for Single-Species Transport.

Chapter 4
Determination of Input Parameters

4.1 Introduction

As stated in the previous chapter, five types of input parameters are required to complete model description, namely geometry, hydraulic conditions, pollutant load, material properties and construction quality. Some of these parameters are considered known with relative certainty and do not require probability distributions to describe them, either because they a) have low natural variability, b) lack sufficient data to characterise their uncertainty, or c) have negligible influence on PFOS risk to groundwater based on preliminary sensitivity analyses. All other input parameters are treated as uncertain and described with probability distributions.

Four different approaches are used to establish deterministic values and probability distributions of input parameters. In what follows we use variable symbols that have already been defined in Table 3.1.

Approaches I and II

Choice of ALL parameters is informed by a review of the relevant literature. However, under Approaches I and II, data is taken exclusively from existing literature. Approach I is applied to a subset of parameters that are known to be PFAS-specific (C_{b0}, D_g, D_{GCL}, S_g, K_d, $t_{1/2}$). Approach II concerns a subset of parameters that are either known, or assumed, to be non-PFAS specific ($h_{p\text{-}top}$, d_s, q_0, 2b, T_{AL}, T_{AQ}, $\theta_{GMB\text{-}GCL}$, k_{AL}, k_{AQ}, n_{GCL}, n_{AL}, n_{AQ}, D_{AL}, $\alpha_{L\text{-}GCL}$, $\alpha_{T\text{-}GCL}$, $\alpha_{L\text{-}AQ}$, $\alpha_{T\text{-}AQ}$).

Non-PFAS specific parameters include porosities of the different layers, parameters governing pressure gradients, width and frequency of leaks, hydraulic transmissivity at the interface between GMB and the clay liner, as well as dispersivities in the clay liner and the aquifer. Hydraulic conductivities may in principle be affected by the chemical composition of the permeant and hence the concentration of PFOS, but no evidence is available that would allow the incorporation of such dependence in the model. For

example, a study by Barakat et al. (2024) did not observe significant dependence of hydraulic conductivities of GCL on PFAS concentrations in permeants. Parameter D_{AL} should also depend on both the porous medium (e.g., porosity, tortuosity, pore size) and the contaminant in question (e.g., diffusion of contaminant in water). However, no PFOS-specific evidence is available in the literature and the value used here is a non-PFAS specific estimate.

It is clear that Approaches I and II have only been applied to a subset of all parameters, because for the remaining parameters, the available information in the literature is too scarce or insufficient to determine usable values or distributions. This limitation motivated the introduction of Approaches III and IV discussed next.

Approach III

As stated above, for some parameters, information available in the literature is insufficient or inconsistent and must hence be combined with expert judgment, leading to Approach III. This is the case for C_{b0}, p_0, ΔH, $V_{ax\text{-}in}$, T_{CCL}, T_{NCL}, T_{AL}, T_{AQ}, D_g, S_g, D_{GCL}, D_{CCL}, D_{NCL}, $\theta_{GMB\text{-}CCL}$, $\theta_{GMB\text{-}NCL}$, k_a, k_b, k_{CCL}, k_{NCL}, $\alpha_{L\text{-}CCL}$, $\alpha_{T\text{-}CCL}$, $\alpha_{L\text{-}NCL}$, $\alpha_{T\text{-}NCL}$, $\alpha_{L\text{-}AL}$, $\alpha_{T\text{-}AL}$, $\alpha_{L\text{-}AQ}$, and $\alpha_{T\text{-}AQ}$. Hence, these parameters were typically determined through discussions conducted by the author with Prof R. Kerry Rowe, a leading authority on contaminant migration through landfill liner systems and geoenvironmental engineering, and Prof Abbas El-Zein, supervising this thesis work. Note that the application of Approach III, as well as Approach IV presented below, are always preceded by Approaches I and II, i.e., a search for evidence in the literature, and only applied after it is found such evidence, either provides a sound but partial quantitative basis, or is largely insufficient or inconsistent to estimate the parameter in question, whether as a fixed constant or probability distribution. Hence, parameters determined through Approaches III and IV are also informed by the literature.

Approach IV

Finally, Approach IV is used to characterise the hydraulic regime generated by leakage through the GMB through calibration against observed leakage rates in New York State landfills (Rowe and Zhao, 2023). This case was adopted because it was a rare case in which data were sufficiently complete to allow calibration. Hence, probability distributions of parameters L_w, 2b, $\theta_{GMB\text{-}GCL}$, k_a and k_b were determined by calibrating

predictions of the liner-system hydraulic model against observed leakage rates. Note that the calibration process also relies on relevant information reported in the literature.

In the following section, details of this calibration work are presented first. Next, to ensure clarity and transparency, fixed values or probability distributions of all input parameters, based on different approaches, are compiled into a single comprehensive table (Table 4.4) with annotations, for the three liner-designs.

4.2 Types of Probability Distributions Used

Two types of probability distributions, triangular and shifted lognormal, were found to well describe all uncertain parameters considered in the models in this thesis. Their generic distribution patterns are shown in Figure 4.1.

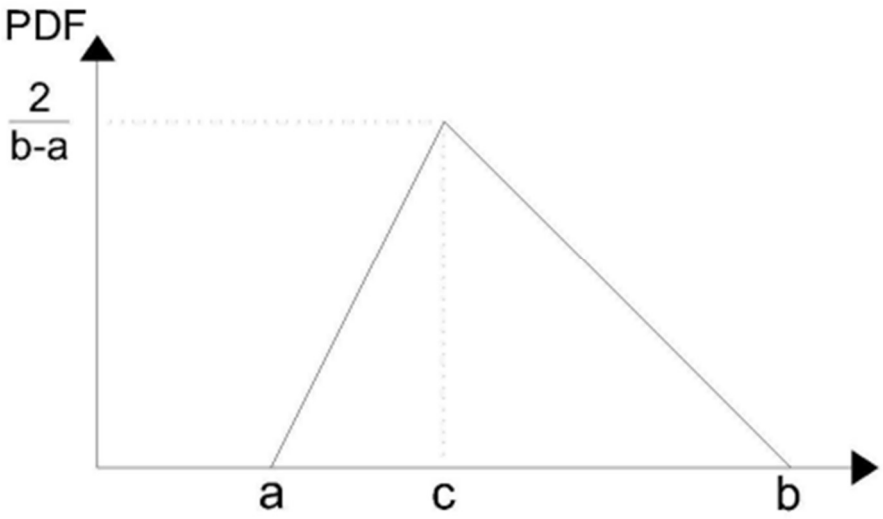

(a) Triangular (a~b: range; c: mode)

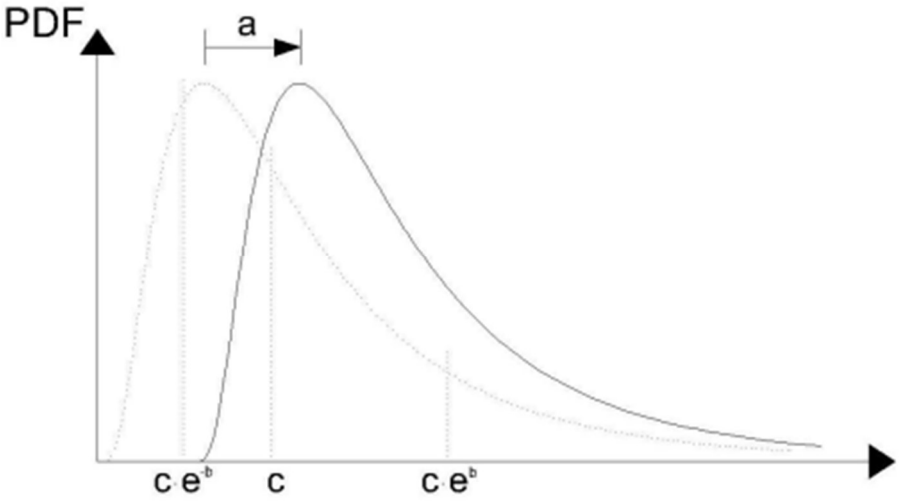

(b) Shifted Lognormal (a: shift; b: ln of geometric standard deviation (GSD) without shift; c: geometric mean (GM) without shift; lognormal distribution can be recovered here by setting a=0)

Figure 4.1. Generic probability distributions used in quantifying uncertainty of variables.

4.3 Calibration to Observed Leakage through a Primary Composite Liner

The MCS based on the Water-Flow solver of SPAS/CONFEM and analytical expressions of leakage implemented in a spreadsheet was used to generate probability distributions of parameters related to the leakage for the GMB/GCL composite liner by calibrating leakage predictions to experimental data, which were associated with good construction quality assurance (CQA) and the absence or presence of electrical leak location (ELL) technologies (Gilson-Beck, 2019). The parameters include the hydraulic conductivity of GCL (k_a, k_b), the GMB/GCL interface transmissivity (θ), the total head difference (ΔH), and the wrinkle geometry (L_w, 2b). The calibration work in this section is adopted from Rowe and Zhao (2023).

4.3.1 Data from Beck (2015)

The establishment of realistic parameters to use for evaluating likely leakage rates and ultimately the probability of PFOS concentrations exceeding allowable levels in the

groundwater, requires data for verification. This subsection describes the data set that was used.

The best available data arises from New York State's requirement for double-lined MSWLs together with annual reporting of actual leakage through the primary liner. Beck (2015) collected and analysed this leakage rate data from 122 discrete landfill cells where there had been good construction quality control but no electrical leak location survey (no ELL). Leakage rate data was also analysed for 60 discrete landfill cells where a dipole method electrical leak location survey was conducted (with ELL). Based on the data, a plot of the probability of leakage exceeding a given value was constructed. This data is given in Figure 4.2(a) for "no ELL" and in Figure 4.2(b) for "with a dipole ELL".

Although, as mentioned above, the data from Beck (2015) pertains to double-lined landfills and the risk assessment in this thesis is for single-lined landfills, the data was used for the following reasons. First, the leakage rates were recorded by Beck (2015) under the primary, not the secondary liner. While the presence of a secondary liner under the primary one will affect leakage rates, these leakage rates nevertheless will have relevance to single-lined systems. Second, the dataset of Beck (2015) is one of the most comprehensive available to the author, based as it is on a large number of cells, and the author has no access to such high-quality data for single-lined landfills. Third, Beck (2015) provided separate leakage data depending on whether a dipole ELL is present or not. This provides a valuable opportunity to evaluate the effect of construction quality and monitoring on the risk of PFOS contamination.

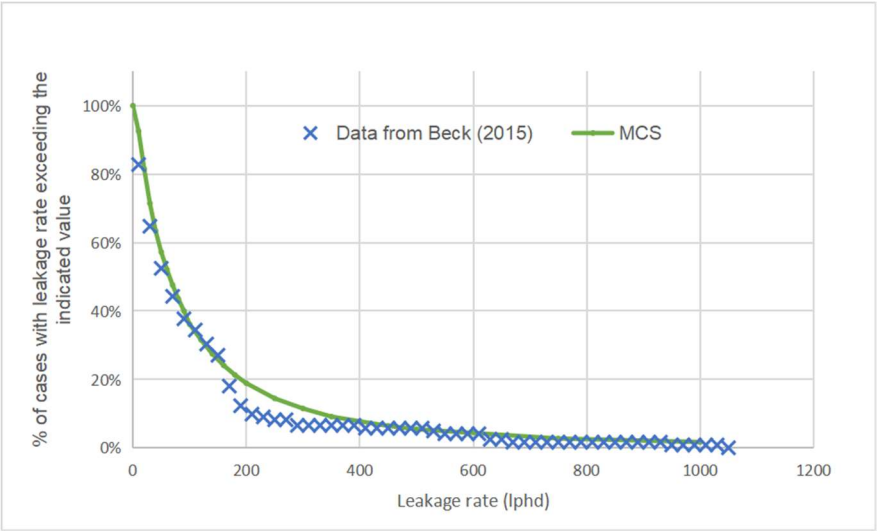

(a) Based on the 122 landfill cells with good CQA and no ELL.

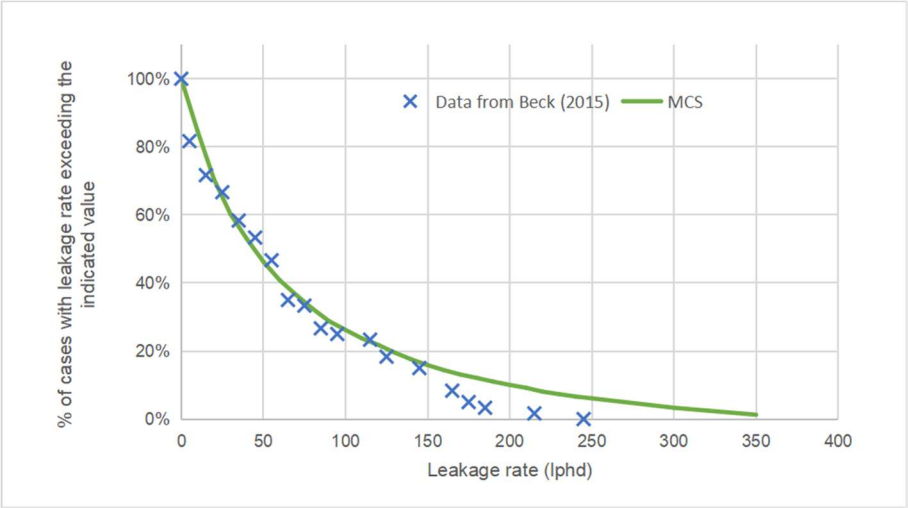

(b) Based on the 60 landfill cells with good CQA and a dipole ELL.

Figure 4.2. Probability (as a percentage of the landfill cells for which data is reported by Beck, 2015) of the leakage rate exceeding a given value, together with calculated rates for GMB/GCL.

4.3.2 Calibration procedure

The calibration procedure is represented in Figure 4.3. The model iteratively calculated in MCS was a single-liner system with a configuration consisting of GMB (0.0015m), GCL (0.007m), and AL (3.743m). The calibration aimed to optimise the fit of the q_a results of MCS to the experimental q_a data by progressively adjusting multiple input distributions. The relevant input distributions include k_a, (k_b/k_a)-1, θ, ΔH, 2b, and L_w. The only difference between cases with no ELL and with ELL lies in the distribution of L_w.

As illustrated in Figure 4.3, based on the good agreement between the q_a results obtained from the Rowe equation (Eq. (A3.1.2)) and SPAS for the calibration model, the core optimisation work was carried out through spreadsheet work in Excel. Note that during the calibration presented in this section, k_{AL} was deliberately set to a sufficiently large value (1×10^{-5} m/s) to ensure the validity of the formula, because the Rowe equation becomes invalid when AL is too thick or when its hydraulic conductivity is not sufficiently large. The starting point of the optimisation was informed by the literature and based on the expert advice by R. Kerry Rowe. The targets of the optimisation lay in the characteristics of the experimental data of q_a, including its statistics (Table 4.1) and probability of exceeding given values (Figure 4.2). Finally, the SPAS-based MCS served as a validation measure to confirm the fit of MCS results to the experimental data, as shown in Figure 4.2 and Table 4.1.

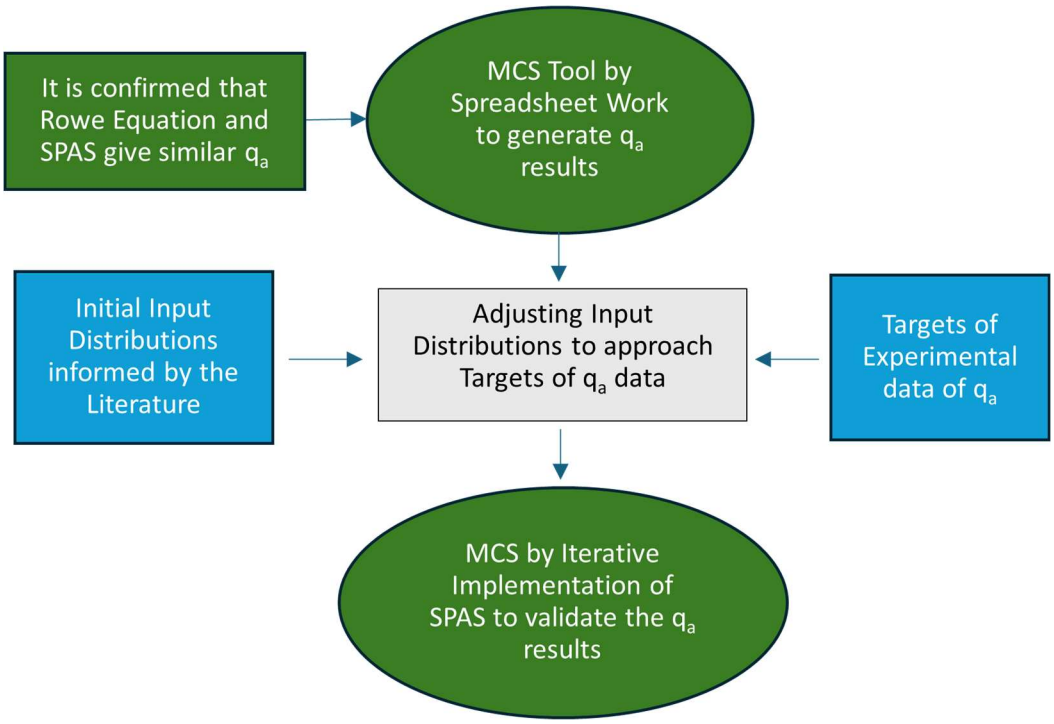

Figure 4.3. Calibration Process

Table 4.1. Characteristics of q_a (lphd) after calibration against experimental data.

	No ELL			With ELL		
	GM (lphd)	AM (lphd)	Exceeding probability	GM (lphd)	AM (lphd)	Exceeding probability
Targets of experimental q_a data	64	123	Figure 4.2(a)	40	60	Figure 4.2(b)
q_a by Equation-based MCS after fitting	66	143		46	100	
q_a by SPAS-based MCS after fitting	60	127	Figure 4.2(a)	42	90	Figure 4.2(b)

4.3.3 Parameters to fit observed data for GMB/GCL composite liner

After the optimisation of input distributions, the experimental data for the cases with no ELL and with ELL were reasonably approximated by MCS (Figure 4.2) using the parameters' distributions given in Table 4.2, with shifted lognormal distributions characterised by δ (shift), GM, and ln(GSD), and triangular distributions by Min, Mode, and Max.

The characteristic of the data points derived from these distributions are given in Table 4.3. The GCL in contact with the GMB is subject to significant vertical stress due to the weight of the overlying waste. The distribution of k_a (GCL's hydraulic conductivity where it is in close contact with GMB) that best fit the data (Figure 4.4(a)) had an arithmetic mean (AM) of 5.8×10^{-11} m/s with an overwhelming majority of values falling between $GM\times e^{-2\times\ln(GSD)}$ (0.3×10^{-11} m/s) and $GM\times e^{2\times\ln(GSD)}$ (30×10^{-11} m/s). The hydraulic conductivity of the GCL is subject to cation-exchange from interaction with the leachate and this affects both k_a and k_b (GCL's hydraulic conductivity under holed wrinkles in GMB). The effect of cation-exchange on k_a is offset by self-healing under the applied stress of the waste over the GMB, giving the relatively low values in Figure 4.4(a) and Table 4.3. However, for the GCL beneath the wrinkle, there is no opportunity for self-healing because the effective stress is essentially zero below the wrinkle remaining after compression. Thus, the ratio k_b/k_a -1, had a GM of 7, a ln(GSD) of 0.3. This gave k_b a range of 5×10^{-12} ~ 1×10^{-8} m/s, a median value of 2.4×10^{-10} m/s, and an AM of 4.8×10^{-10} m/s (Figure 4.4(b)). The transmissivity at the GMB/GCL interface (θ) had a range between $1\times10^{-}$

[12] and 2×10^{-9} m^2/s, a median value of 3.3×10^{-11} m^2/s, an AM of 7.5×10^{-11} m^2/s, and a distribution as shown in Figure 4.4(c).

The statistical parameters for differential head (ΔH), given in Table 4.2, yielded the distribution shown in Figure 4.4(d) with an AM of 0.205 m, a standard deviation of 0.03 m, and a minimum of 0.14 m, with very few values more than 0.3 m. The distribution for the wrinkle width (2b) gave an AM of 0.201 m with a standard deviation (SD) of 0.01 m and a range of 0.17~0.24m (Figure 4.4(e)). Different distributions of the length of holed wrinkle per hectare (L_w) were needed with and without ELL (Table 4.2). With no ELL, the best fits to the data were obtained with holed wrinkles having a minimum length of 20 m/ha, a mode of 250 m/ha and a maximum of 1450 m/ha. With a dipole ELL, the best fits to the data were obtained with holed wrinkles having a minimum length of 0 m/ha, a mode of 20 m/ha and a maximum of 1450 m/ha. When calculating leakages using MCS, outliers were rejected based on Chauvenet's criterion.

All distributions in Table 4.2 were adopted in the probabilistic modelling of the GCL+AL liner design in this thesis except for ΔH. The ΔH distribution in Table 4.2 reflects the situation of the model used for calibration, which is not suitable for the formal MCS of this thesis. The ΔH distribution used for the later formal MCS is specified in Table 4.4.

Table 4.2. Parameter distributions from calibration against observed leakage rate and their characteristics. (Liner thickness: T_{GCL}=0.007 m)

Parameter	Unit	Distribution	δ	GM	ln(GSD)
k_a	m/s	Lognormal	0	3×10^{-11}	1.15
(k_b/k_a) - 1	-	Lognormal	0	7	0.3
θ	m^2/s	Shifted lognormal	1×10^{-12}	3.2×10^{-11}	1.3
ΔH	m	Shifted lognormal	0.1	0.1	0.3
2b	m	Shifted lognormal	0.1	0.1	0.1
			Minimum	Mode	Maximum
L_w (no ELL)	m/ha	Triangular	20	250	1450
L_w (with ELL)	m/ha	Triangular	0	20	1450

Table 4.3. Characteristics of the distributions in Table 4.1.

Parameter	Unit	Range	Median	AM	SD	Figure
k_a	m/s	$9\times10^{-13} \sim 1\times10^{-9}$	3×10^{-11}	5.8×10^{-11}	9.0×10^{-11}	4.4(a)
k_b	m/s	$5\times10^{-12} \sim 1\times10^{-8}$	2.4×10^{-10}	4.8×10^{-10}	7.4×10^{-10}	4.4(b)
θ	m^2/s	$1\times10^{-12} \sim 2\times10^{-9}$	3.3×10^{-11}	7.5×10^{-11}	1.4×10^{-10}	4.4(c)
ΔH	m	0.14 ~ 0.37	0.2	0.205	0.03	4.4(d)
2b	m	0.17 ~ 0.24	0.2	0.201	0.01	4.4(e)
L_w (no ELL)	m/ha	40 ~ 1400	573	524	312	4.4(f)
L_w (with ELL)	m/ha	3 ~ 1380	489	432	337	4.4(g)

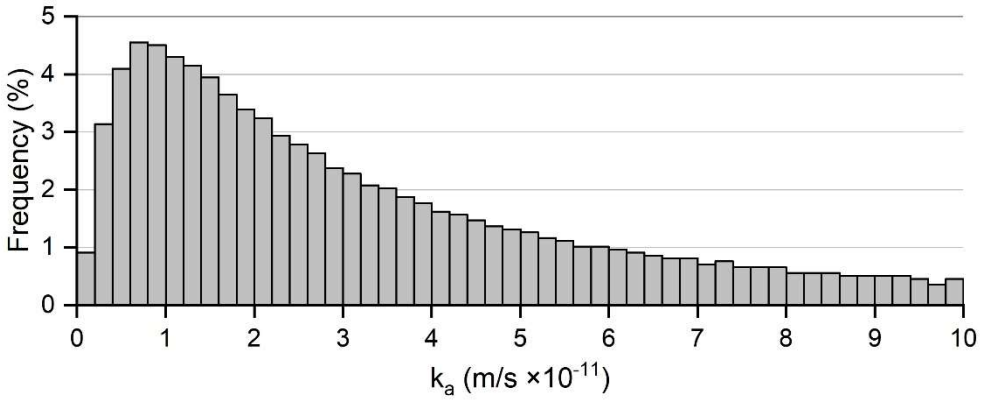

(a) Frequency distribution for k_a

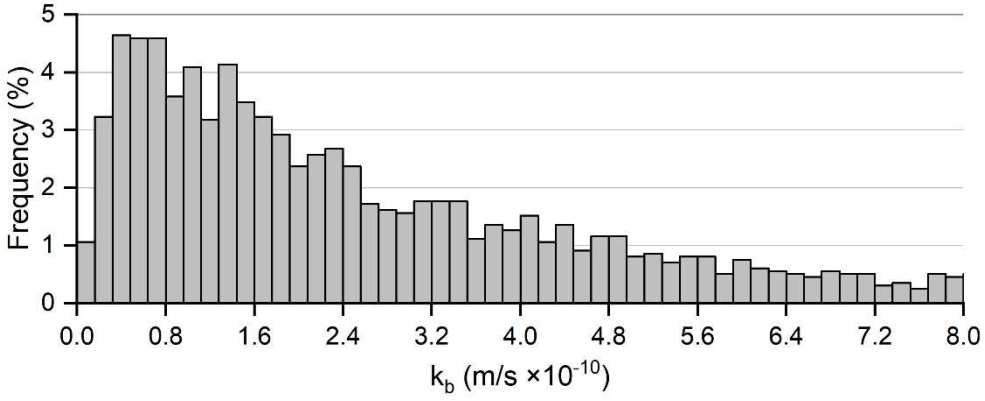

(b) Frequency distribution for k_b

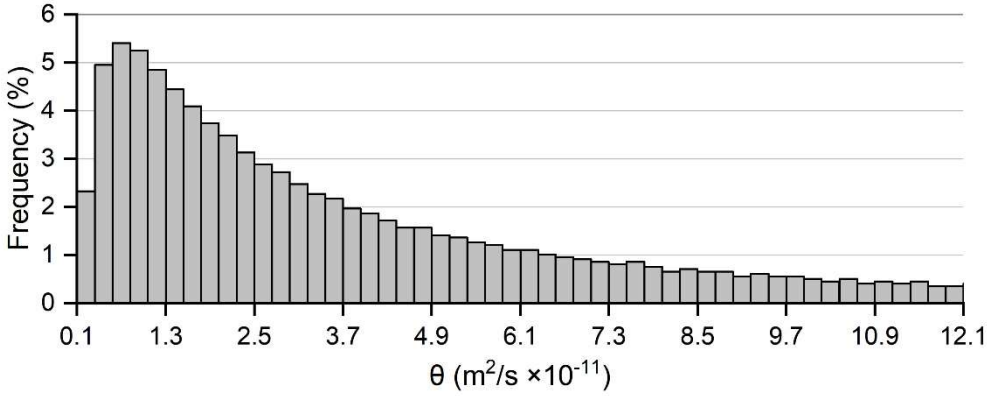

(c) Frequency distribution for θ

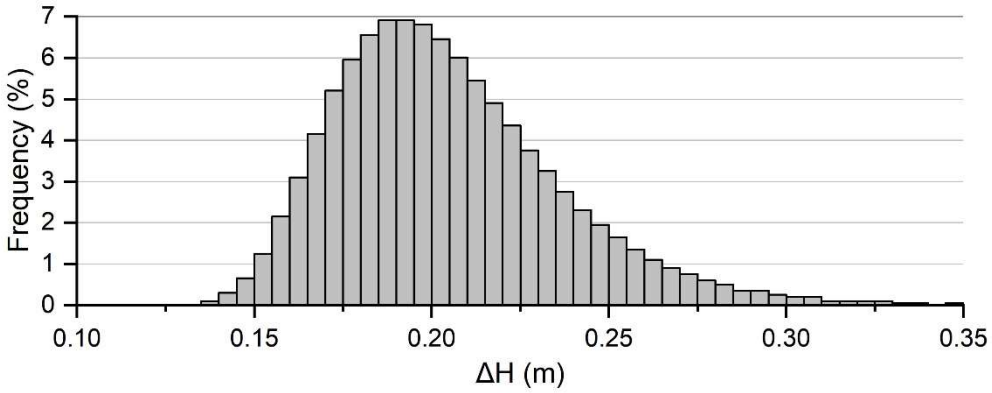

(d) Frequency distribution for ΔH

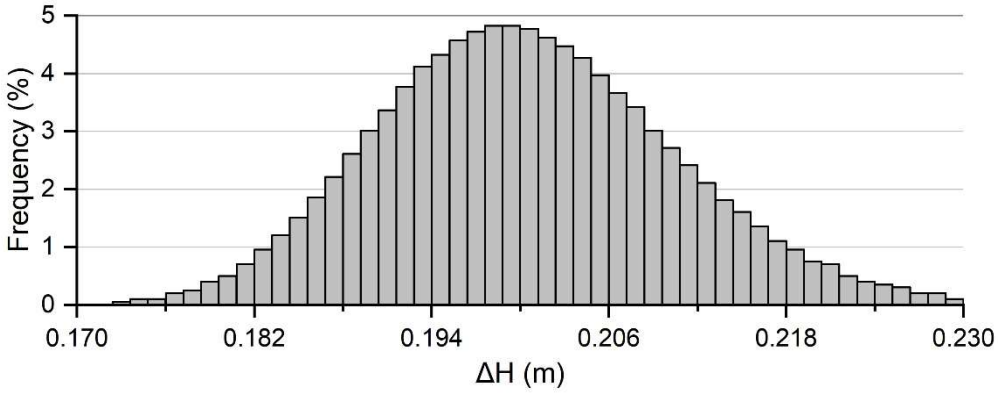

(e) Frequency distribution for 2b

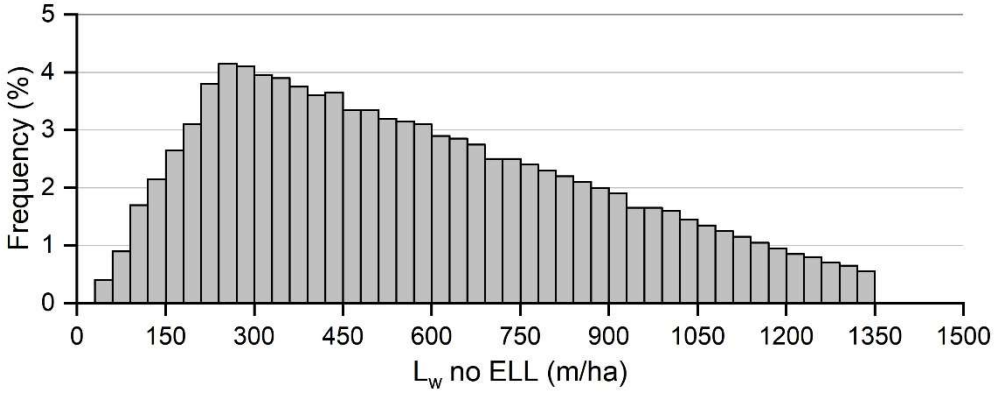

(f) Frequency distribution for L_w (no ELL)

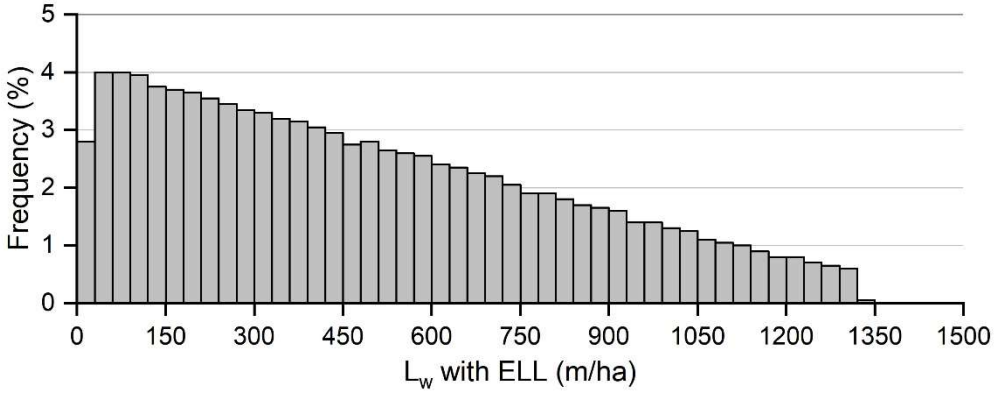

(g) Frequency distribution for L_w (with ELL)

Figure 4.4. Frequency distributions for parameters related to leakage.

4.4 Summary of Input Parameters

Table 4.4 comprehensively shows values or probability distributions of input parameters used for the RSc (good CQA & with ELL) of the three models with different liner designs (marked in the table). Brief descriptions of the source for each parameter, including adopted approach (I, II, III, or IV), are shown. Simulations for the other scenarios are conducted by changing the distribution of L_w as follows (all parameters not specified are identical to those used in RSc):

a) RSc0: L_w=0.
b) Sc- (good CQA & no ELL): L_w follows the triangular distribution with a mode of 250 m/ha, a lower limit of 20 m/ha, and an upper limit of 1450 m/ha.

c) Sc+ (excellent CQA): L_w follows the triangular distribution with a mode of 20 m/ha, a lower limit of 0 m/ha, and an upper limit of 250 m/ha.

The distributions of L_w used for RSc and Sc- are based on the calibration in Section 4.3 for “with ELL” and “no ELL” respectively (Table 4.2). As for Sc+, the L_w distribution is based on expert advice from R. Kerry Rowe to reflect a significantly enhanced level of CQA.

Table 4.4. Certain and uncertain input parameters for the Reference Scenario (RSc).

Variable			Description	Unit	Design	Representative Value[1]	Distribution Type	Probability Distribution Parameters a, c, b [2] a	c	b	Source and Notes[3]
1. Geometry, Hydraulic Conditions and Pollutant Load ('Input')	No Uncertainty Considered	$h_{p\text{-}top}$	Hydraulic pressure head on top of liner	m	All	0.3					II Based on Rowe (1998, 2000a).
		d_s	Mass of waste per surface area in landfill	$kg.m^{-2}$	All	2.5×10^{4}					II Following Rowe and Barakat (2021).
		q_0	Infiltration rate into the landfill	$m.year^{-1}$	All	0.15					II Minimum permitted by MoE (2011).
	Uncertainty Quantified	ΔH	Difference in total hydraulic head between top of GMB and Aquifer	m	I, II	1.05	Triangular	0.3	1.05	2.05	III Expert advice by R. Kerry Rowe based on a deduction of a generic single-liner design for small landfills in Ontario, Canada (MoE, 2011).
		ΔH	Difference in total hydraulic head between top of GMB and Aquifer	m	III	2.425	Triangular	1.675	2.425	3.425	III Given that NCL (Design III) has almost twice the thickness as GCL+AL (Design I) or CCL+AL (Design II), two options are possible for specifying ΔH for III: a) keep the same ΔH as I and II, or b) keep the same pressure in the aquifer as I and II. An intermediate case between these two is selected by setting the average of the two modes from these two options and keeping the same distance between mode and min & max as for I and II.
		L_w	Density of wrinkles	$m.hectare^{-1}$	All	325	Triangular	0	20	1450	IV

									Based on the discussion about holed wrinkle length in Rowe and Barakat (2021) and the calibration presented in Rowe and Zhao (2023).
2b	Width of leak	m	All	0.2	Shifted Lognormal	0.1	0.1	0.1	II, IV Determined through the calibration in Rowe and Zhao (2023), based on a comprehensive study on GMB wrinkle in Chappel (2012).
C_{b0}	Initial PFOS concentration in leachate	$ng.litre^{-1}$	All	900	Shifted Lognormal	0	900	1.1	I, III Expert advice by R. Kerry Rowe based on abundant but variable data on C_{b0} (Zhang et al., 2023).
p_0/C_{b0}	Ratio of PFOS waste content to PFOS initial concentration in leachate	$m^3.kg^{-1}$	All	2×10^{-3}	Shifted Lognormal	0	2×10^{-3}	2.1	III Since data on p_0 is limited (Zhang et al., 2023), expert advice on this ratio is provided by R. Kerry Rowe to address the uncertainty of p_0 and the correlation between p_0 and C_{b0} based on the only information available in Li (2011) and Zhang et al. (2023).
$V_{ax\text{-}in}$	Inward horizontal Darcy velocity in Aquifer	$m.year^{-1}$	All	0.95	Shifted Lognormal	0	0.95	0.4	III Expert advice by R. Kerry Rowe, informed by data from Ronen et al. (1986), Baird et al. (2008), Al-Madhlom et al. (2020), and Innocent et al. (2021).
T_{CCL}	Thickness of CCL	m	II	1.0	Triangular	0.6	1.0	1.5	III Expert advice by R. Kerry Rowe, referring to the requirement of eCFR (n.d.) and NSW EPA (2016).
T_{NCL}	Thickness of NCL	m	III	6.5	Triangular	3.75	6	10	III Expert advice by R. Kerry Rowe, reflecting the field-scale presence of undisturbed low-permeability clay strata, which are typically much thicker than engineered liners.

		T_{AL}	Thickness of Attenuation Layer	m	I	3.743	Shifted Lognormal	0	3.743	0.5	II, III The focus of this study is on landfills built over relatively shallow attenuation layers. The GM of thickness is based on Rowe and Abdelrazek (2019) and Rowe and Barakat (2021), referring to the requirement of MoE (2011). The variability of thickness is based on expert advice by R. Kerry Rowe.
		T_{AL}	Thickness of Attenuation Layer	m	II	2.75	Shifted Lognormal	0	2.75	0.5	III The GM is assumed to keep the average levels of $T_{GCL}+T_{AL}$ and $T_{CCL}+T_{AL}$ the same.
		T_{AQ}	Thickness of Aquifer	m	All	3	Shifted Lognormal	0	3	0.6	II, III The GM of thickness is based on Rowe and Abdelrazek (2019), Guarena et al. (2020), and Rowe and Barakat (2021). The variability of thickness is based on expert advice by R. Kerry Rowe.
2. Material Input Parameters	No Uncertainty Considered	k_{AQ}	Hydraulic conductivity in Aquifer	$m.s^{-1}$	All	1×10^{-5}					II Following Rowe and Barakat (2021).
		D_g	Diffusion coefficient of GMB	$m^2.s^{-1}$	All	1.5×10^{-16}					I, III Preliminary analyses conducted in this study have demonstrated that advection is dominant for PFOS transport in the studied problem, and the uncertainties in diffusion parameters of layers have only a small effect. D_g and S_g are taken from Di Battista et al. (2020) and Rowe et al. (2023). D_{GCL} is based on Barakat et al. (2024).
		S_g	Partitioning coefficient of GMB	1	All	4					
		D_{GCL}	Diffusion coefficient of GCL	$m^2.year^{-1}$	I	1.2×10^{-3}					
		D_{CCL}	Diffusion coefficient of CCL	$m^2.year^{-1}$	II	0.004					III Expert advice by R. Kerry Rowe, which is reasonably higher than D_{GCL} due to the coarser

D_{NCL}	Diffusion coefficient of NCL	$m^2.year^{-1}$	III	0.004	pore structure and weaker sorption capacity of CCL and NCL.
D_{AL}	Diffusion coefficient of Attenuation Layer	$m^2.year^{-1}$	I, II	0.02	II Following Rowe and Barakat (2021), close to a non-PFAS specific value in Schrefler and Delage (2013).
$\alpha_{L\text{-}GCL}$ $\alpha_{T\text{-}GCL}$	Dispersivity of GCL	m	I	0	II Following Rowe and Barakat (2021).
$\alpha_{L\text{-}CCL}$ $\alpha_{T\text{-}CCL}$	Dispersivity of CCL	m	II	0	III Expert advice by R. Kerry Rowe, acknowledging the negligible role of mechanical dispersion in low-permeability domains.
$\alpha_{L\text{-}NCL}$ $\alpha_{T\text{-}NCL}$	Dispersivity of NCL	m	III	0	
K_d	Sorption coefficients of layers	$litre.kg^{-1}$	All	0	I Information on sorption of PFAS on soil and liner material is highly variable, hence the conservative choice of no sorption.
$t_{½}$	Half-life of PFOS in layers	year	All	∞ (no decay)	I PFOS is extremely persistent in the environment (Li et al., 2017), hence decay is assumed to be negligible.
n_{GCL}	Porosity of GCL	1	I	0.7	II Following Rowe and Barakat (2021).
n_{CCL}	Porosity of CCL	1	II	0.4	III
n_{NCL}	Porosity of NCL	1	III	0.35	III
n_{AL}	Porosity of Attenuation Layer	1	I, II	0.3	II Following Rowe and Barakat (2021).
n_{AQ}	Porosity of Aquifer	1	All	0.3	

Uncertainty Quantified	$\theta_{GMB-GCL}$	Transmissivity of the contact region between GMB and GCL	$m^2.year^{-1}$	I	1.0315×10^{-3}	Shifted Lognormal	3.15×10^{-5}	1×10^{-3}	1.3	II, IV Based on a comprehensive review in Rowe (2012) and some following studies (AbdelRazek and Rowe, 2019a, 2019b; Rowe and Jabin, 2021, 2022; Rowe et al., 2024), as well as through a slight adjustment from the calibration in Rowe and Zhao (2023).
	$\theta_{GMB-CCL}$	Transmissivity of the contact region between GMB and CCL	$m^2.year^{-1}$	II	3.15	Shifted Lognormal	0	3.15	1.8	III Giroud and Bonaparte (1989) defined "good" and "poor" GMB-CCL contacts and Rowe (1998) related these two descriptors to transmissivity values of 1.6×10^{-8} m^2/s and 1×10^{-7} m^2/s. The high $\theta_{GMB-CCL}$ is mainly due to the irregularities at the interface. Expert advice by R. Kerry Rowe set the latter as the GM and adopted a high ln(GSD) to conservatively reflect the potential for poor contact or unenhanced construction conditions.
	$\theta_{GMB-NCL}$	Transmissivity of the contact region between GMB and NCL	$m^2.year^{-1}$	III	3.15	Shifted Lognormal	0	3.15	1.2	III Expert advice by R. Kerry Rowe based on the modelling assumption that the contact conditions and surface regularity between GMB and NCL are broadly comparable to those of GMB-CCL.
	k_a	Hydraulic conductivity of GCL in contact with GMB	$m.year^{-1}$	I	9.4×10^{-4}	Shifted Lognormal	0	9.4×10^{-4}	1.15	III, IV Expert advice by R. Kerry Rowe based on existing knowledge on k_{GCL} against leachate containing PFOS (Bouazza, 2021; Barakat et al., 2024) and the calibration in Rowe and Zhao (2023).
	k_b/k_a-1	k_b is hydraulic conductivity of GCL below wrinkles	1	I	7	Shifted Lognormal	0	7	0.3	

k_{CCL}	Hydraulic conductivity of CCL	$m.year^{-1}$	II	9.5×10^{-3}	Shifted Lognormal	3×10^{-3}	6.5×10^{-3}	1.1	III Expert advice by R. Kerry Rowe, based on the PFAS specific information in Yu Tan et al. (2022) and the non-PFAS specific information in Daniel (1993), Benson and Boutwell (2000), Zhai and Benson (2006), Agung et al. (2013), and Hamdi and Srasra (2013).
k_{NCL}	Hydraulic conductivity of NCL	$m.year^{-1}$	III	9.5×10^{-3}	Shifted Lognormal	1.5×10^{-3}	8×10^{-3}	2.0	III Expert advice by R. Kerry Rowe, based on the non-PFAS specific information in Daniel (1993), Cazaux and Didier (2002), and Hamdi and Srasra (2013).
k_{AL}	Hydraulic conductivity of Attenuation Layer	$m.s^{-1}$	I, II	1×10^{-7}	Shifted Lognormal	0	1×10^{-7}	1.15	II Based on a non-PFAS specific reference value in Schrefler and Delage (2013).
$\alpha_{L\text{-}AL}$ $\alpha_{T\text{-}AL}$	Dispersivity of Attenuation Layer	m	I, II	0.052	Shifted Lognormal	0	0.052	0.275	III Expert advice by R. Kerry Rowe, informed by data from Lal and Shukla (2004) and Mahdipanah et al. (2022).
$\alpha_{L\text{-}AQ}$	Longitudinal dispersivity of Aquifer	m	All	2	Shifted Lognormal	0	2	0.75	II, III Based on the data review in Anderson and Cherry (1979), Gelhar et al. (1992), and Schulze-Makuch (2005), as well as the data reliability classification in Zech et al. (2023). Only data of 'high' or 'moderate' reliability are considered.
$\alpha_{T\text{-}AQ}$	Transverse dispersivity of Aquifer	m	All	0.1	Shifted Lognormal	0	0.1	1.5	II, III Based on the data review in Gelhar et al. (1992) and Zech et al. (2019), as well as the data reliability classification in Zech et al. (2019). Data of all reliability levels are considered due to the scarcity of data.

1. For triangular distributions, the representative value is the geometric mean or an easy-to-use value close to it; for shifted lognormal distributions, the representative value is the geometric mean without shift, plus the shift.
2. See Section 4.2 for prototypical distributions and definitions of a, c, and b.
3. Where I or II is shown next to III or IV, both sources from the literature (I or II) and expert advice (III) or calibration (IV) were critical in determining the parameter in question.

Chapter 5
Deterministic Analyses of PFOS Transport through Liner Systems

---

5.1 Comparison between Numerical Solvers

Deterministic analyses provide a reference base for the probabilistic results presented later in this thesis. A comparison of predictions obtained with the principal numerical solver adopted in this thesis (SPAS/CONFEM) and with another solver, POLLUTE v7, for the RSc scenarios of the three designs, is summarised in Table 5.1. Note that the modelling by POLLUTE v7 was performed by Dr Farah B Barakat from Queen's University, Kingston. POLLUTE v7 is based on the 1½-D modelling of solute transport by the finite-layer method, which takes the leakage rate calculated from Rowe equation as a direct input (see Section 2.3.2). Key differences in the way the two solvers simulate the problem are in the estimation of the leakage rate, the representation of wetted distance, and the simulation of solute transport in the aquifer. Given the differences between the two solvers, they are not expected to yield identical results. However, the comparison aims to explore the proximity of these predictions and what may lie behind any differences.

As discussed earlier (Section 3.4.3 and Figure 3.4), three different ways of representing the wetted distance and the leakage pattern in the numerical solver of SPAS/CONFEM, have been used. In summary, under Approach 1, it is assumed that the wetted distance coincides with leak width: this is a reasonable assumption with GCL, given its small transmissivity and is hence adopted for the GCL design. The solutions of Water-Flow and Contaminant-Transport stages are coupled automatedly by SPAS. Under Approaches 2a and 2b, the wetted distance ($2a_0$) is calculated through Rowe equation (Eq. (3.4.1)) for both. Then, while under Approach 2a, the leakage rate (q_a) is calculated by Rowe equation (Eq. (A3.1.1)), under Approach 2b it is calculated by the Water-Flow solver of SPAS. Then a step-function profile of seepage velocity, based on the calculated $2a_0$ and q_a, is input into the Contaminant-Transport solver of SPAS. Given

relatively high transmissivities in CCL and NCL and more accurate SPAS leakage calculations compared to analytical approaches, Approach 2b is adopted for these two designs. Although Approach 2a was not ultimately used in the deterministic or probabilistic simulations, its predictions are shown in Table 5.1 for the purpose of comparison.

The differences in results shown in Table 5.1 originate from two stages of calculation: the water-flow calculation to obtain q_a and the contaminant-transport calculation to obtain $C_{aq\text{-}max}$. Comparing predictions of POLLUTE v7 and Approach 2a demonstrates that, even with the same q_a, $C_{aq\text{-}max}$ predicted by SPAS/CONFEM is about twice that given by POLLUTE. On the other hand, differences in $C_{aq\text{-}max}$ predictions of SPAS/CONFEM under Approaches 2a and 2b are obviously caused by different values of q_a.

The discrepancy in leakage rates (q_a) calculated by Eq. (A3.1.1) and SPAS/CONFEM (i.e., between Approaches 2a and 2b) is attributed to two main reasons, as reflected by Table 5.2. First, the Rowe equation assumes that the hydraulic conductivity of GCL+AL is controlled by the GCL. However, this equation becomes less accurate when the attenuation layer (AL) makes a significant contribution to the overall hydraulic conductivity of the liner, either because it is relatively thick or its hydraulic conductivity (k_{AL}) is low enough to affect the overall conductivity of the combined layers. This is the case for the GCL+AL liner design, and the effect of k_{AL} can be verified by increasing k_{AL} to 1×10^{-5} m/s from the present value (1×10^{-7} m/s) which leads to very similar q_a predictions by Approaches 2a and 2b (204.6 and 218.2). Second, Eq. (A3.1.1) is based on a wetted distance of $2a_0$ which may be an underestimate, as detailed in Appendix 3.1. In fact, the wetted distance is likely larger than $2a_0$. Since Eq. (A3.1.2) assumes a wetted distance of infinity, q_a is expected to be bracketed by the predictions of Eq. (A3.1.1) and Eq. (A3.1.2). As shown in Table 5.2, q_a predictions from SPAS do in fact fall between those of Eq. (A3.1.1) and Eq. (A3.1.2), except for GCL+AL with $k_{AL}=1\times10^{-7}$ m/s, which is due to the abovementioned first limitation of the equation. This is consistent with the above expectation.

A possible explanation for the lower peak concentrations predicted by POLLUTE compared to SPAS/CONFEM, even with the same leakage rate (q_a), lies in the inherent limitations of the 1½-D model under certain conditions. As demonstrated by El-Zein and Rowe (2008), POLLUTE v7 tends to underestimate contaminant concentrations

when either horizontal mixing in the aquifer is limited or when leakage is spatially concentrated beneath dense GMB defects. Under the former, the lack of transverse dispersion allows localized advective plumes to form, resulting in elevated concentrations beneath leaks; with the latter, localized advective fluxes can develop beneath the leaks. These effects may not be fully captured by the 1½-D model of POLLUTE.

Despite the result discrepancies between the two numerical solvers, they predict similar outcomes in terms of comparative performance of the three designs, with GCL+AL and CCL+AL yielding similar q_a and $C_{aq\text{-}max}$ and NCL outperforming both.

Table 5.1. Comparison between software and Approaches 1, 2a, & 2b for calculating RSc.

Software / Liner Design		POLLUTE (q_a calculated by Rowe Equation)	SPAS fully numerical (Approach 1)	SPAS part-analytical (Approach 2a; a_0 & q_a calculated by Rowe Equation)	SPAS part-analytical (Approach 2b; a_0 calculated by Rowe Equation)	Notes on wetted distance ($2a_0$)
GCL+AL	q_a (lphd)	94.1	**197.6**	94.1	197.6	$2a_0$=0.26m, close to the leak width 2b=0.2m
	$C_{aq\text{-}max}$ (ng/l)	131.0	**403.6**	248.5	483.1	
CCL+AL	q_a (lphd)	94.5	222.8	94.5	**222.8**	$2a_0$=6.30m >> 2b=0.2m
	$C_{aq\text{-}max}$ (ng/l)	131.7	9.46	209.6	**463.4**	
NCL	q_a (lphd)	37.2	93.8	37.2	**93.8**	$2a_0$=6.28m >> 2b=0.2m
	$C_{aq\text{-}max}$ (ng/l)	27.2	4.35	56.9	**206.0**	

Table 5.2. Comparison between q_a predictions of Rowe equations and SPAS for different designs and different values of k_{AL}

How to calculate q_a / Liner Design		Eq. (A3.1.1)	Eq. (A3.1.2)	SPAS
GCL+AL	$k_{AL}=1\times10^{-7}$ m/s	94.1	108.7	197.6
	$k_{AL}=1\times10^{-5}$ m/s	204.6	220.3	218.2
CCL+AL	$k_{AL}=1\times10^{-7}$ m/s	94.5	326.4	222.8
	$k_{AL}=1\times10^{-5}$ m/s	94.9	327.8	224.3
NCL		37.2	296.0	93.8

5.2 Deterministic Analysis on PFOS Contamination through Liner Systems

As specified in Chapters 3 and 4, the deterministic analyses are conducted based on a) the models of liner systems in Figure 3.2, b) the SPAS/CONFEM solver with Approaches 1 for GCL+AL and 2b for CCL+AL and NCL, and c) the representative values of input parameters in Table 4.4. Three different CQA scenarios are considered, with a wrinkle length per hectare (L_w, m/ha) set at 475, 325, 75, and 0 for Sc-, RSc, Sc+, and RSc0, respectively.

Key results from deterministic analyses are summarized in Table 5.3, including the leakage rate (q_a), the maximum PFOS concentration in the aquifer ($C_{aq\text{-}max}$), the time (t_{max}) it takes to reach $C_{aq\text{-}max}$, and the horizontal position (x_{max}) at which $C_{aq\text{-}max}$ occurs. The change of PFOS concentration (C_{PFOS}) against time (C_{PFOS} vs t), horizontal dimension (C_{PFOS} vs x), and vertical dimension (C_{PFOS} vs y), as well as the horizontal profile of downward Darcy velocity (v_{ay} vs x), are given in Figures 5.1~5.8. Note that the two groups of Figures, i.e., 5.1~5.4 and 5.5~5.8, are based on the same data, but re-arranged to better highlight the effects of CQA scenarios (5.1~5.4) and liner designs (5.5~5.8), respectively. Identifying $C_{aq\text{-}max}$ (shown in Table 5.3) requires a search across t, x, and y. This is done iteratively by exploring along one dimension (e.g., x), identifying location of maximum concentration (x_{max}), then moving to the next dimension (e.g., y) and so on. Therefore, Figures 5.1~5.3 and 5.5~5.7 show C_{PFOS} along any dimension at point identified through this process (e.g., C_{PFOS} versus y at t_{max} and x_{max}). Note that y_{max} has been consistently found to be at the top of the aquifer. Based on this, values of $C_{aq\text{-}max}$, t_{max}, and x_{max} are summarized in Table 5.3.

The "v_{ay} vs x" curves in Figures 5.4 and 5.8 illustrate the leakage patterns calculated by SPAS as part of Approach 1, which provide a more realistic representation of the flow field. Figure 5.9 compares the curves from Figure 5.4 with the artificially prescribed step-function leakage patterns constructed by "SPAS-derived magnitude of leakage rate" + "analytically determined wetted distance", which is part of Approach 2b. As described in Section 3.4.3 for the GCL+AL design, the flow field shown in Figure 5.4 (a) is automatically incorporated into the solute transport modelling (i.e., Approach 1). The close similarity between the leakage patterns of Approaches 1 and 2b, as well as their wetted distances that are close to the leak width (2b=0.2m), as shown in Figure 5.9 (a1), (a2), (a3), further supports the rationale for using Approach 1 for the GCL+AL design.

In contrast, for the CCL+AL and NCL designs, the flow fields coupled with the solute transport modelling are not those shown in Figures 5.4 (b) and (c), but rather the step-function patterns corresponding to Approach 2b in Figure 5.9 (b1), (b2), (b3) and (c1), (c2), (c3). This compromise is necessary to ensure a more rational representation of the contact between waste and liners in solute transport modelling for the CCL+AL and NCL designs (see the explanation in Section 3.4.3). The necessity of using Approach 2b can be further confirmed by $C_{aq\text{-}max}$ of the CCL+AL and NCL cases based on Approach 1 (Table 5.1), which is obviously a substantial underestimation of $C_{aq\text{-}max}$.

Table 5.3. Summary of key output from deterministic analyses for the three liner designs under different CQA.

		Sc-	RSc	Sc+	RSc0
GCL+AL	q_a (lphd)	300.3	197.6	45.5	0
	$C_{aq\text{-}max}$ (ng/l)	508.5	403.6	176.2	0.55
	t_{max}* (years)	145	155	145	585
	x_{max}** (m)	391	386	335	400
CCL+AL	q_a (lphd)	245.8	222.8	75.4	0
	$C_{aq\text{-}max}$ (ng/l)	488.1	463.4	203.5	0.48
	t_{max} (years)	180	160	155	695
	x_{max} (m)	396	391	340	400
NCL	q_a (lphd)	95.5	93.8	60.7	0
	$C_{aq\text{-}max}$ (ng/l)	208.7	206.0	176.9	0.024 at 1000yr
	t_{max} (years)	525	420	205	>1000yr
	x_{max} (m)	396	391	340	400

* Time to reach $C_{aq\text{-}max}$

** Horizontal position at which $C_{aq\text{-}max}$ occurs

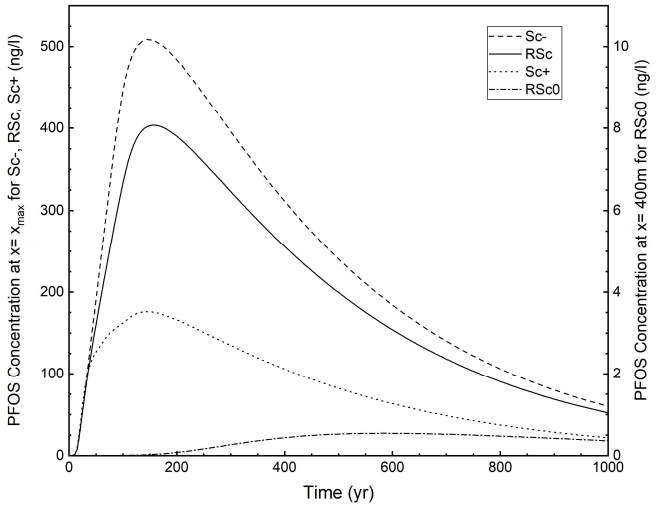

(a) GCL+AL

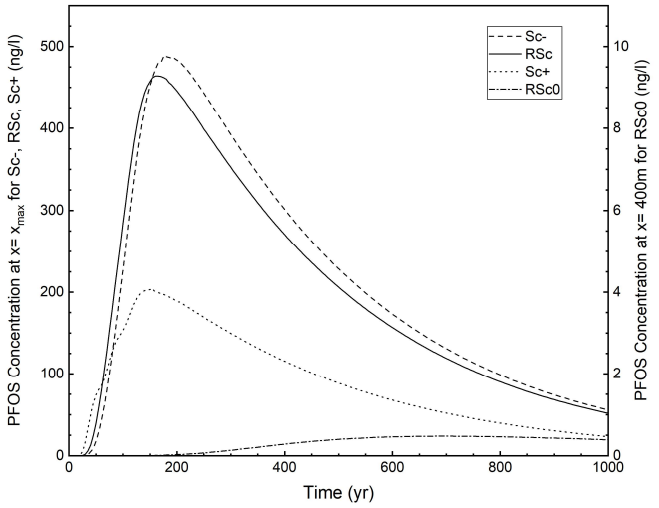

(b) CCL+AL

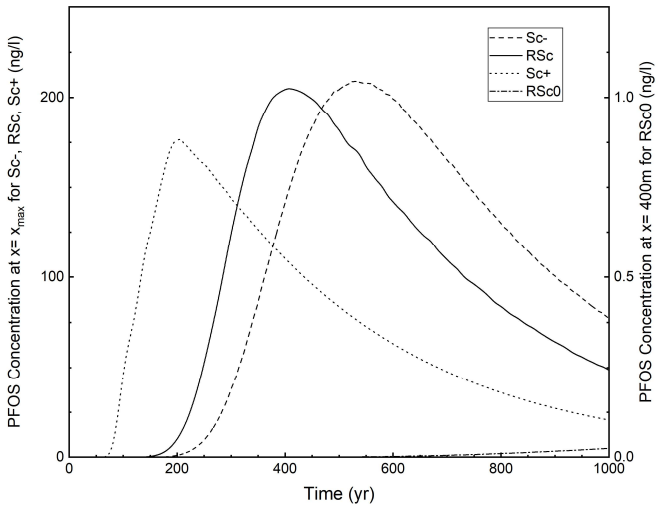

(c) NCL

Figure 5.1. The effect of CQA: change of PFOS concentration (C_{PFOS}) against time (C_{PFOS} vs t at $x=x_{max}$ and the top of aquifer).

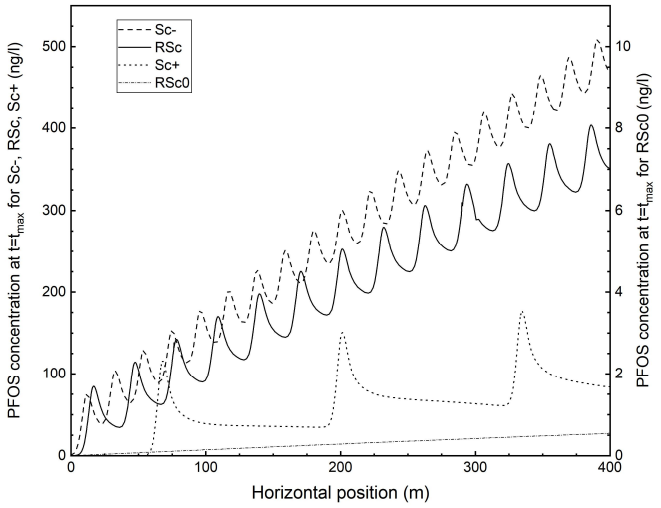

(a) GCL+AL

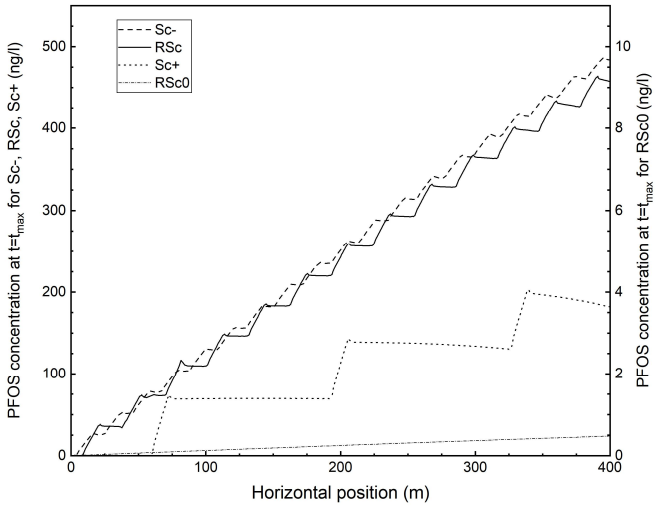

(b) CCL+AL

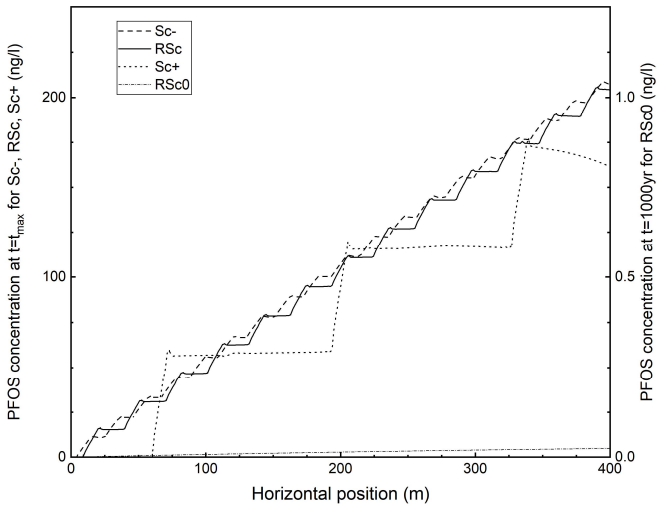

(c) NCL

Figure 5.2. The effect of CQA: change of PFOS concentration (C_{PFOS}) against horizontal dimension (C_{PFOS} vs x at $t=t_{max}$ and the top of aquifer).

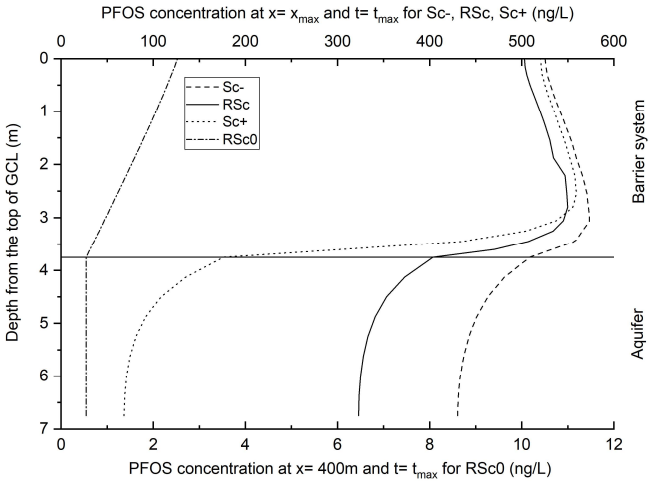

(a) GCL+AL

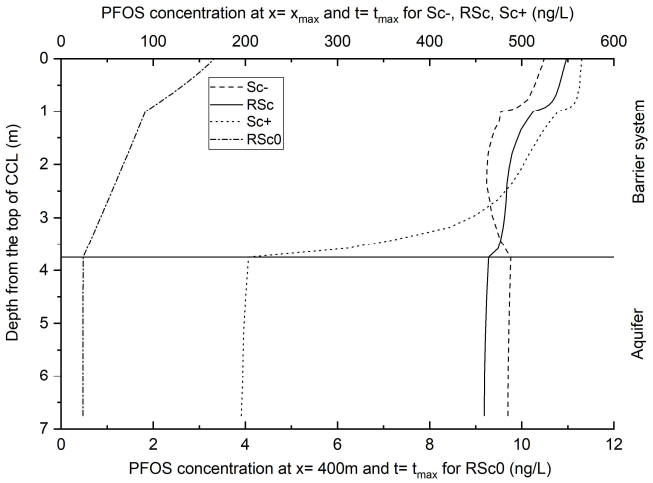

(b) CCL+AL

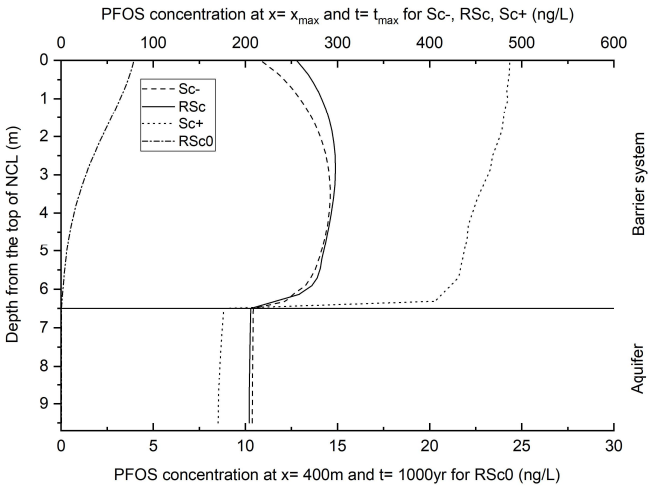

(c) NCL

Figure 5.3. The effect of CQA: change of PFOS concentration (C_{PFOS}) against vertical dimension (C_{PFOS} vs y at $x=x_{max}$ and $t=t_{max}$).

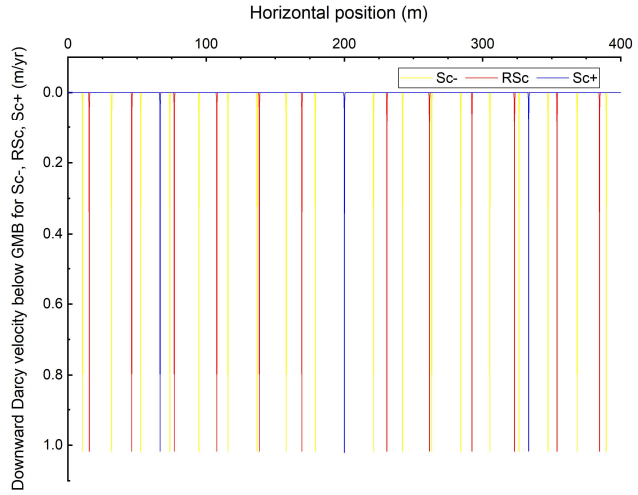

(a) GCL+AL

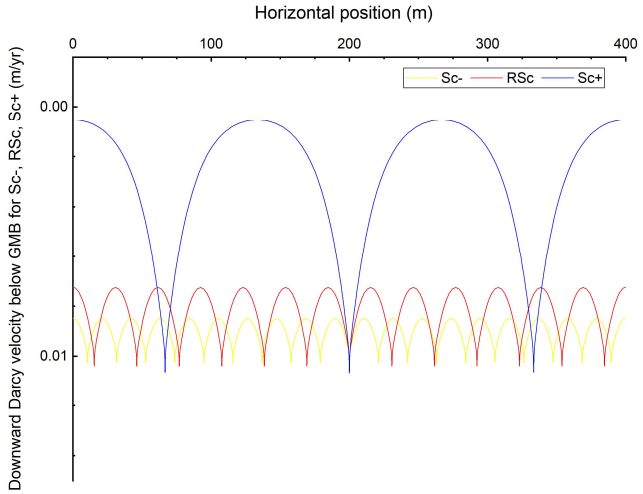

(b) CCL+AL

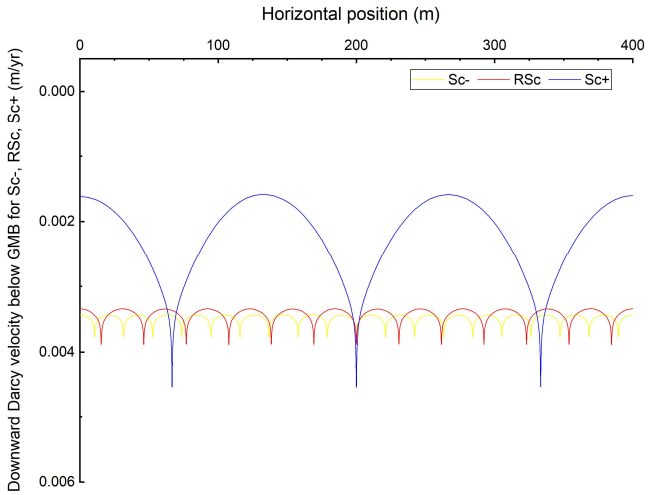

(c) NCL

Figure 5.4. The effect of CQA: horizontal profile of downward Darcy velocity below GMB (v_{ay} vs x below GMB).

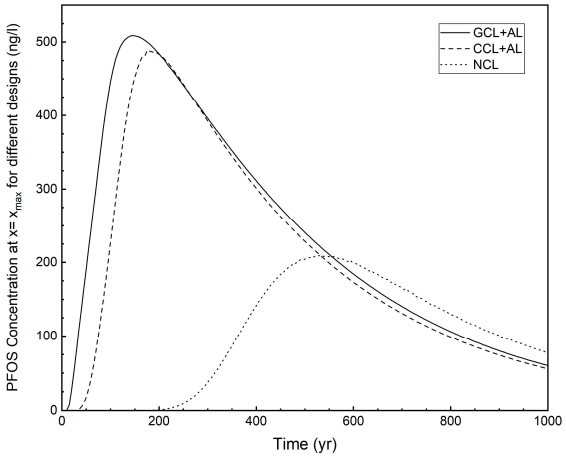

(a) Sc-

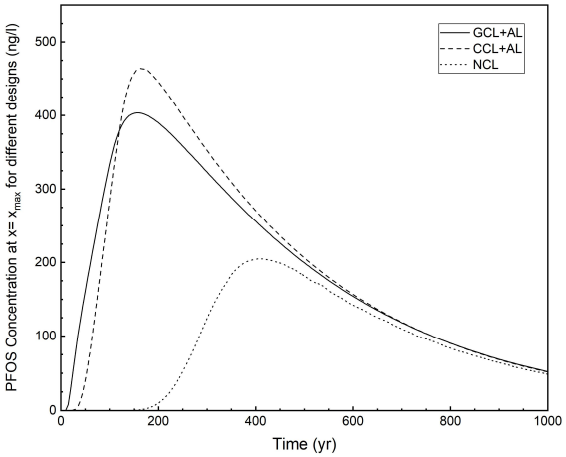

(b) RSc

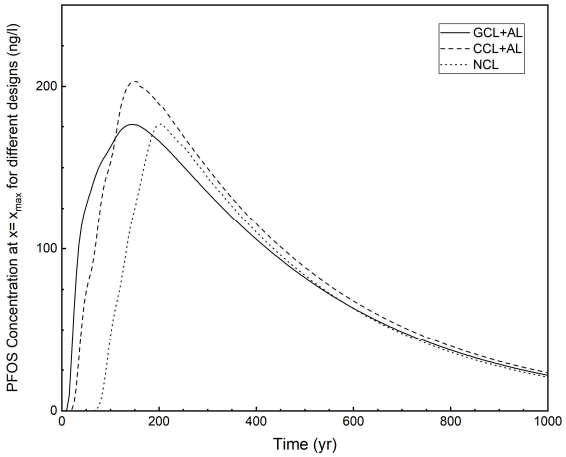

(c) Sc+

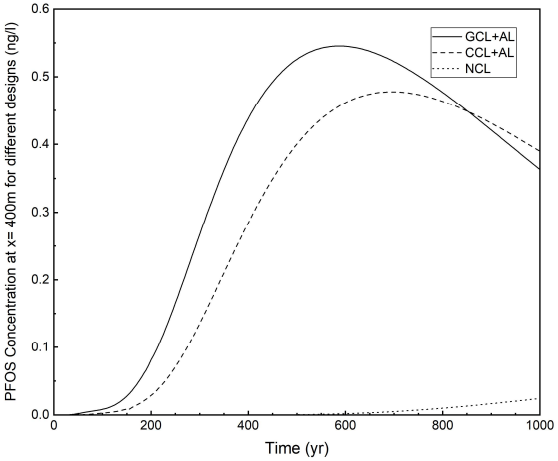

(d) RSc0

Figure 5.5. The effect of liner design: change of PFOS concentration (C_{PFOS}) against time (C_{PFOS} vs t at $x=x_{max}$ and the top of aquifer).

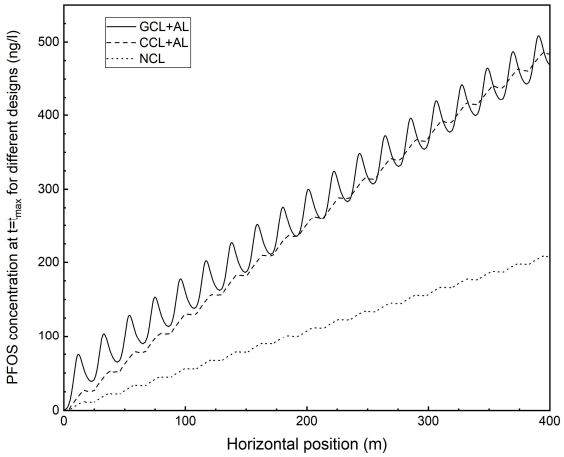

(a) Sc-

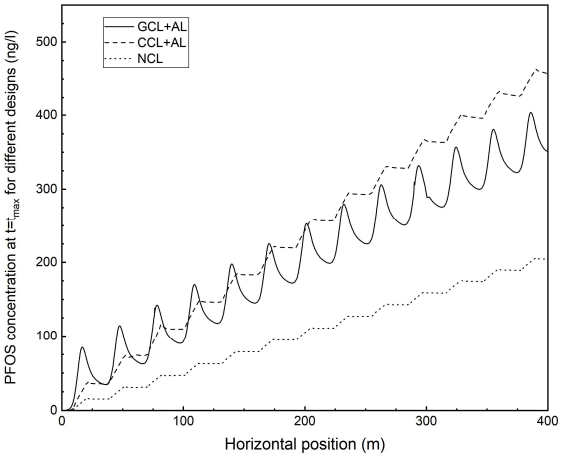

(b) RSc

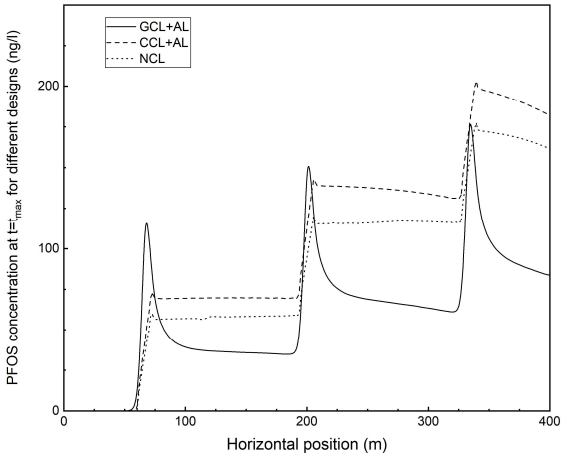

(c) Sc+

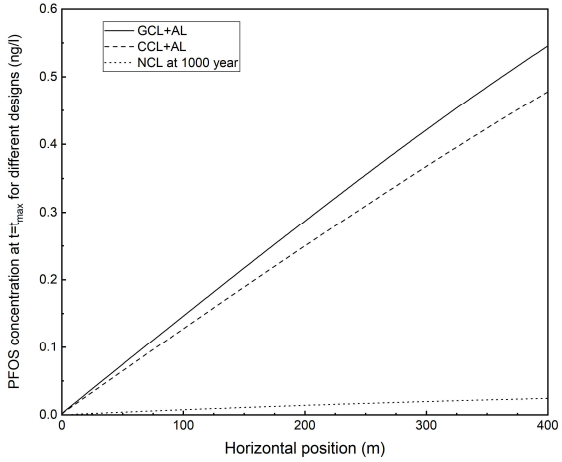

(d) RSc0

Figure 5.6. The effect of liner design: change of PFOS concentration (C_{PFOS}) against horizontal dimension (C_{PFOS} vs x at $t=t_{max}$ and the top of aquifer).

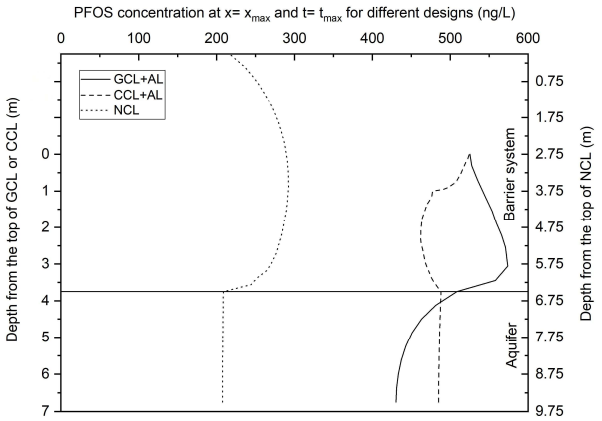

(a) Sc-

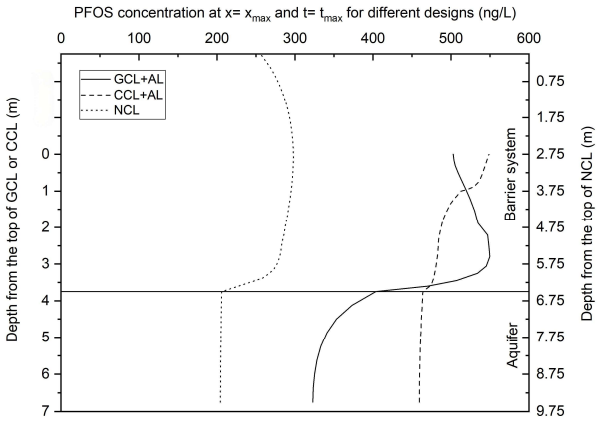

(b) RSc

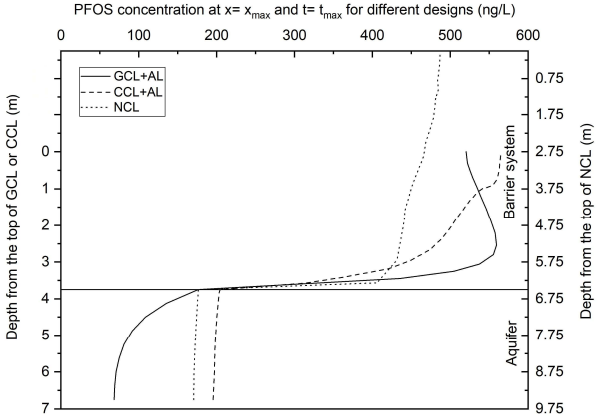

(c) Sc+

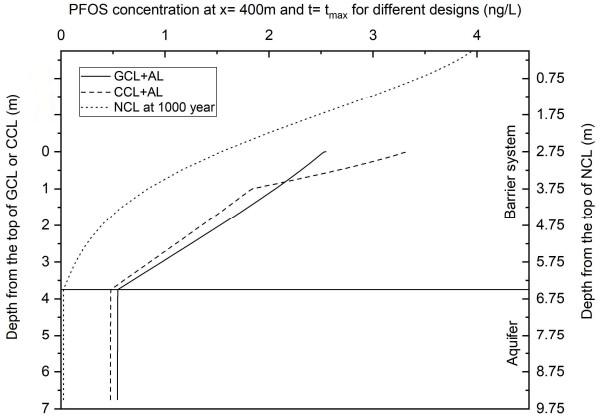

(d) RSc0

Figure 5.7. The effect of liner design: change of PFOS concentration (C_{PFOS}) against vertical dimension (C_{PFOS} vs y at $x=x_{max}$ and $t=t_{max}$).

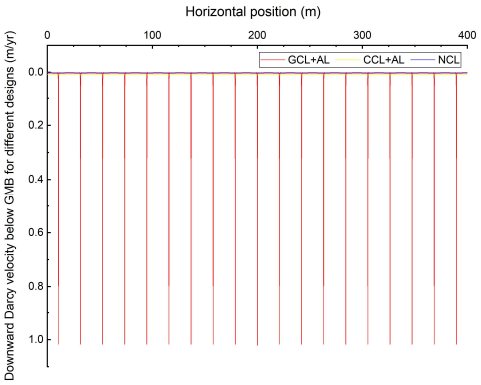

(a1) Sc-: Full dimension

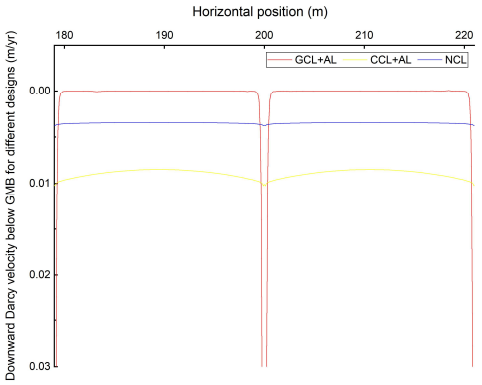

(a2) Sc-: Around one leak

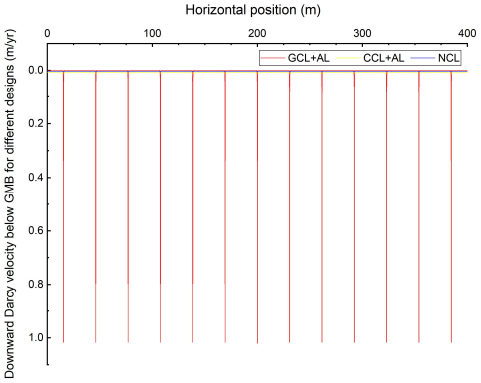

(b1) RSc: Full dimension

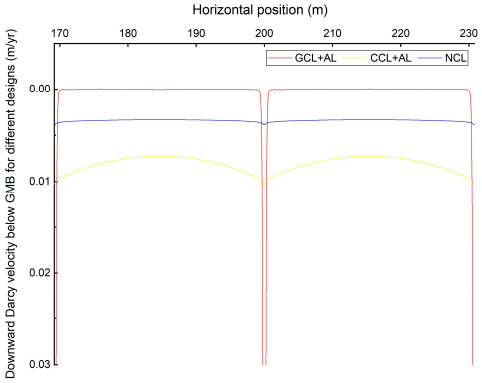

(b2) RSc: Around one leak

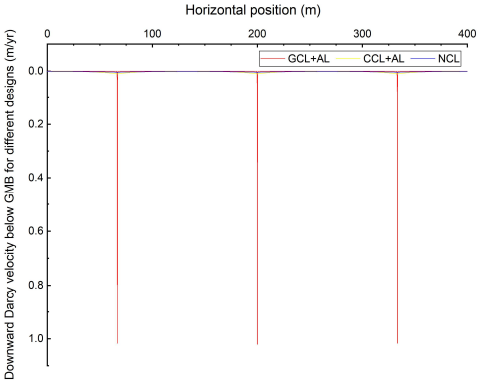

(c1) Sc+: Full dimension

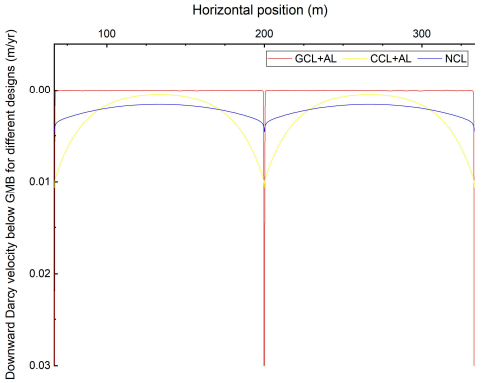

(c2) Sc+: Around one leak

Figure 5.8. The effect of liner design: horizontal profile of downward Darcy velocity below GMB (v_{ay} vs x below GMB).

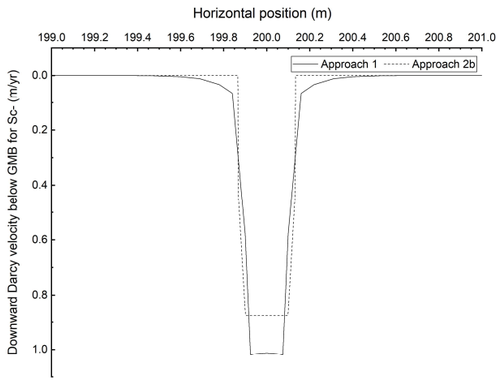

(a1) GCL+AL: Sc- (amplified)

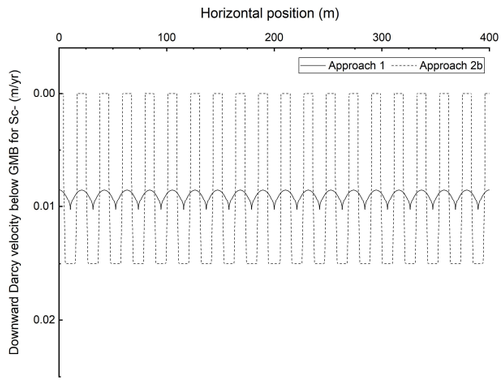

(b1) CCL+AL: Sc-

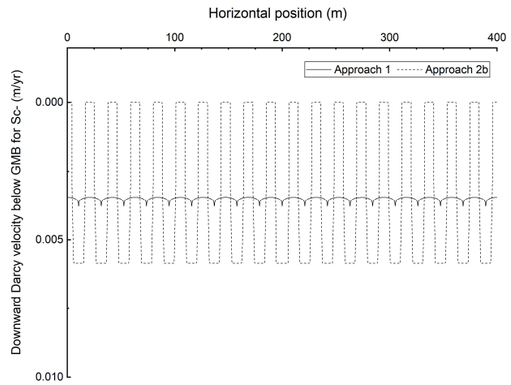

(c1) NCL: Sc-

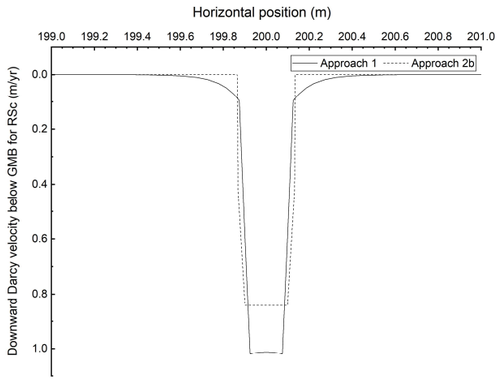

(a2) GCL+AL: RSc (amplified)

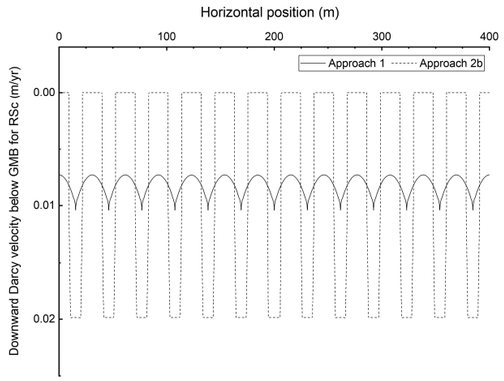

(b2) CCL+AL: RSc

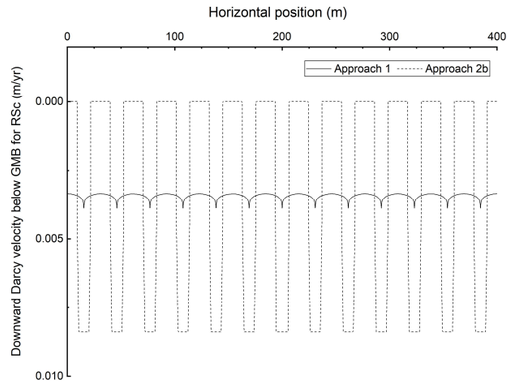

(c2) NCL: RSc

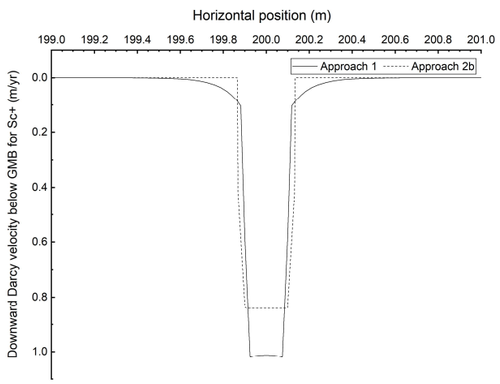

(a3) GCL+AL: Sc+ (amplified)

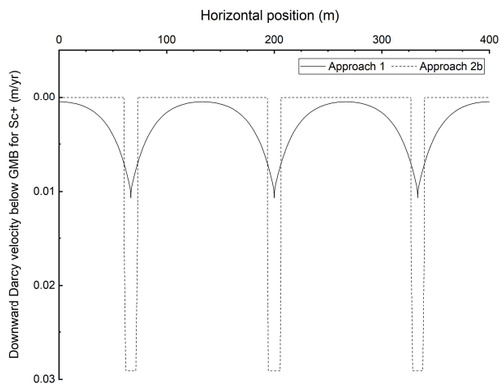

(b3) CCL+AL: Sc+

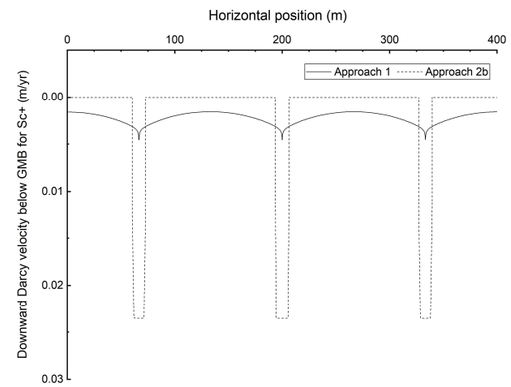

(c3) NCL: Sc+

Figure 5.9. Comparison of leakage patterns obtained using Approach 1 (numerically generated by SPAS) and Approach 2b (idealised step-function).

5.2.1 General spatial and temporal trends

The curves of "C_{PFOS} vs y" (Figures 5.3 and 5.7) show contamination profiles across the depth, at a location along the x axis approximately below the rightmost leak for the three diffusion-advection scenarios (Sc-, RSc, Sc+) and at the rightmost end for the pure-diffusion scenario (RSc0). In the graphs of Sc-, RSc, and Sc+, C_{PFOS} at y=0 represents the concentration at the top of the GCL/CCL/NCL as well as in the waste itself, since the two are directly connected by the presence of leaks in these three scenarios. These values show that, after the period required to reach the peak, the initial PFOS concentration in the waste (900 ng/l) is projected to significantly decrease to around 500 ng/l or even lower, due to the continuous leachate drainage and leakage. On the other hand, under RSc0, no leaks are present and C_{PFOS} at y=0 represents concentrations at the top of GCL/CCL/NCL, just under the intact GMB (less than 2~4 ng/l, see Figure 5.7 (d)). These are, as expected, significantly smaller than the PFOS concentrations in the waste (not shown in the figures), and an indicator of the excellent insulation performance of the liner under these idealised conditions.

Travelling further down in depth below the GCL, C_{PFOS} increases before declining, hence forming a bulge in the curve (Figure 5.3 (a)). The increase in C_{PFOS} in the upper part is due to the declining pollution load at the top, combined with the advective flux due to leakage, and the slow diffusion process in the AL beneath the GCL. On the other hand, high levels of dispersion and horizontal advection in the aquifer exert a draining effect on PFOS in the AL, and lead to the decline in concentration below the peak in the bulge. A similar pattern is observed in NCL for Sc- and RSc (Figure 5.3 (c)). Under Sc+, leakage is smaller in NCL, decline in concentration in the waste hence slower, and this is reflected in a monotonic variability in the y direction and the absence of a bulge.

In the case of CCL+AL, the pattern of variability is reversed, compared to GCL and CCL, with the concentration declining with depth (Figure 5.3 (b)). This is likely due to the relative importance of the rate of drainage and leakage in the waste, compared to the diffusion processes redistributing the contaminant below it. A change in the slope of C_{PFOS} versus y curve at the interface between CCL and AL is clearly visible, reflecting the change in diffusion coefficients in the two layers.

Note that in all scenarios and all designs, there is a visible change in the slope of C_{PFOS} versus y curve at the interface between the AL and the aquifer. This is due to the much

higher dispersion in the latter compared to the former. In addition, it is clear that $C_{aq\text{-}max}$ always occurs at the top of the aquifer. This is expected because the source of contamination is above the aquifer and there is significant dispersion, redistributing PFOS in the y direction in the aquifer, and preventing any accumulation below the AL-aquifer interface.

"C_{PFOS} vs t" (Figures 5.1 and 5.5) shows that, contamination levels in the aquifer reach a peak after a certain period, then decline, under all four scenarios. The initial increase is due to the transport of PFOS from the waste to the aquifer, by advection and/or diffusion. At the same time, due to the finite mass of PFOS specified in the waste, contaminant load in the waste declines and this is reflected, after some delay, in the aquifer. The only exception is the NCL-RSc0 (see Figure 5.5 (d)), in which concentration doesn't reach its peak even after 1000 years, due to the extremely slow transport of PFOS by pure diffusion in this case.

As shown by the curves of horizontal change of concentration ("C_{PFOS} vs x", Figures 5.2 and 5.6), there is an overall increasing trend of C_{PFOS} with distance from the upgradient to the downstream edge of the landfill, which is primarily due to advective horizontal transport caused by groundwater flow. The oscillations, on the other hand, reflect the effect of leakage spikes under GMB defects. In RSc0, no defects are present, and no spikes are observed. The rightmost peak in the curve represents the horizontal maximum, corresponding to a position around the rightmost leak in the GMB. This position is also specified in Table 5.3 by x_{max}.

The curves of downward Darcy velocity below GMB (Figures 5.4 and 5.8) reflect the horizontal distribution of leakage rate. As expected, there are significantly high levels of leakage below the leaks in GMB, which are more extreme for GCL, and much lower ones between them. For GCL+AL cases (Figure 5.4 (a), and red curves in Figure 5.8 (a2), (b2), (c2)), the wetted distance is small and in fact close in value to the leak widths (Figure 5.9 (a1), (a2), (a3)). On the other hand, it can be seen from curves of v_{ay} for CCL+AL and NCL cases (Figure 5.4 (b), (c), and yellow and blue curves in Figure 5.8 (a2), (b2), (c2)) that the leakage spikes below adjacent defects interact with each other even under the scenario with the most sparse defects (Sc+), which means that the actual wetted distance covers all the range between leaks, reinforcing the need, discussed earlier, for using Approach 2b.

5.2.2 Effects of CQA and liner designs

Table 5.3 and Figures 5.1~5.4 and 5.5~5.8 show that, in the pure-diffusion cases (RSc0), values of $C_{aq\text{-}max}$ (0.55 ng/l for GCL+AL, 0.48 ng/l for CCL+AL, 0.024 ng/l for NCL) are two to three orders of magnitude lower than those of the advection-diffusion cases and occur at a much later time (585 years, 695 years, and beyond 1000 years, respectively). This confirms the effectiveness of a single-liner system in containing PFOS, both under conditions of a) GCL or CCL plus relatively thin attenuation layer and b) relatively thick NCL, but only if the GMB remains free of defects. Such a contrast also suggests that advection is the dominant process in PFOS transport through the liner system and causes the vast majority of its impact in the aquifer, while diffusion appears to have a much smaller effect.

Effects of CQA

Comparing $C_{aq\text{-}max}$ between Sc-, RSc and Sc+ highlights the importance of construction and monitoring quality. As expected, applying ELL and enhancing CQA, reflected by a smaller wrinkle length per hectare and thus a smaller density of defects on the GMB in 2D, reduces leakage and hence $C_{aq\text{-}max}$. This importance is clearly manifested for the GCL+AL model among Sc- (q_a=300.3 lphd, $C_{aq\text{-}max}$=508.5 ng/l), RSc (197.6 lphd, 403.6 ng/l), and Sc+ (45.5 lphd, 176.2 ng/l). For the CCL+AL model, the difference between Sc- (245.8 lphd, 488.1 ng/l) and RSc (222.8 lphd, 463.4 ng/l) is not significant, while Sc+ (75.4 lphd, 203.5 ng/l) still leads to an obviously better performance. This may imply that for the CCL+AL design, enhancing CQA is more effective than just applying ELL. In contrast, for the NCL model, although $C_{aq\text{-}max}$ is still sensitive to ELL and CQA, the effect is not very significant (Sc-: 95.5 lphd, 208.7 ng/l; RSc: 93.8 lphd, 206.0 ng/l; Sc+: 60.7 lphd, 176.9 ng/l).

Since the advection appears to be the core PFOS transport process in the simulations, the effect of CQA follows a causal chain linking wrinkle length (defect density), leakage rate, and contaminant concentration. For the GCL+AL model, the leakage rate (300.3 lphd, 197.6 lphd, 45.5 lphd) is proportional to the wrinkle length (475 m/ha, 325 m/ha, 75 m/ha), because the narrow-wetted distance around defects leads to no interaction between adjacent leakage spikes, which is clearly reflected in Figure 5.4 (a). In addition, the relationship between PFOS concentration and leakage rate is positive but not necessarily linear. For the CCL+AL model and the NCL model, the smaller sensitivity

of PFOS concentration to CQA may be attributed to the lower sensitivity of leakage rate to wrinkle length (defect density), which is more obvious when defect density is high. This is because for these two designs, the wetted distance around defects is relatively large, even to the extent of covering the full distance between defects (Figure 5.4 (b), (c)), and denser defects will lead to greater overlaps (interactions) between adjacent leakage spikes that are much broader and lower than those in GCL+AL cases. This overlap also affects the heights of the "rectangles" used to approximate seepage under defects using Approach 2b (Figure 5.9 (b1), (b2), (b3) for CCL+AL and Figure 5.9 (c1), (c2), (c3) for NCL).

The time to reach $C_{aq\text{-}max}$ (t_{max}) for different CQAs in the GCL+AL design tends to be similar (around 150 years, Figure 5.1 (a)). However, counterintuitively, in CCL+AL t_{max} decreases slightly as CQA is enhanced and this effect becomes even more pronounced in NCL (Figure 5.1 (b), (c)). This is due to a limitation of Approach 2b that can be clearly seen in Figure 5.9. The height of the rectangles in Approach 2b is determined by the surface area under the v_{ay} vs x curves and wetted distance, rather than the maximum value of v_{ay}. As a result, as construction quality is upgraded from Sc- to RSc to Sc+, while the leakage rate, surface area under the curve declines and the number of rectangles decreases, the height of each rectangle increases. This can be seen by comparing Figure 5.9 (b1), (b2), (b3) for CCL+AL and Figure 5.9 (c1), (c2), (c3) for NCL. This increase in the height of rectangle, as we move from Sc- to RSc and the Sc+, causes a corresponding decrease in breakthrough time, most clearly visible in Figure 5.1 (c) for NCL, while leakage rate and $C_{aq\text{-}max}$ decrease as expected.

Effects of Liner Design

Next, the performances of different designs are compared. Under Sc- and RSc, the GCL+AL and CCL+AL designs yield comparable $C_{aq\text{-}max}$ (Sc-: 508.5 ng/l for GCL+AL versus 488.1 ng/l for CCL+AL; RSc: 403.6 ng/l versus 463.4 ng/l). NCL design appears to perform much better with 208.7 ng/l under Sc- and 206.0 ng/l under RSc. This is understandable since in the NCL design adopted herein, the hydraulic conductivity of NCL is configured to be sufficiently low to approach that of the CCL although it is called "natural clay liner", while the thickness of NCL is much greater. On the other hand, under Sc+, with CQA enhanced to "excellent" and ELL applied, $C_{aq\text{-}max}$ for the three designs are close (differing by less than 15%) even if leakage rates continue to be significantly different (GCL+AL<NCL<CCL+AL).

Several studies have compared the performance of GCL and CCL in preventing contaminant migration from landfills to aquifers, which can serve as additional references for the findings herein. Barakat and Rowe (2025) conducted numerical simulations of PFOA transport through different composite liners, and found that, when the primary liner consists of GMB+GCL, the best performance of double liner is achieved with a secondary liner of GMB+GCL+CCL, followed by GMB+GCL and then GMB+CCL. Zerenduoji and Yu (2024) and Hu and Yu (2024) both used numerical modelling to evaluate different liner configurations. Both studies found that adding a GCL beneath the GMB significantly reduced leachate flux and peak chloride concentrations in the aquifer, with the GMB+GCL+CCL configuration outperforming simpler alternatives such as GMB+CCL or CCL alone. Kandris and Pantazidou (2012) compared GMB+GCL and GMB+CCL systems regarding their effectiveness in limiting the migration of chloride and benzene, and concluded that GMB+CCL generally offers superior containment, particularly for organic contaminants such as benzene, though GCLs may offer more consistent quality and easier installation. Xie et al. (2009) emphasized that GCLs provide better control of diffusion and adsorption, particularly for hydrophilic organics, compared to CCLs. While direct comparisons involving NCL are limited, it is sometimes used as a barrier against contamination due to its naturally low permeability. However, its performance is highly site-specific and less consistent than engineered liners. Overall, the literature suggests that the performance of GCLs and CCLs varies depending on the context, with each outperforming the other in certain cases; overall, their effectiveness is comparable under controlled conditions, with GCLs offering practical advantages. This is generally consistent with findings in this chapter.

5.2.3 Comparison against drinking water guidelines/standards

$C_{aq\text{-}max}$ predictions in Table 5.3 are compared to four drinking water guidelines/standards: 4 ng/l (USEPA), 70 ng/l (NHMRC), 100 ng/l (EurEau), and 600 ng/l (Health Canada) (see Section 2.2.1.3 for details). Note that Canada and Australia have initiated steps to revise their existing regulatory frameworks, indicating a trend towards stricter control of PFOS in drinking water.

The $C_{aq\text{-}max}$ predicted under RSc0 scenario assuming no leakage (0.55 ng/l in GCL+AL model, 0.48 ng/l in CCL+AL model, 0.024 ng/l in NCL model) is smaller than the most stringent standard, indicating that a single-liner system with an intact GMB may serve as an effective barrier to PFOS.

However, in the presence of defects, $C_{aq\text{-}max}$ values from deterministic analyses under Sc-, RSc and Sc+ indicate a much more negative evaluation of the ability of single-liner systems to contain PFOS. In each of the three scenarios for each of the three liner designs, $C_{aq\text{-}max}$ remains higher than all guidelines/standards except the Canadian one, and significantly higher than the stricter US one. This is true for even the best achievable outcomes among all cases considered in this chapter, i.e., those obtained when ELL and excellent CQA (Sc+) are applied or when the NCL design is adopted, which mean $C_{aq\text{-}max}$ of 170~200 ng/l. This is consistent with earlier findings by Rowe and Barakat (2021), i.e., single-liner systems containing GMB+GCL+AL, even under excellent quality construction, may not be sufficient to protect groundwater from PFOS contamination under landfills unless the PFOS concentration in the landfill is substantially lower than that assumed or there is a substantially higher level of natural attenuation than that considered in this study.

It's important to reiterate here that the results presented in this chapter are based on deterministic analyses and are hence preliminary, prior to the fully probabilistic, and more representative results presented in Chapter 7. Nevertheless, the following preliminary conclusions can be made so far:

1) PFOS transport through single-liner systems is dominated by advection over diffusion, and the presence of GMB defects, serving as the main leaking channel, severely compromises containment performance.
2) The maximum PFOS concentration in the aquifer tends to happen at the top of the aquifer and approximately below the rightmost leak on GMB; as expected, the concentration first increases to a peak level, then gradually declines, with the time to reach the peak to be about 150 years for the GCL+AL design, 170 years for the CCL+AL design, and longer for the NCL design.
3) The performances of liner designs of GCL+AL and CCL+AL are significantly improved by applying ELL and enhancing CQA for the containment of PFOS, while the NCL design is much less sensitive to these two interventions. Generally speaking, the performances of GCL+AL and CCL+AL are comparable, but both are outperformed by NCL. It is important to note here, that NCL requires favourable conditions to exist on site which is not always

possible. The prior site requirements for GCL and CCL designs are far less stringent by comparison.

4) Except in pure-diffusion scenarios, all designs exceed the US, Australian, and EU drinking water guidelines/standards, approaching acceptability only under the Canadian guideline. Even under excellent construction, single-liner systems may be insufficient for PFOS control unless source concentrations are lower or natural attenuation is stronger.

5.3 Preliminary Sensitivity Analysis (Individual-parameter MCS)

Sensitivity analysis of $C_{aq\text{-}max}$ to different variables is conducted in two stages in this thesis. A preliminary analysis is first conducted through a set of consecutive MCS in which only the variable in question is uncertain (1D-MCS or 2D-MCS), as detailed in Section 3.5.2.3. The aim of this analysis is to identify all variables whose uncertainty has little influence on the results. These variables are treated as certain in the subsequent multi-dimensional PCE-enhanced MCS which would make it more computationally efficient at less cost to accuracy. Results of this preliminary analysis are reported in this chapter, since they are a necessary preamble to the multi-dimensional PCE-enhanced MCS. The second stage of sensitivity analyses is conducted as part of the PCE-enhanced MCS, through Sobol' indices of all variables included as uncertain, and will be reported in Chapter 7.

This preliminary sensitivity analysis is conducted only for RSc. Tables 5.4, 5.5, and 5.6 show the range of variance of $C_{aq\text{-}max}$ generated by the MCS, corresponding to the selected variance of each uncertain input variable (or pairs of variables). The frequency distributions and scatterplots of $C_{aq\text{-}max}$ generated by these MCS are given in Figures 5.10, 5.11, and 5.12. A wider range of $C_{aq\text{-}max}$ caused by an uncertainty is considered to indicate greater sensitivity to the variable.

Figure 5.10 shows that all distributions of $C_{aq\text{-}max}$ based on RSc of the GCL+AL model have a well-defined direction of variability with each of the considered input variables. As expected, $C_{aq\text{-}max}$ increases with increasing hydraulic pressure (ΔH), frequency (L_w) and width (2b) of defects, PFOS initial concentration (C_{b0}) in the waste, hydraulic conductivities in the attenuation layer (k_{AL}) and in the GCL under intact (k_a) and defective (k_b) parts of the GMB. A notable point is that the ratio p_0/C_{b0} determines the

equivalent height of leachate (H_f) (see Eq. (3.2.12)), which characterises the total initial PFOS load at the source, assuming that PFOS all exists in the form of leachate at concentration C_{b0}. Consequently, increasing p_0/C_{b0} without changing C_{b0} only slightly increases $C_{aq\text{-}max}$ and delays t_{max}, as shown by the weak correlation in Figure 5.10(e), but its main effect is to slow the post-peak decline, leading to a longer period during which the aquifer concentration remains relatively high. The declining trends observed for Darcy velocity in the aquifer ($V_{ax\text{-}in}$), thicknesses of attenuation layer (T_{AL}) and aquifer (T_{AQ}) and dispersivities in attenuation layer (α_{AL}) and aquifer ($\alpha_{L\text{-}AQ}$ and $\alpha_{T\text{-}AQ}$) are also expected.

Somewhat counterintuitive, however, is the trend of decreasing $C_{aq\text{-}max}$ with transmissivity θ, albeit the change is small (≈25 ng/l). An increase in θ causes wider horizontal spread of leachate around GMB defects in the transmissive layer between GMB and GCL, leading to both a wider wetting area and a higher overall leakage rate. However, the wider wetting area can be underestimated by SPAS because the direct contact between GCL and the waste is assumed to be only within 2b when solving the DAE, which reduces the sensitivity of $C_{aq\text{-}max}$ to θ. This assumption is acceptable because when a GCL is used, θ is small and the resulting wetted area is only slightly larger than the width of the leak. Meanwhile, the higher overall leakage is captured by SPAS and will lead to a faster horizontal flow and thus a higher dispersion in the aquifer, which explains the slight negative correlation between $C_{aq\text{-}max}$ and θ observed in our modelling.

The range of variance of $C_{aq\text{-}max}$ caused by one uncertainty reflects the latter's importance. Hence, the ratio of this range to $C_{aq\text{-}max}$ calculated from the deterministic analysis provides a relative measure of the influence of uncertainty for each variable. Table 5.4 shows that variables C_{b0} & p_0/C_{b0}, k_a & k_b/k_a-1, and L_w have the largest influence on $C_{aq\text{-}max}$, followed by $\alpha_{T\text{-}AQ}$, ΔH, $V_{ax\text{-}in}$, T_{AQ}, k_{AL}, T_{AL}, and 2b. Based on a criterion of the ratio less than 10%, variables $\alpha_{L\text{-}AQ,}$ θ, and α_{AL} have only a small effect on $C_{aq\text{-}max}$; therefore, in multi-dimensional PCE-enhanced MCS conducted later, they are considered known and the representative values of their respective distributions are used in the PCE-enhanced MCS (see Table 4.4).

Table 5.4. Sensitivity analysis for GCL-RSc: Range of variance of $C_{aq\text{-}max}$ (ng/l) caused by uncertainty of single or pairs of variables.

Uncertain Variable	Minimum $C_{aq\text{-}max}$ (ng/l)	Maximum $C_{aq\text{-}max}$ (ng/l)	Range (Max -Min) (ng/l)	Ratio of Range to $C_{aq\text{-}max}$ of deterministic analysis (403.6 ng/l)	Rank
C_{b0} & p_0/C_{b0}	1	>3000	>3000	>743.3%	1
k_a & k_b/k_a-1	16	1343	1327	328.8%	2
L_w	53	939	886	219.5%	3
$\alpha_{T\text{-}AQ}$	347	850	503	124.6%	4
ΔH	150	644	494	122.4%	5
$V_{ax\text{-}in}$	176	634	458	113.5%	6
T_{AQ}	285	720	435	107.8%	7
k_{AL}	137	429	292	72.3%	8
T_{AL}	221	508	287	71.1%	9
2b	353	446	93	23.0%	10
$\alpha_{L\text{-}AQ}$	366	405	39	9.7%	11
θ	381	406	25	6.2%	12
α_{AL}	400	402	2	0.5%	13

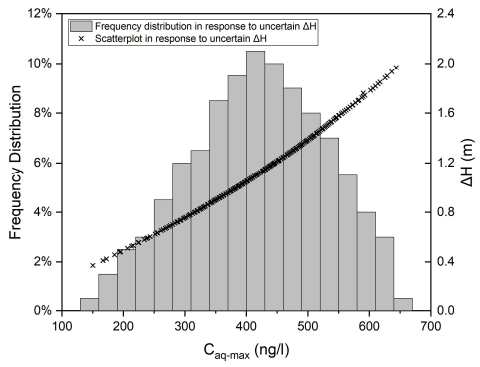

(a) ΔH

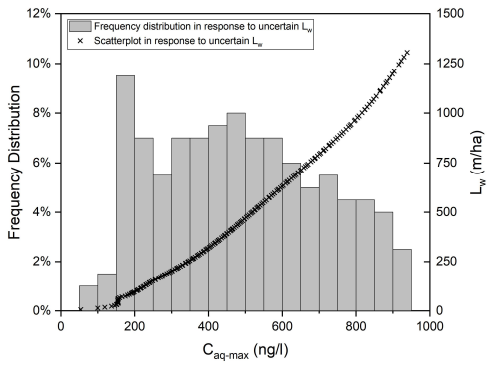

(b) L_w

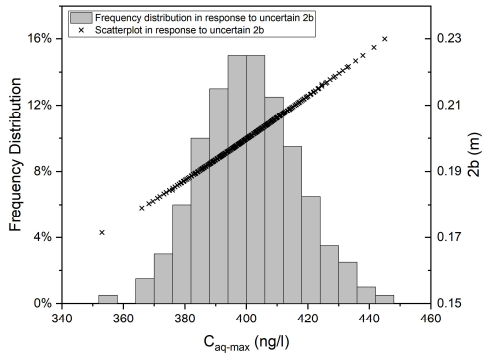

(c) 2b

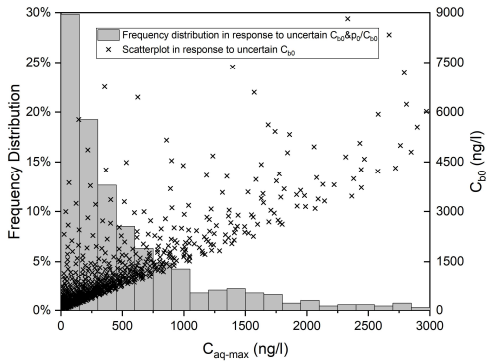

(d) Histogram for C_{b0} & p_0/C_{b0} and scatterplot for C_{b0}

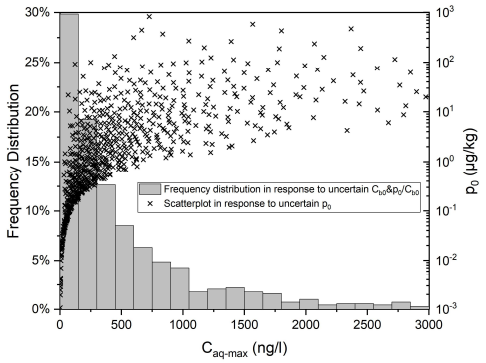

(e) Histogram for C_{b0} & p_0/C_{b0} and scatterplot for p_0

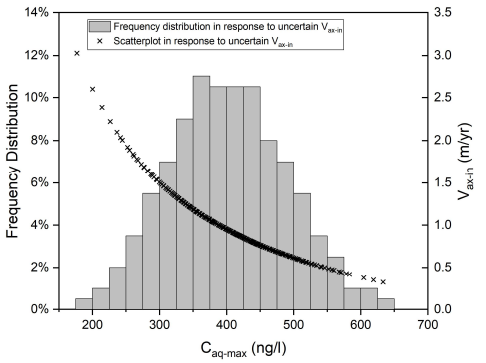

(f) V_{ax-in}

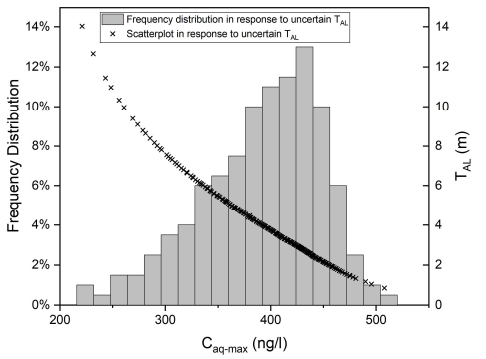

(g) T_{AL}

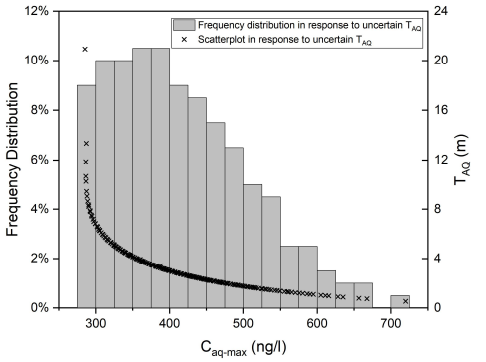

(h) T_{AQ}

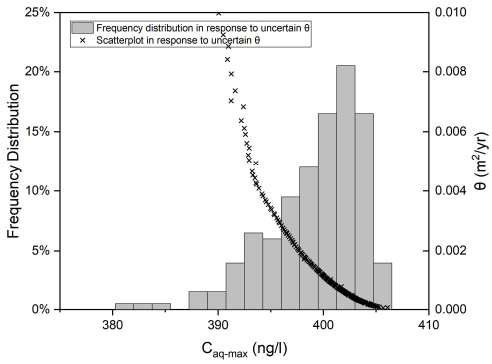

(i) θ

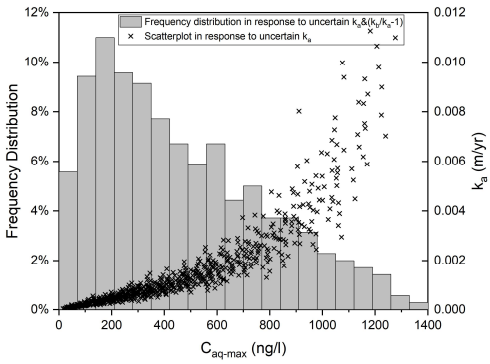

(j) Histogram for k_a & k_b/k_a-1 and scatterplot for k_a

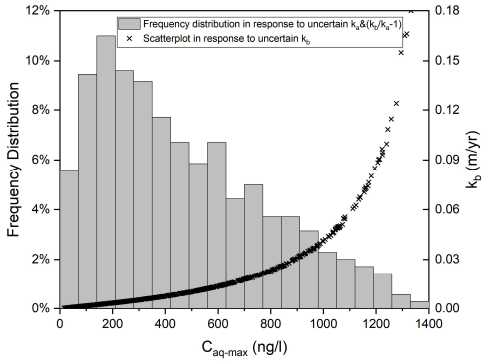

(k) Histogram for k_a & k_b/k_a-1 and scatterplot for k_b

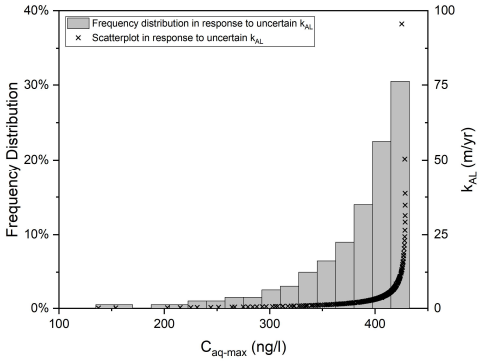

(l) k_{AL}

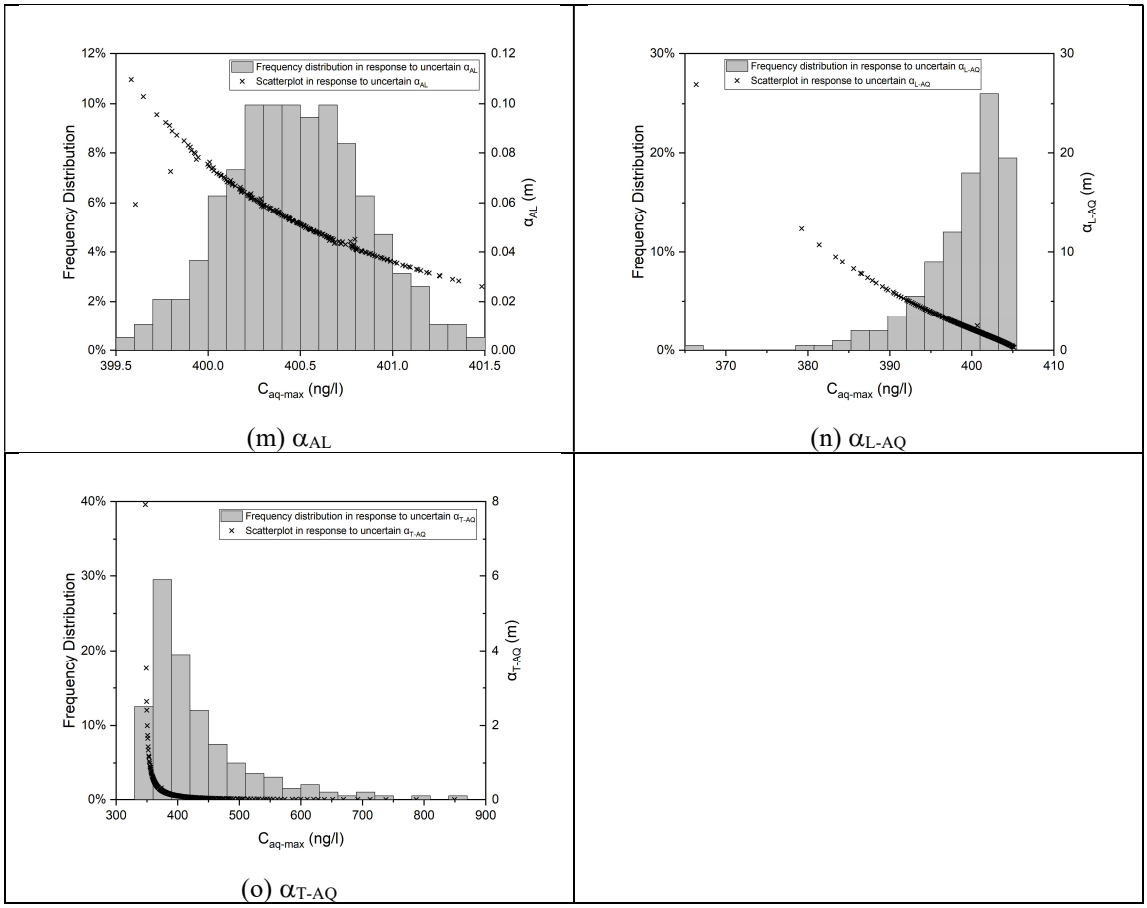

Figure 5.10. Sensitivity analysis for GCL-RSc: Frequency distribution and Scatterplot of $C_{aq\text{-}max}$ in response to individual uncertain inputs.

The influences of most uncertainties in RSc for the CCL+AL model are similar to those for the GCL+AL model. For example, C_{b0} & p_0/C_{b0} and k_{CCL} still lead the list of most influential factors, followed by ΔH, $V_{ax\text{-}in}$, T_{AQ}, L_w, and T_{AL}. While the thickness of GCL is assumed to be known, T_{CCL} has a distribution with low variability, thus causing a modest variability of $C_{aq\text{-}max}$. Furthermore, the influences of $\alpha_{L\text{-}AQ}$ and α_{AL} are still minor in the case of CCL+AL, as they are for GCL+AL.

The biggest difference between GCL+AL and CCL+AL lies in the influence of θ, which has a large positive correlation with $C_{aq\text{-}max}$ for the CCL+AL model. In this model, the overall level of θ is much higher than that in the GCL+AL model, and θ is also very variable (see Table 4.4). Both a wider wetted area and a higher overall leakage rate caused by a higher θ can be well captured by Approach 2b, which yields a higher $C_{aq\text{-}max}$. Another noteworthy point is that the influence of L_w is not as significant as in the GCL model, and its further increase leads to only marginal rises in $C_{aq\text{-}max}$ once a relatively high value is reached. The underlying mechanism has already been discussed in the earlier analysis of CQA: under higher transmissivity and when the defects are

sufficiently dense, the interaction between adjacent leaks causes the non-defective regions to be almost fully affected by leakage, and further increases in L_w have a more limited effect.

In addition, three parameters whose variability has a non-negligible impact in GCL+AL, are found to be far less influential in CCL+AL: $\alpha_{T\text{-}AQ}$, k_{AL}, and 2b. The influence of 2b becomes negligible because, unlike in the GCL model where waste-liner contact is more sensitive to 2b, the much larger wetted distance in the CCL+AL model far exceeds 2b, effectively overshadowing its impact. The smaller influence of k_{AL} for the CCL+AL model could be due to the variability of k_{CCL} affecting the overall permeability of the whole liner more than k_{GCL} (CCL is thicker than GCL) and thus diminishing the influence of k_{AL}.

Table 5.5. Sensitivity analysis for CCL-RSc: Range of variance of $C_{aq\text{-}max}$ (ng/l) caused by uncertainty of single or pairs of variables.

Uncertain Variable	Minimum $C_{aq\text{-}max}$ (ng/l)	Maximum $C_{aq\text{-}max}$ (ng/l)	Range (Max-Min) (ng/l)	Ratio of Range to $C_{aq\text{-}max}$ of deterministic analysis (463.4 ng/l)	Rank
C_{b0} & p_0/C_{b0}	4	>3300	>3300	>712.1%	1
k_{CCL}	186	1096	910	196.4%	2
T_{AQ}	154	888	734	158.4%	3
ΔH	151	719	568	122.6%	4
$V_{ax\text{-}in}$	231	763	532	114.8%	5
L_w	50	514	464	100.1%	6
θ	81	504	423	91.3%	7
T_{CCL}	340	608	268	57.8%	8
T_{AL}	334	510	176	38.0%	9
k_{AL}	421	466	45	9.7%	10
$\alpha_{L\text{-}AQ}$	461	486	25	5.4%	11
$\alpha_{T\text{-}AQ}$	455	464	9	1.9%	12
α_{AL}	461	464	3	0.6%	13
2b	463.1	463.5	0.4	0.1%	14

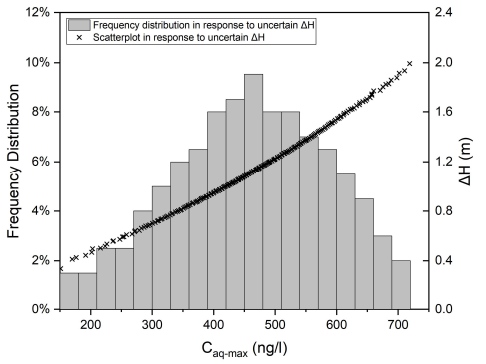

(a) ΔH

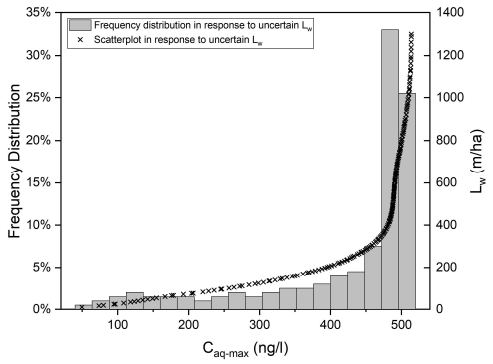

(b) L_w

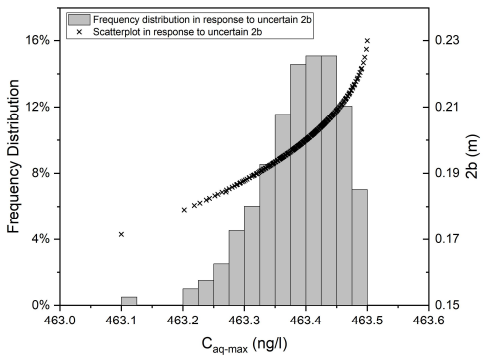

(c) 2b

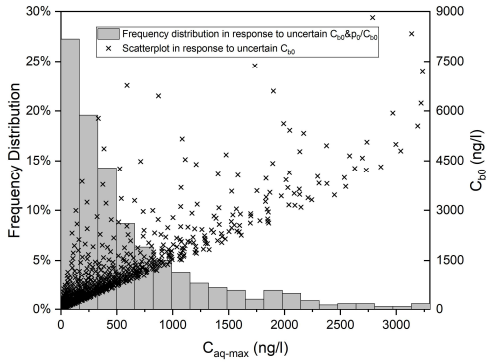

(d) Histogram for C_{b0} & p_0/C_{b0} and scatterplot for C_{b0}

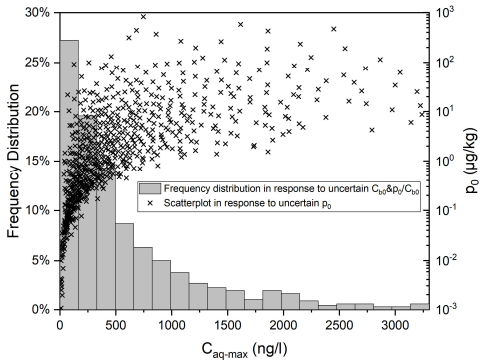

(e) Histogram for C_{b0} & p_0/C_{b0} and scatterplot for p_0

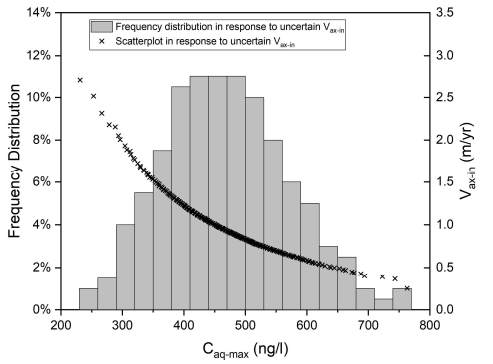

(f) $V_{ax\text{-}in}$

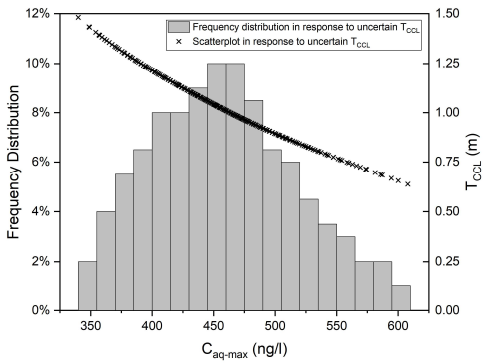

(g) T_{CCL}

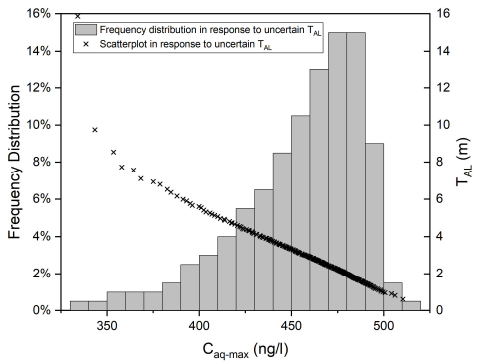

(h) T_{AL}

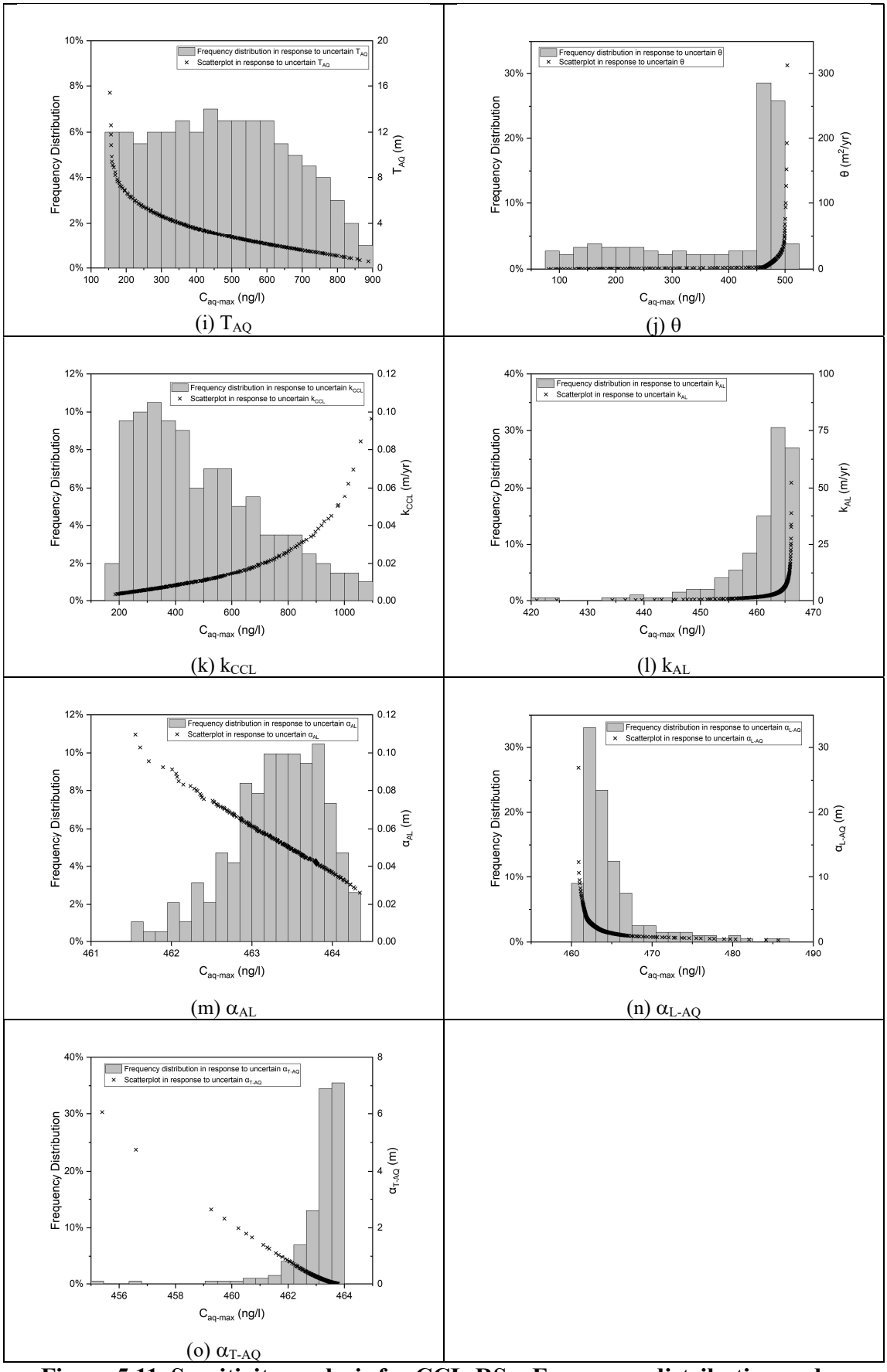

Figure 5.11. Sensitivity analysis for CCL-RSc: Frequency distribution and Scatterplot of $C_{aq\text{-}max}$ in response to individual uncertain inputs.

For the NCL model, the preliminary sensitivity analyses of nearly all parameters can be interpreted analogously to those of the CCL+AL model. The only notable difference is that the influences of NCL's hydraulic conductivity and thickness are higher than their counterpart in CCL. This is expected, given that the NCL is the only soil layer present in this design and is relatively thick.

Table 5.6. Sensitivity analysis for NCL-RSc: Range of variance of $C_{aq\text{-}max}$ (ng/l) caused by uncertainty of single or pairs of variables.

Uncertain Variable	Minimum $C_{aq\text{-}max}$ (ng/l)	Maximum $C_{aq\text{-}max}$ (ng/l)	Range (Max-Min) (ng/l)	Ratio of Range to $C_{aq\text{-}max}$ of deterministic analysis (206.0 ng/l)	Rank
C_{b0} & p_0/C_{b0}	0	>1550	>1550	>752.4%	1
k_{NCL}	12	1267	1255	609.2%	2
T_{AQ}	57	546	489	237.4%	3
$V_{ax\text{-}in}$	87	431	344	167.0%	4
T_{NCL}	101	374	273	132.5%	5
ΔH	116	308	192	93.2%	6
L_w	43	218	175	85.0%	7
θ	138	213	75	36.4%	8
$\alpha_{L\text{-}AQ}$	205	217	12	5.8%	9
$\alpha_{T\text{-}AQ}$	205	206	1	0.5%	10
2b	205.8	206.2	0.4	0.2%	11

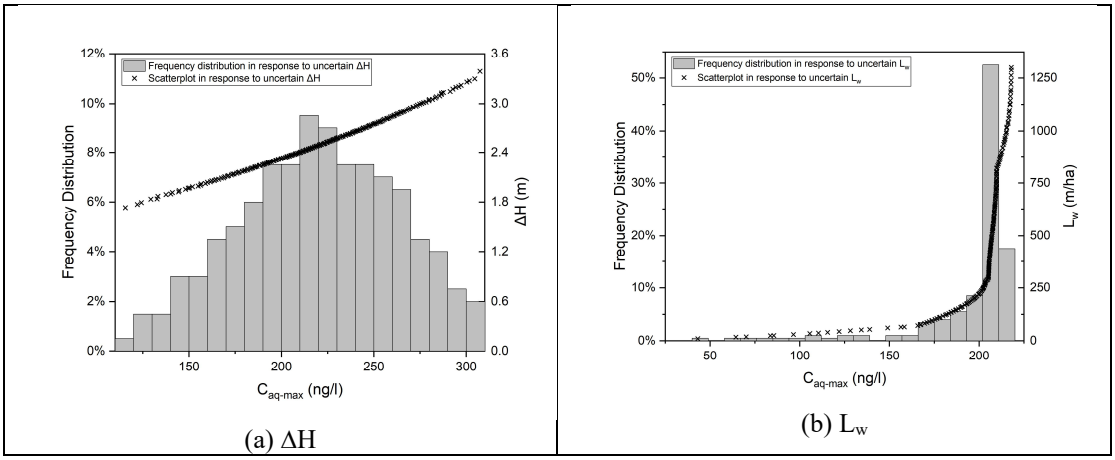

(a) ΔH (b) L_w

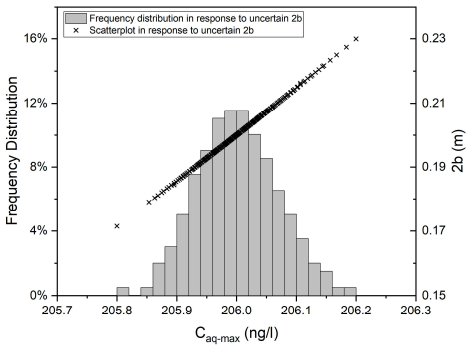

(c) 2b

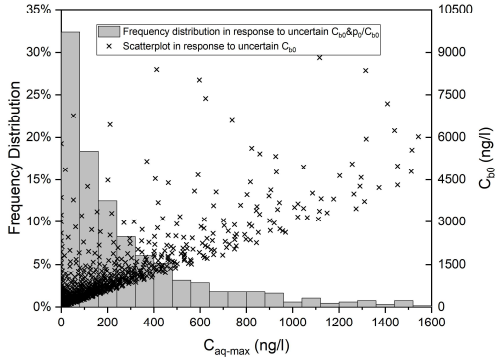

(d) Histogram for C_{b0} & p_0/C_{b0} and scatterplot for C_{b0}

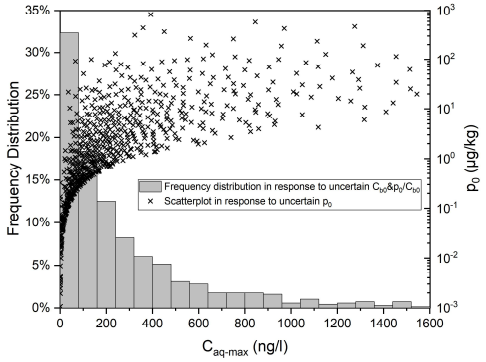

(e) Histogram for C_{b0} & p_0/C_{b0} and scatterplot for p_0

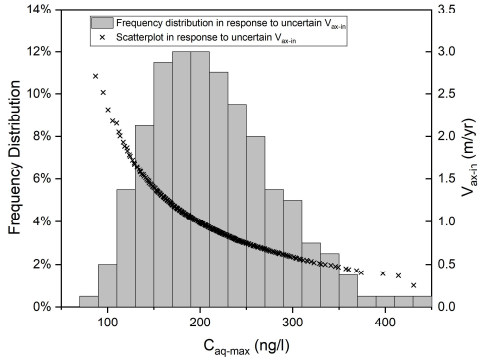

(f) $V_{ax\text{-}in}$

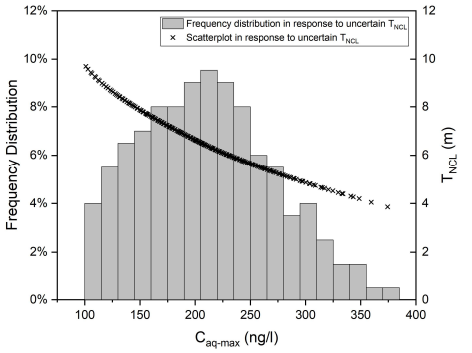

(g) T_{NCL}

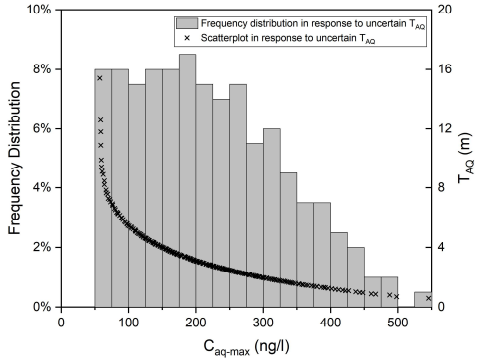

(h) T_{AQ}

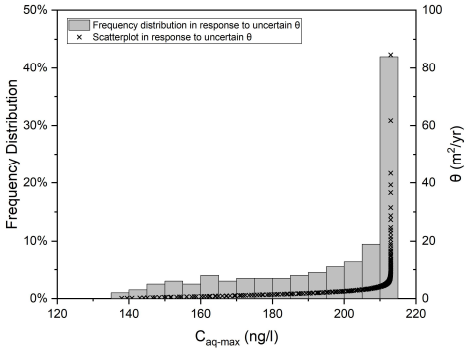

(i) θ

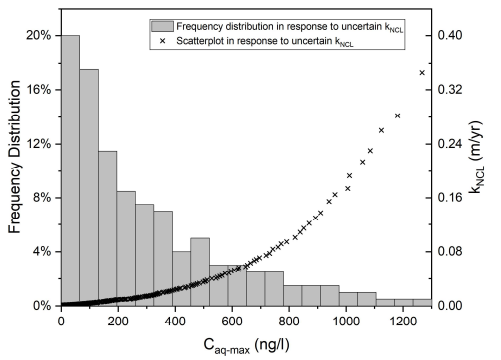

(j) k_{NCL}

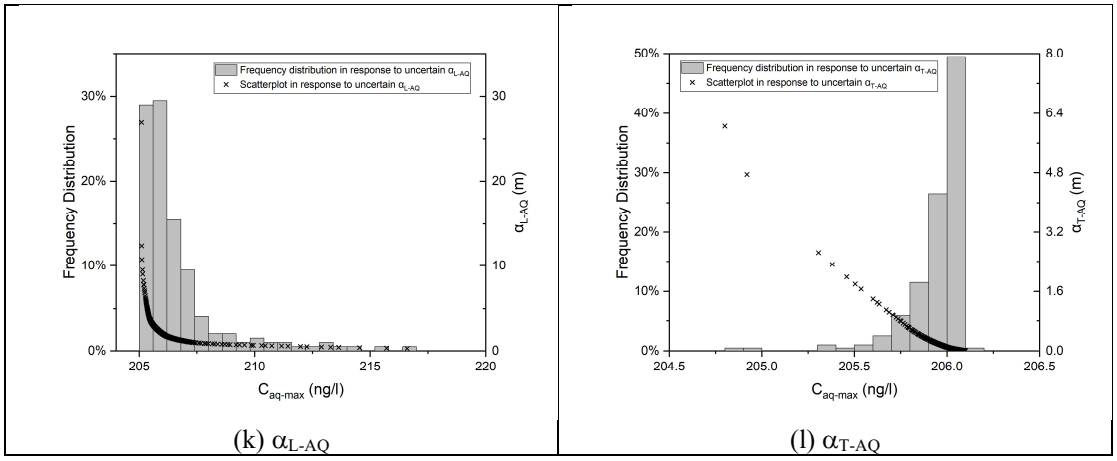

(k) $\alpha_{L\text{-}AQ}$ (l) $\alpha_{T\text{-}AQ}$

Figure 5.12. Sensitivity analysis for NCL-RSc: Frequency distribution and Scatterplot of $C_{aq\text{-}max}$ in response to individual uncertain inputs.

Chapter 6

Results: Performance of Polynomial Chaos Expansion Surrogate Models

---

6.1 Introduction

The deterministic analysis in the previous chapter provides a solution for the problem of PFOS transport in MSWLs by considering mean values of uncertain parameters, yielding a reference estimate of PFOS concentrations in the underlying aquifer. Nevertheless, the core analysis of this thesis is probabilistic in nature, based on Monte Carlo simulations (MCS).

A key variable in any MCS is the total number of realisations (R_{MCS}) conducted to generate probability distributions of the outcome in question. Generally, at a relatively small number of realisations, MCS yields unstable predictions (i.e., ones in which different sampling from the same input distribution with the same number of realisations, generate frequency distributions that differ greatly from each other). A minimum number of realisations, referred to here as R_{stable}, is required before the predictions stabilise and become reliable. The exact value of R_{stable} varies depending on the problem in question and usually increases with increasing number of uncertain input parameters (N_u) for the same problem.

For the problem in this thesis, with ten or more uncertain parameters, R_{stable} is expected to be high, making the associated cost (i.e., computational time) incurred by MCS prohibitive. As discussed in Chapters 2 and 3, an effective way of reducing this cost is to use a relatively small number of MCS realisations as a basis to generate and optimise a Polynomial Chaos Expansion (PCE) surrogate model. The PCE surrogate model is then used to conduct a much larger number of realisations (R_{stable}) that generate stable distributions at much lower computational cost. (Henceforth, we refer to the PCE surrogate model, i.e., the PCE-enhanced MCS as "PCE", for brevity, while the conventional MCS, with no PCE surrogate model, is referred to as MCS).

The number of MCS realisations used as a basis for generating the PCE model is denoted by $R_{MCS\text{-}PCE}$ (these realisations are sometimes called Experimental Design (ED) in the literature). The much larger number of realisations subsequently conducted based on the PCE model are referred to as Prediction Design (PrD) in this thesis. The PCE optimisation process determines optimal $R_{MCS\text{-}PCE}$ ($R_{MCS\text{-}PCE\text{-}opt}$), degree of PCE function (p), hyperbolic truncation norm (q), and optimal method for sparse regression (BCS, LARS, OMP, SP). These have already been introduced and discussed in Chapter 3.

As stated in Chapter 2, to the best of the author's knowledge, PCE has never been applied to any subsurface contaminant transport problem with more than 6 uncertain variables, nor to the problem of contaminant transport in liner systems and aquifers, under waste landfills. Therefore, the applicability of PCE to the problem under study needs to be evaluated. The aim of this chapter is to present the results of this evaluation, by addressing two questions. Does PCE produce the same probability distribution predictions as the conventional MCS for the problem under study? What is the extent of computational gains achieved by PCE, relative to conventional MCS?

This aim is achieved in three stages. In the first stage, a problem with only two uncertain parameters (k_a and k_b/k_a-1), based on the GCL-RSc scenario, is modelled using both conventional MCS and PCE-enhanced MCS, with the latter validated against the former. The small number of uncertain parameters reduces the number of MCS realisations required to achieve stable Monte-Carlo predictions (R_{stable}) and allows a reliable reference output probability distribution for those realisations ($PrD_{ref\text{-}GCL\text{-}2D}$) to be generated by conventional MCS, to which PCE predictions can be compared. Twelve uncertain parameters have been identified in Chapter 5 as influential on $C_{aq\text{-}max}$ and any two of those could have been chosen in principle. However, k_a and k_b/k_a-1 have been found in Chapter 5 to have a particularly large impact on $C_{aq\text{-}max}$, hence their selection here. Using this reference solution, an optimised PCE configuration is built for the problem under study, by determining $R_{MCS\text{-}PCE\text{-}opt}$, optimal p and q and best sparse regression method; this is achieved by trial and error, through comparison of PCE predictions to MCS results of $PrD_{ref\text{-}GCL\text{-}2D}$. Finally, an estimate of the PCE computational gains is made based on the computational time of MCS and PCE.

In the second stage, the GCL-RSc scenario with all 12 uncertain parameters, identified in Chapter 5, is included. During this stage, it is not possible to conduct a large enough

number of MCS realisations to achieve stability. The reliability of PCE is assessed instead by selecting 3 randomly generated sets of MCS realisations ($PrD_{ref\text{-}GCL\text{-}1}$, $PrD_{ref\text{-}GCL\text{-}2}$, and $PrD_{ref\text{-}GCL\text{-}3}$) using R_{MCS}=2000 each time. This number (2000) is much smaller than the required R_{stable} and is selected as a large number whose computational cost is nevertheless still affordable. The MCS results for the three sets are used as reference solutions against which PCE predictions are validated. As in stage 1, an optimised PCE is derived by trial and error, albeit according to the average predictive quality across the 3 sets of $PrD_{ref\text{-}GCL}$. This is followed by an assessment of computational gains achieved by PCE relative to MCS, using R_{stable} established through a PCE stability analysis. Finally, in the third stage, stage 2 is repeated in a simplified manner while using the CCL-RSc and NCL-RSc scenarios with the respective 10 and 9 uncertain parameters, identified in Chapter 5 as influential.

Since the distribution of the maximum concentration of PFOS in the aquifer, $C_{aq\text{-}max}$, is skewed, $\ln(C_{aq\text{-}max})$ is used as the predicted output in all MCS and PCE assessments. The natural logarithm is a suitable transformation because $C_{aq\text{-}max}$ is non-negative. In each stage, once $R_{MCS\text{-}PCE\text{-}opt}$ and R_{stable} have been established, the computational gain (G) generated by PCE, relative to MCS, can be calculated as R_{stable} / $R_{MCS\text{-}PCE\text{-}opt}$. Derivation of this ratio is given in Appendix 6.1.

6.2 Stage 1: Validation of PCE for GCL-RSc with Two Uncertain Parameters

Figure 6.1 shows the mean μ and standard deviation σ of $\ln(C_{aq\text{-}max})$ across all realisations as a function of the number of MCS realisations (no PCE involved), up to 3000 realisations. The figure shows that the mean and standard deviation stabilise, within a band of ±0.25% and ±0.5% of their values at 3000, respectively, after about 1000 MCS realisations. Hence, R_{stable}=1000 is adopted, based on which the reference solution of $PrD_{ref\text{-}GCL\text{-}2D}$ is generated. For $PrD_{ref\text{-}GCL\text{-}2D}$, mean($\ln(C_{aq\text{-}max})$)=5.841 and SD($\ln(C_{aq\text{-}max})$)= 0.862.

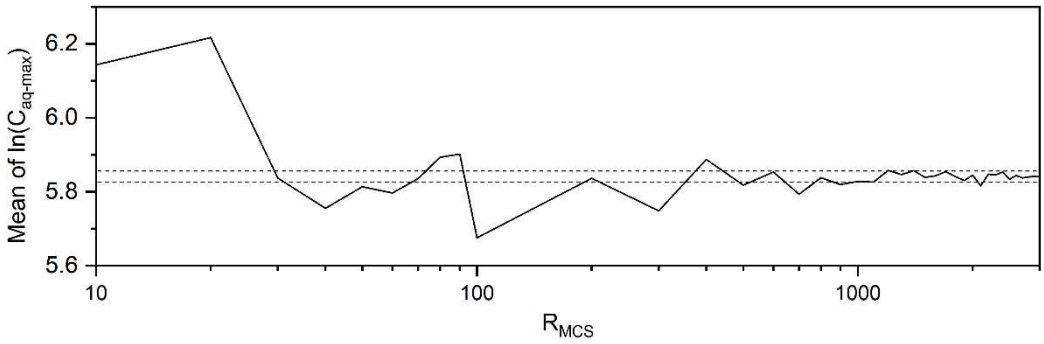

(a)

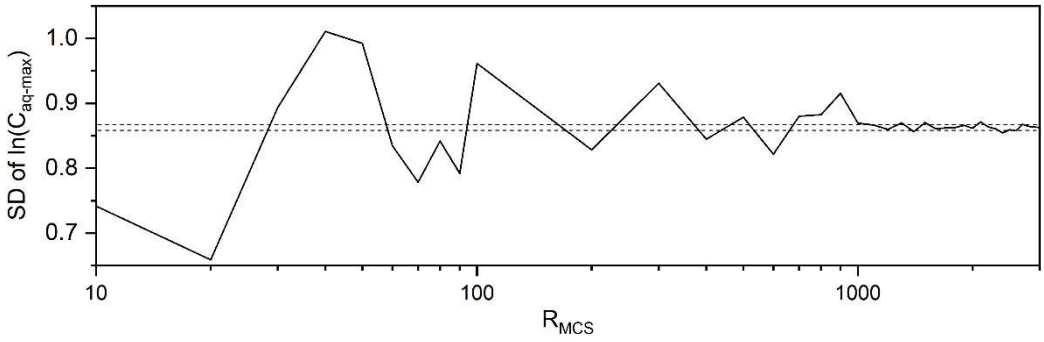

(b)

Figure 6.1. Derivation of $PrD_{ref\text{-}GCL\text{-}2D}$ for GCL-RSc with two uncertain parameters: statistics of $\ln(C_{aq\text{-}max})$ versus R_{MCS} (the dashed lines represent the acceptable tolerance interval of statistical variability, ±0.25% for mean, and ±0.5% for standard deviation).

The optimisation of the PCE is conducted by generating PCE predictions for $PrD_{ref\text{-}GCL\text{-}2D}$ using different values of p and q parameters for four sparse regression techniques, as well as based on different $R_{MCS\text{-}PCE}$. The determination of the optimal combination of "p + q + regression technique" and $R_{MCS\text{-}PCE\text{-}opt}$ is achieved through an alternating trial-and-error procedure. The results presented herein correspond to the final step of this process, with one aspect optimised on the premise that the other is already at its optimal setting. It should be noted that, theoretically speaking, this alternating trial-and-error procedure yields a locally optimal combination rather than guaranteeing the global optimum.

Performance of PCE can be assessed using three evaluation indices reflecting the deviation of PCE from MCS predictions: mean absolute percentage error (MAPE), the absolute error of mean ($\epsilon(\mu)$), and the absolute error of SD ($\epsilon(\sigma)$). Table 6.1 shows MAPE between PCE and MCS predictions under different values of p and q and for different regression techniques. The table shows that the optimal PCE model (identified in red colour) usually has a degree of 4~6 and a relatively high q except for SP. Identical

MAPE values in parts of the table indicate that sometimes higher-degree terms have zero coefficients and make no contribution to the PCE model. To help in selecting the regression technique, Table 6.2 compares MAPE, $\epsilon(\mu)$, and $\epsilon(\sigma)$ under optimal values of p and q for each technique, taken from Table 6.1. It is clear from Table 6.2 that, although BCS performs well, LARS with p=5 and q=0.8, performs best and is adopted here.

Table 6.1. MAPE under different p and q using four sparse regression techniques for $PrD_{ref\text{-}GCL\text{-}2D}$ ($\times 10^{-3}$; $R_{MCS\text{-}PCE}$=60)

q \ p	3	4	5	6	7
0.6	9.54	2.44	1.75	2.04	0.78
0.7	3.14	2.34	1.75	0.65	2.12
0.8	3.14	2.34	0.80	2.12	1.10
0.9	3.14	2.34	0.80	2.12	1.27
1.0	3.14	0.45	1.06	1.27	1.40

(a) BCS

q \ p	3	4	5	6	7
0.6	7.57	2.19	2.19	2.19	0.43
0.7	3.05	2.19	2.19	0.43	0.78
0.8	3.05	2.19	0.43	0.78	0.78
0.9	3.05	2.19	0.43	0.78	0.78
1.0	3.05	0.68	0.78	0.78	0.78

(b) LARS

q \ p	3	4	5	6	7
0.6	7.57	2.19	2.00	2.34	1.72
0.7	3.05	2.19	2.00	1.72	2.45
0.8	3.05	2.19	1.62	2.45	2.45
0.9	3.05	2.19	1.62	2.45	2.45
1.0	3.05	2.19	3.00	2.45	2.45

(c) OMP

q \ p	4	5	6	7	8
0.5	4.89	3.05	4.89	2.20	1.08
0.6	4.89	2.91	4.89	1.08	1.08
0.7	4.89	2.91	2.19	1.91	1.42
0.8	4.89	2.19	1.57	2.13	1.57
0.9	4.89	2.19	1.57	1.42	1.74

(d) SP

Table 6.2. Deviations between PCE and MCS predictions of $\ln(C_{aq\text{-}max})$ for $PrD_{ref\text{-}GCL\text{-}2D}$ using four sparse regression techniques ($R_{MCS\text{-}PCE}$=60)

Configuration	BCS p= 4, q= 1.0	LARS p= 5, q= 0.8	OMP p= 5, q= 0.8	SP p= 7, q= 0.6
MAPE ($\times 10^{-4}$)	4.47	4.32	16.2	10.8
Absolute error of Mean ($\times 10^{-4}$)	1.23	1.18	1.08	0.49
Absolute error of SD ($\times 10^{-4}$)	10.2	7.13	109.8	9.50

Figure 6.2 shows MAPE and absolute errors of mean and standard deviation, relative to the reference solution, as a function of $R_{MCS\text{-}PCE}$. It is clear from the figures that beyond $R_{MCS\text{-}PCE}$=60, error criteria of 0.05% for MAPE, 0.02% for mean and 0.1% for standard deviation, are satisfied, and this size ($R_{MCS\text{-}PCE\text{-}opt}$=60) is adopted, hence completing the process of PCE optimisation for $PrD_{ref\text{-}GCL\text{-}2D}$.

Figure 6.3 shows the accuracy of PCE predictions of $\ln(C_{aq\text{-}max})$, with reference to the conventional MCS. Figure 6.3 (a) shows the probability density curve of $\ln(C_{aq\text{-}max})$

from both methods, while Figure 6.3 (b) shows individual values of $\ln(C_{aq\text{-}max})$ from MCS (horizontal axis) and PCE (vertical axis). The PCE predictions are clearly in excellent agreement with MCS, with very low MAPE (0.043%) and absolute errors of mean (0.012%) and SD (0.071%) (LARS in Table 6.2). Finally, the computational gain ratio (G) achieved by PCE ($R_{stable}/R_{MCS\text{-}PCE\text{-}opt}$) is 16.7 (1000/60), indicating significant savings.

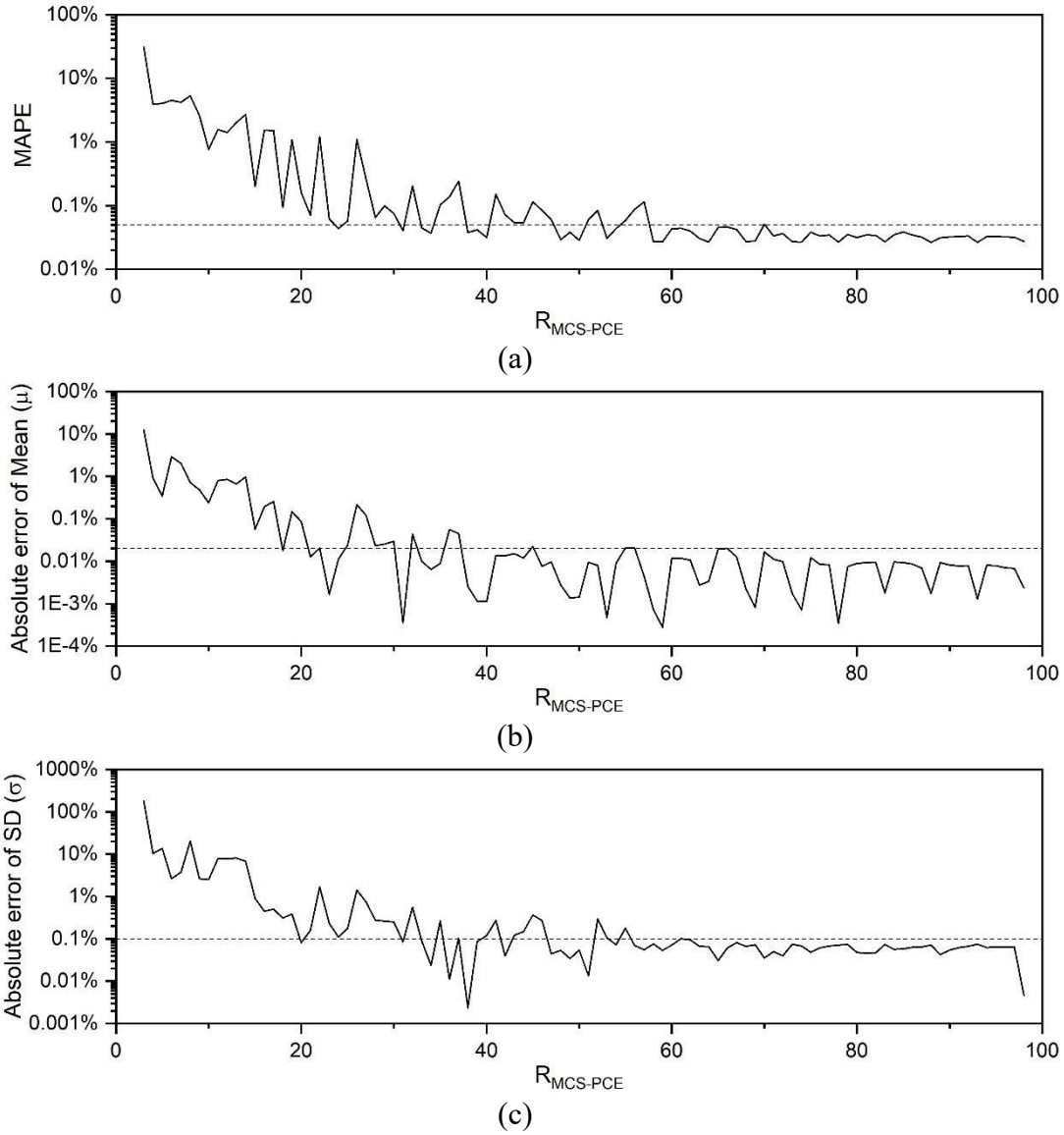

Figure 6.2. Determining $R_{MCS\text{-}PCE\text{-}opt}$: Evaluation indices versus $R_{MCS\text{-}PCE}$ for $PrD_{ref\text{-}GCL\text{-}2D}$ (LARS, p=5, q=0.8; dashed lines in the graphs represent the target value of each evaluation index, 0.05% for MAPE, 0.02% for mean, and 0.1% for standard deviation).

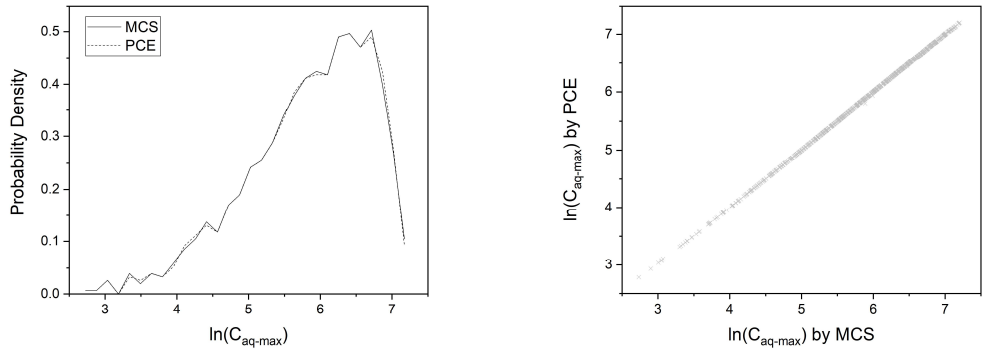

(a) (b)

Figure 6.3. Accuracy of PCE by comparison of $\ln(C_{aq\text{-}max})$ predictions between MCS and PCE for $PrD_{ref\text{-}GCL\text{-}2D}$ (LARS; p=5; q=0.8; $R_{MCS\text{-}PCE}$=60; R_{MCS}=R_{PCE}=R_{stable}=1000): (a) Probability density of $\ln(C_{aq\text{-}max})$; (b) $\ln(C_{aq\text{-}max})$ from each of the 1000 simulations

6.3 Stage 2: Validation of PCE for GCL-RSc with 12 Uncertain Parameters

The MCS-based statistics of $PrD_{ref\text{-}GCL\text{-}1}$, $PrD_{ref\text{-}GCL\text{-}2}$ and $PrD_{ref\text{-}GCL\text{-}3}$, for the GCL-RSc with 12 uncertain variables, are shown in Table 6.3. While they are reasonably close, the difference between them is a reflection of the fact that R_{MCS}=2000<R_{stable}. The alternating trial-and-error procedure still works for searching the optimal combination of "p + q + regression technique" and $R_{MCS\text{-}PCE\text{-}opt}$. Judgements are made based on the average of evaluation indices from the three sets.

Table 6.3. Statistics of $\ln(C_{aq\text{-}max})$ for $PrD_{ref\text{-}GCL\text{-}1}$, $PrD_{ref\text{-}GCL\text{-}2}$, and $PrD_{ref\text{-}GCL\text{-}3}$ by MCS.

	$PrD_{ref\text{-}GCL\text{-}1}$	$PrD_{ref\text{-}GCL\text{-}2}$	$PrD_{ref\text{-}GCL\text{-}3}$
Mean	5.57	5.56	5.57
SD	1.79	1.85	1.82

Results of identifying optimal p, q and regression technique are shown in Tables 6.4 and 6.5. The average MAPE values in Table 6.4 show that, the optimal PCE degree (p) and hyperbolic truncation norm (q), for the studied four sparse regression techniques, are usually 9~11 and 0.5, respectively. These optimal p and q, identified in red colour, are clearly not the highest ones. This highlights the need to maintain a balance between capturing adequate information of the PCE model (high-degree terms and high-order interactions) and avoiding overfitting. The representative performance in predicting $PrD_{ref\text{-}GCL\text{-}1}$, $PrD_{ref\text{-}GCL\text{-}2}$ and $PrD_{ref\text{-}GCL\text{-}3}$ using the four techniques is presented in Table 6.5, suggesting that BCS, with p=9 and q=0.5, leads to the smallest average MAPE, and OMP performs best for minimising $\epsilon(\mu)$ and $\epsilon(\sigma)$. However, all four approaches perform

well, with no large differences identified, which should be attributed to the adequate value of $R_{MCS\text{-}PCE}$. This observation agrees with Lüthen et al. (2020) that no single regression technique significantly outperforms the others. The setting of BCS with p=9 and q=0.5 is adopted for $PrD_{ref\text{-}GCL\text{-}1}$, $PrD_{ref\text{-}GCL\text{-}2}$ and $PrD_{ref\text{-}GCL\text{-}3}$.

Table 6.4. Average MAPE under different p and q using four sparse regression techniques for $PrD_{ref\text{-}GCL\text{-}1}$, $PrD_{ref\text{-}GCL\text{-}2}$ and $PrD_{ref\text{-}GCL\text{-}3}$ ($\times 10^{-2}$; $R_{MCS\text{-}PCE}$=1500).

q \ p	8	9	10	11	12
0.3	6.72	6.72	6.72	3.20	3.22
0.4	3.20	2.58	2.58	2.25	2.14
0.5	2.19	1.64	1.78	1.85	2.11
0.6	1.83	1.85	2.39	2.56	2.46
0.7	1.94	2.41	2.27	2.61	2.71

(a) BCS

q \ p	8	9	10	11	12
0.4	3.22	2.54	2.55	2.20	2.15
0.5	2.22	1.87	1.89	1.89	2.02
0.6	1.95	1.95	2.17	2.36	2.37
0.7	2.20	2.54	2.55	2.64	2.80
0.8	2.44	2.70	2.79	2.91	3.21

(b) LARS

q \ p	8	9	10	11	12
0.3	6.71	6.71	6.75	3.23	3.24
0.4	3.27	2.61	2.61	2.26	2.24
0.5	2.21	1.74	1.88	2.14	2.22
0.6	2.01	1.97	2.43	2.53	2.62
0.7	2.58	3.01	3.79	3.76	3.42

(c) OMP

q \ p	8	9	10	11	12
0.3	6.80	7.16	6.90	3.42	3.50
0.4	3.25	2.58	3.46	2.68	5.26
0.5	2.28	1.78	2.05	1.72	1.89
0.6	1.88	1.85	2.06	2.62	2.32
0.7	2.46	2.97	2.64	2.59	3.89

(d) SP

Table 6.5. Average deviations between PCE and MCS predictions of $\ln(C_{aq\text{-}max})$ for $PrD_{ref\text{-}GCL\text{-}1}$, $PrD_{ref\text{-}GCL\text{-}2}$ and $PrD_{ref\text{-}GCL\text{-}3}$ using four sparse regression techniques ($R_{MCS\text{-}PCE}$=1500).

Configuration	BCS p= 9, q= 0.5	LARS p= 9, q= 0.5	OMP p= 9, q= 0.5	SP p= 11, q= 0.5
MAPE ($\times 10^{-2}$)	1.64	1.87	1.74	1.72
Absolute error of Mean ($\times 10^{-4}$)	4.34	7.88	2.21	5.49
Absolute error of SD ($\times 10^{-3}$)	3.66	4.96	1.83	2.22

Results of the determination of $R_{MCS\text{-}PCE\text{-}opt}$ are shown in Figure 6.4. The figure suggests that a choice $R_{MCS\text{-}PCE\text{-}opt}$=1500 is adequate, as it satisfies the criteria of MAPE≤ 2%, $\epsilon(\mu) \leq 0.1\%$, and $\epsilon(\sigma) \leq 0.5\%$. While the criterion for MAPE may seem lenient, it is reasonable given the complexity generated by the presence of 12 uncertain parameters.

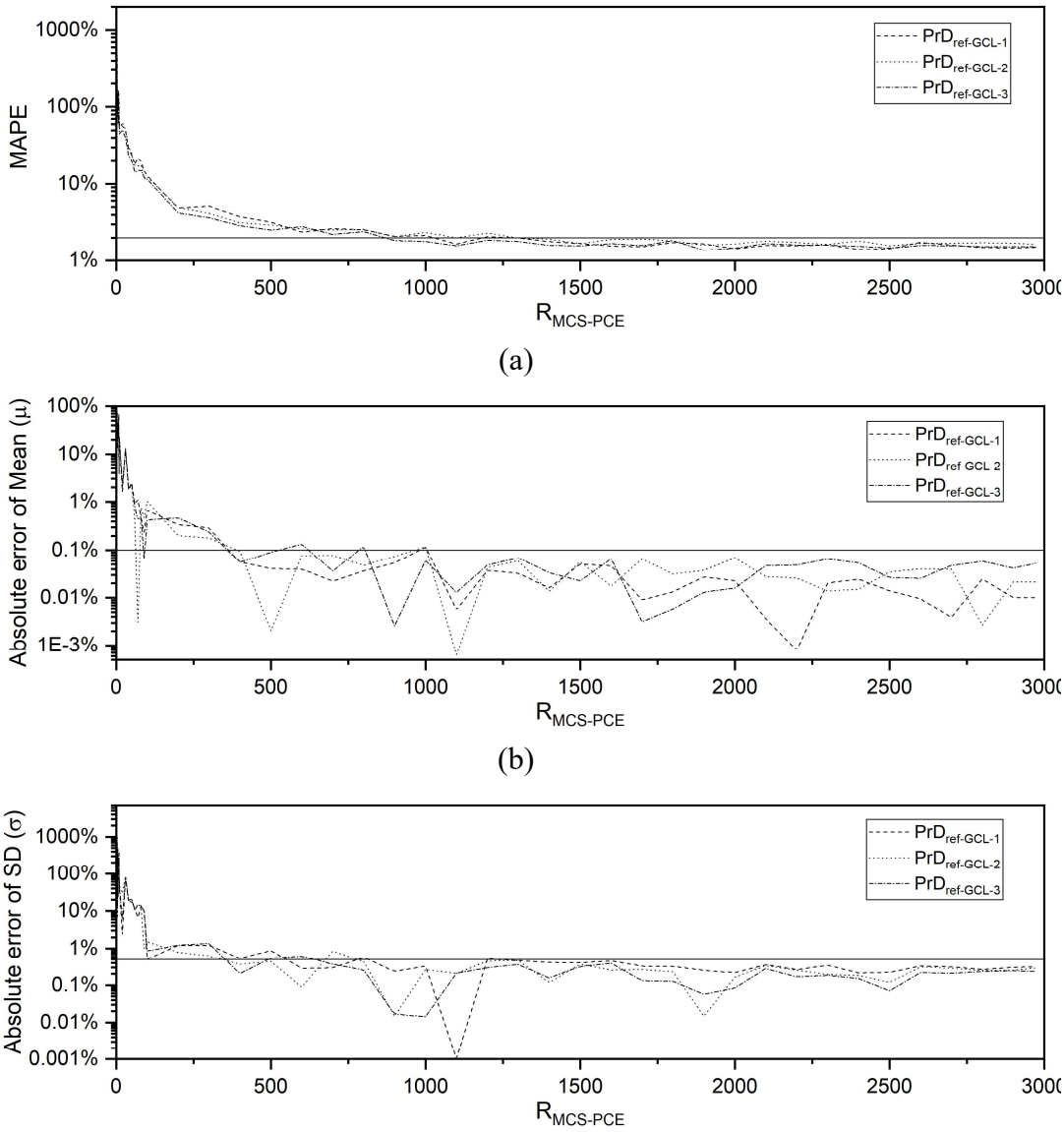

Figure 6.4. Determining $R_{MCS\text{-}PCE\text{-}opt}$: Evaluation indices versus $R_{MCS\text{-}PCE}$ for $PrD_{ref\text{-}GCL\text{-}1}$, $PrD_{ref\text{-}GCL\text{-}2}$, and $PrD_{ref\text{-}GCL\text{-}3}$ (BCS, p=9, q=0.5; solid lines in the graphs represent the target value of each evaluation index, 2% for MAPE, 0.1% for mean, and 0.5% for standard deviation).

Table 6.6 and Figure 6.5 compare predictions from MCS and optimised PCE for $PrD_{ref\text{-}GCL\text{-}1}$, $PrD_{ref\text{-}GCL\text{-}2}$ and $PrD_{ref\text{-}GCL\text{-}3}$, and show very good agreement between the two approaches, confirming the accuracy of PCE for the GCL-RSc problem with 12 uncertain parameters.

Table 6.6. Statistics comparison of $\ln(C_{aq\text{-}max})$ between MCS and PCE for $PrD_{ref\text{-}GCL\text{-}1}$, $PrD_{ref\text{-}GCL\text{-}2}$ and $PrD_{ref\text{-}GCL\text{-}3}$.

		MCS	PCE	MAPE
$PrD_{ref\text{-}GCL\text{-}1}$	Mean	5.57	5.57	1.68%
	SD	1.79	1.78	
$PrD_{ref\text{-}GCL\text{-}2}$	Mean	5.56	5.56	1.68%
	SD	1.85	1.84	
$PrD_{ref\text{-}GCL\text{-}3}$	Mean	5.57	5.57	1.57%
	SD	1.82	1.81	

Now that the optimised PCE model has been validated, a stability analysis can be conducted to determine R_{stable}. The analysis is run for up to 100,000 realisations. Figures 6.6 (a) and (b) show $\mu(\ln(C_{aq\text{-}max}))$ and $\sigma(\ln(C_{aq\text{-}max}))$ versus R_{PCE}. The figures show that 45,000 and 55,000 realisations are required to keep μ within 0.1% and σ within 0.2% of their values at 100,000, respectively. Hence, R_{stable}=60,000 is adopted for the GCL-RSc case with 12 uncertain parameters. The computational gain ratio (G) achieved by PCE ($R_{stable}/R_{MCS\text{-}PCE\text{-}opt}$) is hence 40 (60,000/1,500), an increase from 16.7 for the case of two uncertain parameters. Only limited information on the computational gains associated with PCEs is available in the literature. However, Rajabi et al. (2015b) reported that, in flow and solute transport problems for saturated or unsaturated porous media, PCEs can compute output statistics and PDFs with accuracy at computational cost that is several orders of magnitude lower than standard MCS.

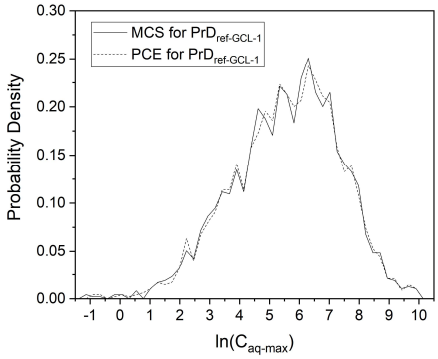

(a1)

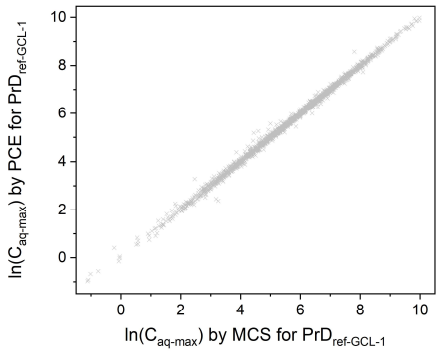

(a2)

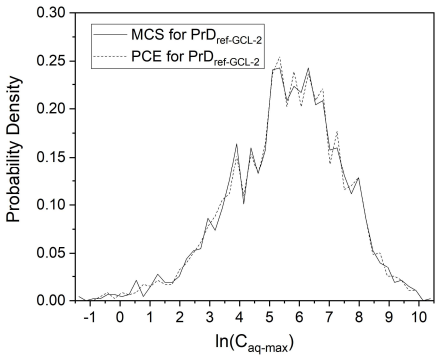

(b1)

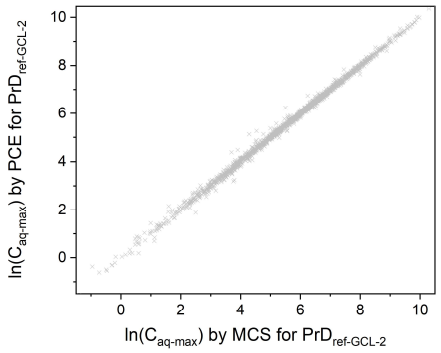

(b2)

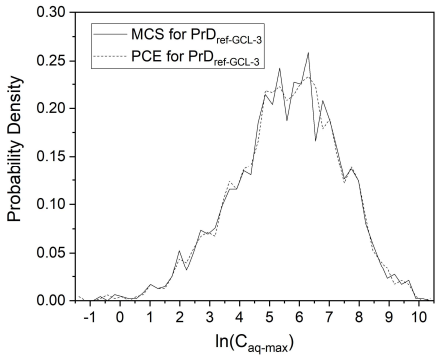

(c1)

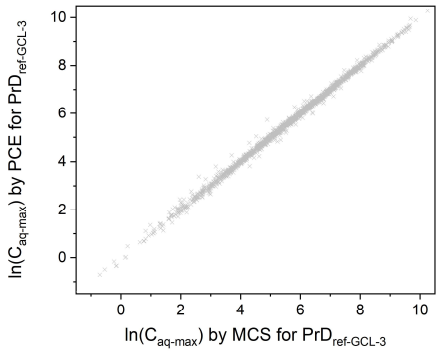

(c2)

Figure 6.5. Accuracy of PCE by comparison of ln(C_{aq-max}) predictions between MCS and PCE for (a) $PrD_{ref-GCL-1}$, (b) $PrD_{ref-GCL-2}$, and (c) $PrD_{ref-GCL-3}$ (BCS, p=9, q=0.5; $R_{MCS-PCE}$=1500; R_{MCS}=R_{PCE}=2000).

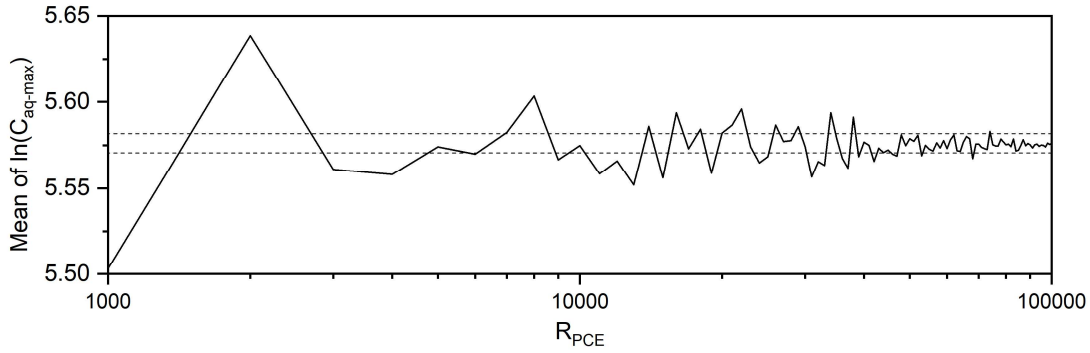

(a)

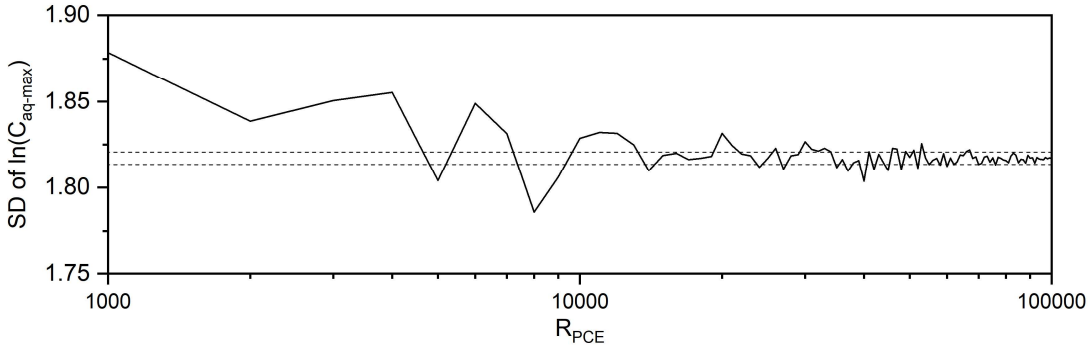

(b)

Figure 6.6. Derivation of R_{stable} for GCL-RSc with 12 uncertain parameters: statistics of $\ln(C_{aq\text{-}max})$ versus R_{MCS} (the dashed lines represent the acceptable tolerance interval of statistical variability, ±0.1% for mean and ±0.2% for standard deviation).

6.4 Stage 3: Validation of PCE for CCL-RSc (10 Uncertain Parameters) and NCL-RSc (9 Uncertain Parameters)

For CCL-RSc with 10 uncertain parameters and NCL-RSc with 9 uncertain parameters, the validation of PCE for each case is conducted based on one randomly generated set of MCS realisations ($PrD_{ref\text{-}CCL}$ and $PrD_{ref\text{-}NCL}$) with R_{MCS}=2000. Following GCL-RSc, BCS is adopted as the sparse regression technique, and $R_{MCS\text{-}PCE}$ is taken as 1500, without optimization. The optimal combinations of p and q for $PrD_{ref\text{-}CCL}$ and $PrD_{ref\text{-}NCL}$ according to MAPE, as shown in Table 6.7, are (p=8, q=0.6) and (p=8, q=0.6), respectively. Table 6.8 and Figure 6.7 indicate that MCS and PCE yield highly consistent results for $PrD_{ref\text{-}CCL}$, while the consistency for $PrD_{ref\text{-}NCL}$ is also satisfactory, albeit slightly reduced (MAPE=3.64%). This validates the performance of PCE for CCL-RSc and NCL-RSc with full uncertainty. Furthermore, R_{stable}=60,000 is also adopted for CCL-RSc and NCL-RSc with full uncertainty, following GCL-RSc with 12 uncertain parameters.

Table 6.7. MAPE under different p and q using BCS for $PrD_{ref\text{-}CCL}$ and $PrD_{ref\text{-}NCL}$ ($\times 10^{-2}$; $R_{MCS\text{-}PCE}$=1500).

q \ p	6	7	8	9	10
0.5	1.94	2.39	1.90	1.30	1.30
0.6	1.94	1.41	1.29	1.96	1.88
0.7	1.87	1.81	1.42	1.85	1.88
0.8	1.71	1.88	1.84	1.90	1.42
0.9	1.91	1.86	1.97	2.06	2.16

(a) BCS for $PrD_{ref\text{-}CCL}$

q \ p	6	7	8	9	10
0.4	6.24	5.68	3.79	3.80	3.80
0.5	5.90	5.13	4.54	3.70	3.80
0.6	5.90	5.44	4.04	3.77	4.38
0.7	6.03	4.80	3.64	3.85	3.83
0.8	5.59	4.12	3.74	4.04	3.84

(b) BCS for $PrD_{ref\text{-}NCL}$

Table 6.8. Statistics comparison of $\ln(C_{aq\text{-}max})$ between MCS and PCE for $PrD_{ref\text{-}CCL}$ and $PrD_{ref\text{-}NCL}$.

		MCS	PCE	MAPE
$PrD_{ref\text{-}CCL}$	Mean	5.45	5.44	1.29%
	SD	1.64	1.64	
$PrD_{ref\text{-}NCL}$	Mean	4.62	4.62	3.64%
	SD	2.22	2.20	

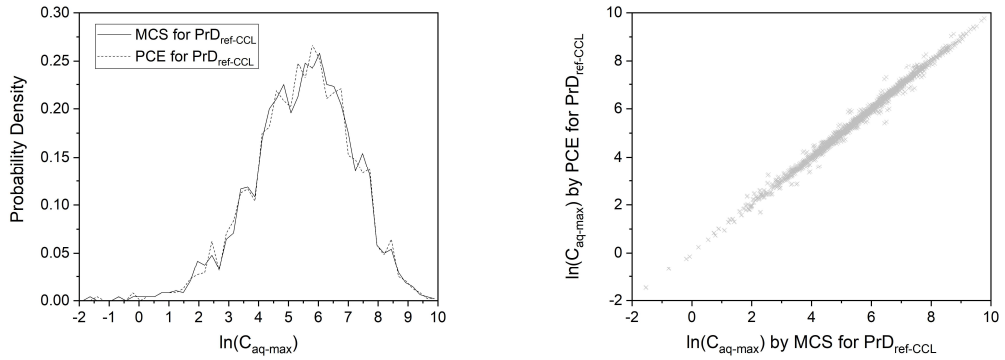

(a1) (a2)

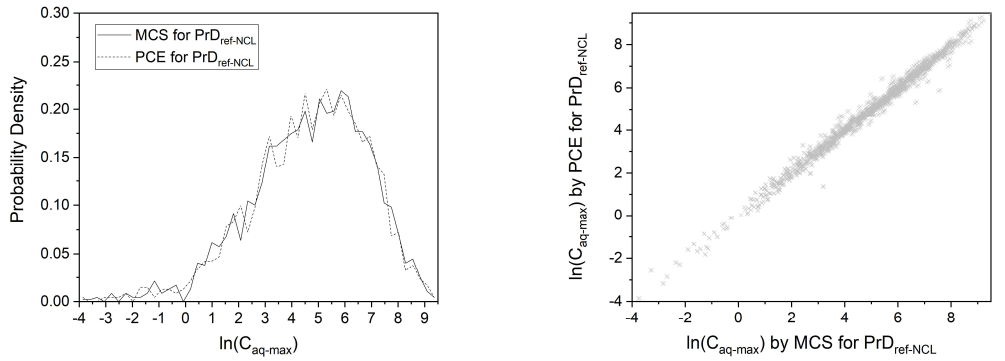

(b1) (b2)

Figure 6.7. Accuracy of PCE by comparison of ln(C_{aq-max}) predictions between MCS and PCE for (a) $PrD_{ref-CCL}$ (p=8, q=0.6) and (b) $PrD_{ref-NCL}$ (p=8, q=0.7) (BCS; $R_{MCS-PCE}$=1500; R_{MCS}=R_{PCE}=2000).

Chapter 7

Probabilistic Analyses of PFOS Transport through Single Composite Liner Systems

---

7.1 Probabilistic Analysis & Risk Assessment

The core research outcomes of this project, namely, the probabilistic analysis of PFOS transport through liner systems and the risk assessment of PFOS contamination in aquifers, are presented and discussed in this chapter. These findings build upon the groundwork laid in the preceding chapters, including the development of models for three different liner designs and the methodological framework centred on PCE-MCS (Chapter 3), the incorporation of uncertain input parameters (Chapter 4), the baseline provided by deterministic analyses and the preliminary evaluation of parameter contributions to output variability (Chapter 5), and the optimisation of PCE (Chapter 6).

All key results of the probabilistic analysis are summarised in Table 7.1 and Table 7.2, including the statistics of $C_{aq\text{-}max}$ yielded by the PCE-MCS, the probability of $C_{aq\text{-}max}$ exceeding four drinking water guidelines/standards, and function parameters of lognormal approximations of probability density (PD) and probability of exceedance (PoE). The three scenarios of Sc-, RSc, Sc+, are simulated for GCL+AL (Design I), CCL+AL (Design II), and NCL (Design III), with RSc0 (diffusion-only) results reported for Design I only, for reasons discussed later in this section. The histograms of $C_{aq\text{-}max}$ under all advection-diffusion scenarios for all the three liner designs are shown in Figure 7.1, uniformly with the interval width of 10 ng/l and the range of >1500 ng/l excluded. The PDF curves by both the kernel density estimation (KDE) fitting and the lognormal fitting are also included in Figure 7.1. Meanwhile, the PoE curves of $C_{aq\text{-}max}$ are shown in Figure 7.2, which are generated by KDE fitting and in line with the PoE values in Table 7.2. Finally, the four referenced guidelines/standards are plotted in each figure as red vertical lines.

7.1.1 General characteristics of probabilistic analysis results

The results of probabilistic analyses in Table 7.1 involve the three liner designs considered in this study, under each of which the different scenarios of CQA are reflected by the different distributions of L_w. Three statistics of $C_{aq\text{-}max}$ are presented, including the geometric mean (GM) reflecting the average level, the natural logarithm of geometric standard deviation (ln(GSD)) reflecting the variability, and the median reflecting the central tendency. Because the distributions of $C_{aq\text{-}max}$ are highly right-skewed, as shown in Figure 7.1, GM and ln(GSD) are better at characterising the distributions than the arithmetic mean (AM) and the standard deviation (SD).

One clear initial observation from Table 7.1 is within the GCL+AL section, namely, under the idealised pure-diffusion scenario with an intact GMB (RSc0), the single-liner system yields an extremely small distribution of $C_{aq\text{-}max}$ (GM =0.34 ng/l, Median =0.39 ng/l), which is much lower than those of the more realistic advection-diffusion scenarios containing GMB with defects. This indicates that advective transport through GMB defects is dominant over diffusive transport in the studied PFOS migration through the liner system, and a single-liner system with an intact GMB is fully capable for containing PFOS. This agrees with the conclusion generated from the deterministic analyses in Section 5.2.2. Moreover, the deterministic analyses yield the same conclusion for both the CCL+AL and NCL designs (Section 5.2.2). Therefore, the probabilistic analyses for the pure-diffusion scenario (RSc0) are not conducted for Design II and Design III, and the perfect containment of PFOS by a single-liner system with an intact GMB can be reasonably extrapolated to Design II and Design III. In the remainder of this chapter, the discussion focuses on the advection-diffusion scenarios Sc-, RSc and Sc+.

It can be observed that, for all calculated cases, the GM of $C_{aq\text{-}max}$ (the average level of all possible outputs) is 40~60% of the $C_{aq\text{-}max}$ from deterministic analyses (the output of an average case), and the medians are slightly higher than the GM. Hence, if defining the contamination level by a single output value, the GM or medians of $C_{aq\text{-}max}$ from probabilistic analyses will give a more optimistic estimation than the deterministic analyses do. Meanwhile, the high values of ln(GSD) (1.6~1.85 for Design I and Design II and ~2.2 for Design III) indicate significant variability of the output.

Table 7.1. $C_{aq\text{-}max}$ Statistics from probabilistic analysis for different CQA scenarios of different liner designs.

		GCL+AL (Design I)				CCL+AL (Design II)			NCL (Design III)		
		Sc-	**RSc**	**Sc+**	**RSc0**	**Sc-**	**RSc**	**Sc+**	**Sc-**	**RSc**	**Sc+**
Key Variable	**L_w (m/ha)**	[20, 250, 1450]	[0, 20, 1450]	[0, 20, 250]	0	[20, 250, 1450]	[0, 20, 1450]	[0, 20, 250]	[20, 250, 1450]	[0, 20, 1450]	[0, 20, 250]
$C_{aq\text{-}max}$ from deterministic analyses*		509	404	176	0.55	488	463	204	209	206	177
$C_{aq\text{-}max}$ Statistics from PCE-MCS	**GM (ng/l)***	315	262	126	0.34	276	229	129	109	102	75
	Median (ng/l)*	352	301	141	0.39	311	259	144	138	128	94
	ln(GSD)	1.67	1.82	1.78	1.84	1.59	1.64	1.76	2.18	2.19	2.22
	$C_{aq\text{-}max\text{-}95\%}$ (ng/l)	4002	4042	2007	5.34	3029	2746	1936	2535	2436	1892

*: The more optimistic estimation based on GM or Median of probabilistic analyses than the deterministic results is not a general rule; rather, it arises from the specific non-linear response characteristics of the present PFOS transport model. In our system, $C_{aq\text{-}max}$ exhibits sub-linear sensitivity to variations in the governing parameters. When combined with the positively skewed (lognormal) input distributions, the lower-tail values have a proportionally stronger influence on the GM of the Monte Carlo outcomes than the upper-tail values, leading to a GM that is lower than the deterministic prediction based on GM inputs. This behaviour is therefore dependent on the modelling assumptions and transport mechanisms considered here and is not universally applicable, although sub-linear response behaviour is common in many physical processes.

While the three statistics in Table 7.1 capture some key features of the $C_{aq\text{-}max}$ distributions, a visual representation of the distributions is provided via histograms in Figure 7.1. On one hand, a significant proportion of $C_{aq\text{-}max}$ fall within the relatively low value range, and the percentage gradually decreases as the value increases. On the other hand, the distribution also extends considerably toward higher values and forms a long right tail, indicating the non-negligible possibility of serious PFOS contamination. Such a pattern reflects the inherent asymmetry and dispersion typical of highly right-skewed distributions, such as a lognormal distribution with high variability. To keep the readability and comparability of figures, $C_{aq\text{-}max}$ values beyond 1500 ng/l are not shown in Figure 7.1. Nevertheless, the extent of right-ward tail is reflected by the 95% percentile of $C_{aq\text{-}max}$ ($C_{aq\text{-}max\text{-}95\%}$) in Table 7.1; in all cases other than RSc0, the value is greater than around 1900 ng/l.

As already stated in Chapter 3, the KDE-based approximation does not provide explicit functional forms for PD and PoE, but fits the original data very well and yields reliable curves for PD and PoE (Figure 7.1 and Figure 7.2). Meanwhile, the lognormal best fit, which provides explicit expressions for PD and PoE in Table 7.2, offers an alternative approximation approach, with slightly lower but still acceptable fidelity to the original data. The marginally superior fit of the KDE over the lognormal distribution can also be observed from the respective PDF curves displayed in Figure 7.1. The PoE values relative to drinking water guidelines/standards, as presented in Table 7.2, are based on KDE and in line with the curves in Figure 7.2. They agree extremely well with the PoE based on the original data. As shown via the curves in Figure 7.2, the PoE declines smoothly along with the increase of $C_{aq\text{-}max}$ but remains considerable even when $C_{aq\text{-}max}$ is relatively high. For example, the PoE corresponding to 1500 ng/l is still over 10% for scenarios of Sc- and RSc, and ~7% for scenarios of Sc+. This is consistent with the fact that there is still a considerable chance of exceeding 1500 ng/l not shown by the histograms in Figure 7.1. A discussion of the PoE, compared to each guideline/standard for all simulated cases, will be presented later in this chapter.

	Sc-	RSc	Sc+
GCL+AL (Design I)	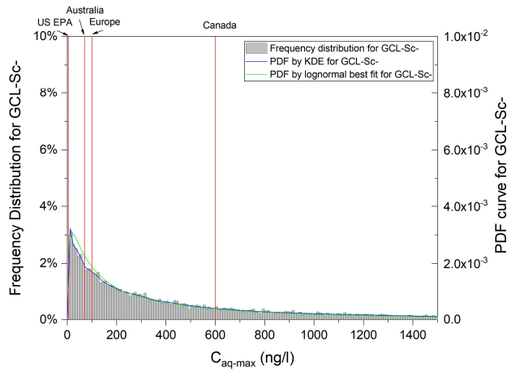 (a1)	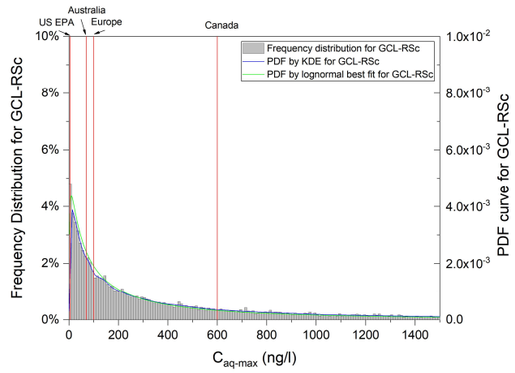 (a2)	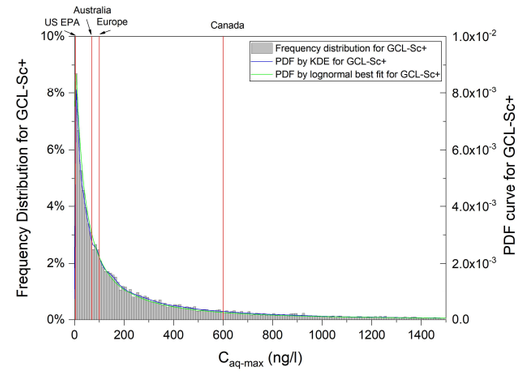 (a3)
CCL+AL (Design II)	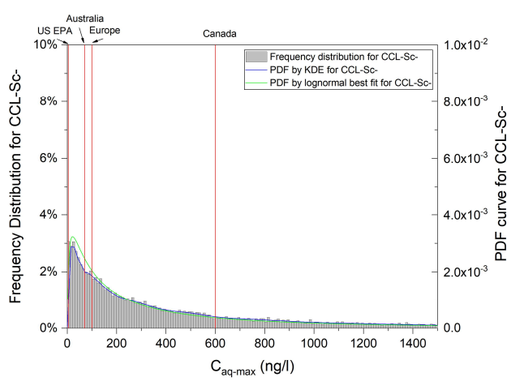 (b1)	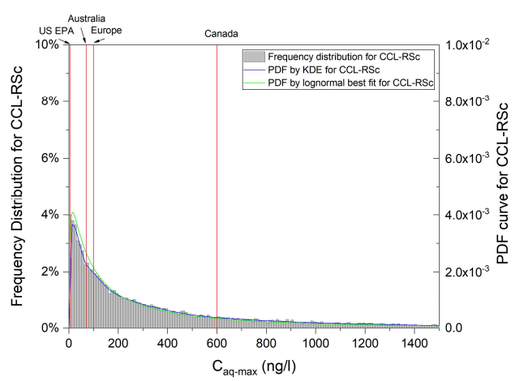 (b2)	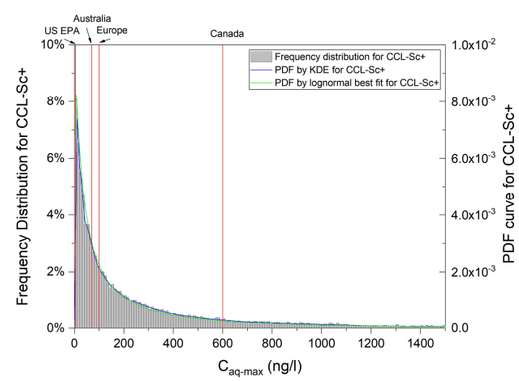 (b3)
NCL (Design III)	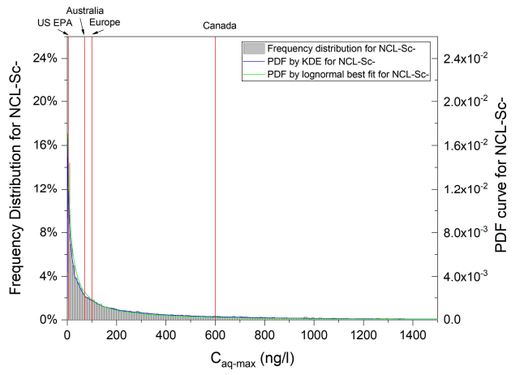 (c1)	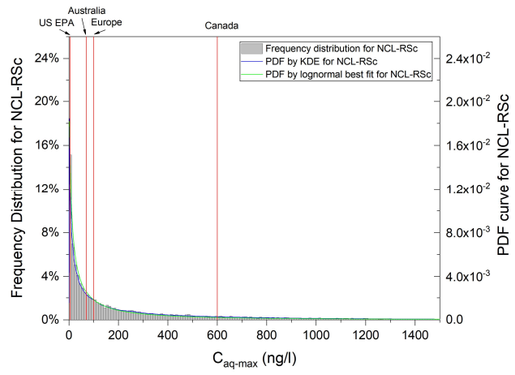 (c2)	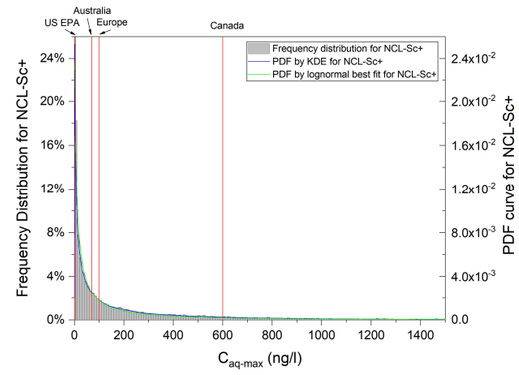 (c3)

Figure 7.1. Frequency distributions (histogram interval width is 10 ng/l) and PDF curves of $C_{aq\text{-}max}$ for different CQA scenarios of different liner designs.

7.1.2 Effects of CQA and liner designs on risk of aquifer contamination

Tables 7.1 & 7.2 and Figures 7.1 & 7.2 can be used to compare the performance of liner systems across different designs (I, II, III) or different scenarios (Sc-, RSc, Sc+). In Figure 7.1, graphs are arranged so as to allow such comparisons within the same row of graphs (different CQA scenarios) or the same column (different designs). The information conveyed by Figure 7.2(a) and Figure 7.2(b) is identical, but arranged differently so as to make it easier to assess the effects of CQA and liner designs, respectively. In general, findings from probabilistic analyses are in broad agreement with those based on deterministic analyses discussed in Chapter 5.

Effects of CQA

It is clear from probabilistic analyses that CQA level has an important effect on risk of PFOS contamination in groundwater. Improving CQA by moving from Sc- (good CQA, no ELL) to RSc (good CQA, with ELL) and then to Sc+ (with excellent CQA and ELL) reduces the aquifer contamination for all the three liner designs. For example, in the case of GCL+AL, improving CQA leads to a decrease in the GM of $C_{aq\text{-}max}$ from 315 ng/l to 262 ng/l, then to 126 ng/l. This is expected since PFOS transport is advection-dominated and enhancing the CQA level is reflected in the models by a reduction in the defects on GMB and thus the leakage rate. As for the extent of improvement, the gain from Sc- to RSc is less significant than that from RSc to Sc+, which can be seen from the GM difference in Table 7.1 and the gap between curves in Figure 7.2(a); this is true for all three designs. This reveals that the application of ELL, while useful, only produces a partial improvement, and ensuring excellent construction quality is more impactful. This trend is broadly consistent with outcomes of the deterministic analysis; its underlying mechanism, previously discussed in Section 5.2.2, lies in the causal chain linking defect density, leakage rate, and contaminant concentration. Another noteworthy point is that the performance gain associated with improved CQA is more pronounced in the GCL+AL and CCL+AL designs (Figure 7.2(a1)(a2)), where the GM reduction from Sc- to Sc+ is 315 to 126 ng/l for GCL+AL and 276 to 129 ng/l for CCL+AL. In contrast, the NCL design exhibits much lower sensitivity to CQA improvements (Figure 7.2(a3); from Sc-'s 109 to Sc+'s 75 ng/l). This implies that investing in higher CQA under the GCL+AL and CCL+AL designs may yield greater returns compared to the NCL design.

Effects of Liner Design

As demonstrated by the PoE curves in Figure 7.2(b) and the PoE values in Table 7.2, under each level of CQA, the performance of the GCL+AL and CCL+AL designs is nearly identical, especially in relation to the three more stringent guidelines/standards (4 ng/l, USEPA; 70 ng/l, Australia; 100 ng/l, Europe), and the NCL design clearly outperforms them. This is consistent with the conclusions based on the deterministic analyses (Section 5.2.2). However, judging by the statistics, the performance of the CCL+AL design is slightly but clearly better than that of the GCL+AL design under Sc- (GM of $C_{aq\text{-}max}$: 276 ng/l vs 315 ng/l) and RSc (GM of $C_{aq\text{-}max}$: 229 ng/l vs 262 ng/l). This highlights the importance of examining the full dataset rather than relying solely on summary statistics, which may not fully reflect certain aspects of the underlying data. In addition, while all three designs produce widely varying possibilities of $C_{aq\text{-}max}$, the NCL design exhibits the highest variability, indicated by comparing ln(GSD) (e.g., 1.82, 1.64 and 2.19 for Designs I, II and III, respectively, under RSc). The next important trend is reflected by the gap between curves in Figure 7.2(b). That is, the distinctions among the three designs, particularly the superior performance of the NCL design, are more pronounced under the Sc- and RSc scenarios (Design III outperforms Design I by GM of $C_{aq\text{-}max}$: 109 ng/l vs 315 ng/l for Sc-, and 102 ng/l vs 262 ng/l for RSc), suggesting that when the CQA level is expected to be relatively low, the NCL design may be a more favourable choice. In contrast, under the Sc+ scenario, the sensitivity to liner design diminishes considerably (Design III outperforms Design I by GM of $C_{aq\text{-}max}$: 75 ng/l vs 126 ng/l), indicating that with ideal CQA conditions, all three designs perform similarly well.

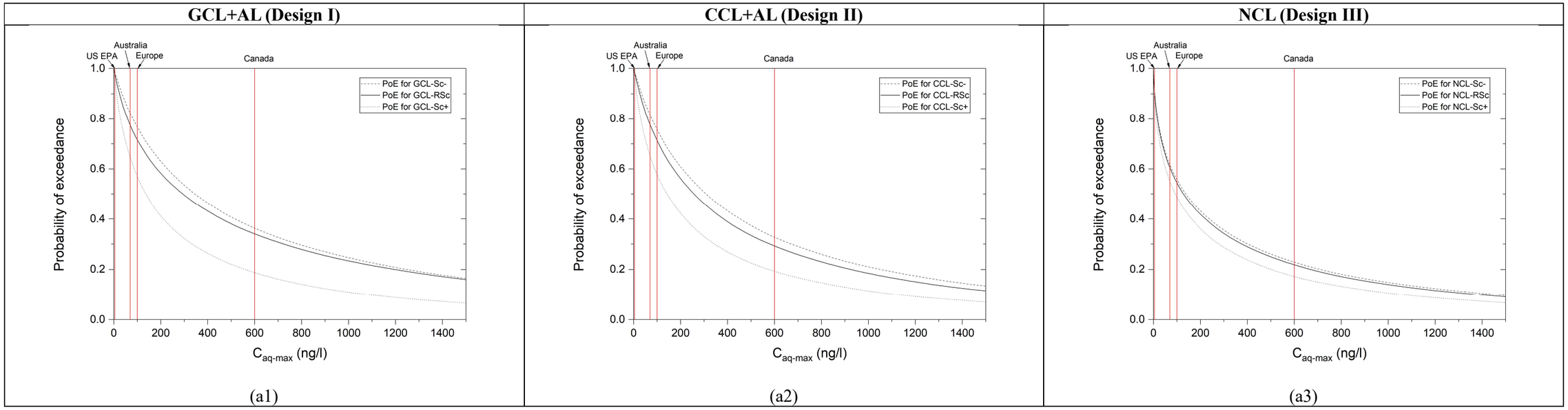

(a) The effect of CQA on $C_{aq\text{-}max}$ exceedance probability.

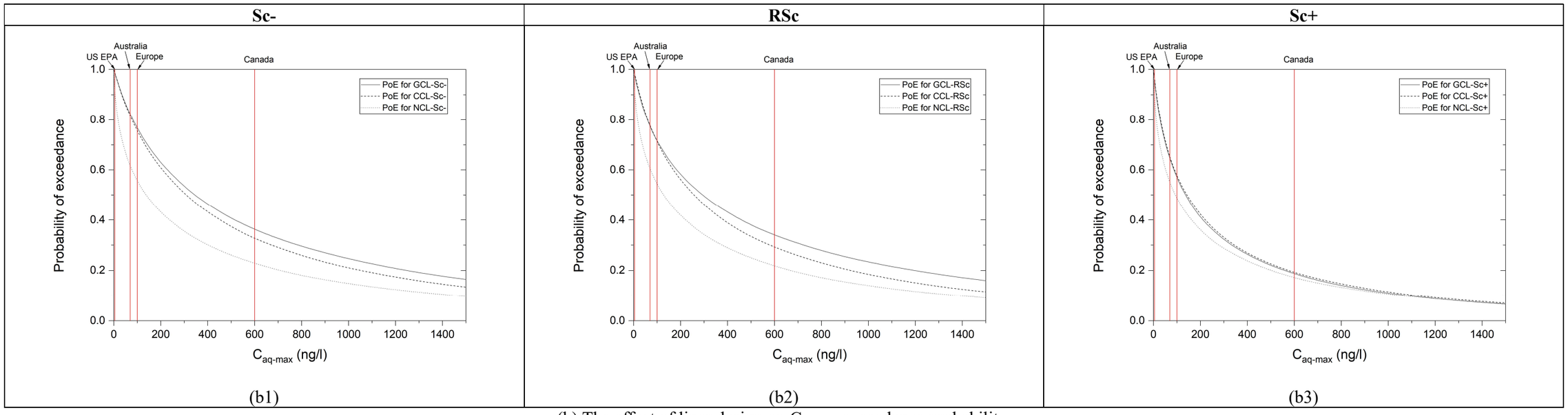

(b) The effect of liner design on $C_{aq\text{-}max}$ exceedance probability.

Figure 7.2. $C_{aq\text{-}max}$ exceedance probability by KDE for different CQA scenarios of different liner designs.

Table 7.2. PoE by KDE & Functions by Lognormal best fit from probabilistic analysis for different CQA scenarios of different liner designs.

		GCL+AL (Design I)				CCL+AL (Design II)			NCL (Design III)		
		Sc-	**RSc**	**Sc+**	**RSc0**	**Sc-**	**RSc**	**Sc+**	**Sc-**	**RSc**	**Sc+**
Key Variable	**L_w (m/ha)**	[20, 250, 1450]	[0, 20, 1450]	[0, 20, 250]	0	[20, 250, 1450]	[0, 20, 1450]	[0, 20, 250]	[20, 250, 1450]	[0, 20, 1450]	[0, 20, 250]
C_{aq-max} from deterministic analyses		509	404	176	0.55	488	463	204	209	206	177
Probability of Exceedance by KDE	**USEPA (C_{ref}=4 ng/l)**	99%	98%	97%	7.5%	99%	99%	97%	92%	92%	90%
	Australia (C_{ref}=70 ng/l)	82%	78%	65%	0%	82%	78%	65%	62%	61%	55%
	Europe (C_{ref}=100 ng/l)	77%	72%	57%	0%	76%	71%	58%	56%	55%	49%
	Canada (C_{ref}=600 ng/l)	36%	34%	19%	0%	33%	29%	19%	23%	22%	17%
Functions by Lognormal best fit	**PDF: m_1,m_2,m_3***	4.19, 5.59, 5.75	4.56, 6.62, 5.57	4.47, 6.37, 4.84	4.62, 6.79, -1.09	3.99, 5.08, 5.62	4.12, 5.40, 5.44	4.41, 6.18, 4.86	5.47, 9.53, 4.69	5.49, 9.59, 4.62	5.56, 9.83, 4.31
	R^2 of PDF	0.980	0.990	0.993	0.998	0.959	0.976	0.991	0.985	0.985	0.988
	PoE function: n_1,n_2**	5.75, 2.36	5.57, 2.57	4.84, 2.52	-1.09, 2.60	5.62, 2.25	5.44, 2.32	4.86, 2.49	4.69, 3.09	4.62, 3.10	4.31, 3.14

$$*PD = \frac{1}{m_1 C_{aq-max}} \exp\left\{-\frac{1}{m_2}\left[\ln\left(C_{aq-max}\right) - m_3\right]^2\right\} \quad (7.1)$$

$$**PoE = \frac{1}{2}\left\{1 - \text{erf}\left[\frac{\ln\left(C_{aq-max}\right) - n_1}{n_2}\right]\right\} \quad (7.2)$$

7.1.3 Risk assessment relative to drinking water guidelines/standards

Based on the PoE associated with the four regulatory guidelines/standards shown in Table 7.2, a comprehensive assessment of the PFOS contamination risk across all cases is presented in this subsection. The effects of CQA and design configurations on contamination, discussed above, can also be reflected and further supported by the PoE values.

The specific PoE-based risk assessment largely depends on the guideline/standard. For the most stringent standard (4 ng/l, USEPA), PoE is over 95% for Design I and Design II and around 90% for Design III, indicating an extremely high risk of contamination. For the moderate guideline in Australia (70 ng/l) and standard in Europe (100 ng/l), the contamination risks are still unacceptably high as their PoE ranges from 49% (Design III, Sc+, Europe) to 82% (Design I, Sc-, Australia). Even under the most lenient guideline (600 ng/l, Canada), PoE ranges between 17% and 36%, depending on specific design and scenarios (Sc-, RSc, Sc+). Although an excellent construction quality (Sc+) reduces the risk substantially, it does not eliminate it (PoE=19%, 19%, 17% for Designs I, II, III). Note here that, as mentioned earlier, both Australian and Canadian guidelines are undergoing a process of revision which is likely to result in more stringent ceilings.

When PoE is used as the criterion, the effect of improving construction quality and introducing ELL varies depending on the standard/guideline referenced. CQA improvement is marginally effective in the case of USEPA standard (PoE dropping from 99% to 96% when upgrading from Sc- to Sc+, for the GCL+AL design) and moderately so for others (e.g., corresponding change in PoE for Australian guideline is a drop from 82% to 65%). Continuing with the Australian guideline, performance gains from refining construction quality (RSc to Sc+) are larger than applying ELL (Sc- to RSc) with PoE decreasing from 82% for Sc- to 78% for RSc and then to 65% for Sc+, under Designs I and II (coincidentally identical). The corresponding values for Design III are 62%-61%-55%. In addition, the gap between Sc- and Sc+ (82%-65% for Designs I, II and 62%-55% for Design III) further supports the earlier finding that the effect of improved CQA is more significant in Designs I, II than in Design III, and that Design III performs significantly better under the poorer construction quality scenario.

In summary, using USEPA (4 ng/l), Australian (70 ng/l) and European (100 ng/l) drinking water guidelines/standards as a reference, the PoE remains significantly high across all studied single-lined cases, regardless of the CQA level or liner design applied.

7.2 Global Sensitivity Analysis (GSA) based on Sobol' Indices

Assessing the sensitivity of contamination to all uncertain variables is important for two reasons. First, such analyses can identify the leverage variables with most impact and hence help in pointing out possible modifications to liner design or operational practices so as to reduce the risk of PFOS contamination. Second, outcomes of sensitivity analysis can help in identifying which variables need to be known with more certainty to achieve better prediction accuracy, and hence suggest future research priorities, towards narrowing uncertainty associated with high-impact variables.

As introduced in Section 2.4.3 and Appendix 3.3, the Sobol' indices (SIs) are used herein as a measure of the global sensitivity of $C_{aq\text{-}max}$ to various uncertain variables. The first-order Sobol' index (SI) of a variable represents its singular effect on $C_{aq\text{-}max}$. Higher-order indices, also known as multiple-term indices, add the effects of interactions between multiple variables. The total Sobol' index of a variable is the sum of all indices involving this variable, including first and higher order ones. Both the first-order indices and the total indices, under the three CQA levels and for the three liner designs, are shown in Figure 7.3. In addition, Tables 7.3 (a) to (c) show all uncertain variables for the three designs, respectively, arranged by descending order of Sobol' indices as obtained under scenario RSc.

For the cases considered in this thesis, the total indices are found to be close to the corresponding first-order indices, indicating minimal effect of interactions between variables. As previously determined in the analyses in Section 5.3, the simulation of GCL+AL incorporates 12 uncertain parameters (10 factors after merging correlated pairs), that of CCL+AL 10 uncertain parameters (9 factors), and for NCL 9 uncertain parameters (8 factors).

The two factors with the most dominant influence on $C_{aq\text{-}max}$ are always the PFOS load in the waste (C_{b0}, p_0) and the hydraulic conductivity of the functional clay liner (k_{FCL}); the latter refers to k_a/ k_b, k_{CCL}, k_{NCL} for the three designs respectively. The second set of most influential factors includes L_w and ΔH for the GCL+AL design; L_w, T_{AQ}, θ, and

ΔH for the CCL+AL design; and T_{AQ}, T_{NCL}, and L_w for the NCL design. The other factors do not make significant contributions to the uncertainty of the output. These findings are generally consistent with the results of preliminary sensitivity analyses in Section 5.3.

Different liner designs seem to exhibit some differences among Table 7.3 (a), (b) and (c). First, the Sobol' indices of C_{b0} & p_0 and k_{FCL} in Design III are comparable, in contrast to the more succinct dominance of C_{b0} & p_0 in Design I and Design II, with ratios of Sobol' indices of C_{b0} & p_0 to those of k_{FCL} ranging from 2 to 3 for GCL+AL and 6 to 9 for CCL+AL (depending on the CQA scenario). The large thickness of NCL likely explains the particularly strong influence of k_{FCL} within Design III.

Second, the importance of θ is substantially greater for Design II and Design III compared to Design I. This behaviour, as already discussed in Section 5.3, is attributed to the higher values and larger variabilities of θ in Designs II and III (Table 4.4), which result in greater variability in wetted distance and overall leakage rate, thereby exerting a stronger influence on $C_{aq\text{-}max}$.

Third, both similarities and discrepancies are observed in the sensitivities to layer thicknesses, with comparisons between T_{AL} (Design I), T_{CCL}+T_{AL} (Design II) and T_{NCL} (Design III) especially instructive (given that T_{GCL} is small and there is only one clay layer in Design III). While for RSc and Sc-, the sensitivity to T_{AL} in Design I is similar to the sensitivity to T_{CCL}+T_{AL} in Design II, for Sc+, the former is much higher. As for Design III, the sensitivity to T_{NCL} is nearly twice that of T_{CCL}+T_{AL} in Design II across all three scenarios, which is expected given the greater thickness and the exclusive role of NCL in its design. Nevertheless, for Sc+, sensitivity to T_{AL} in Design I is still larger than that of T_{NCL} in Design III, indicating that a better control of leakage in the GCL+AL model increases the sensitivity to T_{AL} significantly, likely because of an increase in the importance of diffusion relative to advection.

In each of Table 7.3 (a), (b), and (c), the sensitivity ranks of variables across the three scenarios also exhibit certain discrepancies. For the GCL+AL design, L_w declines from 3rd to 6th and $\alpha_{T\text{-}AQ}$ rises from 9th to 3rd between Sc- and Sc+. The former is due to the narrower range of holed wrinkle length in Sc+ ([0, 20, 250] m/ha) compared to Sc- ([20, 250, 1450] m/ha) and RSc ([0, 20, 1450] m/ha), and thus a reduced variability in leakage rate. The latter can be primarily attributed to the lower overall level of L_w in Sc+, which

leads to a weaker advective flux of PFOS into the aquifer and thus greater sensitivity to dispersion effects in the aquifer.

For the CCL+AL design, there are two notable trends. (1) L_w ranks 7th under Sc- but 3rd under RSc and Sc+, which is an inverse trend to that in the GCL+AL design. This is attributed to the different extents of overlapping of wetted ranges around adjacent leaks (Figure 5.8) between Design I and Design II. In Design I, there are nearly no interactions between leaks no matter how dense they are, so the sensitivity contribution of L_w is simply related to its own variability. In Design II, the overlapping caused by the large wetted distance is pronounced when the leaks are denser, weakening the contribution of higher L_w to increasing the whole leakage rate and $C_{aq\text{-}max}$. In other words, with L_w taking [0, 20, 1450] m/ha or [20, 250, 1450] m/ha, the change of L_w among relatively large range approaching 1450 m/ha won't make a big difference to the leakage level and $C_{aq\text{-}max}$, while with L_w taking [0, 20, 250] m/ha, its change can propagate to $C_{aq\text{-}max}$ more sensitively. (2) Between Sc-/RSc and Sc+, θ rises from 5th to 2nd, and k_{CCL} declines from 2nd to 4th. This is also associated with the overlapping of wetted ranges, as under Sc+, the sparser leaks can better reflect the increased horizontal spread of leachate around one leak in the transmissive layer caused by a higher θ. The change of the rank of k_{CCL} should be an ancillary effect, since θ and k_{CCL} are both factors affecting leachate flow.

For the NCL design, the only notable change across scenarios is about L_w, whose rank rises from 8th to 5th then 3rd among Sc-, RSc, and Sc+. The underlying mechanism is supposed to be the same to what just discussed for the CCL+AL design.

<table>
<tr><th></th><th>Sc-</th><th>RSc</th><th>Sc+</th></tr>
<tr><td>GCL+AL (Design I)</td>
<td> 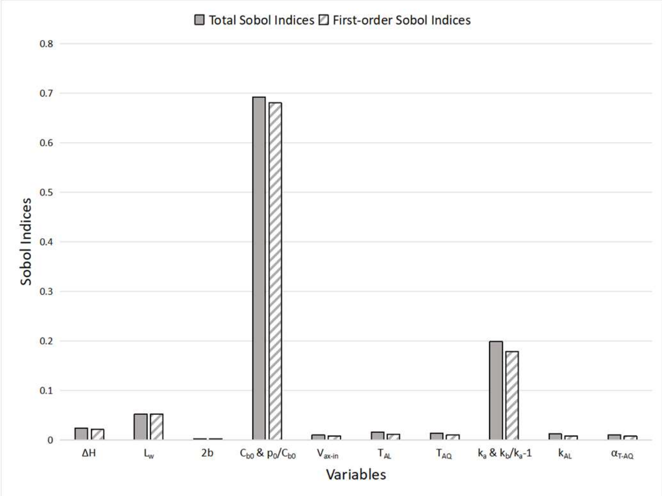

(a1)</td>
<td> 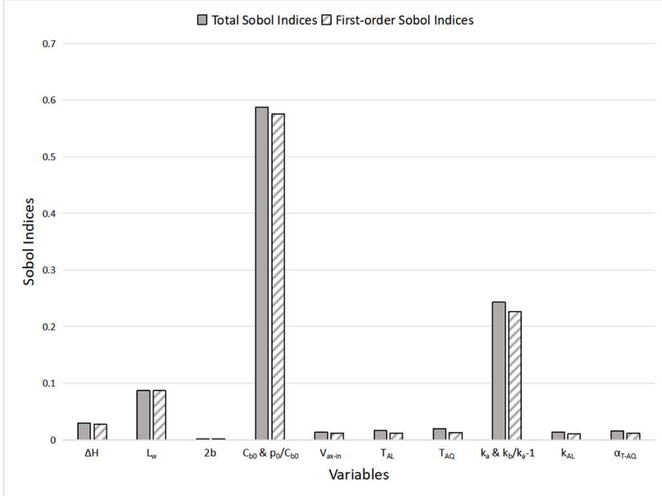

(a2)</td>
<td> 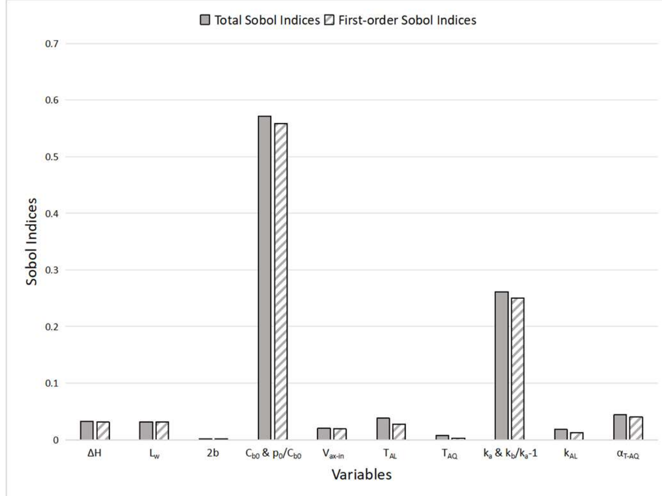

(a3)</td></tr>
<tr><td>CCL+AL (Design II)</td>
<td> 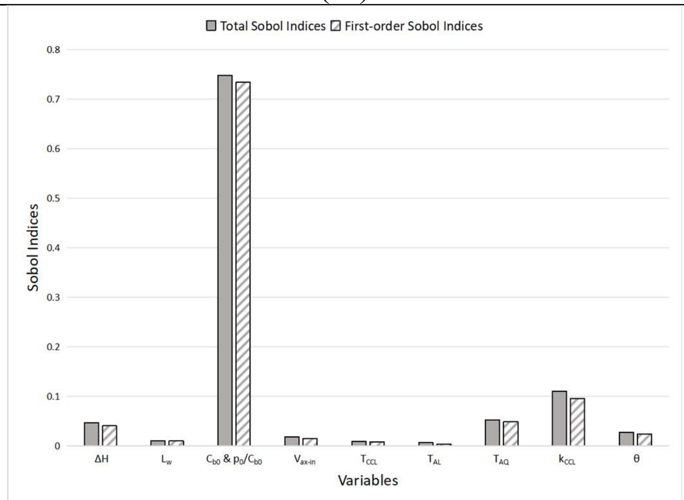

(b1)</td>
<td> 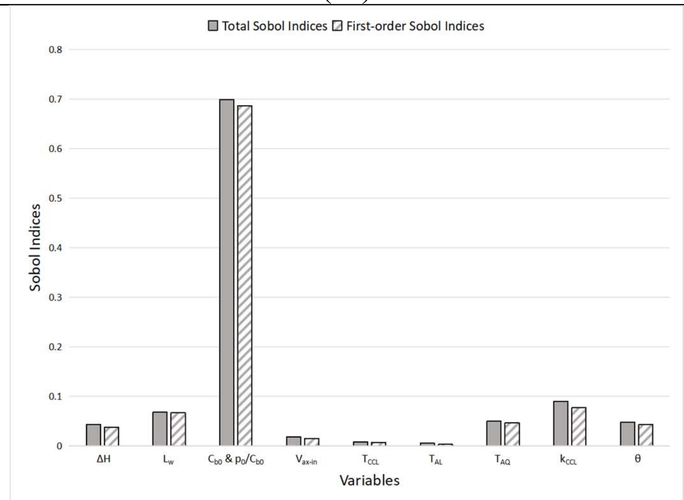

(b2)</td>
<td> 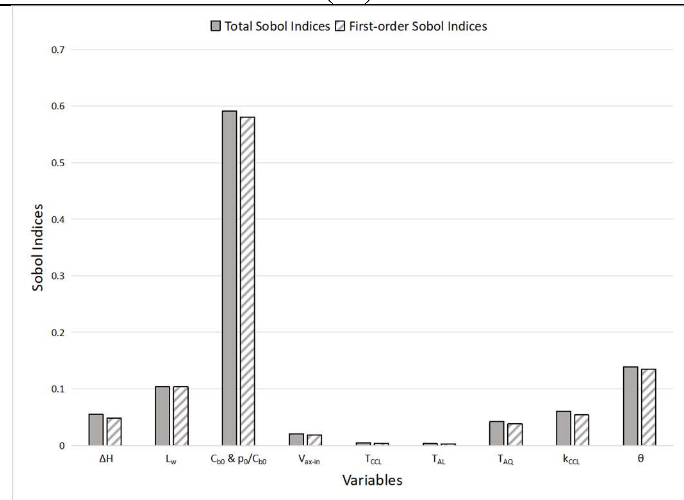

(b3)</td></tr>
<tr><td>NCL (Design III)</td>
<td> 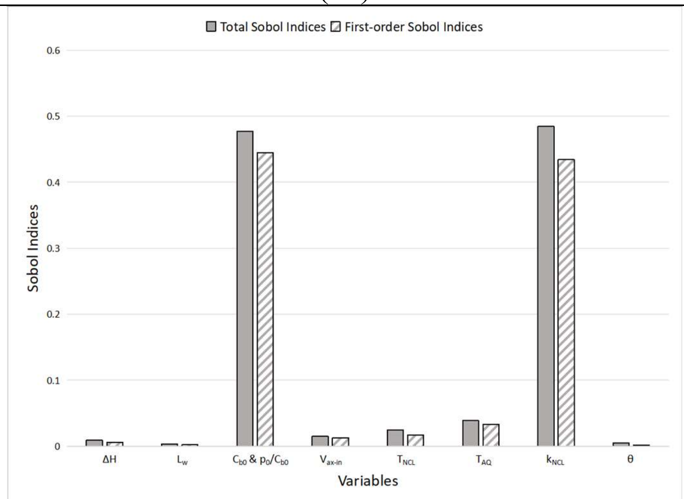

(c1)</td>
<td> 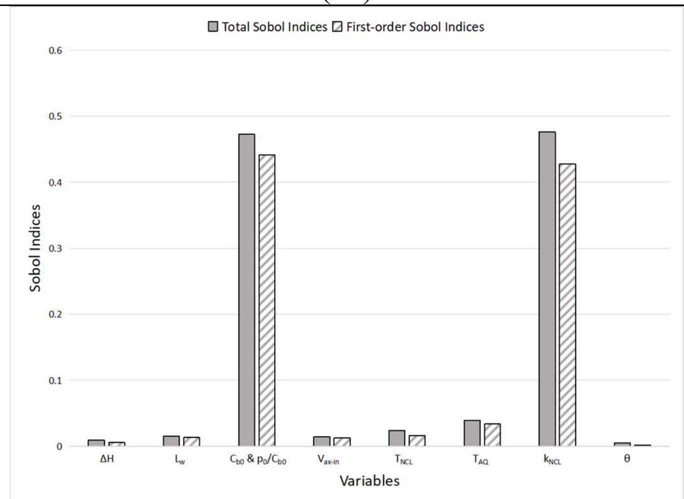

(c2)</td>
<td> 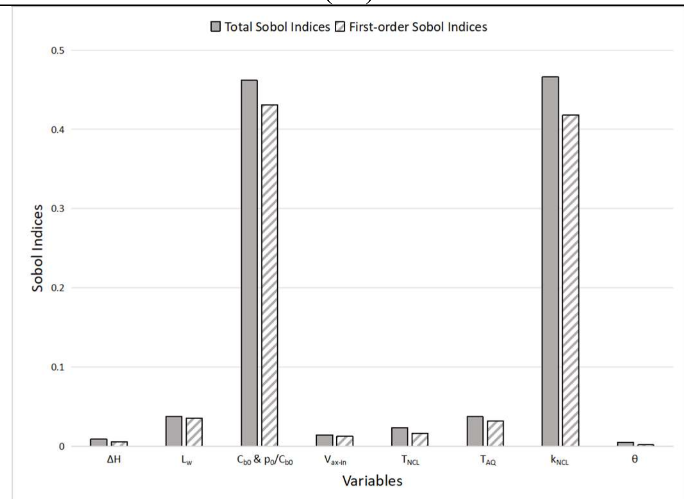

(c3)</td></tr>
</table>

Figure 7.3. Relative effects of input parameters for different CQA scenarios of different liner designs.

Table 7.3(a). Total Sobol' indices for uncertain parameters under different CQA scenarios of the GCL+AL design (Design I) (ordered by sensitivity from highest to lowest based on RSc).

Total Sobol' Index	Sc-		RSc		Sc+	
	Value	Rank	Value	Rank	Value	Rank
C_{b0} & p_0/C_{b0}	0.692	1	0.587	1	0.572	1
k_a & k_b/k_a-1	0.199	2	0.243	2	0.261	2
L_w	0.052	3	0.087	3	0.032	6
ΔH	0.023	4	0.030	4	0.032	5
T_{AQ}	0.014	6	0.020	5	0.008	9
T_{AL}	0.015	5	0.016	6	0.038	4
$\alpha_{T\text{-}AQ}$	0.010	9	0.016	7	0.044	3
k_{AL}	0.012	7	0.014	8	0.018	8
$V_{ax\text{-}in}$	0.010	8	0.014	9	0.021	7
2b	3.5×10^{-4}	10	4.4×10^{-4}	10	5.2×10^{-4}	10
$\alpha_{L\text{-}AQ}$	*		*		*	
θ	*		*		*	
α_{AL}	*		*		*	

*Variables having minor influences on variance of $C_{aq\text{-}max}$ for GCL-RSc according to preliminary sensitivity analyses in Section 5.3.

Table 7.3(b). Total Sobol' indices for uncertain parameters under different CQA scenarios of the CCL+AL design (Design II) (ordered by sensitivity from highest to lowest based on RSc).

Total Sobol' Index	Sc-		RSc		Sc+	
	Value	Rank	Value	Rank	Value	Rank
C_{b0} & p_0/C_{b0}	0.748	1	0.699	1	0.592	1
k_{CCL}	0.110	2	0.089	2	0.060	4
L_w	0.010	7	0.067	3	0.104	3
T_{AQ}	0.052	3	0.050	4	0.042	6
θ	0.027	5	0.047	5	0.139	2
ΔH	0.046	4	0.043	6	0.055	5
$V_{ax\text{-}in}$	0.018	6	0.017	7	0.021	7
T_{CCL}	0.009	8	0.008	8	0.005	8
T_{AL}	0.006	9	0.005	9	0.003	9
2b	*		*		*	
$\alpha_{T\text{-}AQ}$	*		*		*	
$\alpha_{L\text{-}AQ}$	*		*		*	
k_{AL}	*		*		*	
α_{AL}	*		*		*	

*Variables having minor influences on variance of $C_{aq\text{-}max}$ for CCL-RSc according to preliminary sensitivity analyses in Section 5.3.

Table 7.3(c). Total Sobol' indices for uncertain parameters under different CQA scenarios of the NCL design (Design III) (ordered by sensitivity from highest to lowest based on RSc).

Total Sobol' Index	Sc-		RSc		Sc+	
	Value	Rank	Value	Rank	Value	Rank
k_{NCL}	0.484	1	0.476	1	0.466	1
C_{b0} & p_0/C_{b0}	0.477	2	0.472	2	0.462	2
T_{AQ}	0.039	3	0.039	3	0.037	4
T_{NCL}	0.024	4	0.024	4	0.023	5
L_w	0.003	8	0.015	5	0.038	3
$V_{ax\text{-}in}$	0.015	5	0.014	6	0.014	6
ΔH	0.009	6	0.009	7	0.009	7
θ	0.005	7	0.005	8	0.005	8
2b	*		*		*	
$\alpha_{T\text{-}AQ}$	*		*		*	
$\alpha_{L\text{-}AQ}$	*		*		*	

*Variables having minor influences on variance of $C_{aq\text{-}max}$ for NCL-RSc according to preliminary sensitivity analyses in Section 5.3.

7.3 Temporal Evolution of PFOS Contamination: Analysis based on RSc for GCL+AL

So far, maximum concentrations of PFOS at all times have been considered. An understanding of the evolution in time of PFOS aquifer contamination can also be useful. Focusing on GCL+AL (Design I), Figure 7.4 shows the change in time of the GM, median, and ln(GSD) of $C_{aq\text{-}max\text{-}xy}$ which is defined as the maximum concentration anywhere in the aquifer as a function of time (as discussed in Section 3.5.2.3, the maximum is assumed to occur at the top of the aquifer under the right-most leak). Figure 7.5 shows the corresponding change in PoE with time, relative to the four drinking water guidelines/standards considered here. Finally, Figures 7.6 and 7.7 show the change over time of Sobol' indices, with a stacked chart emphasizing the overall composition and the curves highlighting the sensitivity of individual parameters, respectively.

7.3.1 Temporal evolution of statistics and PoE of $C_{aq\text{-}max\text{-}xy}$

The GM and Median of $C_{aq\text{-}max\text{-}xy}(t)$ reach their peak values, i.e., 142.9 ng/l and 187.6 ng/l, at 160 years, which are considerably smaller than the GM and Median of $C_{aq\text{-}max}$ (262 ng/l and 301 ng/l). Meanwhile, the peak values for the PoE against the four drinking water guidelines/standards are 93% at 160 years, 67% at 160 years, 61% at 140 years, and 28% at 140 years respectively, which are somewhat smaller than the corresponding PoE values of $C_{aq\text{-}max}$ (98%, 78%, 72%, and 34%). Therefore, assessing the PFOS contamination risk throughout the whole timescale will give a slightly more optimistic estimation than based on $C_{aq\text{-}max}$, although the conclusion of a very high risk level doesn't change. The highest concentrations occur around 140~160 years, which agrees with the result of the corresponding deterministic analysis (i.e., 155 years). Figure 7.5 shows that for the most stringent standard (4 ng/l, USEPA), the PoE is almost always larger than 50% throughout the whole studied period; for the two moderate guidelines/standards (70 ng/l, Australia; 100 ng/l Europe), the PoE exceeds 50% from 60 years to 500 years and exceeds 30% in the period after; for the least stringent guideline (600 ng/l, Canada), the PoE is always between 10% and 30%, which is relatively low but still non-negligible. As for the ln(GSD) of $C_{aq\text{-}max\text{-}xy}(t)$ over time, it is always greater than 2, meaning that at any time-node, the uncertainty of $C_{aq\text{-}max\text{-}xy}(t)$ is

high. In addition, the inverse trend of ln(GSD) relative to GM and Median reveals that the higher the average level of concentration, the lower the degree of variability.

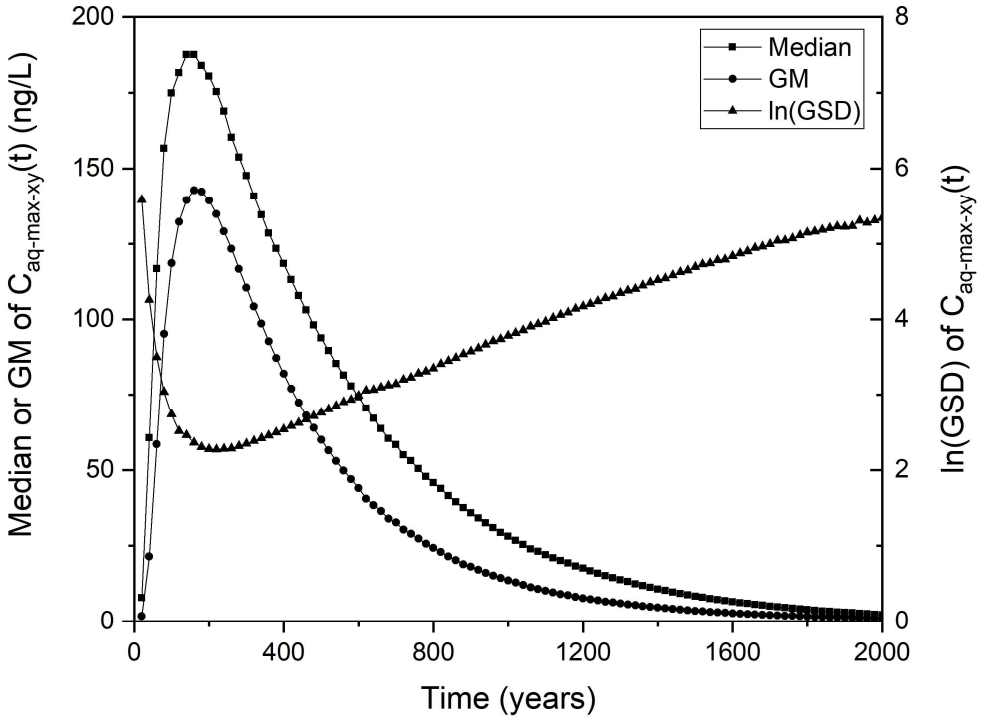

Figure 7.4. Statistics of $C_{aq\text{-}max\text{-}xy}(t)$ over time.

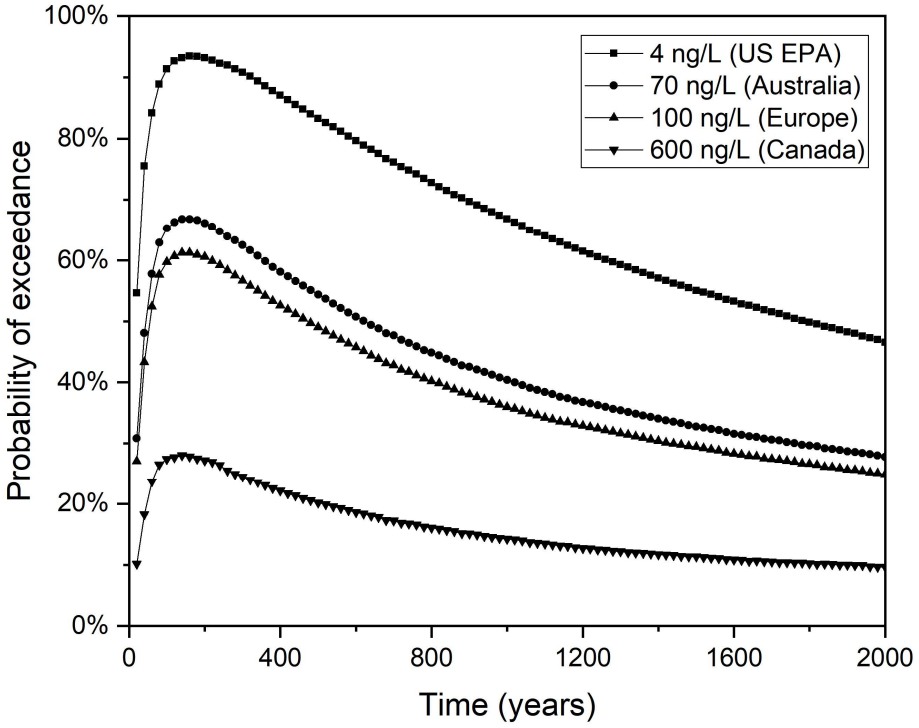

Figure 7.5. $C_{aq\text{-}max\text{-}xy}(t)$ exceedance probability relative to four guidelines/standards over time.

7.3.2 Temporal evolution of Sobol' indices

As shown in Figure 7.6 and Figure 7.7(a), the three most prominent factors in the temporal sensitivity analysis are C_{b0} & p_0/C_{b0}, k_a & k_b/k_a-1, and T_{AL}. Note that in the GSA analyses in Section 7.2, T_{AL} has not been found to cause high variability of outcome. Besides these three variables, only the SIs of ΔH and L_w are discernible during the early to middle period. To better visualise factors with small effect, Figure 7.7(b) shows the SIs of parameters, with the three most prominent ones removed. The following observations can be made based on Figures 7.6 and 7.7:

a) In the early stages (before 100 years), T_{AL} is the most influential factor, followed by k_a & k_b/k_a-1, while the influence of C_{b0} & p_0/C_{b0} starts low and rises rapidly. In this stage, PFOS has not yet reached the aquifer in significant amounts, and the concentration in the aquifer mostly depends on the barriers to advection, hence the importance of hydraulic conductivities and thickness of attenuation layer. At this early stage, almost all the initial mass of contaminant in the waste is available for downward transport, and C_{b0} & p_0/C_{b0} does not have a large influence on $C_{aq\text{-}max\text{-}xy}(t)$.
b) The influence of C_{b0} & p_0/C_{b0} increases before reaching a peak at 300 years and maintains it thereafter. At this stage, the available mass of contaminant in the waste becomes an important limiting factor for $C_{aq\text{-}max\text{-}xy}(t)$, and its influence is amplified by the high levels of uncertainty associated with C_{b0} & p_0/C_{b0}. Meanwhile, the importance of k_a & k_b/k_a-1 is decreasing but still considerable, and the influence of T_{AL} declines rapidly and becomes insignificant from 250 years to 500 years. During the peak-concentration period (100~300 years), the relative importance of various parameters is similar to those identified for $C_{aq\text{-}max}$ (Figure 7.3(a2)). From 300 to 500 years, the transport of PFOS is dominated by advection, and thus the parameters related to advective transport, i.e., k_a & k_b/k_a-1, L_w, ΔH, and k_{AL}, reach the peak of their respective influences.
c) As time progresses beyond 600 years, the pollution load keeps its dominant influence, as it governs the residual mass available for long-term migration. Notably, the effect of T_{AL} climbs back to second place, which can be explained by its role in regulating the delayed release of PFOS retained in the system. At the same time, the flow-related parameters (k_a & k_b/k_a-1, L_w and ΔH) make only small contributions to the uncertainty of $C_{aq\text{-}max\text{-}xy}(t)$. A possible explanation is

that, over longer time scales, solute transport becomes increasingly controlled by decline and depletion at the source and diffusion processes in the attenuation layer, at the expense of advection processes.

d) $V_{ax\text{-}in}$, T_{AQ}, and $\alpha_{T\text{-}AQ}$ make a difference by influencing the mechanical dispersion in the aquifer. With a greater dispersion in the aquifer, the peak concentration is reduced. Therefore, these three parameters always have small but stable influences (Figure 7.7(b)). Finally, the influence of 2b is always negligible because of its very small inherent variability.

In summary, the temporal sensitivity analysis based on the "GCL+AL, RSc" case revealed that for the most dangerous period concerning PFOS contamination risk (100~300 years), the most influential factor for $C_{aq\text{-}max\text{-}xy}(t)$ is the pollution load in the waste (C_{b0} & p_0/C_{b0}), while the influence of k_a & k_b/k_a-1, L_w, and ΔH is also considerable due to their impact on the advective transport. Other parameters only have minor influences. The importance of parameters related to water flow declines during the later stage of the studied time span. The thickness of the liner system has a significant effect on the concentration during the initial stage (before 100 years) and the later stage (after 600 years), by retarding the initial breakthrough and by governing the delayed release of residual PFOS, respectively. The parameters mainly affecting the mechanical dispersion in the aquifer ($V_{ax\text{-}in}$, T_{AQ}, and $\alpha_{T\text{-}AQ}$) have small but stable influences on $C_{aq\text{-}max\text{-}xy}(t)$.

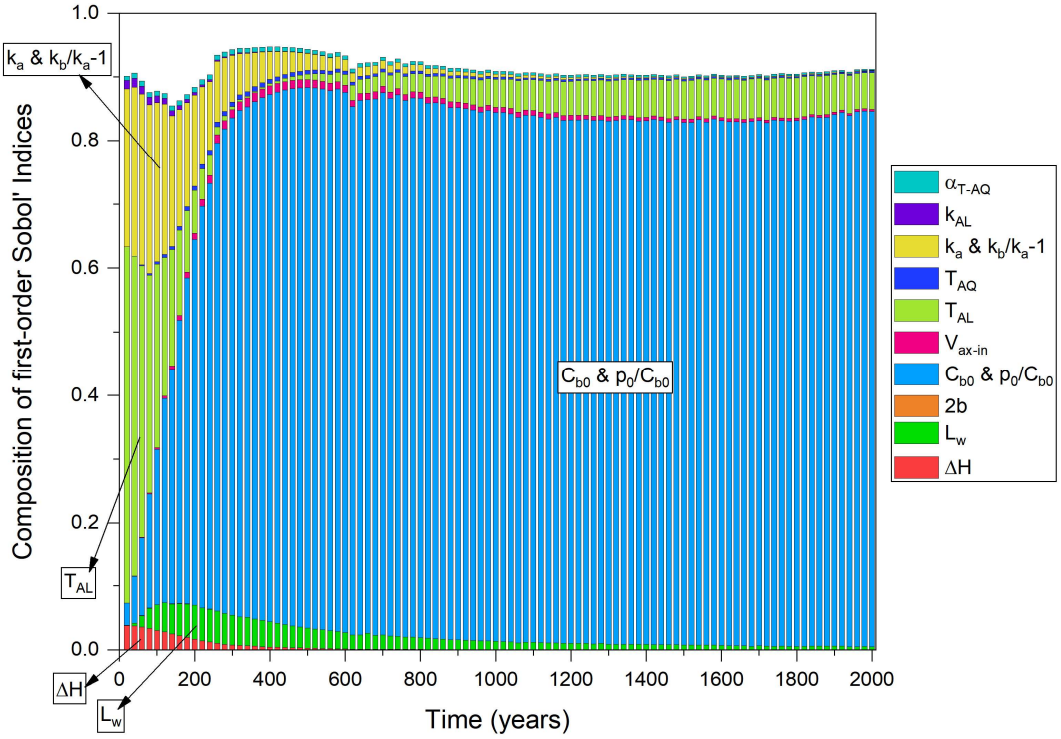

Figure 7.6. Stacked chart of first-order Sobol' indices of ln($C_{aq\text{-}max\text{-}xy}$(t)) over time.

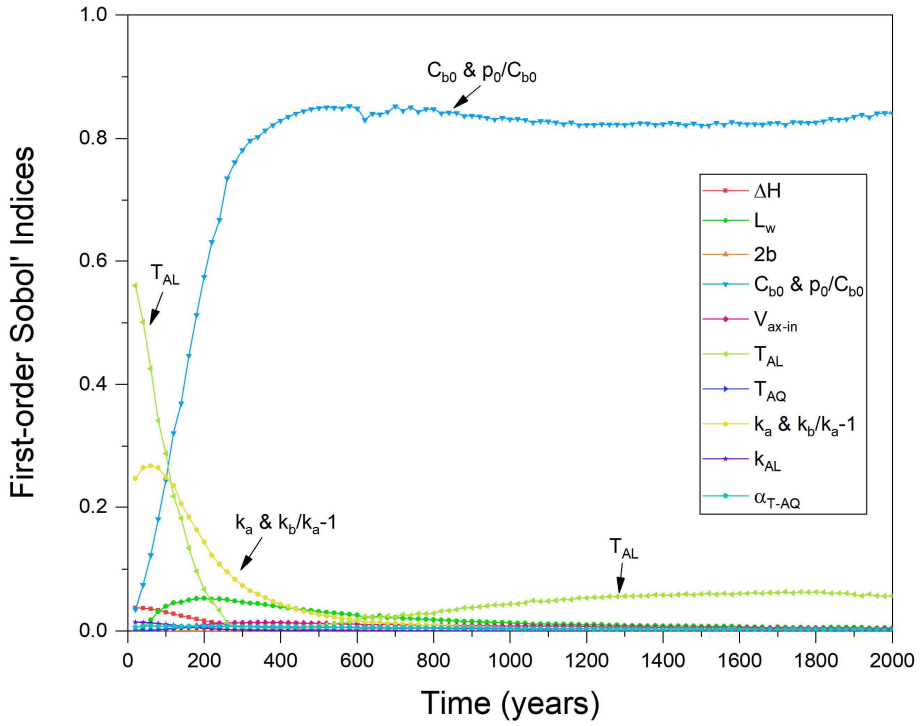

(a) Full factor

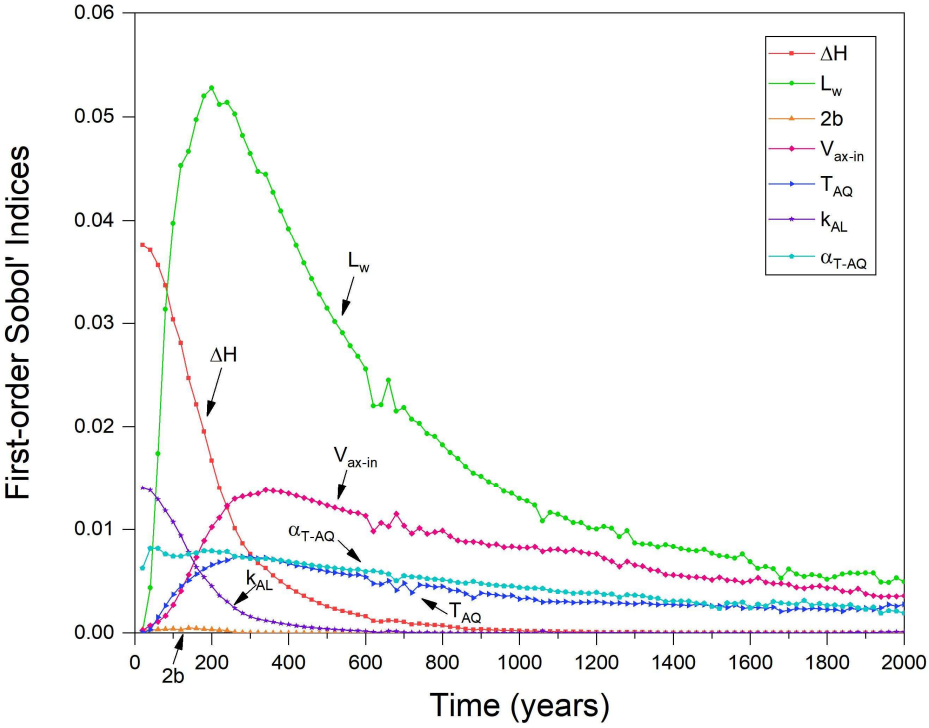

(b) Excluding the three most influential factors

Figure 7.7. First-order Sobol' indices for ln($C_{aq\text{-}max\text{-}xy}$(t)) over time.

7.4 Summary and Conclusions

The probabilistic analyses reported in this chapter have identified a high risk of PFOS contamination in aquifers underlying landfills equipped with three different kinds of single composite liner systems (Design I: GMB+GCL+AL, Design II: GMB+CCL+AL, Design III: GMB+NCL). The high risk has been found regardless of the construction quality applied and even if ELL is incorporated. The variables with the most impact on PFOS concentrations in groundwater have been found to be related to the mass of PFOS accepted into the landfill waste (C_{b0} and p_0), followed by the quality of construction and/or insulation material chosen (k_{FCL} for all designs, L_w for Designs I and II, and θ for Desing II) and the site conditions (ΔH for Designs I and II, and T_{AQ} for Designs II and III).

On the positive side, each one of the construction/material variables can be leveraged, within limits, by engineers, based on extensive knowledge of liner construction and management that has accrued over the past three decades. Selecting a GMB with a long service life is critical to ensure maximal insulation over the longest possible time (Di Battista et al., 2020; Rowe, 2018, 2020a, b). In addition, taking GCL as an example, the hydraulic conductivities of the GCL under the intact (k_a) and wrinkled (k_b) parts of the GMB can be kept at low values (e.g., $< 10^{-10}$ m/s) through well-documented quality assurance practices (Rowe et al., 2004; D35 Committee, n.d.). These include, amongst others, adequate testing of GCL samples; adequate treatment of overlapping edges of GCL to avoid leakage; careful consideration of the liner quality when applying GCL and its suitability for the ultimate use in service, relative to other alternatives such as CCL and NCL; and mitigation of the potentially damaging effects of exposure such as wet/dry or freeze/thaw cycles or downslope erosion (Rowe, 2018, 2020a). As for L_w, protocols for minimising wrinkles and holes in GMBs can be followed which include careful timing of GMB placement to minimise the formation of wrinkles and a quality construction program, likely including an ELL for detecting and repairing leaks.

On the downside, results of the analyses conducted herein show that even under the most favourable scenario (Sc+), the risk of exceeding drinking water guidelines/standards remains unacceptably high. While better construction quality reduces peak PFOS concentrations in the aquifer, it does not eliminate the risk. Simulations also show that PFOS concentrations in the aquifer may reach their peaks around 150 years or even later after PFOS is first accepted into the waste landfill.

Conditions in individual landfills will vary, leading to different times for peak concentrations. Nevertheless, given that PFOS production grew significantly over the second half of the 20th century until curbs were introduced, it is possible that peak PFOS concentrations in landfill-underlying aquifers may not be encountered until the end of this century and beyond. This raises obvious ethical questions of inter-generational equity, in addition to intra-generational ones often associated with environmentally degraded land.

Several complementary measures can be taken to address the problem. For new landfills expected to receive PFOS-polluted waste, double composite base liners, often used in hazardous waste landfills, are a safer choice. However, whether protection offered by the added composite liner can reduce risk to acceptable levels remains to be assessed. Another possible measure, given the high sensitivity of PFOS concentrations in the aquifer to C_{b0} and p_0, is to put in place a strict limit on the amount of PFOS-polluted waste accepted into the landfill and to divert any unaccepted PFOS to specialized landfills designed for the purpose. The advantage of this measure is that it can be applied to both new and existing landfills. On the other hand, implementing such controls is likely to be very challenging in practice, given the presence of PFAS, including PFOS, in a wide range of consumer products that may be very difficult to separate from the municipal waste stream. This observation highlights the critical importance of eliminating PFAS from consumer and industrial products upstream, at the design and manufacture stages, rather than attempting to address the problem at the waste disposal stage.

Chapter 8
Conclusions

8.1 Summary of Research

Per- and polyfluoroalkyl substances (PFAS) are a class of synthetic organic chemicals widely used in industrial and consumer products due to their thermal and chemical stability and surfactant properties. However, their persistence in the environment and potential adverse health impacts have raised increasing concerns regarding their long-term contamination risk. Among PFAS, perfluorooctane sulfonic acid (PFOS) has emerged as a particularly concerning compound due to its global occurrence, extreme persistence, and well-documented toxicity. In municipal solid waste landfills (MSWLs), a major terminal destination for PFAS-laden waste, PFOS can leach into surrounding groundwater, posing substantial environmental risks. To mitigate such risks, engineered liner systems, specifically, single composite liner systems (SCLS), are commonly installed at the base of landfills to prevent contaminant migration. However, these systems were not originally designed to handle persistent organic contaminants such as PFOS. This has underscored the importance of studying PFOS migration within engineered landfill liner systems, which has become an increasingly relevant research topic in light of growing environmental concerns.

The literature reveals several important research gaps that this study seeks to address. First, although numerous experimental studies have reported PFOS sorption and transport behaviours, no effort has been made to systematically quantify the uncertainty of key parameters governing PFOS migration in landfill liner systems based on available evidence. Second, there have been only two known numerical attempts to model PFAS transport through such systems, which were both conducted in a deterministic manner, with one study specifically focusing on PFOS but considering only one SCLS design and relying on a dimensionally reduced modelling approach. Third, no probabilistic risk assessment has been undertaken to evaluate the potential for PFOS or other PFAS to contaminate groundwater beneath landfills, despite growing

recognition of their environmental persistence and toxicity. Following from this lack, and considering the high computational cost of Monte Carlo analyses, a fourth gap emerged in relation to surrogate models that can reduce this cost. While Polynomial Chaos Expansion (PCE) methods have been shown to be amongst the most effective in reducing the computational burden of Monte Carlo simulations (MCS) for contaminant transport, no previous applications have involved more than six uncertain variables. In contrast, PFOS migration through landfill liners was found in this thesis to be influenced by a considerably larger set of uncertainties. These four gaps have motivated the present research, which aims to simulate and analyse the migration of PFOS through typical SCLS designs, in a probabilistic manner, and to evaluate the associated contamination risks to underlying aquifers.

To achieve the research objectives, a comprehensive probabilistic analysis framework was developed and implemented, centred on a PCE-enhanced MCS approach. The finite element solver SPAS/CONFEM, specifically developed for modelling contaminant transport in landfill liner systems, was employed to solve the coupled equations governing water flow and PFOS migration in the studied synthetic models. To efficiently generate the high-dimensional input samples, the Latin Hypercube Sampling with Multidimensional Uniformity (LHSMDU) method was adopted. A preliminary MCS with a relatively small number of realisations, based on iterative runs of the original numerical model, was conducted to generate training data for the PCE surrogate model. The PCE surrogate model was established through a MATLAB-based uncertainty quantification framework, UQLab. This surrogate model was subsequently used in a second MCS with a significantly larger number of realisations to produce the target output, namely, the maximum PFOS concentration in the aquifer ($C_{aq\text{-}max}$). These simulations formed the basis for a) a contamination risk assessment (expressed as the probability of $C_{aq\text{-}max}$ exceeding drinking water guidelines/standards) and b) a global sensitivity analysis (GSA, conducted via Sobol' indices).

Building on the above framework, this study investigated three representative SCLS designs, namely GMB+GCL+AL (Design I), GMB+CCL+AL (Design II), and GMB+NCL (Design III), under four levels of construction quality: Sc- (good CQA but no ELL), RSc (good CQA with ELL), Sc+ (excellent CQA with ELL), and RSc0 (no leakage). (CQA: construction quality assurance; ELL: electrical leak location.) The research work consisted of several key components. First, the determination of input

parameters, including both fixed values and probability distributions, was carried out using a combination of approaches: literature synthesis, expert judgment, and a calibration study based on observed leakage rates from municipal landfills in New York State. Second, a series of deterministic simulations was conducted for the three liner designs across the four construction quality scenarios, providing representative reference levels of PFOS concentration for different cases, as well as insights into the spatial and temporal variation patterns. These simulations were followed by a preliminary sensitivity analysis based on the conventional MCS, which helped identify those uncertain parameters with negligible influence on the variability of the results. These parameters were then excluded from the set of uncertain variables in subsequent probabilistic analyses, which reduced their computational cost. Third, the predictive accuracy and computational efficiency of the PCE surrogate model were evaluated. This involved validating the surrogate predictions against conventional MCS results and identifying a relatively optimal PCE configuration based on RSc of the three designs. Finally, a formal probabilistic analysis of PFOS transport was performed using the PCE-enhanced MCS framework, covering multiple combinations of liner design and construction quality (Design I: RSc0, Sc+, RSc, Sc-; Design II: Sc+, RSc, Sc-; Design III: Sc+, RSc, Sc-). Key outputs related to $C_{aq\text{-}max}$ included statistical summaries, fitted probability density functions, and probabilities of exceedance (PoE) with respect to selected regulatory guidelines/standards. The contamination risk assessment was based on these PoE outcomes. Through comparative analyses, the influence of liner design and construction quality on the mitigation of PFOS migration was examined. Benefiting from the computational efficiency of the PCE model, a global sensitivity analysis (GSA) based on Sobol' indices was also performed to quantify the contributions of individual uncertain parameters to the variability of $C_{aq\text{-}max}$. In addition, a temporal analysis of spatially peak PFOS concentration was conducted for Design I under RSc, to gain insights into the change in time of both PFOS contamination risk and its sensitivity to key variables.

8.2 Main Research Findings

Deterministic Simulations (Chapter 5)

- PFOS transport through single-liner systems is primarily governed by advection, with GMB defects acting as major leakage pathways that substantially undermine containment performance.
- Generally, maximum PFOS concentrations ($C_{aq\text{-}max}$) occur at the top of aquifer and approximately beneath the rightmost defect on the GMB. The concentration follows a typical temporal pattern of initial increase, peak, and gradual decline, with the time to peak varying across designs, approximately 150 years for Design I, 170 years for Design II, and even longer for Design III.
- The effectiveness of GCL+AL (Design I) and CCL+AL (Design II) designs can be considerably improved by applying ELL and enhancing CQA, while the NCL design (Design III) shows much less sensitivity to such improvements.
- Overall, the performances of Design I and Design II are broadly comparable, and are both outperformed by Design III, although the practical implementation of NCL is subject to strict site-specific constraints.
- Importantly, except under the idealised diffusion-only scenario, all simulated designs exceed the regulatory limits for PFOS in drinking water as specified by the US, Australian, and EU guidelines/standards, and only approach acceptability under the Canadian guideline. Note, however, that in Australia a newly revised guideline has just been published, while in Canada the guideline is undergoing a revision process, which is likely to result in more stringent requirements in both jurisdictions.
- These results suggest that, even with excellent construction quality, single-liner systems, under the best knowledge available, may be inadequate for PFOS containment unless aided by lower source concentrations or more favourable natural attenuation.

PCE Performance (Chapter 6)

- The PCE surrogate model is found to be a computationally efficient alternative to the finite element numerical model for implementing MCS with up to 12 uncertain parameters, while maintaining the predictive capability of the original model.

- It is found that the use of PCE enables more than one order of magnitude reductions in computational time. Specifically, a sixteen-fold reduction in computational cost is achieved when moving from MCS to PCE-enhanced MCS under two uncertain parameters, which rises to a forty-fold gain in the case of twelve uncertain parameters.

Probabilistic Analysis (Chapter 7)

- Findings from probabilistic analyses are broadly consistent with the conclusions drawn from the deterministic analyses, thereby reinforcing the latter's validity, while extending them by incorporating the effects of parameter uncertainty and enabling a more comprehensive risk-based interpretation.
- Under the idealised no-leakage scenario (RSc0), which is highly improbable in reality, single-liner systems are able to fully contain PFOS migration, confirming that if liner integrity is maintained, PFOS groundwater contamination risks can be effectively minimised.
- The probability distributions of $C_{aq\text{-}max}$ are highly variable and highly right-skewed with long tails, indicating that while most values cluster around moderate levels, there is a non-negligible risk of extremely high values.
- Improving construction quality consistently reduces PFOS contamination risk across all three liner designs, with the enhancement from RSc to Sc+ (i.e., from good to excellent CQA) yielding more substantial risk reduction than the mere application of ELL technologies (from Sc- to RSc).
- The risk reduction achieved through construction quality improvements is more significant in Design I and Design II than in Design III, suggesting that investment in construction quality yields higher returns for the former two systems.
- Across all construction quality levels, Design III consistently outperforms both Design I and Design II, with the latter two showing nearly identical performance in terms of PoE, though Design II slightly surpasses Design I based on statistical summaries under Sc- and RSc. This underscores the value of combining multiple metrics for a more complete performance assessment.
- The superiority of Design III becomes more evident under lower CQA scenarios (Sc- and RSc), while under excellent construction (Sc+), the differences among

the three designs narrow significantly, suggesting that NCL may be more advantageous when construction quality is unassured.

- For all studied single-liner cases, the probability of PFOS concentrations exceeding drinking water guidelines/standards remains high under both stringent and moderately lenient criteria, regardless of liner design or construction quality.
- Preliminary sensitivity analysis in Chapter 5 and GSA based on Sobol' indices in Chapter 7 reveal similar importance ranks of contributors to the variance in $C_{aq\text{-}max}$. For all three liner designs, PFOS load in waste (C_{b0} & p_0/C_{b0}), the hydraulic conductivity of functional clay liner, and L_w are consistently among the most influential, followed by ΔH, $V_{ax\text{-}in}$, and thicknesses of layers.
- In contrast to the minor influence of θ in Design I, θ has a largely positive correlation with $C_{aq\text{-}max}$ in Design II and Design III. This is due to the higher values and larger variabilities of θ in these two designs, leading to greater variability of wetted area and overall leakage rate.
- The most critical contamination window is around 140~160 years, with PoE consistently exceeding 50% for the USEPA standard and remaining non-negligible for all other guidelines/standards across the studied period (0~2000 years).
- During the high-risk period (100~300 years), the most influential factor is PFOS load in waste (C_{b0} & p_0/C_{b0}), with advective transport parameters also playing important roles.

8.3 Limitations of Research

The study's findings must be qualified by a number of limitations, which have been discussed in Section 3.6 and are summarised here. Several simplifying assumptions have been made, on ground of empirical evidence, past knowledge in the literature, feasibility, and data availability. Key assumptions are: the soil is fully saturated; the flow is steady state, reducible to two spatial dimensions; sorption and degradation of PFOS are negligible; and the liner's performance does not deteriorate over time.

The modelling choices made in this study, where possible, erred on the conservative side. For example, no sorption or biodegradation was assumed to be present. On the

other hand, some uncertainties could not be incorporated and may not be conservative. One such assumption is that the liner will continue to be functional over hundreds of years. There is evidence that a well-selected GMB may function for 500 years to millennia (Rowe, 2020b). However, GMBs are usually selected based on a minimum standard (often GRI-GM13, i.e., Geosynthetic Institute, 2021) and price, without serious consideration of longevity. Research indicates that even with good construction and design, the service life of these GMBs at normal MSWL temperatures of up to 40°C is likely to be in the order of 150 years. If the temperature is allowed to exceed 40°C, the service life drops rapidly; except for specialty GMBs, it is likely to be only a few decades at 60°C and less than a decade at 80°C (Rowe and Islam, 2009; Rowe et al., 2014; Abdelaal et al., 2014).

The choice of probability distributions for critical variables was based on best available evidence, including expert judgment. It is, however, impossible to capture all variability inherent to all MSWLs with SCLS. It is important to remember here that the aim of the study is to make an overall assessment of the safety of SCLS in relation to PFOS based on generically typical designs. Quantitative and qualitative findings, including PoE functions presented in Table 7.2, must therefore be used with caution and only if the landfill in question falls within the range of designs and scenarios considered here. For example, the simulations of landfills with Design I or Design II assume the presence of only a shallow combination of GCL+AL or CCL+AL between GMB and the aquifer (average level of 3.75 m). However, in some landfills, the AL is much thicker, and its hydraulic conductivity may be lower than the values considered here. In such conditions, our findings of high risk of PFOS contamination cannot be applied without further analysis. Meanwhile, the hydraulic conductivity of NCL was assumed to be quite low, approaching that of CCL in our modelling, which was a key element in its superior performance. However, the in-situ soils (NCL) in reality vary greatly from site to site, and the evaluation of liner systems dominated by NCL needs to be based on site-specific investigations. In addition, some variables, especially the total percolation rate into the overall system (q_0), were treated as deterministic values, whereas in reality they may exhibit considerable variability, which could introduce additional uncertainty into the predicted PFOS impact. For example, the placement of a final cover and the associated reduction in leachate generation may affect contamination patterns. However, the direction of this effect is not straightforward. On the one hand, after cover placement,

q_0 is expected to decrease. If the hydraulic conditions governing leachate leakage are assumed to remain unchanged, the leakage rate through the liner system (q_a) would not vary, and, given $q_0 = q_a + q_c$, the collection rate by the drainage system (q_c) would decrease. This would result in less PFOS being removed by the drainage system and potentially a greater proportion entering the underlying aquifer. On the other hand, cover placement may alter the hydraulic conditions acting on the liner system, by reducing the pressure head at the top of the liner. In this case, the leakage rate through defects in the geomembrane (q_a) would decrease, which would in turn reduce the mass of PFOS migrating into the aquifer. Therefore, predictions may change if landfill closure and cover placement are explicitly considered from a certain time point onward in numerical simulations and warrants further investigation.

While the above limitations need to be borne in mind, the study is nevertheless the first to assess the risk of PFOS contamination to aquifers underlying landfills while systematically accounting for a set of important uncertainties, and its findings are thus highly instructive.

8.4 Implications of Findings

The findings of this study highlight the considerable challenges associated with managing PFOS contamination in landfills equipped with single composite liner systems (SCLS). Even under excellent construction quality, the probabilistic results demonstrate that the risk of PFOS concentrations in underlying aquifers exceeding regulatory thresholds remains unacceptably high. This suggests that current SCLS designs, while technologically mature and widely applied, may be inherently insufficient to ensure long-term containment of highly persistent PFAS compounds such as PFOS. Additionally, given the extended timeframes over which peak PFOS concentrations may emerge, potentially 150 years or more, these findings also raise ethical concerns related to long-term environmental liabilities and inter-generational exposure risks.

Another critical finding from the study is that the variables with the most impact on PFOS contamination risk are directly related to the mass of PFOS in the landfill waste and the quality of construction and/or insulation material chosen. This finding has two key implications.

First, regarding containment enhancement, the performance of SCLS can be improved to some extent through established engineering practices, such as selecting GMBs with longer service lives, ensuring low hydraulic conductivity in clay components through rigorous quality control measures, and minimising holed wrinkles in GMB through proper placement timing and leak detection. Building upon these incremental enhancements, a more thorough solution may involve the use of double composite liner systems, which incorporate a secondary barrier layer. Although double liners have been successfully employed in hazardous waste landfills, their effectiveness for PFOS containment has not been assessed, either experimentally or through risk assessments, and thus requires further research.

Second, there is a strong case for placing limits on the volumes of PFOS received, and hence reducing total contaminant load in landfills, especially those equipped with single composite liner systems. This should be an important part of any strategy to reduce PFOS contamination risk in aquifers underlying landfills. Such reduction may be difficult to implement in practice due to the diffuse, extensive, and often unidentifiable presence of PFAS in various consumer and industrial products. This limitation, however, raises a more fundamental point: meaningful risk reduction requires upstream interventions at the design and production stages of consumer and industrial products containing PFOS, and by implication, PFAS more generally. This is to say that eliminating, substituting, or reducing PFOS in manufacturing processes is essential for mitigating its long-term environmental threat to groundwater within landfill contexts, and relying on engineering solutions alone at the downstream end may not be the most rational approach.

8.5 Future Research

Building upon the current study, several directions are recommended for future research to enhance the understanding and predictive capacity of PFAS transport through landfill liner systems.

- PFAS compounds other than PFOS need to be considered in future studies, especially PFOA and PFHxS, which are important contaminants and may exhibit different behaviour to PFOS.

- On the other hand, whether assessing PFOS or other PFAS compounds, many of the input variables used in the current probabilistic framework are subject to considerable uncertainty. This study has revealed some particularly influential variables that require focused and prioritised investigation, such as the contaminant load in waste, the permeability of clay material in the liner, and the density of defects on the GMB. Future experimental studies should aim to reduce associated uncertainty by generating more consistent and representative data for various PFAS compounds under landfill-relevant conditions.
- Another important avenue for research is a probabilistic assessment of PFAS contamination risk under double composite liners or hybrid configurations, which may offer superior containment performance under realistic conditions.
- While the present study covered large variabilities corresponding to different single-liner configurations in landfills, site-specific modelling based on field measurements can provide a higher level of confidence required in risk assessments.
- There is also scope for improvement of numerical solvers and their computational efficiencies, including extending into 3D space and better accounting for variability in space and time of key variables.

In conclusion, the main advancement of this study lies in the shift from a purely deterministic perspective to a probabilistic one. In reality, environmental processes are inherently uncertain, and viewing them through a probabilistic lens allows for a more accurate and informative understanding. Although this study only represents a modest step towards that ideal, it establishes a foundation for further developments. The proposed directions above all aim to progressively close the gap between modelling assumptions and the complexity of real-world landfill systems.

Appendix 3.1 Original Expression of Rowe Equation

Rowe (1998) developed a closed-form analytical equation for calculating the leakage through a GMB hole coincident with a wrinkle (Figure A3.1), which is also known as the Rowe equation. Afterward, this analytical solution was examined in a comparison study with numerical solutions by SPAS (El-Zein and Rowe, 2008), employed in several contaminant transport modelling studies (Rowe and Abdelrazek, 2019; Rowe and Barakat, 2021), and further modified to achieve better universality (Yu et al., 2024). The definition of wetted distance and the Rowe equation are presented below, taking the GCL-liner model as an example.

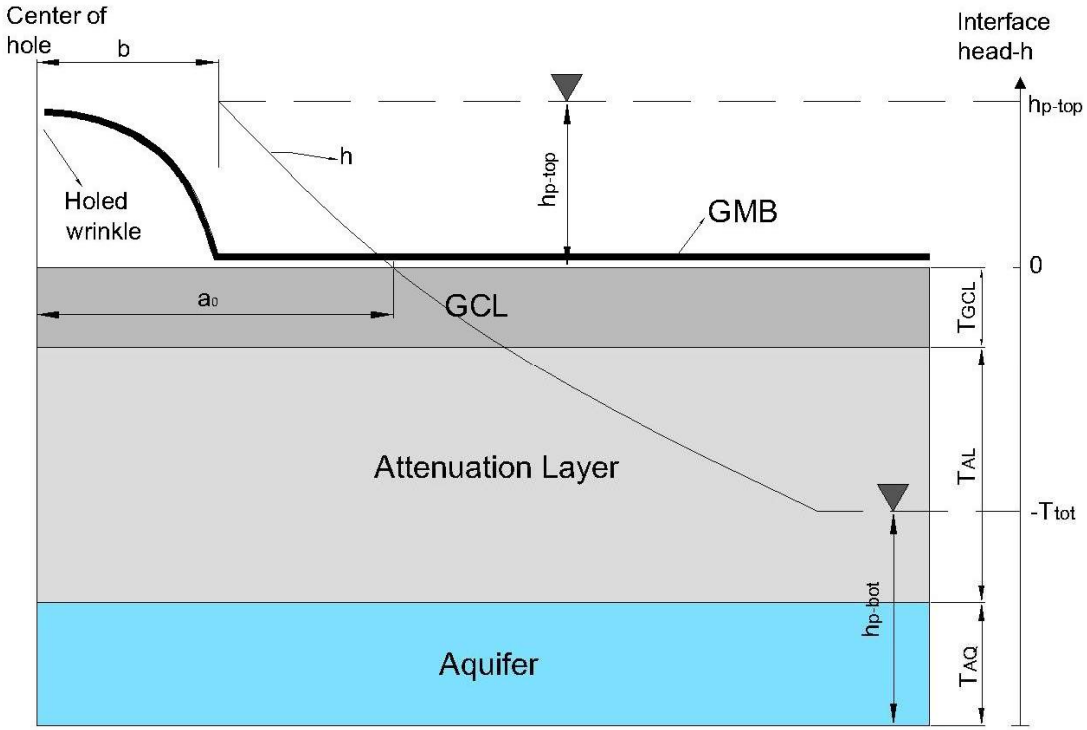

Figure A3.1. Schematic showing wetted distance beneath a holed wrinkle. Adapted from Rowe and Barakat (2021)

The GMB and GCL of a composite liner are not in perfect direct contact. Thus, when leachate passes through a holed wrinkle, there is downward flow through the unstressed GCL directly beneath the wrinkle as well as lateral flow between the GMB and GCL and downward through the confined GCL. As shown in Figure A3.1, the pressure head acting between the GMB and GCL (h [L]) reaches a maximum at the centre of the holed wrinkle and decreases with distance away from the centre (Rowe, 2005, 2012, 2020). This head on the GCL is typically calculated by setting the top of the GCL as datum. If the pressure head at the aquifer bottom, $h_{p\text{-}bot}$, rises to below the GCL, the wetted

distance of a_0 is where the head h = 0 (Rowe, 1998; Rowe et al., 2004; Barakat and Rowe, 2020). The interface head will continuously decrease until h ~ -T_{tot} where $T_{tot} = T_{GCL} + T_{AL} + T_{AQ} - h_{p-bot}$.

Rowe (1998) proposed several versions of an equation estimating q_a depending on assumptions about wetted distance. Two versions are presented below with slight adjustments which are for considering the effects of the aquifer thickness and different hydraulic conductivities under the wrinkle and under the intact part of the GMB.

The first version, assuming the spacing of leaks is significantly larger than the wetted range (wetted distance ends at the point of h=0), can be expressed as:

$$q_a = 2L_w \left[k_{sb} \cdot b + k_{sa} \frac{1}{\alpha}\left(1 - e^{-\alpha(a_0 - b)}\right)\right] \frac{T_{tot} + h_{p-to}}{T_{GCL} + T_{AL}} \qquad \text{(A3.1.1)}$$

The second version, assuming a very large wetted distance can be written as

$$q_a = 2L_w \left(k_{sb} \cdot b + k_{sa} \frac{1}{\alpha}\right) \frac{T_{tot} + h_{p-top}}{T_{GCL} + T_{AL}} \qquad \text{(A3.1.2)}$$

where k_{sa} and k_{sb} are the harmonic means of hydraulic conductivities in the liner under the intact and wrinkled parts of the GMB, respectively, and expressed as

$$k_{sa} = \frac{T_{GCL} + T_{AL}}{\frac{T_{GCL}}{k_a} + \frac{T_{AL}}{k_{AL}}} \qquad \text{(A3.1.3)}$$

$$k_{sb} = \frac{T_{GCL} + T_{AL}}{\frac{T_{GCL}}{k_b} + \frac{T_{AL}}{k_{AL}}} \qquad \text{(A3.1.4)}$$

The wetted distance ($2a_0$) around each wrinkle in Eq. (A3.1.1) can be expressed as

$$a_0 = b - \ln \frac{T_{tot}}{h_{p-top} + T_{tot}} \cdot \frac{1}{\alpha} \qquad \text{(A3.1.5)}$$

where

$$\alpha = \left[\frac{k_{sa}}{(T_{GCL} + T_{AL})\theta}\right]^{0.5} \qquad \text{(A3.1.6)}$$

$$T_{tot} = T_{GCL} + T_{AL} + T_{AQ} - h_{p-bot} \qquad \text{(A3.1.7)}$$

All other symbols appearing in Eqs. (A3.1.1) to (A3.1.7) can be found in Table 3.1. For the models with CCL-liner or NCL-liner, very little difference is expected between hydraulic conductivities of clay under wrinkled and intact parts of the GMB; hence, $k_a \approx k_b$, and the above equations can be adjusted accordingly.

It is expected that the actual leakage rate, for the model shown in Figure A3.1, will fall between predictions of Eq. (A3.1.1) and Eq. (A3.1.2), given their respective assumptions about wetted distance, described above (Rowe and Barakat, 2021).

Appendix 3.2 MATLAB Scripts for Conventional MCS

The core MATLAB script is named "MCSfrommatlab_test7_7_b_9_2_js_tnode.m". It corresponds to the MCS version applying Approach 1 (Figure 3.4(a)), and the script corresponding to Approach 2b (Figure 3.4(b)) is slightly different and isn't shown here. Another notable version of script, which is also not shown, is for the pure-diffusion case where GMB is ideally considered without defects and there is no leakage (RSc0 in 3.3.2), where the execution of Water-Flow Solver is omitted.

```
% This function is to get the values of multi variables at multi time
stations and multi nodes.
% What users input in Excel is variable name/ node coordinates/ time-
stations.

function
MCSfrommatlab_test7_7_b_9_2_js_tnode(MCSfrommatlab_input_file)
tic;
rng('shuffle');
fprintf('spas MCS starting\n')
fprintf('reading Excel file\n')
% At first, some variables are extracted from Excel and plt.
basic_information=readtable(MCSfrommatlab_input_file,'Range','A1:B100
','ReadVariableNames',false);
spafile=char(basic_information{11,2});
pltfile=char(basic_information{13,2});
MCS_times=xlsread(MCSfrommatlab_input_file,'B5:B5');
TotalTime_TotalNode=importfile(pltfile,1,2);
TotalTime=TotalTime_TotalNode(2,1);
TotalNode=TotalTime_TotalNode(2,2);

spafile_WF=char(basic_information{17,2});
pltfile_WF=char(basic_information{19,2});
TotalTime_TotalNode_WF=importfile(pltfile_WF,1,2);
TotalTime_WF=TotalTime_TotalNode_WF(2,1);
TotalNode_WF=TotalTime_TotalNode_WF(2,2);

% Read variable names from Excel, then transfer them into variable
codes.
variable_names=readtable(MCSfrommatlab_input_file,'Range','I3:I100','
ReadVariableNames',false);
i=1;
while length(char(variable_names{i,1}))~=0
i=i+1;
end
variable_number=i-1;
variable_names=variable_names(1:variable_number,1:1);
fID=fopen(pltfile);
for j=1:variable_number
for i=1:3
fgetl(fID);
end
for i=1:17
if ~isempty(strfind(fgetl(fID),char(variable_names{j,1})))
```

```
variable_code(j)=i;
end
end
fseek(fID,0,'bof');
end
fclose(fID);
% From node coordinates to node codes
node_coordinates=xlsread(MCSfrommatlab_input_file,'S3:T100');
node_number=size(node_coordinates,1);
for_fromcoordinatetocode=plt_to_array(pltfile,TotalTime,TotalNode);
All_coordinates=for_fromcoordinatetocode(1:TotalNode,2:3);
for j=1:node_number
min_distance=sqrt((node_coordinates(j,1)-
All_coordinates(1,1))^2+(node_coordinates(j,2)-
All_coordinates(1,2))^2);
for i=1:TotalNode
distance=sqrt((node_coordinates(j,1)-
All_coordinates(i,1))^2+(node_coordinates(j,2)-
All_coordinates(i,2))^2);
if distance<=min_distance
min_distance=distance;
closest_node_x(j)=All_coordinates(i,1);
closest_node_y(j)=All_coordinates(i,2);
node_code(j)=i;
end
end
end
fprintf('x-coordinates for closest nodes are ');closest_node_x
fprintf('y-coordinates for closest nodes are ');closest_node_y

% Get the array of all_times for later use.
fID=fopen(pltfile);
first_time=cell2mat(textscan(fID,'%f',1,'HeaderLines',20));
fseek(fID,0,'bof');
second_time=cell2mat(textscan(fID,'%f',1,'HeaderLines',20+TotalNode+1
));
fclose(fID);
All_times=linspace(first_time,first_time+(second_time-
first_time)*(TotalTime-1),TotalTime);

% read probabilistic parameters' mean and SD from Excel and generate
random
% values for them.
% meanwhile, draw distributions for these parameters
all_probabilistic_parameters=xlsread(MCSfrommatlab_input_file,'F3:H10
0');
dist_type=readtable(MCSfrommatlab_input_file,'Range','C3:C100','ReadV
ariableNames',false);
probabilistic_parameter_number=xlsread(MCSfrommatlab_input_file,'B3:B
3');
probabilistic_parameter_number_WF=xlsread(MCSfrommatlab_input_file,'B
15:B15');
figure('Name','Probabilistic Parameters');hold on;
for i=1:probabilistic_parameter_number
if strcmp(char(dist_type{i,1}),'norm')

P(i).randomvalues_initial=LHS_normrnd(all_probabilistic_parameters(i,
1),all_probabilistic_parameters(i,2),1,MCS_times);
elseif strcmp(char(dist_type{i,1}),'logn')
```

```
P(i).randomvalues_initial=LHS_lognrnd(all_probabilistic_parameters(i,
1),all_probabilistic_parameters(i,2),1,MCS_times);
elseif strcmp(char(dist_type{i,1}),'tria')

P(i).randomvalues_initial=LHS_triarnd(all_probabilistic_parameters(i,
1),all_probabilistic_parameters(i,2),all_probabilistic_parameters(i,3
),1,MCS_times);
elseif strcmp(char(dist_type{i,1}),'logn+cons')

P(i).randomvalues_initial=LHS_lognrnd(all_probabilistic_parameters(i,
1),all_probabilistic_parameters(i,2),1,MCS_times)+all_probabilistic_p
arameters(i,3);
end
P(i).randomvalues_inorder=sort(P(i).randomvalues_initial);
samples_input(i,:)=P(i).randomvalues_inorder;
end
samples_LHSMDU = LHSMDU(probabilistic_parameter_number, 5, MCS_times,
samples_input);
for i=1:probabilistic_parameter_number
    P(i).randomvalues=samples_LHSMDU(i,:);
end
for i=1:probabilistic_parameter_number
fprintf('Random values for P%u are ',i);P(i).randomvalues
xlswrite('Random input parameters.xlsx',{['Random values for
P',num2str(i),' are ']},'Sheet1',['A',num2str(2*i-1)]);
xlswrite('Random input
parameters.xlsx',P(i).randomvalues,'Sheet1',['A',num2str(2*i)]);
subplot(1,probabilistic_parameter_number,i);histfit(P(i).randomvalues
);title(['P' num2str(i)]);
end
set(gcf,'outerposition',get(0,'screensize'));
saveas(gcf,['Random input parameters.png']);
hold off;

% get line numbers for lines starting with "PARAMETER" in Water Flow
spa file
fID=fopen(spafile_WF,'r');
j=1;
for i=1:50
if startsWith(fgetl(fID),"PARAMETER")
parameter_linenumbers_WF(j)=i;j=j+1;
end
end
fclose(fID);
parameter_linenumbers_WF=parameter_linenumbers_WF(1:1,1:probabilistic
_parameter_number_WF);

% get line numbers for lines starting with "PARAMETER" in spa file
fID=fopen(spafile,'r');
j=1;
for i=1:50
if startsWith(fgetl(fID),"PARAMETER")
parameter_linenumbers(j)=i;j=j+1;
end
end
fclose(fID);
parameter_linenumbers=parameter_linenumbers(1:1,1:probabilistic_param
eter_number);

for i=1:MCS_times
```

```
    fprintf('doing simulation %u\n',i)

% update values of P(i) in Water Flow spa file
fprintf('updating WF spafile\n')
fID=fopen(spafile_WF,'r+');
for k=1:probabilistic_parameter_number_WF
    for l=1:(parameter_linenumbers_WF(k)-1)
        fgets(fID);
    end
fprintf(fID,'PARAMETER %u %26.20f',k,P(k).randomvalues(i));
fseek(fID,0,'bof');
end
fclose(fID);
% confemfrommatlab for Water Flow
fprintf('doing confem for WF\n')
fID=fopen('confem3d.nam','r+');
fprintf(fID,'Project2');
fclose(fID);
confemfrommatlab;
% read leakage rate from Water Flow plt file
fprintf('reading leakage rate\n')
allresults_WF=plt_to_array_WF(pltfile_WF,TotalTime_WF,TotalNode_WF);
clear leakage_integral_table;
p=1;
for q=1:TotalNode_WF
if abs(allresults_WF(q,3))<1e-6
leakage_integral_table(p,1)=allresults_WF(q,2);
leakage_integral_table(p,2)=allresults_WF(q,12);
p=p+1;
end
end
leakage_integral_table_sort=sortrows(leakage_integral_table,1);
leakage_integral_x=leakage_integral_table_sort(:,1);
leakage_integral_Vay=leakage_integral_table_sort(:,2);
leakage=-trapz(leakage_integral_x,leakage_integral_Vay);
leakage_rate(i)=leakage/(leakage_integral_x(length(leakage_integral_t
able_sort))-leakage_integral_x(1));

% update values of P(i) in spa file and update leakage_rate(i) in spa
file
fprintf('updating spafile\n')
fID=fopen(spafile,'r+');
for k=1:probabilistic_parameter_number
    for l=1:(parameter_linenumbers(k)-1)
        fgets(fID);
    end
fprintf(fID,'PARAMETER %u %26.20f',k,P(k).randomvalues(i));
fseek(fID,0,'bof');
end
for l=1:(parameter_linenumbers(probabilistic_parameter_number)+2)
        fgets(fID);
    end
fprintf(fID,'PARAMETER %u %26.20f',(probabilistic_parameter_number+1)
,leakage_rate(i));
fclose(fID);
% confemfrommatlab
fprintf('doing confem\n')
fID=fopen('confem3d.nam','r+');
fprintf(fID,'Project1');
fclose(fID);
confemfrommatlab;
```

```
% read results from plt file
% importfile is a function generated by matlab itself (not built-in,
not
% written by me). It can read information into numeric matrix form
(here
% from line 21 to line inf).
% But later, it's found that importfile is too slow for large plt
file. So
% another way is presented, that is the function of 'plt_to_array'.
fprintf('reading results\n')
if exist(pltfile,'file')
allresults=plt_to_array(pltfile,TotalTime,TotalNode);
% 2024.6.3 record desired variable at all timenodes
for j=1:node_number
    for a=1:TotalTime

desired_information_at_all_timenode(i).variable(j).timenode(a)=allres
ults((a-1)*TotalNode+node_code(j),variable_code(j)+3);
    end
end
% find and record all the peak information into a structure.
for j=1:node_number
    peak_variable_value=allresults(node_code(j),variable_code(j)+3);
    for a=1:TotalNode*TotalTime
        if allresults(a,1)==node_code(j)
           variable_value=allresults(a,variable_code(j)+3);
           if variable_value>=peak_variable_value
               peak_variable_value=variable_value;

desired_peak_information_at_given_yandx(i).variable(j)=peak_variable_
value;
               overall_linenumber(j)=a;
           end
        end
    end

desired_peak_information_at_given_yandx(i).x(j)=allresults(overall_li
nenumber(j),2);

desired_peak_information_at_given_yandx(i).y(j)=allresults(overall_li
nenumber(j),3);

desired_peak_information_at_given_yandx(i).nodecode(j)=allresults(ove
rall_linenumber(j),1);

desired_peak_information_at_given_yandx(i).T(j)=All_times(floor((over
all_linenumber(j)-1)/TotalNode)+1);

desired_peak_information_at_given_yandx(i).timestationcode(j)=floor((
overall_linenumber(j)-1)/TotalNode)+1;

    % judge if this peak variable is a spike
    if
desired_peak_information_at_given_yandx(i).timestationcode(j)<=2

desired_peak_information_at_given_yandx(i).variable_Tadd1(j)=allresul
ts((desired_peak_information_at_given_yandx(i).timestationcode(j)+1-
1)*TotalNode+desired_peak_information_at_given_yandx(i).nodecode(j),v
ariable_code(j)+3);

desired_peak_information_at_given_yandx(i).variable_Tadd2(j)=allresul
```

```
ts((desired_peak_information_at_given_yandx(i).timestationcode(j)+2-
1)*TotalNode+desired_peak_information_at_given_yandx(i).nodecode(j),v
ariable_code(j)+3);
        if
abs(desired_peak_information_at_given_yandx(i).variable(j)-
desired_peak_information_at_given_yandx(i).variable_Tadd1(j))<=abs(de
sired_peak_information_at_given_yandx(i).variable_Tadd1(j)-
desired_peak_information_at_given_yandx(i).variable_Tadd2(j))
            desired_peak_information_at_given_yandx(i).js(j)=0;
        else
            desired_peak_information_at_given_yandx(i).js(j)=1;
        end
    elseif
desired_peak_information_at_given_yandx(i).timestationcode(j)>=TotalT
ime-1

desired_peak_information_at_given_yandx(i).variable_Tminus1(j)=allres
ults((desired_peak_information_at_given_yandx(i).timestationcode(j)-
1-
1)*TotalNode+desired_peak_information_at_given_yandx(i).nodecode(j),v
ariable_code(j)+3);

desired_peak_information_at_given_yandx(i).variable_Tminus2(j)=allres
ults((desired_peak_information_at_given_yandx(i).timestationcode(j)-
2-
1)*TotalNode+desired_peak_information_at_given_yandx(i).nodecode(j),v
ariable_code(j)+3);
        if
abs(desired_peak_information_at_given_yandx(i).variable(j)-
desired_peak_information_at_given_yandx(i).variable_Tminus1(j))<=abs(
desired_peak_information_at_given_yandx(i).variable_Tminus1(j)-
desired_peak_information_at_given_yandx(i).variable_Tminus2(j))
            desired_peak_information_at_given_yandx(i).js(j)=0;
        else
            desired_peak_information_at_given_yandx(i).js(j)=1;
        end
    else

desired_peak_information_at_given_yandx(i).variable_Tminus1(j)=allres
ults((desired_peak_information_at_given_yandx(i).timestationcode(j)-
1-
1)*TotalNode+desired_peak_information_at_given_yandx(i).nodecode(j),v
ariable_code(j)+3);

desired_peak_information_at_given_yandx(i).variable_Tminus2(j)=allres
ults((desired_peak_information_at_given_yandx(i).timestationcode(j)-
2-
1)*TotalNode+desired_peak_information_at_given_yandx(i).nodecode(j),v
ariable_code(j)+3);

desired_peak_information_at_given_yandx(i).variable_Tadd1(j)=allresul
ts((desired_peak_information_at_given_yandx(i).timestationcode(j)+1-
1)*TotalNode+desired_peak_information_at_given_yandx(i).nodecode(j),v
ariable_code(j)+3);

desired_peak_information_at_given_yandx(i).variable_Tadd2(j)=allresul
ts((desired_peak_information_at_given_yandx(i).timestationcode(j)+2-
1)*TotalNode+desired_peak_information_at_given_yandx(i).nodecode(j),v
ariable_code(j)+3);
        if
abs(desired_peak_information_at_given_yandx(i).variable(j)-
```

```
desired_peak_information_at_given_yandx(i).variable_Tminus1(j))<=abs(
desired_peak_information_at_given_yandx(i).variable_Tminus1(j)-
desired_peak_information_at_given_yandx(i).variable_Tminus2(j)) &
abs(desired_peak_information_at_given_yandx(i).variable(j)-
desired_peak_information_at_given_yandx(i).variable_Tadd1(j))<=abs(de
sired_peak_information_at_given_yandx(i).variable_Tadd1(j)-
desired_peak_information_at_given_yandx(i).variable_Tadd2(j))
            desired_peak_information_at_given_yandx(i).js(j)=0;
        else
            desired_peak_information_at_given_yandx(i).js(j)=1;
        end
    end

end
else
    fprintf('plt file missing');
    for j=1:node_number
        desired_peak_information_at_given_yandx(i).variable(j)=0;
        desired_peak_information_at_given_yandx(i).x(j)=0;
        desired_peak_information_at_given_yandx(i).y(j)=0;
        desired_peak_information_at_given_yandx(i).nodecode(j)=0;
        desired_peak_information_at_given_yandx(i).T(j)=0;

desired_peak_information_at_given_yandx(i).timestationcode(j)=0;

        % "judge spike" is -1 here
        desired_peak_information_at_given_yandx(i).js(j)=-1;

        % 2024.6.3 echo above
        for a=1:TotalTime

desired_information_at_all_timenode(i).variable(j).timenode(a)=0;
        end

    end
end
end
% show the results by listing them and drawing their distributions

figure('Name','Leakage Rate');hold on;
fprintf('The %u results for leakage rate are
',MCS_times);leakage_rate
xlswrite('Leakage rate.xlsx',{['The ',num2str(MCS_times),' results
for leakage rate are ']},'Sheet1','A1');
xlswrite('Leakage rate.xlsx',leakage_rate,'Sheet1','A2');
histfit(leakage_rate);
set(gcf,'outerposition',get(0,'screensize'));
saveas(gcf,['Leakage rate.png']);
hold off;

figure('Name','Output Variables');hold on;
for j=1:node_number
    for i=1:MCS_times

output(i)=desired_peak_information_at_given_yandx(i).variable(j);
        output_x(i)=desired_peak_information_at_given_yandx(i).x(j);
        output_y(i)=desired_peak_information_at_given_yandx(i).y(j);

output_nodecode(i)=desired_peak_information_at_given_yandx(i).nodecod
e(j);
```

```
        output_T(i)=desired_peak_information_at_given_yandx(i).T(j);

output_timestationcode(i)=desired_peak_information_at_given_yandx(i).
timestationcode(j);

output_js(i)=desired_peak_information_at_given_yandx(i).js(j);
    end
    fprintf('The %u results for peak values of variable %u at node %u
are ',MCS_times,variable_code(j),node_code(j));output
    xlswrite('Desired peak values of variables.xlsx',{['The
',num2str(MCS_times),' results for peak values of variable
',num2str(variable_code(j)),' at node ',num2str(node_code(j)),' are
']},'Sheet1',['A',num2str(2*j-1)]);
    xlswrite('Desired peak values of
variables.xlsx',output,'Sheet1',['A',num2str(2*j)]);
    xlswrite(['Peak x,y,T for set',num2str(j),'.xlsx'],{'Peak
x'},'Sheet1','A1');
    xlswrite(['Peak x,y,T for
set',num2str(j),'.xlsx'],output_x,'Sheet1','A2');
    xlswrite(['Peak x,y,T for set',num2str(j),'.xlsx'],{'Peak
y'},'Sheet1','A3');
    xlswrite(['Peak x,y,T for
set',num2str(j),'.xlsx'],output_y,'Sheet1','A4');
    xlswrite(['Peak x,y,T for set',num2str(j),'.xlsx'],{'Peak
nodecode'},'Sheet1','A5');
    xlswrite(['Peak x,y,T for
set',num2str(j),'.xlsx'],output_nodecode,'Sheet1','A6');
    xlswrite(['Peak x,y,T for set',num2str(j),'.xlsx'],{'Peak
T'},'Sheet1','A7');
    xlswrite(['Peak x,y,T for
set',num2str(j),'.xlsx'],output_T,'Sheet1','A8');
    xlswrite(['Peak x,y,T for set',num2str(j),'.xlsx'],{'Peak
timestationcode'},'Sheet1','A9');
    xlswrite(['Peak x,y,T for
set',num2str(j),'.xlsx'],output_timestationcode,'Sheet1','A10');
    xlswrite(['Judge-Spike for
set',num2str(j),'.xlsx'],output_js,'Sheet1','A1');
    subplot(1,node_number,j);histfit(output);title(['variable'
num2str(variable_code(j)) ' at node ' num2str(node_code(j))]);
end
set(gcf,'outerposition',get(0,'screensize'));
saveas(gcf,['Desired variables.png']);
hold off;

% 2024.6.3 echo above
for j=1:node_number
    for a=1:TotalTime
        for i=1:MCS_times

outputt(i)=desired_information_at_all_timenode(i).variable(j).timenod
e(a);
        end
        xlswrite('Desired variables at all
timenodes.xlsx',outputt,['Sheet',num2str(j)],['A',num2str(a)]);
    end
end

% use tic toc to record the calculation time
toc;
t=toc
end
```

Script 3-1. “MCSfrommatlab_test7_7_b_9_2_js_tnode.m”

The generation of input samples requires a series of subscripts, including “LHS_normrnd.m”, “LHS_lognrnd.m”, “LHS_triarnd.m” for the 1D LHS of normal, lognormal, triangular distributions, respectively, referring to “f_norm.m”, “f_logn.m”, “f_tria.m” for the cumulative distribution functions of the three types, as well as “LHSMDU.m” for the generation of high-dimensional samples by LHSMDU.

```
function
samples_InRandomOrder_InMatrixForm=LHS_normrnd(miu,sigma,row_number,c
olumn_number)

if miu<1
    Index=ceil(1/miu);
    miu=miu*Index;
    sigma=sigma*Index;
else
    Index=1;
end

segment_number=row_number*column_number;
segment_node_CDF=linspace(0,1,segment_number+1);
for i=1:segment_number
    rng('shuffle');

samples_CDF(i)=unifrnd(segment_node_CDF(i),segment_node_CDF(i+1));
end
for i=1:segment_number
    fID=fopen('f_norm.m','w+');
    fprintf(fID,'function y=f_norm(x)\n');

fprintf(fID,'y=normcdf(x,%26.20f,%26.20f)-%26.20f;',miu,sigma,samples
_CDF(i));
    fclose(fID);
    fun=@f_norm;
    x0=miu;
    samples(i)=fsolve(fun,x0);
end
rng('shuffle');
samples_InRandomOrder=samples(randperm(length(samples)));
samples_InRandomOrder_InMatrixForm=reshape(samples_InRandomOrder,row_
number,column_number);

samples_InRandomOrder_InMatrixForm=samples_InRandomOrder_InMatrixForm
/Index;
end
```

Script 3-2. “LHS_normrnd.m”

```
function
samples_InRandomOrder_InMatrixForm=LHS_lognrnd(miu,sigma,row_number,c
olumn_number)

segment_number=row_number*column_number;
segment_node_CDF=linspace(0,1,segment_number+1);
for i=1:segment_number
```

```
    rng('shuffle');

samples_CDF(i)=unifrnd(segment_node_CDF(i),segment_node_CDF(i+1));
end
for i=1:segment_number
    fID=fopen('f_logn.m','w+');
    fprintf(fID,'function y=f_logn(x)\n');

fprintf(fID,'y=normcdf(x,%26.20f,%26.20f)-%26.20f;',miu,sigma,samples
_CDF(i));
    fclose(fID);
    fun=@f_logn;
    x0=miu;
    samples(i)=exp(fsolve(fun,x0));
end
rng('shuffle');
samples_InRandomOrder=samples(randperm(length(samples)));
samples_InRandomOrder_InMatrixForm=reshape(samples_InRandomOrder,row_
number,column_number);

end
```

Script 3-3. “LHS_lognrnd.m”

```
function
samples_InRandomOrder_InMatrixForm=LHS_triarnd(min,mode,max,row_numbe
r,column_number)

if mode<1
    Index=ceil(1/mode);
    mode=mode*Index;
    min=min*Index;
    max=max*Index;
else
    Index=1;
end

segment_number=row_number*column_number;
segment_node_CDF=linspace(0,1,segment_number+1);
for i=1:segment_number
    rng('shuffle');

samples_CDF(i)=unifrnd(segment_node_CDF(i),segment_node_CDF(i+1));
end
for i=1:segment_number
    fID=fopen('f_tria.m','w+');
    fprintf(fID,'function y=f_tria(x)\n');

fprintf(fID,"pd=makedist('Triangular','A',%26.20f,'B',%26.20f,'C',%26
.20f);\n",min,mode,max);
    fprintf(fID,'y=cdf(pd,x)-%26.20f;',samples_CDF(i));
    fclose(fID);
    fun=@f_tria;
    x0=mode;
    samples(i)=fsolve(fun,x0);
end
rng('shuffle');
samples_InRandomOrder=samples(randperm(length(samples)));
samples_InRandomOrder_InMatrixForm=reshape(samples_InRandomOrder,row_
number,column_number);
```

```
samples_InRandomOrder_InMatrixForm=samples_InRandomOrder_InMatrixForm
/Index;
end
```

Script 3-4. “LHS_triarnd.m”

```
function y=f_norm(x)
y=normcdf(x,    1.1000000000000008882,    0.2000000000000001110)-
0.99958993000829432507;
```

Script 3-5. “f_norm.m”

```
function y=f_logn(x)
y=normcdf(x,    1.0116008999999991406,    0.5000000000000000000)-
0.99999859455602035929;
```

Script 3-6. “f_logn.m”

```
function y=f_tria(x)
pd=makedist('Triangular','A',    0.0000000000000000000,'B',
20.000000000000000000,'C', 1450.0000000000000000000);
y=cdf(pd,x)-    0.99910043259062297771;
```

Script 3-7. “f_tria.m”

```
function samples_LHSMDU = LHSMDU(N, M, L, samples_input)
% N is the number of variables, M is the redundant factor, L is the
number
% of realizations, samples_input is the 1-row-L-column*N and in-order
LHS
% samples. (samples_input must be in a form of N-row-L-column, and
must be in order.) The output, samples_LHSMDU, is the 1-row-L-
column*N and
% in-MDU-order samples.
% Note: here, it's assumed that the N variables are independent to
each
% other.

rng('shuffle');
N_ML_01matrix=unifrnd(0,1,N,M*L);
for i=1:size(N_ML_01matrix,2)
    for j=1:size(N_ML_01matrix,2)
        D(i,j)=norm(N_ML_01matrix(:,i)-N_ML_01matrix(:,j));
    end
end

for i=1:(M-1)*L
    for j=1:size(N_ML_01matrix,2)
        D_sort=sort(D(j,:));
        smallest_distance(j)=(D_sort(2)+D_sort(3))/2;
        clear D_sort;
    end
    [min_smallest_distance,position]=min(smallest_distance);
    N_ML_01matrix(:,position)=[];
    D(:,position)=[];
    D(position,:)=[];
    clear smallest_distance;
end
N_L_01matrix=N_ML_01matrix;

for k=1:N
    [A,I]=sort(N_L_01matrix(k,:));
    [B,II]=sort(I);
```

```
    N_L_ranking_matrix(k,:)=II;
end

for k=1:N
    P(k).values_in_order=samples_input(k,:);
    for l=1:L

P(k).values_in_MDUorder(l)=P(k).values_in_order(N_L_ranking_matrix(k,
l));
    end
    samples_LHSMDU(k,:)=P(k).values_in_MDUorder;
end

end
```

Script 3-8. “LHSMDU.m”

Calling CONFEM by MATLAB requires the subscript of “confemfrommatlab.m”. Reading information from input data files of CONFEM requires “importfile.m” and “plt_to_array.m” to transfer information in the file to numeric matrix form so that specific information can be located more easily.

```
confemfolder ='C:\Users\Linxue Zhao\Documents\MATLAB\PFOS transport
MCS\3e-13leak\wholeInput_multitimenode\';
confemfile = [confemfolder,'confem_noscreen.exe'];
dos(confemfile);
```

Script 3-9. “confemfrommatlab.m”

```
function caseproblem1 = importfile(filename, startRow, endRow)
%IMPORTFILE Import numeric data from a text file as a matrix.
%   CASEPROBLEM1 = IMPORTFILE(FILENAME) Reads data from text file
FILENAME
%   for the default selection.
%
%   CASEPROBLEM1 = IMPORTFILE(FILENAME, STARTROW, ENDROW) Reads data
from
%   rows STARTROW through ENDROW of text file FILENAME.
%
% Example:
%   caseproblem1 = importfile('case problem 1.plt', 2, 1370);
%
%    See also TEXTSCAN.

% Auto-generated by MATLAB on 2022/01/27 19:54:45

%% Initialize variables.
if nargin<=2
    startRow = 2;
    endRow = inf;
end

%% Read columns of data as text:
% For more information, see the TEXTSCAN documentation.
formatSpec =
'%6s%16s%15s%15s%15s%15s%15s%15s%15s%15s%15s%15s%15s%15s%15s%15s%15s%
15s%15s%s%[^\n\r]';
```

```
%% Open the text file.
fileID = fopen(filename,'r');

%% Read columns of data according to the format.
% This call is based on the structure of the file used to generate
this
% code. If an error occurs for a different file, try regenerating the
code
% from the Import Tool.
dataArray = textscan(fileID, formatSpec, endRow(1)-startRow(1)+1,
'Delimiter', '', 'WhiteSpace', '', 'TextType', 'string',
'HeaderLines', startRow(1)-1, 'ReturnOnError', false, 'EndOfLine',
'\r\n');
for block=2:length(startRow)
    frewind(fileID);
    dataArrayBlock = textscan(fileID, formatSpec, endRow(block)-
startRow(block)+1, 'Delimiter', '', 'WhiteSpace', '', 'TextType',
'string', 'HeaderLines', startRow(block)-1, 'ReturnOnError', false,
'EndOfLine', '\r\n');
    for col=1:length(dataArray)
        dataArray{col} = [dataArray{col};dataArrayBlock{col}];
    end
end

%% Close the text file.
fclose(fileID);

%% Convert the contents of columns containing numeric text to
numbers.
% Replace non-numeric text with NaN.
raw = repmat({''},length(dataArray{1}),length(dataArray)-1);
for col=1:length(dataArray)-1
    raw(1:length(dataArray{col}),col) = mat2cell(dataArray{col},
ones(length(dataArray{col}), 1));
end
numericData = NaN(size(dataArray{1},1),size(dataArray,2));

for col=[1,2,3,4,5,6,7,8,9,10,11,12,13,14,15,16,17,18,19,20]
    % Converts text in the input cell array to numbers. Replaced non-
numeric
    % text with NaN.
    rawData = dataArray{col};
    for row=1:size(rawData, 1)
        % Create a regular expression to detect and remove non-
numeric prefixes and
        % suffixes.
        regexstr =
'(?<prefix>.*?)(?<numbers>([-]*(\d+[\,]*)+[\.]{0,1}\d*[eEdD]{0,1}[-
+]*\d*[i]{0,1})|([-]*(\d+[\,]*)*[\.]{1,1}\d+[eEdD]{0,1}[-
+]*\d*[i]{0,1}))(?<suffix>.*)';
        try
            result = regexp(rawData(row), regexstr, 'names');
            numbers = result.numbers;

            % Detected commas in non-thousand locations.
            invalidThousandsSeparator = false;
            if numbers.contains(',')
                thousandsRegExp = '^[-/+]*\d+?(\,\d{3})*\.{0,1}\d*$';
                if isempty(regexp(numbers, thousandsRegExp, 'once'))
                    numbers = NaN;
```

```
                    invalidThousandsSeparator = true;
                end
            end
            % Convert numeric text to numbers.
            if ~invalidThousandsSeparator
                numbers = textscan(char(strrep(numbers, ',', '')),
'%f');
                numericData(row, col) = numbers{1};
                raw{row, col} = numbers{1};
            end
        catch
            raw{row, col} = rawData{row};
        end
    end
end


%% Replace non-numeric cells with NaN
R = cellfun(@(x) ~isnumeric(x) && ~islogical(x),raw); % Find non-
numeric cells
raw(R) = {NaN}; % Replace non-numeric cells

%% Create output variable
caseproblem1 = cell2mat(raw);
```

Script 3-10. “importfile.m”

```
function allresults=plt_to_array(pltfile,TotalTime,TotalNode)
fID=fopen(pltfile);
str=[];
for i=1:20
fgetl(fID);
end
for i=1:TotalTime
fgetl(fID);
for j=1:TotalNode
tmp=fgets(fID);
str=[str tmp];
end
end
fclose(fID);
fID=fopen('neat plt.txt','w+');
fprintf(fID,str);
fclose(fID);
allresults=importdata('neat plt.txt');
end
```

Script 3-11. “plt_to_array.m”

Appendix 3.3 Mathematical Formulation of Polynomial Chaos Expansion and Global Sensitivity Analysis

The following presents a compact mathematical description of the framework comprising PCE and subsequent GSA employed herein (Deman et al., 2016; Marelli et al., 2024a, 2024b). More details are available in Sudret (2008), Blatman and Sudret (2010), and Gratiet et al. (2016).

Let us consider a computational model, $Y = \mathcal{M}(\mathbf{x})$, describing the relationship between the random output Y and the M-dimensional random input vector $\mathbf{x} = \{x_1, \dots, x_\mathrm{M}\}$ in the investigated physical system. Let $f_\mathbf{x}(\mathbf{x})$ and $f_{x_i}(x_i)$ denote the joint probability density function (PDF) and the marginal PDFs of the input variables. The M input variables are assumed to be independent in the following introduction to the theory, which is also the case for the uncertain modelling in this study. Thus, the above computational model can be described by a map from $\mathbf{x} \in \mathcal{D}_\mathbf{x} \subset \mathbb{R}^\mathrm{M}$ to $Y = \mathcal{M}(\mathbf{x}) \in \mathbb{R}$ where $\mathcal{D}_\mathbf{x}$ is the support of $\mathbf{x}$.

As mentioned in Introduction, GSA aims to estimate the attribution of output uncertainties to the uncertainties in input parameters, which can be associated with single parameters or combinations of several parameters. A prevalent variance-based sensitivity metric, the Sobol' indices (SIs), can quantify such an attribution. PCE provides an efficient approximation to the original computational model, which also facilitates the calculation of SIs.

A3.3.1 Sobol' indices

Sobol' indices (Sobol', 1993) are derived from the concept of defining the expansion of the computational model into summands of increasing dimension. The total variance of the model is characterized by the sum of the variances of these summands. Assuming the function $\mathcal{M}(\mathbf{x})$ to be square-integrable with respect to the PDF of $f_\mathbf{x}(\mathbf{x})$, the Sobol' decomposition of $Y = \mathcal{M}(\mathbf{x})$ in summands of increasing dimension is defined as:

$$\mathcal{M}(\mathbf{x}) = \mathcal{M}_0 + \sum_{i=1}^{\mathrm{M}} \mathcal{M}_i(x_i) + \sum_{1 \le i < j \le \mathrm{M}} \mathcal{M}_{ij}(x_i, x_j) + \cdots + \mathcal{M}_{12\dots\mathrm{M}}(x_1, \dots, x_\mathrm{M}) \quad \text{(A3.3.1)}$$

which is only valid for independent input variables and can also be written as

$$\mathcal{M}(\mathbf{x}) = \mathcal{M}_0 + \sum_{\boldsymbol{u} \neq \emptyset} \mathcal{M}_{\boldsymbol{u}}(\mathbf{x}_{\boldsymbol{u}}) \quad \text{(A3.3.2)}$$

where $\boldsymbol{u} = \{i_1, \dots, i_s\} \subset \{1, \dots, \mathrm{M}\}$ are index sets and $\mathbf{x}_{\boldsymbol{u}}$ mean the subvectors of $\mathbf{x}$ involving only the components with indices belonging to $\boldsymbol{u}$.

The Sobol' decomposition is shown to be existing and unique under the following conditions by Sobol' (1993).

1) $\mathcal{M}_0$ is constant and equal to the expected value of $\mathcal{M}(\mathbf{x})$.

2) $\int_{\mathcal{D}_{x_k}} \mathcal{M}_{\boldsymbol{u}}(\mathbf{x}_{\boldsymbol{u}}) f_{x_k}(x_k) \mathrm{d}x_k = 0$, if $k \in \boldsymbol{u}$, where $\mathcal{D}_{x_k}$ and $f_{x_k}(x_k)$ stand for the support and marginal PDF of x_k respectively.

The second condition results in the orthogonality between terms of the decomposition.

$$E[\mathcal{M}_{\boldsymbol{u}}(\mathbf{x}_{\boldsymbol{u}})\mathcal{M}_{\boldsymbol{v}}(\mathbf{x}_{\boldsymbol{v}})] = 0, \text{ if } \boldsymbol{u} \neq \boldsymbol{v} \tag{A3.3.3}$$

Due to the uniqueness and orthogonality of the Sobol' decomposition, the total variance D of $Y = \mathcal{M}(\mathbf{x})$ can be decomposed as

$$D = \mathrm{Var}[\mathcal{M}(\mathbf{x})] = \sum_{\boldsymbol{u} \neq \emptyset} D_{\boldsymbol{u}} \tag{A3.3.4}$$

where $D_{\boldsymbol{u}}$ are the partial variances expressed as

$$D_{\boldsymbol{u}} = \mathrm{Var}[\mathcal{M}_{\boldsymbol{u}}(\mathbf{x}_{\boldsymbol{u}})] = E[\mathcal{M}_{\boldsymbol{u}}^2(\mathbf{x}_{\boldsymbol{u}})] \tag{A3.3.5}$$

The variance decomposition leads to a natural definition of the Sobol' index as

$$S_{\boldsymbol{u}} = D_{\boldsymbol{u}}/D \tag{A3.3.6}$$

which quantifies the attribution of the total variance to the interaction between the variables comprising $\mathbf{x}_{\boldsymbol{u}}$. The index with respect to one input variable x_i is defined as the first-order Sobol' index, $S_i = D_i/D$, representing the influence of x_i alone. Second-order indices, S_{ij}, represents the influence of the interaction between $\{x_i, x_j\}$ that cannot be decomposed into their separate contributions. Further higher-order indices can be interpreted analogously.

The total Sobol' indices, S_i^T, quantifies the total contribution of x_i, including its separate contribution and all contributions of interactions involving it. This definition leads to a derivation of S_i^T as the sum of all partial indices involving x_i, i.e., $S_i^T = \sum_{\vartheta_i} S_{\boldsymbol{u}}, \vartheta_i = \{\boldsymbol{u} \supset i\}$. Another derivation of S_i^T is expressed as $S_i^T = 1 - S_{\sim i}$, where $S_{\sim i}$ denotes the sum of all $S_{\boldsymbol{u}}$ with $\boldsymbol{u}$ not including i.

Traditionally, the evaluation of Sobol' indices can be achieved through MCS, requiring multiple integrations of the model $\mathcal{M}(\mathbf{x})$ and its square, for different combinations of the variables (Sobol', 2001). This is computationally unaffordable when the model is time-consuming, or the number of variables is large (Sudret, 2008).

A3.3.2 Polynomial chaos expansions

Still assuming the square-integrable function $\mathcal{M}(\mathbf{x})$ of the independent input vector **x**, the PCE of $Y = \mathcal{M}(\mathbf{x})$ is defined as

$$Y \approx \hat{Y} = \mathcal{M}^{\mathrm{PCE}}(\mathbf{x}) = \sum_{\boldsymbol{\alpha} \in \mathcal{A}} y_{\boldsymbol{\alpha}} \boldsymbol{\Psi}_{\boldsymbol{\alpha}}(\mathbf{x}) \tag{A3.3.7}$$

where $\{\boldsymbol{\Psi}_{\boldsymbol{\alpha}}, \boldsymbol{\alpha} \in \mathcal{A}\}$ is a set of multivariate polynomials orthonormal with respect to $f_{\mathbf{x}}(\mathbf{x})$, $\mathcal{A}$ is a set of multi-indices $\boldsymbol{\alpha} = (\alpha_1, \dots, \alpha_{\mathrm{M}})$ that identifies the components of $\boldsymbol{\Psi}_{\boldsymbol{\alpha}}$, and $\{y_{\boldsymbol{\alpha}}, \boldsymbol{\alpha} \in \mathcal{A}\}$ is the corresponding set of coefficients.

The multivariate polynomials comprising the PCE basis are assembled as the tensor product of their univariate counterparts, i.e.,

$$\boldsymbol{\Psi}_{\boldsymbol{\alpha}}(\mathbf{x}) = \prod_{i=1}^{\mathrm{M}} \Psi_{\alpha_i}^{(x_i)}(x_i) \tag{A3.3.8}$$

where $\Psi_{\alpha_i}^{(x_i)}(x_i)$ represents the polynomial of degree α_i for x_i, which belongs to a family of polynomials that are orthonormal with respect to $f_{x_i}(x_i)$. The well-known classical families of univariate orthonormal polynomials (Askey-Scheme) and their corresponding distributions are widely available in the literature (e.g., Xiu and Karniadakis, 2002). For example, the family of Hermite polynomials corresponds to a standard normal distribution and also suits a log-normal distribution through a simple transformation. If the input vector contains arbitrary probability distributions, like the triangular distribution adopted in this paper, there are two common approaches to address this. The first is to perform an isoprobabilistic transformation to a vector with independent standard components, where the transformation may be highly non-linear, causing a considerable negative impact on the accuracy of PCE (Marelli et al., 2024a). The second is to construct an associated family of univariate polynomials for the non-standard distribution, which can be realized through the Stieltjes procedure (Gautschi, 2004).

Assuming the degree of $\mathcal{M}^{\mathrm{PCE}}(\mathbf{x})$ to be p, the number of terms in PCE, P, depends on p and M, so $\mathcal{A}$ can be rewritten as $\mathcal{A}^{\mathrm{M,p}} = \{\boldsymbol{\alpha} \in \mathbb{N}^{\mathrm{M}} : |\boldsymbol{\alpha}| \leq \mathrm{p}\}$, and card $\mathcal{A}^{\mathrm{M,p}} = \mathrm{P} =$

$\frac{(\mathrm{M}+\mathrm{p})!}{\mathrm{M}!\mathrm{p}!}$. However, not every term is equally important. Typically, the most crucial terms in the expansion are those involving only a few variables (Marelli et al., 2024a). A hyperbolic truncation scheme can be applied to exclude terms of high interaction order (Blatman, 2009), so that the complexity of the expansion can be significantly reduced without losing considerable accuracy. By introducing a norm $0 < q \leq 1$, the set of multi-indices is contracted to

$$\mathcal{A}^{\mathrm{M,p,q}} = \left\{\boldsymbol{\alpha} \in \mathcal{A}^{\mathrm{M,p}} : \|\boldsymbol{\alpha}\|_{\mathrm{q}} \leq \mathrm{p}\right\}, \|\boldsymbol{\alpha}\|_{\mathrm{q}} = \left(\sum_{i=1}^{\mathrm{M}} \alpha_i^{\mathrm{q}}\right)^{1/\mathrm{q}} \tag{A3.3.9}$$

For $\mathrm{q} = 1$, the total-degree set of multi-indices is retained. For $\mathrm{q} < 1$, all the univariate high-degree terms remain, but high-degree terms with many interacting variables are excluded.

After determining the basis, the coefficients $\boldsymbol{y} = \{y_{\boldsymbol{\alpha}}, \boldsymbol{\alpha} \in \mathcal{A}^{\mathrm{M,p,q}}\}$ need to be calculated based on a set of correspondences between samples of the input vector and corresponding outputs through the original model, namely the experimental design (Marelli et al., 2024a). The two principal methods for the non-intrusive calculation of polynomial chaos coefficients are projection and regression. The regression method proceeds by conducting a least-squares minimization problem (Berveiller et al., 2006), which aims to minimize an objective function representing the difference between the meta-model $\hat{Y}$ and original model Y with respect to the unknown vector of coefficients $\boldsymbol{v}$, and can be expressed as

$$\boldsymbol{y} = \underset{\boldsymbol{v} \in \mathbb{R}^{\mathrm{card}\, \mathcal{A}^{\mathrm{M,p,q}}}}{\arg\min}\ E\left[\left(\sum_{\boldsymbol{\alpha} \in \mathcal{A}^{\mathrm{M,p,q}}} v_{\boldsymbol{\alpha}} \boldsymbol{\Psi}_{\boldsymbol{\alpha}}(\mathbf{x}) - \mathcal{M}(\mathbf{x})\right)^2\right] \tag{A3.3.10}$$

Sparse regression techniques can be used to further discard irrelevant terms in the truncated PCE and thus reduce the needed number of experimental evaluations. Several approaches have been developed for this purpose, such as hybrid least angle regression (LARS, Blatman and Sudret, 2011), orthogonal matching pursuit (OMP, Pati et al., 1993), subspace pursuit (SP, Diaz et al., 2018), Bayesian compressive sensing (BCS, Sargsyan et al., 2014), etc. Comparative estimations on these techniques can be found in Lüthen et al. (2020) and Lüthen et al. (2021). As available options in UQLab, the above four sparse regression approaches were compared for their performance in solving the investigated problem in this work.

A3.3.3 PCE-based Sobol' indices

As mentioned earlier, when a PCE of a quantity of interest (QoI) is established, the Sobol' indices associated with this QoI can be derived analytically (Sudret, 2008). Through a comparative observation on the PCE $\hat{Y} = \mathcal{M}^{\mathrm{PCE}}(\mathbf{x})$ and the Sobol' decomposition of $Y = \mathcal{M}(\mathbf{x})$, it is straightforward to derive the Sobol' decomposition of $\hat{Y}$ from the sum of corresponding terms in Eq. (A3.3.7), which can be expressed as

$$\mathcal{M}_{\boldsymbol{u}}{}^{\mathrm{PCE}}(\mathbf{x}_{\boldsymbol{u}}) = \sum_{\boldsymbol{\alpha}\in\mathcal{A}_{\boldsymbol{u}}} y_{\boldsymbol{\alpha}} \boldsymbol{\Psi}_{\boldsymbol{\alpha}}(\mathbf{x}) \tag{A3.3.11}$$

Where $\mathcal{A}_{\boldsymbol{u}} = \{\boldsymbol{\alpha} \in \mathcal{A}: \alpha_k \neq 0 \text{ if and only if } k \in \boldsymbol{u}\}$.

Because of the orthonormality of the polynomial chaos basis, the partial variance $D_{\boldsymbol{u}}$ and the total variance D can be estimated as

$$\widehat{D}_{\boldsymbol{u}} = \mathrm{Var}[\mathcal{M}_{\boldsymbol{u}}^{\mathrm{PCE}}(\mathbf{x}_{\boldsymbol{u}})] = \sum_{\boldsymbol{\alpha}\in\mathcal{A}_{\boldsymbol{u}}} y_{\boldsymbol{\alpha}}^2 \tag{A3.3.12}$$

and

$$\widehat{D} = \mathrm{Var}[\mathcal{M}^{\mathrm{PCE}}(\mathbf{x})] = \sum_{\boldsymbol{\alpha}\in\mathcal{A}\setminus\{0\}} y_{\boldsymbol{\alpha}}^2 \tag{A3.3.13}$$

Therefore, the Sobol' indices of any order involving the interaction between any variable are available by $\hat{S}_{\boldsymbol{u}} = \widehat{D}_{\boldsymbol{u}}/\widehat{D}$. In particular, the PCE-based first-order and total Sobol' indices can respectively be expressed as

$$\hat{S}_i = \sum_{\boldsymbol{\alpha}\in\mathcal{A}_i} y_{\boldsymbol{\alpha}}^2 / \widehat{D}, \mathcal{A}_i = \left\{\boldsymbol{\alpha} \in \mathcal{A}: \alpha_i > 0, \alpha_{j\neq i} = 0\right\} \tag{A3.3.14}$$

and

$$\hat{S}_i^T = \sum_{\boldsymbol{\alpha}\in\mathcal{A}_i^T} y_{\boldsymbol{\alpha}}^2 / \widehat{D}, \mathcal{A}_i^T = \{\boldsymbol{\alpha} \in \mathcal{A}: \alpha_i > 0\} \tag{A3.3.15}$$

Appendix 3.4 MATLAB Scripts for PCE-enhanced MCS

The generation of input samples is realized by the script of "PCE_MCS_Sample_generation.m", which is a segment of Script 3-1. The relevant subscripts (Script 3-2 to 3-8) are also employed in conjunction herein.

```
function PCE_MCS_Sample_generation(MCSfrommatlab_input_file)
tic;
rng('shuffle');
fprintf('generating samples\n')
% At first, some variables are extracted from Excel and plt.
basic_information=readtable(MCSfrommatlab_input_file,'Range','A1:B100
','ReadVariableNames',false);

MCS_times=xlsread(MCSfrommatlab_input_file,'B5:B5');


% read probabilistic parameters' mean and SD from Excel and generate
random
% values for them.
% meanwhile, draw distributions for these parameters
all_probabilistic_parameters=xlsread(MCSfrommatlab_input_file,'F3:H10
0');
dist_type=readtable(MCSfrommatlab_input_file,'Range','C3:C100','ReadV
ariableNames',false);
probabilistic_parameter_number=xlsread(MCSfrommatlab_input_file,'B3:B
3');
probabilistic_parameter_number_WF=xlsread(MCSfrommatlab_input_file,'B
15:B15');
figure('Name','Probabilistic Parameters');hold on;
for i=1:probabilistic_parameter_number
if strcmp(char(dist_type{i,1}),'norm')

P(i).randomvalues_initial=LHS_normrnd(all_probabilistic_parameters(i,
1),all_probabilistic_parameters(i,2),1,MCS_times);
elseif strcmp(char(dist_type{i,1}),'logn')

P(i).randomvalues_initial=LHS_lognrnd(all_probabilistic_parameters(i,
1),all_probabilistic_parameters(i,2),1,MCS_times);
elseif strcmp(char(dist_type{i,1}),'tria')

P(i).randomvalues_initial=LHS_triarnd(all_probabilistic_parameters(i,
1),all_probabilistic_parameters(i,2),all_probabilistic_parameters(i,3
),1,MCS_times);
elseif strcmp(char(dist_type{i,1}),'logn+cons')

P(i).randomvalues_initial=LHS_lognrnd(all_probabilistic_parameters(i,
1),all_probabilistic_parameters(i,2),1,MCS_times)+all_probabilistic_p
arameters(i,3);
end
P(i).randomvalues_inorder=sort(P(i).randomvalues_initial);
samples_input(i,:)=P(i).randomvalues_inorder;
end
samples_LHSMDU = LHSMDU(probabilistic_parameter_number, 5, MCS_times,
samples_input);
for i=1:probabilistic_parameter_number
    P(i).randomvalues=samples_LHSMDU(i,:);
end
```

```
for i=1:probabilistic_parameter_number
fprintf('Random values for P%u are ',i);P(i).randomvalues
xlswrite('Random input parameters.xlsx',{['Random values for
P',num2str(i),' are ']},'Sheet1',['A',num2str(2*i-1)]);
xlswrite('Random input
parameters.xlsx',P(i).randomvalues,'Sheet1',['A',num2str(2*i)]);
subplot(1,probabilistic_parameter_number,i);histfit(P(i).randomvalues
);title(['P' num2str(i)]);
end
set(gcf,'outerposition',get(0,'screensize'));
saveas(gcf,['Random input parameters.png']);
hold off;

% use tic toc to record the calculation time
toc;
t=toc
end
```

Script 3-11. "PCE_MCS_Sample_generation.m"

The establishment of PCE model based on ED and the subsequent calculation of PrD (Steps 2 to 4 in Section 3.5.3.2) are realized by the script of "PCE_prediction.m".

```
clearvars
rng(100,'twister')
uqlab

tic;
% Read the input and output data of experimental design (ED).
X_ED=xlsread('X.xlsx','Sheet1','A1:L1980');
Y_ED=xlsread('Y.xlsx','Sheet1','A:A');
MetaOpts.ExpDesign.X = X_ED;
MetaOpts.ExpDesign.Y = Y_ED;

% Define the types and statistics of input distributions.
IOpts.Marginals(1).Type = 'Lognormal' ;
IOpts.Marginals(1).Parameters = [-2.302585 0.1] ;
IOpts.Marginals(2).Type = 'Lognormal' ;
IOpts.Marginals(2).Parameters = [-6.9696307 1.15] ;
IOpts.Marginals(3).Type = 'Lognormal' ;
IOpts.Marginals(3).Parameters = [1.94591015 0.3] ;
IOpts.Marginals(4).Type = 'Lognormal' ;
IOpts.Marginals(4).Parameters = [1.148544657 1.15] ;
IOpts.Marginals(5).Type = 'Triangular' ;
IOpts.Marginals(5).Parameters = [0.3 2.05 1.05] ;
IOpts.Marginals(6).Type = 'Lognormal' ;
IOpts.Marginals(6).Parameters = [1.31989 0.5] ;
IOpts.Marginals(7).Type = 'Lognormal' ;
IOpts.Marginals(7).Parameters = [1.0986 0.6] ;
IOpts.Marginals(8).Type = 'Lognormal' ;
IOpts.Marginals(8).Parameters = [6.802394763 1.1] ;
IOpts.Marginals(9).Type = 'Lognormal' ;
IOpts.Marginals(9).Parameters = [-6.2146081 2.1] ;
IOpts.Marginals(10).Type = 'Lognormal' ;
IOpts.Marginals(10).Parameters = [-0.051293294 0.4] ;
IOpts.Marginals(11).Type = 'Lognormal' ;
IOpts.Marginals(11).Parameters = [-2.3025851 1.5] ;
IOpts.Marginals(12).Type = 'Triangular' ;
IOpts.Marginals(12).Parameters = [0 1450 20] ;
```

```
% Set the configuration of the PCE model and establish the PCE model.
myInput = uq_createInput(IOpts);
MetaOpts.Type = 'Metamodel';
MetaOpts.MetaType = 'PCE';
MetaOpts.PolyTypes={'Hermite', 'Hermite', 'Hermite', 'Hermite',
'Arbitrary', 'Hermite', 'Hermite', 'Hermite', 'Hermite', 'Hermite',
'Hermite', 'Arbitrary'};
MetaOpts.TruncOptions.qNorm = 0.5;
MetaOpts.Degree =10;
MetaOpts.DegreeEarlyStop = false;
MetaOpts.Method = 'BCS';
myPCE_sparse = uq_createModel(MetaOpts);
toc;t=toc

% Print the basis information of the established PCE model.
uq_print(myPCE_sparse)
uq_display(myPCE_sparse);
YPCE = uq_evalModel(X_ED);

% Calculate the output of the prediction design (PrD).
X_predictor=xlsread('20000X-1.xlsx','Sheet1','A1:L20000');
YPCE_predictor=uq_evalModel(X_predictor);
xlswrite('YPCE_predictor.xlsx',YPCE_predictor,'Sheet1','A1');

% Calculate the Sobol' Indices of the first two orders.
PCESobol.Type = 'Sensitivity';
PCESobol.Method = 'Sobol';
PCESobol.Sobol.Order = 2;
PCESobolAnalysis = uq_createAnalysis(PCESobol);
PCESobolAnalysis.Results
```

Script 3-12. “PCE_prediction.m”

Appendix 6.1 Definition of Computational Gain (G) of PCE over MCS

The computational gain (G) obtained by using PCE relative to MCS can be defined as the ratio of computational time required to conduct MCS (T_{MCS}) to that of PCE (T_{PCE}). The time cost of conducting MCS is made of two components:

a) $T_{LHS\text{-}stable}$: the time it takes to generate high-dimensional input samples by Latin hypercube sampling with multidimensional uniformity (LHSMDU) for the large number (R_{stable}) of realisations to reach output stability,
b) $R_{stable} \times t_{SPAS}$: the time it takes to run the MCS analyses with R_{stable} realisations.

where t_{SPAS} is the calculation time of one simulation in SPAS, which ranges between 6 and 11 minutes for problems studied in this thesis. The numerical simulations are performed on a desktop computer equipped with an AMD Ryzen 5 2600X 6-core processor (3.6 GHz) and 32 GB DDR4 RAM, running Windows 10 Pro 64-bit.

Hence, $T_{MCS} = T_{LHS\text{-}stable} + R_{stable} \times t_{SPAS}$.

As for PCE, the time cost of conducting it is made of five components:

a) $T_{LHS\text{-}ED}$: the time it takes to generate high-dimensional input samples by LHSMDU for the ED ($T_{LHS\text{-}ED} << T_{LHS\text{-}stable}$),
b) $R_{MCS\text{-}PCE\text{-}opt} \times t_{SPAS}$: the time it takes to run the MCS analyses with $R_{MCS\text{-}PCE\text{-}opt}$ (the optimised size of ED) realisations,
c) T_{train}: the time required to establish PCE model by UQLab based on the ED,
d) $T_{LHS\text{-}stable}$,
e) $R_{stable} \times t_0$: the time it takes to predict the R_{stable} realisations via the PCE model.

Hence, $T_{PCE} = T_{LHS\text{-}ED} + R_{MCS\text{-}PCE\text{-}opt} \times t_{SPAS} + T_{train} + T_{LHS\text{-}stable} + R_{stable} \times t_0$.

And G can be expressed as

$$G = \frac{T_{MCS}}{T_{PCE}} = \frac{T_{LHS-stable} + R_{stable} \times t_{SPAS}}{T_{LHS-E} + R_{MCS-PCE-op} \times t_{SPAS} + T_{train} + T_{LHS-stable} + R_{stable} \times t_0} \quad \text{(A6.1.1)},$$

Expression A6.1.1 can be further simplified as follows. Both T_{train} and $R_{stable} \times t_0$ have a negligible effect, with the first completed in under one hour and the second in a few seconds. Hence:

$$G \approx \frac{T_{LHS-stable} + R_{stable} \times t_{SPAS}}{R_{MCS-PCE-opt} \times t_{SPAS} + T_{LHS-stabl}} \qquad \text{(A6.1.2).}$$

Finally, $T_{LHS\text{-}stable} << R_{stable} \times t_{SPAS}$ and $R_{MCS\text{-}PCE\text{-}opt} \times t_{SPAS}$, therefore:

$$G \approx \frac{R_{stable}}{R_{MCS-PCE-op}} \qquad \text{(A6.1.3).}$$

References

3M Company. (1999a). *Fluorochemical Use, Distribution and Release Overview*. https://www.regulations.gov/document/EPA-HQ-OPPT-2002-0043-0008

3M Company. (1999b). *The Science of Organic Fluorochemistry*.

3M Company. (2000). *Voluntary Use and Exposure Information Profile for Perfluorooctanoic Acid and Salts*. https://www.regulations.gov/document/EPA-HQ-OPPT-2002-0051-0009

Abbaspour, K. C., Schulin, R., Van Genuchten, M. Th., & Schlappi, E. (1998). Procedures for Uncertainty Analyses Applied to a Landfill Leachate Plume. *Groundwater*, *36*(6), 874–883. https://doi.org/10.1111/j.1745-6584.1998.tb02094.x

Abdelaal, F. B., Rowe, R. K., & Islam, M. Z. (2014). Effect of leachate composition on the long-term performance of a HDPE geomembrane. *Geotextiles and Geomembranes*, *42*(4), 348–362. https://doi.org/10.1016/j.geotexmem.2014.06.001

AbdelRazek, A. Y., & Rowe, R. K. (2019a). Interface transmissivity of conventional and multicomponent GCLs for three permeants. *Geotextiles and Geomembranes*, *47*(1), 60–74. https://doi.org/10.1016/j.geotexmem.2018.10.001

AbdelRazek, A. Y., & Rowe, R. K. (2019b). Performance of GCLs in high salinity impoundment applications. *Geosynthetics International*, *26*(6), 611–628. https://doi.org/10.1680/jgein.19.00043

Abdulle, A., & Huber, M. E. (2014). Discontinuous Galerkin finite element heterogeneous multiscale method for advection–diffusion problems with multiple scales. *Numerische Mathematik*, *126*(4), 589–633. https://doi.org/10.1007/s00211-013-0578-9

ACRP. (2017). *Use and Potential Impacts of AFFF Containing PFASs at Airports.* Washington, DC: The National Academies Press.

Agung, P., Damianto, B., & Pramusandi, S. (2013). Hydraulic conductivity measurement of compacted clay soil liners for waste containment structures. *Journal of Earth Sciences and Geotechnical Engineering*, *3*(4), 125–145.

Aliewi, A., Hadi, K., Bhandary, H., Al-Qallaf, H., Rashed, T., Abdulhadi, A., & Al-Salem, S. M. (2021). Investigation of landfill leachate pollution impact on shallow aquifers using numerical simulation. *Arabian Journal of Geosciences*, *14*(20), 2158. https://doi.org/10.1007/s12517-021-08536-8

Allred, B. M., Lang, J. R., Barlaz, M. A., & Field, J. A. (2014). Orthogonal zirconium diol/C18 liquid chromatography–tandem mass spectrometry analysis of poly and perfluoroalkyl substances in landfill leachate. *Journal of Chromatography A*, *1359*, 202–211. https://doi.org/10.1016/j.chroma.2014.07.056

Allred, B. M., Lang, J. R., Barlaz, M. A., & Field, J. A. (2015). Physical and Biological Release of Poly- and Perfluoroalkyl Substances (PFASs) from Municipal Solid Waste in Anaerobic Model Landfill Reactors. *Environmental Science & Technology*, *49*(13), 7648–7656. https://doi.org/10.1021/acs.est.5b01040

Al-Madhlom, Q., Al-Ansari, N., Hamza, B. A., Laue, J., & Hussain, H. M. (2020). Seepage Velocity: Large Scale Mapping and the Evaluation of Two Different Aquifer Conditions (Silty Clayey and Sandy). *Hydrology*, *7*(3), 60. https://doi.org/10.3390/hydrology7030060

Anderson, M. P., & Cherry, J. A. (1979). Using models to simulate the movement of contaminants through groundwater flow systems. *C R C Critical Reviews in Environmental Control*, *9*(2), 97–156. https://doi.org/10.1080/10643387909381669

Armitage, J., Cousins, I. T., Buck, R. C., Prevedouros, K., Russell, M. H., MacLeod, M., & Korzeniowski, S. H. (2006). Modeling Global-Scale Fate and Transport of Perfluorooctanoate Emitted from Direct Sources. *Environmental Science & Technology*, *40*(22), 6969–6975. https://doi.org/10.1021/es0614870

Arvaniti, O. S., Asimakopoulos, A. G., Dasenaki, M. E., Ventouri, E. I., Stasinakis, A. S., & Thomaidis, N. S. (2014). Simultaneous determination of eighteen perfluorinated compounds in dissolved and particulate phases of wastewater, and in sewage sludge by liquid chromatography-tandem mass spectrometry. *Anal. Methods*, *6*(5), 1341–1349. https://doi.org/10.1039/C3AY42015A

ATSDR. (2021). *Toxicological Profile for Perfluoroalkyls*. https://www.atsdr.cdc.gov/toxprofiles/tp200.pdf

Baetsle, L. H. (1969). Migration of radionuclides in porous media. In A. M. F. Duhamel (Ed.). *Progress in Nuclear Energy Series XII: Health Physics (Pp. 707–730). Pergamon Press*.

Baird, D., Le Gal La Salle, C., Love, A., & Simmons, C. (2008). Groundwater residence time and flow velocity in confined tertiary aquifers of the Northern Adelaide Plains, South Australia. *Paper Presented at Water Down Under 2008 Incorporating 31st Hydrology and Water Resources Symposium and 4th International Conference on Water Resources and Environment Research*.

Bakr, A. A., Gelhar, L. W., Gutjahr, A. L., & MacMillan, J. R. (1978). Stochastic analysis of spatial variability in subsurface flows: 1. Comparison of one- and three-dimensional flows. *Water Resources Research*, *14*(2), 263–271. https://doi.org/10.1029/WR014i002p00263

Balaguer, A., Conde, C., Hidalgo, A., Lopez, J. A., & Martinez, V. (1995). Finite Volume Methods For Two-dimensional Groundwater Pollutant Transport. *WIT Transactions on Ecology and the Environment, 13*.

Bannour, H. (2023). Effect of the durability of GCLs on Contaminants transfer through a composite liner exhibiting a hole in the geomembrane: A numerical approach. *E3S Web of Conferences*, *368*, 02001. https://doi.org/10.1051/e3sconf/202336802001

Banzhaf, S., Filipovic, M., Lewis, J., Sparrenbom, C. J., & Barthel, R. (2017). A review of contamination of surface-, ground-, and drinking water in Sweden by perfluoroalkyl and polyfluoroalkyl substances (PFASs). *Ambio*, *46*(3), 335–346. https://doi.org/10.1007/s13280-016-0848-8

Barakat, F. B., & Rowe, R. K. (2025). Implications of single and double liners on the impact of PFOA in landfills on an underlying aquifer. *Geotextiles and*

Geomembranes, *53*(1), 140–154. https://doi.org/10.1016/j.geotexmem.2024.09.009

Barakat, F. B., Rowe, R. K., Patch, D., & Weber, K. (2024). Transport parameters for PFOA and PFOS migration through GCL's and composite liners used in landfills. *Geotextiles and Geomembranes*, *52*(4), 762–772. https://doi.org/10.1016/j.geotexmem.2024.04.002

Barakat F.B., & Rowe, R.K. (2020). The Effect of Local Contact Variability on Interface Transmissivity and Implications for Mine Waste Covers. *GeoVirtual 2020, Vancouver, BC*.

Bear, J. (1972). *Dynamics of Fluids in Porous Media (1st ed.)*. Dover Publications.

Bear, J., & Cheng, A. H.-D. (2010). *Modeling Groundwater Flow and Contaminant Transport*. Springer Netherlands. https://doi.org/10.1007/978-1-4020-6682-5

Bečanová, J., Melymuk, L., Vojta, Š., Komprdová, K., & Klánová, J. (2016). Screening for perfluoroalkyl acids in consumer products, building materials and wastes. *Chemosphere*, *164*, 322–329. https://doi.org/10.1016/j.chemosphere.2016.08.112

Beck, A. (2015). Available technologies to approach zero leaks. *In Proc., of the Geosynthetics 2015 Conf. Roseville, CA: Industrial Fabrics Association International*.

Benskin, J. P., Li, B., Ikonomou, M. G., Grace, J. R., & Li, L. Y. (2012). Per- and Polyfluoroalkyl Substances in Landfill Leachate: Patterns, Time Trends, and Sources. *Environmental Science & Technology*, *46*(21), 11532–11540. https://doi.org/10.1021/es302471n

Benson, C., & Boutwell, G. (2000). Compaction Conditions and Scale-Dependent Hydraulic Conductivity of Compacted Clay Liners. In D. Shanklin, J. Talbot, & K. Rademacher, *Constructing and Controlling Compaction of Earth Fills* (pp. 254–273). ASTM International100 Barr Harbor Drive, PO Box C700, West Conshohocken, PA 19428-2959. https://doi.org/10.1520/STP15289S

Benson, C. H., Ören, A. H., & Gates, W. P. (2010). Hydraulic conductivity of two geosynthetic clay liners permeated with a hyperalkaline solution. *Geotextiles and Geomembranes*, *28*(2), 206–218. https://doi.org/10.1016/j.geotexmem.2009.10.002

Berrone, S., Borio, A., & Manzini, G. (2018). SUPG stabilization for the nonconforming virtual element method for advection–diffusion–reaction equations. *Computer Methods in Applied Mechanics and Engineering*, *340*, 500–529. https://doi.org/10.1016/j.cma.2018.05.027

Bertolazzi, E., & Manzini, G. (2004). A finite volume method for transport of contaminants in porous media. *Applied Numerical Mathematics*, *49*(3–4), 291–305. https://doi.org/10.1016/j.apnum.2003.12.008

Berveiller, M., Sudret, B., & Lemaire, M. (2006). Stochastic finite element: A non intrusive approach by regression. *European Journal of Computational Mechanics*, *15*(1–3), 81–92. https://doi.org/10.3166/remn.15.81-92

Bianchi Janetti, E., Guadagnini, L., Riva, M., & Guadagnini, A. (2019). Global sensitivity analyses of multiple conceptual models with uncertain parameters

driving groundwater flow in a regional-scale sedimentary aquifer. *Journal of Hydrology*, *574*, 544–556. https://doi.org/10.1016/j.jhydrol.2019.04.035

Bieda, B. (2013). Stochastic approach to municipal solid waste landfill life based on the contaminant transit time modeling using the Monte Carlo (MC) simulation. *Science of The Total Environment*, *442*, 489–496. https://doi.org/10.1016/j.scitotenv.2012.10.032

Blatman, G. (2009). *Adaptive sparse polynomial chaos expansion for uncertainty propagation and sensitivity analysis*. Ph. D. thesis, Blaise Pascal University - Clermont II.

Blatman, G., & Sudret, B. (2010). Efficient computation of global sensitivity indices using sparse polynomial chaos expansions. *Reliability Engineering & System Safety*, *95*(11), 1216–1229. https://doi.org/10.1016/j.ress.2010.06.015

Blatman, G., & Sudret, B. (2011). Adaptive sparse polynomial chaos expansion based on least angle regression. *Journal of Computational Physics*, *230*(6), 2345–2367. https://doi.org/10.1016/j.jcp.2010.12.021

Bong, T., & Son, Y. (2019). Impact of Probability Distribution of Hydraulic Conductivity on Groundwater Contaminant Transport. *KSCE Journal of Civil Engineering*, *23*(5), 1963–1973. https://doi.org/10.1007/s12205-019-0140-0

Botti, M., Fumagalli, A., & Scotti, A. (2023). Uncertainty quantification for mineral precipitation and dissolution in fractured porous media. *GEM - International Journal on Geomathematics*, *14*(1), 21. https://doi.org/10.1007/s13137-023-00231-y

Bouazza, A. (2021). Interaction between PFASs and geosynthetic liners: Current status and the way forward. *Geosynthetics International*, *28*(2), 214–223. https://doi.org/10.1680/jgein.20.00033

Bouazza, A., & Gates, W. P. (2014). Overview of performance compatibility issues of GCLs with respect to leachates of extreme chemistry. *Geosynthetics International*, *21*(2), 151–167. https://doi.org/10.1680/gein.14.00006

Bouazza, A., Rouf, M. A., Singh, R. M., Rowe, R. K., & Gates, W. P. (2017). Gas advection-diffusion in geosynthetic clay liners with powder and granular bentonites. *Geosynthetics International*, *24*(6), 607–614. https://doi.org/10.1680/jgein.17.00027

Boulanger, B., Vargo, J. D., Schnoor, J. L., & Hornbuckle, K. C. (2005). Evaluation of Perfluorooctane Surfactants in a Wastewater Treatment System and in a Commercial Surface Protection Product. *Environmental Science & Technology*, *39*(15), 5524–5530. https://doi.org/10.1021/es050213u

Bradshaw, S. L., Benson, C. H., & Rauen, T. L. (2016). Hydraulic Conductivity of Geosynthetic Clay Liners to Recirculated Municipal Solid Waste Leachates. *Journal of Geotechnical and Geoenvironmental Engineering*, *142*(2), 04015074. https://doi.org/10.1061/(ASCE)GT.1943-5606.0001387

Brenner, K., Chorfi, N., & Masson, R. (2023). Algebraic flux correction finite element method with semi-implicit time stepping for solute transport in fractured porous media. *Computational Geosciences*, *27*(1), 103–126. https://doi.org/10.1007/s10596-022-10178-y

Brooke, D., Footitt, A., & Nwaogu, T. A. (2004). *ENVIRONMENTAL RISK EVALUATION REPORT: PERFLUOROOCTANESULPHONATE (PFOS)*. https://assets.publishing.service.gov.uk/media/5a7b984540f0b645ba3c5549/scho1009brbl-e-e.pdf

Brusseau, M. L., Khan, N., Wang, Y., Yan, N., Van Glubt, S., & Carroll, K. C. (2019). Nonideal Transport and Extended Elution Tailing of PFOS in Soil. *Environmental Science & Technology*, *53*(18), 10654–10664. https://doi.org/10.1021/acs.est.9b02343

Buck, R. C., Franklin, J., Berger, U., Conder, J. M., Cousins, I. T., De Voogt, P., Jensen, A. A., Kannan, K., Mabury, S. A., & Van Leeuwen, S. P. (2011). Perfluoroalkyl and polyfluoroalkyl substances in the environment: Terminology, classification, and origins. *Integrated Environmental Assessment and Management*, *7*(4), 513–541. https://doi.org/10.1002/ieam.258

Busch, J., Ahrens, L., Sturm, R., & Ebinghaus, R. (2010). Polyfluoroalkyl compounds in landfill leachates. *Environmental Pollution*, *158*(5), 1467–1471. https://doi.org/10.1016/j.envpol.2009.12.031

Cadini, F., De Sanctis, J., Bertoli, I., & Zio, E. (2013). Monte Carlo simulation of radionuclide migration in fractured rock for the performance assessment of radioactive waste repositories. *Reliability Engineering & System Safety*, *111*, 241–247. https://doi.org/10.1016/j.ress.2012.10.002

CalEPA. (2020). *Response Levels Lowered for Water Systems Statewide as PFAS Investigation Continues New Stricter Standard Established for PFOA and PFOS*. State Water Resources Control Board. https://www.waterboards.ca.gov/press_room/press_releases/2020/pr02062020_pfoa_pfos_response_levels.pdf

Campo, J., Masiá, A., Picó, Y., Farré, M., & Barceló, D. (2014). Distribution and fate of perfluoroalkyl substances in Mediterranean Spanish sewage treatment plants. *Science of The Total Environment*, *472*, 912–922. https://doi.org/10.1016/j.scitotenv.2013.11.056

Canada. Environment Canada. (2010). *Risk management scope for perfluorooctanoic acid (PFOA), its salts and its precursors, and long-chain (C9-C20) perfluorocarboxylic acids (PFCAs), their salts, and their precursors*. https://publications.gc.ca/site/eng/459874/publication.html

Carey, G. R., McGregor, R., Pham, A. L., Sleep, B., & Hakimabadi, S. G. (2019). Evaluating the longevity of a PFAS *in situ* colloidal activated carbon remedy. *Remediation Journal*, *29*(2), 17–31. https://doi.org/10.1002/rem.21593

Cazaux, D., & Didier, G. (2002). Comparison between various Field and Laboratory Measurements of the Hydraulic Conductivity of three Clay Liners. In M. Sara & L. Everett, *Evaluation and Remediation of Low Permeability and Dual Porosity Environments* (pp. 3–24). ASTM International100 Barr Harbor Drive, PO Box C700, West Conshohocken, PA 19428-2959. https://doi.org/10.1520/STP10616S

Chang, S.-Y., & Boateng, L. K. (2012). Adaptive Kalman Filtering Scheme for the Simulation of Benzene in Subsurface Environment. *Journal of Environmental Engineering*, *138*(5), 542–551. https://doi.org/10.1061/(ASCE)EE.1943-7870.0000500

Chappel, M. J. (2012). *A Field Scale Evaluation of Wrinkles in Exposed HDPE Geomembranes*. Ph. D. thesis, Queen's University.

Chaudhary, E., Swami, D., Joshi, N., & Reddy, K. R. (2024). Sustainable Landfill Liner Using Local Soils and Wastes Amended with Bentonite: Hydraulic Conductivity and Stochastic Leachate Transport Modeling. *Journal of Geotechnical and Geoenvironmental Engineering*, *150*(1), 04023126. https://doi.org/10.1061/JGGEFK.GTENG-11470

Chaudhuri, A., & Sekhar, M. (2005). Probabilistic Analysis of Pollutant Migration from a Landfill Using Stochastic Finite Element Method. *Journal of Geotechnical and Geoenvironmental Engineering*, *131*(8), 1042–1049. https://doi.org/10.1061/(ASCE)1090-0241(2005)131:8(1042)

Chaudhuri, S. (2019). *Transport Potential of Anionic, Cationic, and Zwitterionic Per- and Polyfluoroalkyl Substances (PFASs) through a Saturated Porous Medium*. ProQuest Dissertations Publishing.

Chen, C., Zhan, L., Wang, Y., Zhang, S., & Chen, Y. (2020). Stochastic evaluation of leakages through holes in wrinkle networks of composite liners. *Geotextiles and Geomembranes*, *48*(3), 284–296. https://doi.org/10.1016/j.geotexmem.2019.12.001

Chen, R., Ge, Y., Chen, Z., Liu, J., Zhao, Y., & Li, Z. (2019). Analytical solution for one-dimensional contaminant diffusion through unsaturated soils beneath geomembrane. *Journal of Hydrology*, *568*, 260–274. https://doi.org/10.1016/j.jhydrol.2018.10.057

Chen, Y., Xie, H., Ke, H., & Chen, R. (2009). An analytical solution for one-dimensional contaminant diffusion through multi-layered system and its applications. *Environmental Geology*, *58*(5), 1083–1094. https://doi.org/10.1007/s00254-008-1587-3

Cheng, R. T., Casulli, V., & Milford, S. N. (1984). Eulerian-Lagrangian Solution of the Convection-Dispersion Equation in Natural Coordinates. *Water Resources Research*, *20*(7), 944–952. https://doi.org/10.1029/WR020i007p00944

Ciriello, V., & De Barros, F. P. J. (2020). Characterizing the Influence of Multiple Uncertainties on Predictions of Contaminant Discharge in Groundwater Within a Lagrangian Stochastic Formulation. *Water Resources Research*, *56*(10), e2020WR027867. https://doi.org/10.1029/2020WR027867

Ciriello, V., Di Federico, V., Riva, M., Cadini, F., De Sanctis, J., Zio, E., & Guadagnini, A. (2013). Polynomial chaos expansion for global sensitivity analysis applied to a model of radionuclide migration in a randomly heterogeneous aquifer. *Stochastic Environmental Research and Risk Assessment*, *27*(4), 945–954. https://doi.org/10.1007/s00477-012-0616-7

Clarke, B. O., Anumol, T., Barlaz, M., & Snyder, S. A. (2015). Investigating landfill leachate as a source of trace organic pollutants. *Chemosphere*, *127*, 269–275. https://doi.org/10.1016/j.chemosphere.2015.02.030

Costanza, J., Arshadi, M., Abriola, L. M., & Pennell, K. D. (2019). Accumulation of PFOA and PFOS at the Air–Water Interface. *Environmental Science & Technology Letters*, *6*(8), 487–491. https://doi.org/10.1021/acs.estlett.9b00355

D35 Committee. (n.d.). *Guide for Installation of Geosynthetic Clay Liners*. ASTM International. https://doi.org/10.1520/D6102-23

Daniel, D. E. (Ed.). (1993). *Geotechnical Practice for Waste Disposal*. Springer US. https://doi.org/10.1007/978-1-4615-3070-1

De Barros, F. P. J. (2018). Evaluating the combined effects of source zone mass release rates and aquifer heterogeneity on solute discharge uncertainty. *Advances in Water Resources*, *117*, 140–150. https://doi.org/10.1016/j.advwatres.2018.05.010

De Barros, F. P. J., Bolster, D., Sanchez-Vila, X., & Nowak, W. (2011). A divide and conquer approach to cope with uncertainty, human health risk, and decision making in contaminant hydrology. *Water Resources Research*, *47*(5), 2010WR009954. https://doi.org/10.1029/2010WR009954

De Barros, F. P. J., & Nowak, W. (2010). On the link between contaminant source release conditions and plume prediction uncertainty. *Journal of Contaminant Hydrology*, *116*(1–4), 24–34. https://doi.org/10.1016/j.jconhyd.2010.05.004

Deman, G., Konakli, K., Sudret, B., Kerrou, J., Perrochet, P., & Benabderrahmane, H. (2016). Using sparse polynomial chaos expansions for the global sensitivity analysis of groundwater lifetime expectancy in a multi-layered hydrogeological model. *Reliability Engineering & System Safety*, *147*, 156–169. https://doi.org/10.1016/j.ress.2015.11.005

Deutsch, J. L., & Deutsch, C. V. (2012). Latin hypercube sampling with multidimensional uniformity. *Journal of Statistical Planning and Inference*, *142*(3), 763–772. https://doi.org/10.1016/j.jspi.2011.09.016

Dhanraj, M. R., & Ganesha, A. (2023). Modelling and Simulation of Pollutant Transport in Porous Media—A Simulation and Validation Study. In M. S. Ranadive, B. B. Das, Y. A. Mehta, & R. Gupta (Eds.), *Recent Trends in Construction Technology and Management* (Vol. 260, pp. 387–399). Springer Nature Singapore. https://doi.org/10.1007/978-981-19-2145-2_30

Di Battista, V., Rowe, R. K., Patch, D., & Weber, K. (2020). PFOA and PFOS diffusion through LLDPE and LLDPE coextruded with EVOH at 22 °C, 35 °C, and 50 °C. *Waste Management*, *117*, 93–103. https://doi.org/10.1016/j.wasman.2020.07.036

Diaz, P., Doostan, A., & Hampton, J. (2018). Sparse polynomial chaos expansions via compressed sensing and D-optimal design. *Computer Methods in Applied Mechanics and Engineering*, *336*, 640–666. https://doi.org/10.1016/j.cma.2018.03.020

Diersch, H.-J. G. (2014). *FEFLOW: Finite Element Modeling of Flow, Mass and Heat Transport in Porous and Fractured Media*. Springer Berlin Heidelberg. https://doi.org/10.1007/978-3-642-38739-5

Ding, X.-H., & Feng, S.-J. (2022). Analytical model for degradable contaminant transport through a cutoff wall-aquifer system under time-dependent point source pollution. *Computers and Geotechnics*, *143*, 104627. https://doi.org/10.1016/j.compgeo.2021.104627

Ding, X.-H., Feng, S.-J., & Zheng, Q.-T. (2021). A two-dimensional analytical model for contaminant transport in a finite domain subjected to multiple arbitrary time-

dependent point injection sources. *Journal of Hydrology*, *597*, 126318. https://doi.org/10.1016/j.jhydrol.2021.126318

Divya, A., Shrihari, S., & Ramesh, H. (2020). Predictive simulation of leachate transport in a coastal lateritic aquifer when remediated with reactive barrier of nano iron. *Groundwater for Sustainable Development*, *11*, 100382. https://doi.org/10.1016/j.gsd.2020.100382

Djordjevich, A., Savović, S., & Janićijević, A. (2017). Explicit finite-difference solution of two-dimensional solute transport with periodic flow in homogenous porous media. *Journal of Hydrology and Hydromechanics*, *65*(4), 426–432. https://doi.org/10.1515/johh-2017-0040

Dogan, M., Van Dam, R. L., Liu, G., Meerschaert, M. M., Butler, J. J., Bohling, G. C., Benson, D. A., & Hyndman, D. W. (2014). Predicting flow and transport in highly heterogeneous alluvial aquifers. *Geophysical Research Letters*, *41*(21), 7560–7565. https://doi.org/10.1002/2014GL061800

Domenico, P. A., & Robbins, G. A. (1985). A New Method of Contaminant Plume Analysis. *Groundwater*, *23*(4), 476–485. https://doi.org/10.1111/j.1745-6584.1985.tb01497.x

Douglas, Jr., J., & Russell, T. F. (1982). Numerical Methods for Convection-Dominated Diffusion Problems Based on Combining the Method of Characteristics with Finite Element or Finite Difference Procedures. *SIAM Journal on Numerical Analysis*, *19*(5), 871–885. https://doi.org/10.1137/0719063

Du, Z., Deng, S., Bei, Y., Huang, Q., Wang, B., Huang, J., & Yu, G. (2014). Adsorption behavior and mechanism of perfluorinated compounds on various adsorbents—A review. *Journal of Hazardous Materials*, *274*, 443–454. https://doi.org/10.1016/j.jhazmat.2014.04.038

eCFR. (n.d.). *Title 40—Protection of Environment. Part 258—Criteria for municipal solid waste landfills. 258.40—Design criteria*. Electronic Code of Federal Regulations. https://www.ecfr.gov/current/title-40/chapter-I/subchapter-I/part-258/subpart-D/section-258.40

Eggen, T., Moeder, M., & Arukwe, A. (2010). Municipal landfill leachates: A significant source for new and emerging pollutants. *Science of The Total Environment*, *408*(21), 5147–5157. https://doi.org/10.1016/j.scitotenv.2010.07.049

EGLE. (2020). *PFAS Maximum Contaminant Levels (MCLs)*. https://www.michigan.gov/pfasresponse/drinking-water/mcl

El-Zein, A. (2005). Exponential finite elements for diffusion–advection problems. *International Journal for Numerical Methods in Engineering*, *62*(15), 2086–2103. https://doi.org/10.1002/nme.1249

El-Zein, A. & Balaam, N. (2012). Saturated- unsaturated flow and solute transport in engineered liner systems: A new special-purpose finite element analysis software. *Australian Geomechanics Journal*, *47*, 11–26.

Elzein, A. H., & Booker, J. R. (1999). Groundwater pollution by organic compounds: A two-dimensional analysis of contaminant transport in stratified porous media with multiple sources of non-equilibrium partitioning. *International Journal for Numerical and Analytical Methods in Geomechanics*, *23*(14), 1717–1732.

https://doi.org/10.1002/(SICI)1096-9853(19991210)23:14<1717::AID-NAG991>3.0.CO;2-E

El-Zein, A. H., Carter, J. P., & Airey, D. W. (2005). Multiple-Porosity Contaminant Transport by Finite-Element Method. *International Journal of Geomechanics*, *5*(1), 24–34. https://doi.org/10.1061/(ASCE)1532-3641(2005)5:1(24)

El-Zein, A., McCarroll, I., & Masoudian, M. (2016). Inorganic transport through composite geosynthetics and compacted clay liners under geomembranes with multiple defects. *Australian Geomechanics Journal*, *51*(1), 23–39.

El-Zein, A., McCarroll, I., & Touze-Foltz, N. (2012). Three-dimensional finite-element analyses of seepage and contaminant transport through composite geosynthetics clay liners with multiple defects. *Geotextiles and Geomembranes*, *33*, 34–42. https://doi.org/10.1016/j.geotexmem.2012.02.004

El-Zein, A., & Rowe, R. K. (2008). Impact on groundwater of concurrent leakage and diffusion of dichloromethane through geomembranes in landfill liners. *Geosynthetics International*, *15*(1), 55–71. https://doi.org/10.1680/gein.2008.15.1.55

Eriksen, K. T., Raaschou-Nielsen, O., McLaughlin, J. K., Lipworth, L., Tjønneland, A., Overvad, K., & Sørensen, M. (2013). Association between Plasma PFOA and PFOS Levels and Total Cholesterol in a Middle-Aged Danish Population. *PLoS ONE*, *8*(2), e56969. https://doi.org/10.1371/journal.pone.0056969

EurEau. (2018). *Drinking Water Directive Plenary Vote*. https://www.eureau.org/resources/briefing-notes/3011-drinking-water-directive-plenary-vote-eureau-explanatory-memorandum/file

European Parliament & Council of the European Union. (2020). *Directive (EU) 2020/2184 of 16 December 2020 on the quality of water intended for human consumption (recast)*. Official Journal of the European Union, L 435, 1-62. https://eur-lex.europa.eu/eli/dir/2020/2184/oj

Fahs, M., Younes, A., & Ackerer, P. (2011). An Efficient Implementation of the Method of Lines for Multicomponent Reactive Transport Equations. *Water, Air, & Soil Pollution*, *215*(1–4), 273–283. https://doi.org/10.1007/s11270-010-0477-y

Fajraoui, N., Ramasomanana, F., Younes, A., Mara, T. A., Ackerer, P., & Guadagnini, A. (2011). Use of global sensitivity analysis and polynomial chaos expansion for interpretation of nonreactive transport experiments in laboratory-scale porous media. *Water Resources Research*, *47*(2), 2010WR009639. https://doi.org/10.1029/2010WR009639

Faroughi, S. A., Soltanmohammadi, R., Datta, P., Mahjour, S. K., & Faroughi, S. (2023). Physics-Informed Neural Networks with Periodic Activation Functions for Solute Transport in Heterogeneous Porous Media. *Mathematics*, *12*(1), 63. https://doi.org/10.3390/math12010063

Feng, S.-J., Peng, M.-Q., Chen, H.-X., & Chen, Z.-L. (2019). Fully transient analytical solution for degradable organic contaminant transport through GMB/GCL/AL composite liners. *Geotextiles and Geomembranes*, *47*(3), 282–294. https://doi.org/10.1016/j.geotexmem.2019.01.017

Ferraresi, M., & Marinelli, A. (1996). An extended formulation of the integrated finite difference method for groundwater flow and transport. *Journal of Hydrology*, *175*(1–4), 453–471. https://doi.org/10.1016/S0022-1694(96)80020-5

Ferrey, M. L., Wilson, J. T., Adair, C., Su, C., Fine, D. D., Liu, X., & Washington, J. W. (2012). Behavior and Fate of PFOA and PFOS in Sandy Aquifer Sediment. *Groundwater Monitoring & Remediation*, *32*(4), 63–71. https://doi.org/10.1111/j.1745-6592.2012.01395.x

Focaccia, S., Panini, G., Pedrazzoli, P., & Ciriello, V. (2021). A meta-modeling approach for hydrological forecasting under uncertainty: Application to groundwater nitrate response to climate change. *Journal of Hydrology*, *603*, 127173. https://doi.org/10.1016/j.jhydrol.2021.127173

Fox, P. J., & Berles, J. D. (1997). CS2: A PIECEWISE-LINEAR MODEL FOR LARGE STRAIN CONSOLIDATION. *International Journal for Numerical and Analytical Methods in Geomechanics*, *21*(7), 453–475. https://doi.org/10.1002/(SICI)1096-9853(199707)21:7<453::AID-NAG887>3.0.CO;2-B

Fox, P. J., & Pu, H. (2012). Enhanced CS2 Model for Large Strain Consolidation. *International Journal of Geomechanics*, *12*(5), 574–583. https://doi.org/10.1061/(ASCE)GM.1943-5622.0000171

Fuertes, I., Gómez-Lavín, S., Elizalde, M. P., & Urtiaga, A. (2017). Perfluorinated alkyl substances (PFASs) in northern Spain municipal solid waste landfill leachates. *Chemosphere*, *168*, 399–407. https://doi.org/10.1016/j.chemosphere.2016.10.072

Gallen, C., Drage, D., Eaglesham, G., Grant, S., Bowman, M., & Mueller, J. F. (2017). Australia-wide assessment of perfluoroalkyl substances (PFASs) in landfill leachates. *Journal of Hazardous Materials*, *331*, 132–141. https://doi.org/10.1016/j.jhazmat.2017.02.006

Gallen, C., Drage, D., Kaserzon, S., Baduel, C., Gallen, M., Banks, A., Broomhall, S., & Mueller, J. F. (2016). Occurrence and distribution of brominated flame retardants and perfluoroalkyl substances in Australian landfill leachate and biosolids. *Journal of Hazardous Materials*, *312*, 55–64. https://doi.org/10.1016/j.jhazmat.2016.03.031

Gambolati, G., Paniconi, C., & Putti, M. (1993). Numerical Modeling of Contaminant Transport in Groundwater. In D. Petruzzelli & F. G. Helfferich (Eds.), *Migration and Fate of Pollutants in Soils and Subsoils* (pp. 381–410). Springer Berlin Heidelberg. https://doi.org/10.1007/978-3-642-77862-9_16

Gates, W. P., & Bouazza, A. (2010). Bentonite transformations in strongly alkaline solutions. *Geotextiles and Geomembranes*, *28*(2), 219–225. https://doi.org/10.1016/j.geotexmem.2009.10.010

Gates, W. P., Bouazza, A., & Churchman, G. J. (2009). Bentonite Clay Keeps Pollutants at Bay. *Elements*, *5*(2), 105–110. https://doi.org/10.2113/gselements.5.2.105

Gautschi, W. (2004). *Orthogonal Polynomials: Computation and Approximation*. Oxford University Press. https://doi.org/10.1093/oso/9780198506720.001.0001

Geetha Manjari, K., & Sivakumar Babu, G. L. (2018). Probabilistic analysis of groundwater and radionuclide transport model from near surface disposal facilities. *Georisk: Assessment and Management of Risk for Engineered Systems and Geohazards*, *12*(1), 60–73. https://doi.org/10.1080/17499518.2017.1329538

Gelhar, L. W., Welty, C., & Rehfeldt, K. R. (1992). A critical review of data on field-scale dispersion in aquifers. *Water Resources Research*, *28*(7), 1955–1974. https://doi.org/10.1029/92WR00607

Geo-Slope International. (2018a). *GeoStudio SEEP/W*. https://www.geoslope.com/products/seep-w

Geo-Slope International. (2018b). *GeoStudio CTRAN/W*. https://www.geoslope.com/products/ctran-w

Geosynthetic Institute. (2021). *Standard specification for test methods, test properties, and testing frequency for high-density polyethylene (HDPE) smooth and textured geomembranes (GRI-GM13)*. https://geosynthetic-institute.org/grispecs/gm13.pdf

Gewurtz, S. B., Backus, S. M., De Silva, A. O., Ahrens, L., Armellin, A., Evans, M., Fraser, S., Gledhill, M., Guerra, P., Harner, T., Helm, P. A., Hung, H., Khera, N., Kim, M. G., King, M., Lee, S. C., Letcher, R. J., Martin, P., Marvin, C., … Waltho, J. (2013). Perfluoroalkyl acids in the Canadian environment: Multi-media assessment of current status and trends. *Environment International*, *59*, 183–200. https://doi.org/10.1016/j.envint.2013.05.008

Gharehbaghi, A. (2021). A Numerical Model with Finite Difference Schemes for Multi-Species Solute Transport in Porous Media. *Journal of Engineering Research*. https://doi.org/10.36909/jer.13705

Giesy, J. P., & Kannan, K. (2001). Global Distribution of Perfluorooctane Sulfonate in Wildlife. *Environmental Science & Technology*, *35*(7), 1339–1342. https://doi.org/10.1021/es001834k

Gilson-Beck, A. (2019). Controlling leakage through installed geomembranes using electrical leak location. *Geotextiles and Geomembranes*, *47*(5), 697–710. https://doi.org/10.1016/j.geotexmem.2019.103501

Giroud, J. P. (1997). Equations for Calculating the Rate of Liquid Migration Through Composite Liners Due to Geomembrane Defects. *Geosynthetics International*, *4*(3–4), 335–348. https://doi.org/10.1680/gein.4.0097

Giroud, J. P. (2016). Leakage Control using Geomembrane Liners. *Soils and Rocks*, *39*(3), 213–235. https://doi.org/10.28927/SR.393213

Giroud, J. P., Badu-Tweneboah, K., & Bonaparte, R. (1992). Rate of leakage through a composite liner due to geomembrane defects. *Geotextiles and Geomembranes*, *11*(1), 1–28. https://doi.org/10.1016/0266-1144(92)90010-8

Giroud, J. P., & Bonaparte, R. (1989). Leakage through liners constructed with geomembranes—Part II. Composite liners. *Geotextiles and Geomembranes*, *8*(2), 71–111. https://doi.org/10.1016/0266-1144(89)90022-8

Giroud, J. P., Khatami, A., & Badu-Tweneboah, K. (1989). Evaluation of the rate of leakage through composite liners. *Geotextiles and Geomembranes*, *8*(4), 337–340. https://doi.org/10.1016/0266-1144(89)90016-2

Giroud, J. P., & Touze-Foltz, N. (2005). Equations for calculating the rate of liquid flow through geomembrane defects of uniform width and finite or infinite length. *Geosynthetics International*, *12*(4), 191–204. https://doi.org/10.1680/gein.2005.12.4.191

Grant, R. W. (2002). Political Theory, Political Science, and Politics. *Political Theory*, *30*(4), 577–595. https://doi.org/10.1177/0090591702030004007

Gratiet, L. L., Marelli, S., & Sudret, B. (2016). *Metamodel-based sensitivity analysis: Polynomial chaos expansions and Gaussian processes*. https://doi.org/10.48550/ARXIV.1606.04273

Guarena, N., Dominijanni, A., & Manassero, M. (2020). From the design of bottom landfill liner systems to the impact assessment of contaminants on underlying aquifers. *Innovative Infrastructure Solutions*, *5*(1), 2. https://doi.org/10.1007/s41062-019-0251-y

Guo, Z., Fogg, G. E., Brusseau, M. L., LaBolle, E. M., & Lopez, J. (2019). Modeling groundwater contaminant transport in the presence of large heterogeneity: A case study comparing MT3D and RWhet. *Hydrogeology Journal*, *27*(4), 1363–1371. https://doi.org/10.1007/s10040-019-01938-9

Hamdi, N., & Srasra, E. (2013). Hydraulic conductivity study of compacted clay soils used as landfill liners for an acidic waste. *Waste Management*, *33*(1), 60–66. https://doi.org/10.1016/j.wasman.2012.08.012

Hamid, H., Li, L. Y., & Grace, J. R. (2018). Review of the fate and transformation of per- and polyfluoroalkyl substances (PFASs) in landfills. *Environmental Pollution*, *235*, 74–84. https://doi.org/10.1016/j.envpol.2017.12.030

Hanna, M., & El-Zein, A. (2023). Estimation of Soil Water Retention Curves by Inversion of the Richards Equation: A Comparison of Nature-Inspired and Gradient Algorithms. In M. Barla, A. Di Donna, D. Sterpi, & A. Insana (Eds.), *Challenges and Innovations in Geomechanics* (Vol. 288, pp. 247–254). Springer International Publishing. https://doi.org/10.1007/978-3-031-12851-6_30

Hansen, K. J., Clemen, L. A., Ellefson, M. E., & Johnson, H. O. (2001). Compound-Specific, Quantitative Characterization of Organic Fluorochemicals in Biological Matrices. *Environmental Science & Technology*, *35*(4), 766–770. https://doi.org/10.1021/es001489z

Harrad, S., Drage, D. S., Sharkey, M., & Berresheim, H. (2019). Brominated flame retardants and perfluoroalkyl substances in landfill leachate from Ireland. *Science of The Total Environment*, *695*, 133810. https://doi.org/10.1016/j.scitotenv.2019.133810

Harter, T. (2000). Application of stochastic theory in groundwater contamination risk analysis: Suggestions for the consulting geologist and/or engineer. In D. Zhang & C. L. Winter, *Theory, modeling, and field investigation in hydrogeology: A special volume in honor of Shlomo P. Neumans 60th birthday*. Geological Society of America. https://doi.org/10.1130/0-8137-2348-5.43

Hassan, A. E. (2004). Validation of Numerical Ground Water Models Used to Guide Decision Making. *Groundwater*, *42*(2), 277–290. https://doi.org/10.1111/j.1745-6584.2004.tb02674.x

He, Q., & Tartakovsky, A. M. (2021). Physics-Informed Neural Network Method for Forward and Backward Advection-Dispersion Equations. *Water Resources Research*, *57*(7), e2020WR029479. https://doi.org/10.1029/2020WR029479

Health Canada. (2018). *Guidelines for Canadian Drinking Water Quality: Guideline Technical Document – Perfluorooctane Sulfonate (PFOS)*. https://publications.gc.ca/collections/collection_2018/sc-hc/H144-13-9-2018-eng.pdf

Health Canada. (2024). *Objective for Canadian drinking water quality- per- and polyfluoroalkyl substances*. https://www.canada.ca/content/dam/hc-sc/documents/services/publications/healthy-living/objective-drinking-water-quality-per-polyfluoroalkyl-substances/objective-for-canadian-drinking-water-quality-en-final.pdf

HEPA. (2023). *PFAS National Environmental Management Plan (NEMP) 3.0*. Heads of EPAs Australia and New Zealand. https://www.dcceew.gov.au/sites/default/files/documents/pfas-nemp-3.pdf

Hepburn, E., Madden, C., Szabo, D., Coggan, T. L., Clarke, B., & Currell, M. (2019). Contamination of groundwater with per- and polyfluoroalkyl substances (PFAS) from legacy landfills in an urban re-development precinct. *Environmental Pollution*, *248*, 101–113. https://doi.org/10.1016/j.envpol.2019.02.018

Higgins, C. P., & Luthy, R. G. (2006). Sorption of Perfluorinated Surfactants on Sediments. *Environmental Science & Technology*, *40*(23), 7251–7256. https://doi.org/10.1021/es061000n

Houde, M., De Silva, A. O., Muir, D. C. G., & Letcher, R. J. (2011). Monitoring of Perfluorinated Compounds in Aquatic Biota: An Updated Review: PFCs in Aquatic Biota. *Environmental Science & Technology*, *45*(19), 7962–7973. https://doi.org/10.1021/es104326w

Hu, W., & Yu, Y. (2024). Modelling of Leachate Leakage and Contaminant Migration Through Municipal Solid Waste Landfill Liner Systems. In S. Wang, R. Huang, R. Azzam, & V. P. Marinos (Eds.), *Engineering Geology for a Habitable Earth: IAEG XIV Congress 2023 Proceedings, Chengdu, China* (pp. 321–329). Springer Nature Singapore. https://doi.org/10.1007/978-981-99-9065-8_23

Hulagabali, A. M., Solanki, C. H., & Dodagoudar, G. R. (2014). Contaminant transport modeling through saturated porous media using finite difference and finite element methods. *IOSR Journal of Mechanical and Civil Engineering (IOSR-JMCE)*, *ICAET-2014*, 29–33.

Huset, C. A., Barlaz, M. A., Barofsky, D. F., & Field, J. A. (2011). Quantitative determination of fluorochemicals in municipal landfill leachates. *Chemosphere*, *82*(10), 1380–1386. https://doi.org/10.1016/j.chemosphere.2010.11.072

Hwang, G. (2021). ANALYTICAL SOLUTION FOR THE TWO-DIMENSIONAL LINEAR ADVECTION-DISPERSION EQUATION IN POROUS MEDIA VIA THE FOKAS METHOD. *Journal of Applied Analysis & Computation*, *11*(5), 2334–2354. https://doi.org/10.11948/20200383

Innocent, C., Kloppmann, W., Millot, R., & Vaute, L. (2021). A multi-isotopic study of the groundwaters from the Lower Triassic Sandstones aquifer of northeastern France: Groundwater origin, mixing and flowing velocity. *Applied Geochemistry*, *131*, 105012. https://doi.org/10.1016/j.apgeochem.2021.105012

Iooss, B., & Lemaître, P. (2015). A Review on Global Sensitivity Analysis Methods. In G. Dellino & C. Meloni (Eds.), *Uncertainty Management in Simulation-Optimization of Complex Systems* (Vol. 59, pp. 101–122). Springer US. https://doi.org/10.1007/978-1-4899-7547-8_5

Islam, M. Z., & Rowe, R. K. (2009). Permeation of BTEX through Unaged and Aged HDPE Geomembranes. *Journal of Geotechnical and Geoenvironmental Engineering*, *135*(8), 1130–1140. https://doi.org/10.1061/(ASCE)GT.1943-5606.0000056

Jaiswal, D. K., Kumar, A., & Yadav, R. R. (2011). Analytical Solution to the One-Dimensional Advection-Diffusion Equation with Temporally Dependent Coefficients. *Journal of Water Resource and Protection*, *03*(01), 76–84. https://doi.org/10.4236/jwarp.2011.31009

Jeon, J., Kannan, K., Lim, B. J., An, K. G., & Kim, S. D. (2011). Effects of salinity and organic matter on the partitioning of perfluoroalkyl acid (PFAs) to clay particles. *Journal of Environmental Monitoring*, *13*(6), 1803. https://doi.org/10.1039/c0em00791a

Jiang, W., Li, J., & Ge, S. (2025). Numerical study for one-dimensional non-isothermal transport of organic contaminant in the three-layer composite liner containing a defective geomembrane. *International Journal of Heat and Mass Transfer*, *237*, 126417. https://doi.org/10.1016/j.ijheatmasstransfer.2024.126417

Jin, R., Chen, W., & Simpson, T. W. (2001). Comparative studies of metamodelling techniques under multiple modelling criteria. *Structural and Multidisciplinary Optimization*, *23*(1), 1–13. https://doi.org/10.1007/s00158-001-0160-4

Jones, M. C. (1993). Simple boundary correction for kernel density estimation. *Statistics and Computing*, *3*(3), 135–146. https://doi.org/10.1007/BF00147776

Jones, R. V., & Dixon, N. (2011). European perspectives on sustainable development using Geosynthetics. *In Proceedings of the 24th Annual GRI Conference: Optimizing Sustainability Using Geosynthetics, Dallas, Texas, USA*, 1–7.

Kameoka, H., Ito, K., Ono, J., Banno, A., Matsumura, C., Haga, Y., Endo, K., Mizutani, S., & Yabuki, Y. (2022). Investigation of perfluoroalkyl carboxylic and sulfonic acids in leachates from industrial and municipal solid waste landfills, and their treated waters and effluents from their closest leachate treatment plants. *Journal of Material Cycles and Waste Management*, *24*(1), 287–296. https://doi.org/10.1007/s10163-021-01319-z

Kamil, H., Soulaïmani, A., & Beljadid, A. (2025). A comparative study of physics-informed neural network strategies for modeling water and nitrogen transport in unsaturated soils. *Journal of Hydrology*, *661*, 133624. https://doi.org/10.1016/j.jhydrol.2025.133624

Kandris, K., & Pantazidou, M. (2012). Landfill Base Liners: Assessment of Material Equivalency and Impact to Groundwater. *Geotechnical and Geological Engineering*, *30*(1), 27–44. https://doi.org/10.1007/s10706-011-9447-4

Kanney, J. F., Miller, C. T., & Kelley, C. T. (2003). Convergence of iterative split-operator approaches for approximating nonlinear reactive transport problems. *Advances in Water Resources*, *26*(3), 247–261. https://doi.org/10.1016/S0309-1708(02)00162-8

Kelkar, S., Ding, M., Chu, S., Robinson, B. A., Arnold, B., Meijer, A., & Eddebbarh, A.-A. (2010). Modeling solute transport through saturated zone ground water at 10km scale: Example from the Yucca Mountain license application. *Journal of Contaminant Hydrology*, *117*(1–4), 7–25. https://doi.org/10.1016/j.jconhyd.2010.05.003

Khan, V., Roy, S., & Rajesh, S. (2022). Numerical investigation on hydraulic and gas flow response of MSW landfill cover system comprising a geosynthetic clay liner under arid climatic conditions. *Geotextiles and Geomembranes*, *50*(6), 1159–1171. https://doi.org/10.1016/j.geotexmem.2022.08.001

Kia, S. (1991). Subsurface multiphase flow of organic contaminants: Model development and validation. *Water Research*, *25*(10), 1225–1236. https://doi.org/10.1016/0043-1354(91)90061-T

Kim, M., Li, L. Y., Grace, J. R., Benskin, J. P., & Ikonomou, M. G. (2015). Compositional Effects on Leaching of Stain-Guarded (Perfluoroalkyl and Polyfluoroalkyl Substance-Treated) Carpet in Landfill Leachate. *Environmental Science & Technology*, *49*(11), 6564–6573. https://doi.org/10.1021/es505333y

Kissa, E. (2001). *Fluorinated surfactants and repellents (2nd ed., rev. And expanded.)*. Marcel Dekker. https://openlibrary.org/books/OL3944888M/Fluorinated_surfactants_and_repellents

Knutsen, H., Mæhlum, T., Haarstad, K., Slinde, G. A., & Arp, H. P. H. (2019). Leachate emissions of short- and long-chain per- and polyfluoralkyl substances (PFASs) from various Norwegian landfills. *Environmental Science: Processes & Impacts*, *21*(11), 1970–1979. https://doi.org/10.1039/C9EM00170K

Kolditz, O. (2002). *Computational Methods in Environmental Fluid Mechanics*. Springer Berlin Heidelberg. https://doi.org/10.1007/978-3-662-04761-3

Koohbor, B., Fahs, M., Ataie-Ashtiani, B., Belfort, B., Simmons, C. T., & Younes, A. (2019). Uncertainty analysis for seawater intrusion in fractured coastal aquifers: Effects of fracture location, aperture, density and hydrodynamic parameters. *Journal of Hydrology*, *571*, 159–177. https://doi.org/10.1016/j.jhydrol.2019.01.052

Kotthoff, M., Müller, J., Jürling, H., Schlummer, M., & Fiedler, D. (2015). Perfluoroalkyl and polyfluoroalkyl substances in consumer products. *Environmental Science and Pollution Research*, *22*(19), 14546–14559. https://doi.org/10.1007/s11356-015-4202-7

Lal, R., & Shukla, M. K. (2004). *Principles of Soil Physics* (0 ed.). CRC Press. https://doi.org/10.4324/9780203021231

Lang, J. R., Allred, B. M., Field, J. A., Levis, J. W., & Barlaz, M. A. (2017). National Estimate of Per- and Polyfluoroalkyl Substance (PFAS) Release to U.S. Municipal Landfill Leachate. *Environmental Science & Technology*, *51*(4), 2197–2205. https://doi.org/10.1021/acs.est.6b05005

Lang, J. R., Allred, B. M., Peaslee, G. F., Field, J. A., & Barlaz, M. A. (2016). Release of Per- and Polyfluoroalkyl Substances (PFASs) from Carpet and Clothing in Model Anaerobic Landfill Reactors. *Environmental Science & Technology*, *50*(10), 5024–5032. https://doi.org/10.1021/acs.est.5b06237

Lee, H. (2013). *Environmental Chemistry of Commercial Fluorinated Surfactants: Transport, Fate, and Source of Perfluoroalkyl Acid Contamination in the Environment* [University of Toronto]. https://utoronto.scholaris.ca/server/api/core/bitstreams/e92ab1da-0079-4fce-a18b-ba93dc83cac2/content

Leij, F. J., Toride, N., & Van Genuchten, M. Th. (1993). Analytical solutions for non-equilibrium solute transport in three-dimensional porous media. *Journal of Hydrology*, *151*(2–4), 193–228. https://doi.org/10.1016/0022-1694(93)90236-3

Li, B. (2011). *Perfluorinated compounds in landfill leachate and their effect on the performance of sodium bentonite landfill liners*. https://doi.org/10.14288/1.0063208

Li, B., Danon-Schaffer, M. N., Li, L. Y., Ikonomou, M. G., & Grace, J. R. (2012). Occurrence of PFCs and PBDEs in Landfill Leachates from Across Canada. *Water, Air, & Soil Pollution*, *223*(6), 3365–3372. https://doi.org/10.1007/s11270-012-1115-7

Li, B., Li, L. Y., & Grace, J. R. (2015). Adsorption and hydraulic conductivity of landfill-leachate perfluorinated compounds in bentonite barrier mixtures. *Journal of Environmental Management*, *156*, 236–243. https://doi.org/10.1016/j.jenvman.2015.04.003

Li, J., Huang, C., Zhang, J., & Zhang, Z. (2022a). Review of the Anti-Pollution Performance of Triple-Layer GM/GCL/AL Composite Liners. *Membranes*, *12*(10), 922. https://doi.org/10.3390/membranes12100922

Li, J., Jiang, W., Ge, S., Feng, C., Huang, X., & Wang, P. (2022b). Coupled model for consolidation and organic contaminant transport in GMB/CCL composite liner under non-isothermal distribution condition. *Computers and Geotechnics*, *150*, 104893. https://doi.org/10.1016/j.compgeo.2022.104893

Li, L., Liu, J., Hu, J., & Wania, F. (2017). Degradation of Fluorotelomer-Based Polymers Contributes to the Global Occurrence of Fluorotelomer Alcohol and Perfluoroalkyl Carboxylates: A Combined Dynamic Substance Flow and Environmental Fate Modeling Analysis. *Environmental Science & Technology*, *51*(8), 4461–4470. https://doi.org/10.1021/acs.est.6b04021

Li, L. Y., & Denham, W. T. (2000). The Hydraulic Conductivity and Adsorptivity of Organoclay in a Sand-Bentonite Barrier to Hydrophobic Organic Chemicals. *Environmental Technology*, *21*(12), 1429–1443. https://doi.org/10.1080/09593332208618176

Lin, G., & Tartakovsky, A. M. (2010). Numerical Studies of Three-dimensional Stochastic Darcy's Equation and Stochastic Advection-Diffusion-Dispersion Equation. *Journal of Scientific Computing*, *43*(1), 92–117. https://doi.org/10.1007/s10915-010-9346-5

Liu, C., & Liu, J. (2016). Aerobic biotransformation of polyfluoroalkyl phosphate esters (PAPs) in soil. *Environmental Pollution*, *212*, 230–237. https://doi.org/10.1016/j.envpol.2016.01.069

Liu, L., Cheng, S. Y., & Guo, H. C. (2004). A Simulation-Assessment Modeling Approach for Analyzing Environmental Risks of Groundwater Contamination at Waste Landfill Sites. *Human and Ecological Risk Assessment: An International Journal*, *10*(2), 373–388. https://doi.org/10.1080/10807030490438436

Liu, T., & Hu, L. (2014). Organic acid transport through a partially saturated liner system beneath a landfill. *Geotextiles and Geomembranes*, *42*(5), 428–436. https://doi.org/10.1016/j.geotexmem.2014.06.007

Liu, W., Wu, J., He, W., & Xu, F. (2019). A review on perfluoroalkyl acids studies: Environmental behaviors, toxic effects, and ecological and health risks. *Ecosystem Health and Sustainability*, *5*(1), 1–19. https://doi.org/10.1080/20964129.2018.1558031

Lüthen, N., Marelli, S., & Sudret, B. (2020). *Automatic selection of basis-adaptive sparse polynomial chaos expansions for engineering applications* (Version 3). arXiv. https://doi.org/10.48550/ARXIV.2009.04800

Lüthen, N., Marelli, S., & Sudret, B. (2021). Sparse Polynomial Chaos Expansions: Literature Survey and Benchmark. *SIAM/ASA Journal on Uncertainty Quantification*, *9*(2), 593–649. https://doi.org/10.1137/20M1315774

Mahdipanah, H., Tashakori, A., Emamgholizadeh, S., & Maroufpoor, E. (2022). An experimental study on the determination of dispersion coefficient in layered soils. *Water Supply*, *22*(3), 2377–2394. https://doi.org/10.2166/ws.2021.359

Mahjouri, N., & Shamsoddinpour, M. (2016). Developing a methodology for early leakage detection in landfills: Application of the fuzzy transformation technique and probabilistic artificial neural networks. *Environmental Earth Sciences*, *75*(12), 1000. https://doi.org/10.1007/s12665-016-5757-4

Marelli, S., Luthen, N., & Sudret, B. (2024a). *UQLab—Polynomial chaos expansions (PCE) user manuals*. Uqlab. https://www.uqlab.com/pce-user-manual

Marelli, S., Lamas, C., Konakli, K., Mylonas, C., Wiederkehr, P., & Sudret, B. (2024b). *UQLab—Sensitivity analysis user manual*. Uqlab. https://www.uqlab.com/sensitivity-user-manual

Marelli, S., & Sudret, B. (2014). UQLab: A Framework for Uncertainty Quantification in Matlab. *Vulnerability, Uncertainty, and Risk*, 2554–2563. https://doi.org/10.1061/9780784413609.257

Markhali, S. P., & Ehteshami, M. (2016). Environmental assessment of leachate transport in saturated homogeneous media using finite element modeling. *Environmental Earth Sciences*, *75*(16), 1193. https://doi.org/10.1007/s12665-016-5994-6

Martz, M., Heil, J., Marschner, B., & Stumpe, B. (2019). Effects of soil organic carbon (SOC) content and accessibility in subsoils on the sorption processes of the model pollutants nonylphenol (4-n-NP) and perfluorooctanoic acid (PFOA). *Science of The Total Environment*, *672*, 162–173. https://doi.org/10.1016/j.scitotenv.2019.03.369

Masi, M., Paz-Garcia, J. M., Gomez-Lahoz, C., Villen-Guzman, M., Ceccarini, A., & Iannelli, R. (2019). Modeling of electrokinetic remediation combining local chemical equilibrium and chemical reaction kinetics. *Journal of Hazardous Materials*, *371*, 728–733. https://doi.org/10.1016/j.jhazmat.2019.03.014

Masum, S. A., Zhang, Z., Tian, G., & Sultana, M. (2023). Three-dimensional fully coupled hydro-mechanical-chemical model for solute transport under mechanical and osmotic loading conditions. *Environmental Science and Pollution Research*, *30*(3), 5983–6000. https://doi.org/10.1007/s11356-022-22600-0

McCaulou, D. R., & Huling, S. G. (1999). Compatibility of Bentonite and DNAPLs. *Groundwater Monitoring & Remediation*, *19*(2), 78–86. https://doi.org/10.1111/j.1745-6592.1999.tb00208.x

McDougall, M. R. R., & Kalinovich, I. (2021). Developing Hazard Rating Calculation Methodologies for Per- and Polyfluoroalkyl Substances. *Environmental Toxicology and Chemistry*, *40*(3), 937–946. https://doi.org/10.1002/etc.4981

McGregor, R. (2018). *In Situ* treatment of PFAS-impacted groundwater using colloidal activated Carbon. *Remediation Journal*, *28*(3), 33–41. https://doi.org/10.1002/rem.21558

McGregor, R., & Zhao, Y. (2021). The in situ treatment of TCE and PFAS in groundwater within a silty sand aquifer. *Remediation Journal*, *31*(2), 7–17. https://doi.org/10.1002/rem.21675

McKay, M. D. (1992). Latin hypercube sampling as a tool in uncertainty analysis of computer models. *Proceedings of the 24th Conference on Winter Simulation - WSC '92*, 557–564. https://doi.org/10.1145/167293.167637

McKay, M. D., Beckman, R. J., & Conover, W. J. (1979). Comparison of Three Methods for Selecting Values of Input Variables in the Analysis of Output from a Computer Code. *Technometrics*, *21*(2), 239–245. https://doi.org/10.1080/00401706.1979.10489755

Mendoza-Sanchez, I., & Cunningham, J. (2012). Efficient Algorithms for Modeling the Transport and Biodegradation of Chlorinated Ethenes in Groundwater. *Transport in Porous Media*, *92*(1), 165–185. https://doi.org/10.1007/s11242-011-9896-5

Miao, Y., Guo, X., Dan Peng, Fan, T., & Yang, C. (2017). Rates and equilibria of perfluorooctanoate (PFOA) sorption on soils from different regions of China. *Ecotoxicology and Environmental Safety*, *139*, 102–108. https://doi.org/10.1016/j.ecoenv.2017.01.022

Mikhael, E., Bouazza, A., Gates, W. P., & Haque, A. (2024). Unlocking the sorption mechanism of perfluoroalkyl acids (PFAAs) on geosynthetics: Case of the geotextile components of geosynthetic clay liners. *Geotextiles and Geomembranes*, *52*(1), 59–71. https://doi.org/10.1016/j.geotexmem.2023.09.002

Milley, S. A., Koch, I., Fortin, P., Archer, J., Reynolds, D., & Weber, K. P. (2018). Estimating the number of airports potentially contaminated with perfluoroalkyl and polyfluoroalkyl substances from aqueous film forming foam: A Canadian

example. *Journal of Environmental Management*, *222*, 122–131. https://doi.org/10.1016/j.jenvman.2018.05.028

Mishra, H., Karmakar, S., Kumar, R., & Singh, J. (2017). A Framework for Assessing Uncertainty Associated with Human Health Risks from MSW Landfill Leachate Contamination. *Risk Analysis*, *37*(7), 1237–1255. https://doi.org/10.1111/risa.12713

MoE. (2011). *Ontario Regulation 232/98: Landfilling Sites, Environmental protection act, R.S.O. 1990, Amendment of October 2011*. Government of Ontario. https://www.ontario.ca/laws/regulation/980232

Mumford, K. G., Mustafa, N., & Gerhard, J. I. (2016). Probabilistic risk assessment of contaminant transport in groundwater and vapour intrusion following remediation of a contaminant source. *Stochastic Environmental Research and Risk Assessment*, *30*(3), 1017–1031. https://doi.org/10.1007/s00477-015-1156-8

Nadukandi, P., Oñate, E., & García, J. (2012). A high-resolution Petrov–Galerkin method for the convection–diffusion–reaction problem. Part II—A multidimensional extension. *Computer Methods in Applied Mechanics and Engineering*, *213–216*, 327–352. https://doi.org/10.1016/j.cma.2011.10.003

Napa-García, G. F, Godoy, V. A., & Zuquette, L. V. (2014). Probabilistic Analysis of Contaminant Transport via Monte Carlo Simulation. *Electronic Journal of Geotechnical Engineering*, *19*, 6847–6856.

Natarajan, N., & Suresh Kumar, G. (2010). Finite difference approach for modeling multispecies transport in porous media. *International Journal of Engineering Science and Technology*, *2*(8), 3344–3350.

Naylor, T. D. (1989). 20 – Permeation Properties. *Comprehensive Polymer Science and Supplements*, *20*, 643–668.

Neuman, S. P. (1984). Adaptive Eulerian–Lagrangian finite element method for advection–dispersion. *International Journal for Numerical Methods in Engineering*, *20*(2), 321–337. https://doi.org/10.1002/nme.1620200211

Nguyen, T. M. H., Bräunig, J., Thompson, K., Thompson, J., Kabiri, S., Navarro, D. A., Kookana, R. S., Grimison, C., Barnes, C. M., Higgins, C. P., McLaughlin, M. J., & Mueller, J. F. (2020). Influences of Chemical Properties, Soil Properties, and Solution pH on Soil–Water Partitioning Coefficients of Per- and Polyfluoroalkyl Substances (PFASs). *Environmental Science & Technology*, *54*(24), 15883–15892. https://doi.org/10.1021/acs.est.0c05705

Nguyen, T.-B., Lim, J., Choi, H., & Stark, T. D. (2011). Numerical modeling of diffusion for volatile organic compounds through composite landfill liner systems. *KSCE Journal of Civil Engineering*, *15*(6), 1033–1039. https://doi.org/10.1007/s12205-011-1293-7

NHMRC. (2022). *Australian Drinking Water Guidelines Version 3.8*.

NHMRC. (2025). *Australian Drinking Water Guidelines Version 4.0*. https://www.nhmrc.gov.au/about-us/news-centre/updated-australian-drinking-water-guidelines

NJDEP. (2019). *Safe Drinking Water Act Rules, N.J.A.C. 7:10*. https://dep.nj.gov/rules/notice-of-rule-proposal-archive/20190401a/

NSW EPA. (2016). *Environmental guidelines: Solid waste landfills (2nd ed.)*. https://www.epa.nsw.gov.au/sites/default/files/solid-waste-landfill-guidelines-160259.pdf

NSW EPA. (2022). *Regulation of PFAS firefighting foams*. https://www.epa.nsw.gov.au/Your-environment/Chemicals/PFAS-in-NSW/Regulation-of-PFAS-firefighting-foams

NYSDOH. (2020). *Public Water Systems and NYS Drinking Water Standards for PFOA, PFOS and 1,4-Dioxane*. Center for Environmental Health. https://www.westchesterwaterworks.org/water_supplier_fact_sheet_new_mcls.pdf

OECD. (2020). *Per and poly-fluorinated chemicals (PFAS)*. OECD. https://www.oecd.org/en/topics/sub-issues/risk-management-risk-reduction-and-sustainable-chemistry/per-and-poly-fluorinated-chemicals.html

Ogata, A., & Banks, R. B. (1961). *A solution of the differential equation of longitudinal dispersion in porous media: Fluid movement in earth materials (Vols. 411-A.)*. U.S. Govt. Print. Off.

Oladyshkin, S., & Nowak, W. (2012). Data-driven uncertainty quantification using the arbitrary polynomial chaos expansion. *Reliability Engineering & System Safety*, *106*, 179–190. https://doi.org/10.1016/j.ress.2012.05.002

Oliver, D. P., Navarro, D. A., Baldock, J., Simpson, S. L., & Kookana, R. S. (2020a). Sorption behaviour of per- and polyfluoroalkyl substances (PFASs) as affected by the properties of coastal estuarine sediments. *Science of The Total Environment*, *720*, 137263. https://doi.org/10.1016/j.scitotenv.2020.137263

Oliver, D. P., Li, Y., Orr, R., Nelson, P., Barnes, M., McLaughlin, M. J., & Kookana, R. S. (2020b). Sorption behaviour of per- and polyfluoroalkyl substances (PFASs) in tropical soils. *Environmental Pollution*, *258*, 113726. https://doi.org/10.1016/j.envpol.2019.113726

Olsen, G. W., Chang, S.-C., Noker, P. E., Gorman, G. S., Ehresman, D. J., Lieder, P. H., & Butenhoff, J. L. (2009). A comparison of the pharmacokinetics of perfluorobutanesulfonate (PFBS) in rats, monkeys, and humans. *Toxicology*, *256*(1–2), 65–74. https://doi.org/10.1016/j.tox.2008.11.008

Oñate, E., Nadukandi, P., & Miquel, J. (2017). Accurate FIC-FEM formulation for the multidimensional steady-state advection–diffusion–absorption equation. *Computer Methods in Applied Mechanics and Engineering*, *327*, 352–368. https://doi.org/10.1016/j.cma.2017.08.012

Oreskes, N., Shrader-Frechette, K., & Belitz, K. (1994). Verification, Validation, and Confirmation of Numerical Models in the Earth Sciences. *Science*, *263*(5147), 641–646. https://doi.org/10.1126/science.263.5147.641

Orion. (2020). https://www.orion-fire.com/technical/foam-concentrate-storage/

Pati, Y. C., Rezaiifar, R., & Krishnaprasad, P. S. (1993). Orthogonal matching pursuit: Recursive function approximation with applications to wavelet decomposition.

Proceedings of 27th Asilomar Conference on Signals, Systems and Computers, 40–44. https://doi.org/10.1109/ACSSC.1993.342465

Patrick Wang, P., & Zheng, C. (2005). Contaminant transport models under random sources. *Groundwater*, *43*(3), 423–433. https://doi.org/10.1111/j.1745-6584.2005.0034.x

Paul, A. G., Jones, K. C., & Sweetman, A. J. (2009). A First Global Production, Emission, And Environmental Inventory For Perfluorooctane Sulfonate. *Environmental Science & Technology*, *43*(2), 386–392. https://doi.org/10.1021/es802216n

Peng, M.-Q., Feng, S.-J., Chen, H.-X., & Chen, Z.-L. (2023). The role of thermodiffusion in organic pollutant transport in landfill composite liner system. *Computers and Geotechnics*, *153*, 105108. https://doi.org/10.1016/j.compgeo.2022.105108

Peng, M.-Q., Feng, S.-J., Chen, H.-X., Chen, Z.-L., & Xie, H.-J. (2021). Analytical model for organic contaminant transport through GMB/CCL composite liner with finite thickness considering adsorption, diffusion and thermodiffusion. *Waste Management*, *120*, 448–458. https://doi.org/10.1016/j.wasman.2020.10.004

Pérez Guerrero, J. S., Skaggs, T. H., & Van Genuchten, M. Th. (2009). Analytical Solution for Multi-Species Contaminant Transport Subject to Sequential First-Order Decay Reactions in Finite Media. *Transport in Porous Media*, *80*(2), 373–387. https://doi.org/10.1007/s11242-009-9368-3

Perkola, N., & Sainio, P. (2013). Survey of perfluorinated alkyl acids in Finnish effluents, storm water, landfill leachate and sludge. *Environmental Science and Pollution Research*, *20*(11), 7979–7987. https://doi.org/10.1007/s11356-013-1518-z

Piggott, J. H., & Cawlfield, J. D. (1996). Probabilistic sensitivity analysis for one-dimensional contaminant transport in the vadose zone. *Journal of Contaminant Hydrology*, *24*(2), 97–115. https://doi.org/10.1016/S0169-7722(96)00003-4

Plimmer, B. R., Pringle, A. B., & Moncaster, S. J. (1999). A probabilistic risk assessment methodology for landfills, with particular reference to the representation of chemical containment. *Geological Society, London, Special Publications*, *157*(1), 275–280. https://doi.org/10.1144/GSL.SP.1999.157.01.19

Praveen Kumar, R., & Dodagoudar, G. R. (2010). Two-dimensional meshfree modelling of contaminant transport through saturated porous media using RPIM. *Environmental Earth Sciences*, *61*(2), 341–353. https://doi.org/10.1007/s12665-009-0346-4

Pu, H., & Fox, P. J. (2016). Model for Coupled Large Strain Consolidation and Solute Transport in Layered Soils. *International Journal of Geomechanics*, *16*(2), 04015064. https://doi.org/10.1061/(ASCE)GM.1943-5622.0000539

Pu, H., Qiu, J., Zhang, R., & Zheng, J. (2018). Assessment of consolidation-induced VOC transport for a GML/GCL/CCL composite liner system. *Geotextiles and Geomembranes*, *46*(4), 455–469. https://doi.org/10.1016/j.geotexmem.2018.04.002

Pu, H., Qiu, J., Zhang, R., & Zheng, J. (2020a). Analytical solutions for organic contaminant diffusion in triple-layer composite liner system considering the effect of degradation. *Acta Geotechnica*, *15*(4), 907–921. https://doi.org/10.1007/s11440-019-00783-0

Pu, H., Wang, K., Qiu, J., & Chen, X. (2020b). Large-strain numerical solution for coupled self-weight consolidation and contaminant transport considering nonlinear compressibility and permeability. *Applied Mathematical Modelling*, *88*, 916–932. https://doi.org/10.1016/j.apm.2020.07.010

Qiu, J., He, Y., Song, D., & Tong, J. (2023a). Analytical solution for solute transport in a triple liner under non-isothermal conditions. *Geosynthetics International*, *30*(4), 364–381. https://doi.org/10.1680/jgein.21.00122

Qiu, J.-W., Jiang, L.-S., Pu, H.-F., Song, D.-B., Min, M., & Tong, J. (2023b). Analytical solutions for contaminant transport through a GMB/CCL composite liner system considering effective porosity and thermodiffusion. *Computers and Geotechnics*, *163*, 105713. https://doi.org/10.1016/j.compgeo.2023.105713

Qiu, P., Xu, Y., Yao, G., Liu, Y., Dong, L., & Huang, Q. (2024). Deterioration modes, mechanisms, and effects of flexible landfill facilities disposing hazardous waste. *Journal of Cleaner Production*, *451*, 142030. https://doi.org/10.1016/j.jclepro.2024.142030

Queensland Government. (2021). *Firefighting foam management policy (Version 2)*. Department of Environment and Science. https://www.qld.gov.au/environment/management/environmental/pfas/firefighting-foam

Rajabi, M. M., & Ataie-Ashtiani, B. (2014). Sampling efficiency in Monte Carlo based uncertainty propagation strategies: Application in seawater intrusion simulations. *Advances in Water Resources*, *67*, 46–64. https://doi.org/10.1016/j.advwatres.2014.02.004

Rajabi, M. M., Ataie-Ashtiani, B., & Janssen, H. (2015a). Efficiency enhancement of optimized Latin hypercube sampling strategies: Application to Monte Carlo uncertainty analysis and meta-modeling. *Advances in Water Resources*, *76*, 127–139. https://doi.org/10.1016/j.advwatres.2014.12.008

Rajabi, M. M., Ataie-Ashtiani, B., & Simmons, C. T. (2015b). Polynomial chaos expansions for uncertainty propagation and moment independent sensitivity analysis of seawater intrusion simulations. *Journal of Hydrology*, *520*, 101–122. https://doi.org/10.1016/j.jhydrol.2014.11.020

Rasmusson, K., & Fagerlund, F. (2024). Per- and polyfluoroalkyl substances (PFAS) as contaminants in groundwater resources – A comprehensive review of subsurface transport processes. *Chemosphere*, *362*, 142663. https://doi.org/10.1016/j.chemosphere.2024.142663

Ravindiran, G., Rajamanickam, S., Sivarethinamohan, S., Karupaiya Sathaiah, B., Ravindran, G., Muniasamy, S. K., & Hayder, G. (2023). A Review of the Status, Effects, Prevention, and Remediation of Groundwater Contamination for Sustainable Environment. *Water*, *15*(20), 3662. https://doi.org/10.3390/w15203662

Razavi, S., Tolson, B. A., & Burn, D. H. (2012). Review of surrogate modeling in water resources. *Water Resources Research*, *48*(7), 2011WR011527. https://doi.org/10.1029/2011WR011527

Reddy, K. R., Kumar, G., & Giri, R. K. (2017). Influence of dynamic coupled hydro-bio-mechanical processes on response of municipal solid waste and liner system in bioreactor landfills. *Waste Management*, *63*, 143–160. https://doi.org/10.1016/j.wasman.2016.12.040

Renner, R. (2001). Growing Concern Over Perfluorinated Chemicals. *Environmental Science & Technology*, *35*(7), 154A-160A. https://doi.org/10.1021/es012317k

Renou, S., Givaudan, J. G., Poulain, S., Dirassouyan, F., & Moulin, P. (2008). Landfill leachate treatment: Review and opportunity. *Journal of Hazardous Materials*, *150*(3), 468–493. https://doi.org/10.1016/j.jhazmat.2007.09.077

Rhoads, K. R., Janssen, E. M.-L., Luthy, R. G., & Criddle, C. S. (2008). Aerobic Biotransformation and Fate of *N* -Ethyl Perfluorooctane Sulfonamidoethanol (*N* -EtFOSE) in Activated Sludge. *Environmental Science & Technology*, *42*(8), 2873–2878. https://doi.org/10.1021/es702866c

Richards, S., & Bouazza, A. (2007). Phenol adsorption in organo-modified basaltic clay and bentonite. *Applied Clay Science*, *37*(1–2), 133–142. https://doi.org/10.1016/j.clay.2006.11.006

Roco, M. C., Khadilkar, J., & Zhang, J. (1989). Probabilistic approach for transport of contaminants through porous media. *International Journal for Numerical Methods in Fluids*, *9*(12), 1431–1451. https://doi.org/10.1002/fld.1650091202

Ronen, D., Magaritz, M., Paldor, N., & Bachmat, Y. (1986). The Behavior of Groundwater in the Vicinity of the Water Table Evidenced by Specific Discharge Profiles. *Water Resources Research*, *22*(8), 1217–1224. https://doi.org/10.1029/WR022i008p01217

Rowe, R. K. (1998). Geosynthetics and the minimization of contaminant migration through barrier systems beneath solid waste. *In Proceedings of the 6th International Conference on Geosynthetics, Atlanta, Ga. 25–29 March 1998. Edited by R.K. Rowe. Industrial Fabrics Association International*, 27–103.

Rowe, R. K. (2005). Long-term performance of contaminant barrier systems. *Géotechnique*, *55*(9), 631–678. https://doi.org/10.1680/geot.2005.55.9.631

Rowe, R. K. (2012). Short- and long-term leakage through composite liners. The 7th Arthur Casagrande Lecture[1] This lecture was presented at the 14th Pan-American Conference on Soil Mechanics and Geotechnical Engineering, Toronto, Ont., October 2011, and a pre-print appeared in the conference proceedings. *Canadian Geotechnical Journal*, *49*(2), 141–169. https://doi.org/10.1139/t11-092

Rowe, R. K. (2018). Environmental geotechnics: Looking back, looking forward. *Italian Geotechnical Journal*, *1156*(4), 8–040. https://doi.org/10.19199/2018.4.0557-1405.008

Rowe, R. K. (2020a). Geosynthetic clay liners: Perceptions and misconceptions. *Geotextiles and Geomembranes*, *48*(2), 137–156. https://doi.org/10.1016/j.geotexmem.2019.11.012

Rowe, R. K. (2020b). Protecting the Environment with Geosynthetics: 53rd Karl Terzaghi Lecture. *Journal of Geotechnical and Geoenvironmental Engineering*, *146*(9), 04020081. https://doi.org/10.1061/(ASCE)GT.1943-5606.0002239

Rowe, R. K., Abdelaal, F. B., & Islam, M. Z. (2014). Aging of High-Density Polyethylene Geomembranes of Three Different Thicknesses. *Journal of Geotechnical and Geoenvironmental Engineering*, *140*(5), 04014005. https://doi.org/10.1061/(ASCE)GT.1943-5606.0001090

Rowe, R. K., & AbdelRazek, A. Y. (2019). Effect of interface transmissivity and hydraulic conductivity on contaminant migration through composite liners with wrinkles or failed seams. *Canadian Geotechnical Journal*, *56*(11), 1650–1667. https://doi.org/10.1139/cgj-2018-0660

Rowe, R. K., & Barakat, F. B. (2021). Modelling the transport of PFOS from single lined municipal solid waste landfill. *Computers and Geotechnics*, *137*, 104280. https://doi.org/10.1016/j.compgeo.2021.104280

Rowe, R. K., Barakat, F. B., Patch, D., & Weber, K. (2023). Diffusion and partitioning of different PFAS compounds through thermoplastic polyurethane and three different PVC-EIA liners. *Science of The Total Environment*, *892*, 164229. https://doi.org/10.1016/j.scitotenv.2023.164229

Rowe, R. K., & Booker, J. R. (1984). The analysis of pollutant migration in a non-homogeneous soil. *Géotechnique*, *34*(4), 601–612. https://doi.org/10.1680/geot.1984.34.4.601

Rowe, R. K., & Booker, J. R. (1985). 1-D Pollutant Migration in Soils of Finite Depth. *Journal of Geotechnical Engineering*, *111*(4), 479–499. https://doi.org/10.1061/(ASCE)0733-9410(1985)111:4(479)

Rowe, R. K., & Islam, M. Z. (2009). Impact of landfill liner time–temperature history on the service life of HDPE geomembranes. *Waste Management*, *29*(10), 2689–2699. https://doi.org/10.1016/j.wasman.2009.05.010

Rowe, R. K., & Jabin, F. (2021). Effect of prehydration, permeant, and desiccation on GCL/Geomembrane interface transmissivity. *Geotextiles and Geomembranes*, *49*(6), 1451–1469. https://doi.org/10.1016/j.geotexmem.2021.04.006

Rowe, R. K., & Jabin, F. (2022). Factors affecting multicomponent GCL-geomembrane interface transmissivity for landfills. *Geosynthetics International*, *29*(5), 476–494. https://doi.org/10.1680/jgein.21.00042

Rowe, R. K., Martinez Noboa, N., & Brachman, R. W. I. (2024). Effect of closed and open system freeze–thaw cycles on GMB–GCL interface transmissivity. *Geosynthetics International*, *31*(1), 42–53. https://doi.org/10.1680/jgein.22.00297

Rowe, R. K., Quigley, R. M., Brachman, R., & Booker, J. R. (2004). *Barrier Systems for Waste Disposal Facilities* (0 ed.). CRC Press. https://doi.org/10.1201/9781482271935

Rowe, R.K., & Booker, J.R. (2004). *POLLUTE Version 7 –1½ D Pollutant Migration through a Non-homogenous Soil*. GAEA Technologies Ltd. https://gaea.ca/products.php

Rowe, R.K., & Zhao, L. (2023). Implications of double composite liner behaviour for PFAS containment. *ISSMGE*. https://doi.org/10.53243/ICEG2023-64

Rupali, S., & Sawant, V. A. (2016). Contaminant Transport Through Geomembranes Overlying Clay and Sand Using Element Free Galerkin Method. *International Journal of Geosynthetics and Ground Engineering*, *2*(2), 14. https://doi.org/10.1007/s40891-016-0054-6

Sangam, H. P., & Rowe, R. K. (2005). Effect of Surface Fluorination on Diffusion through a High Density Polyethylene Geomembrane. *Journal of Geotechnical and Geoenvironmental Engineering*, *131*(6), 694–704. https://doi.org/10.1061/(ASCE)1090-0241(2005)131:6(694)

Santhosh, L. G., Lakshmikanthan, P., & Babu, G. L. S. (2017). Reliability Based Approach for the Prediction of Leachate Head in MSW Landfills. *International Journal of Geosynthetics and Ground Engineering*, *3*(1), 4. https://doi.org/10.1007/s40891-016-0080-4

Sargsyan, K., Safta, C., Najm, H. N., Debusschere, B. J., Ricciuto, D., & Thornton, P. (2014). DIMENSIONALITY REDUCTION FOR COMPLEX MODELS VIA BAYESIAN COMPRESSIVE SENSING. *International Journal for Uncertainty Quantification*, *4*(1), 63–93. https://doi.org/10.1615/Int.J.UncertaintyQuantification.2013006821

Schaefer, C. E., Drennan, D. M., Tran, D. N., Garcia, R., Christie, E., Higgins, C. P., & Field, J. A. (2019). Measurement of Aqueous Diffusivities for Perfluoroalkyl Acids. *Journal of Environmental Engineering*, *145*(11), 06019006. https://doi.org/10.1061/(ASCE)EE.1943-7870.0001585

Schaefer, C. E., Drennan, D., Nickerson, A., Maizel, A., & Higgins, C. P. (2021). Diffusion of perfluoroalkyl acids through clay-rich soil. *Journal of Contaminant Hydrology*, *241*, 103814. https://doi.org/10.1016/j.jconhyd.2021.103814

Schrefler, B. A., & Delage, P. (2010). *Environmental geomechanics*. ISTE.

Schrefler, B., & Delage, P. (Eds.). (2013). *Environmental Geomechanics* (1st ed.). Wiley. https://doi.org/10.1002/9781118619834

Schulze-Makuch, D. (2005). Longitudinal dispersivity data and implications for scaling behavior. *Groundwater*, *43*(3), 443–456. https://doi.org/10.1111/j.1745-6584.2005.0051.x

Selvadurai, A. P. S. (2008). On nonclassical analytical solutions for advective transport problems. *Water Resources Research*, *44*(5), 2007WR006312. https://doi.org/10.1029/2007WR006312

Shi, Y., Xie, H., Ding, H., & Wang, L. (2025). Contaminant transport through the heterogeneous GCL/SL composite liner: Experimental and analytical studies. *Journal of Hydrology*, *651*, 132607. https://doi.org/10.1016/j.jhydrol.2024.132607

Simmons, N. (2019). *PFAS concentrations of landfill leachates in Victoria, Australia-implications for discharge of leachate to sewer*. Proceedings 17th International Waste Management and Landfill Symposium, Sardinia, Italy, CISA. https://www.researchgate.net/publication/336603065_PFAS_concentrations_of_landfill_leachates_in_Victoria_Australia_-_implications_for_discharge_of_leachate_to_sewer

Simon, J. A., Abrams, S., Bradburne, T., Bryant, D., Burns, M., Cassidy, D., Cherry, J., Chiang, S. (Dora), Cox, D., Crimi, M., Denly, E., DiGuiseppi, B., Fenstermacher, J., Fiorenza, S., Guarnaccia, J., Hagelin, N., Hall, L., Hesemann, J., Houtz, E., … Wice, R. (2019). PFAS Experts Symposium: Statements on regulatory policy, chemistry and analytics, toxicology, transport/fate, and remediation for per- and polyfluoroalkyl substances (PFAS) contamination issues. *Remediation Journal*, *29*(4), 31–48. https://doi.org/10.1002/rem.21624

Singh, P., Kumari, P., & Jaiswal, D. K. (2024). *Analytical solution of three-dimensional advection-dispersion equation along porous media with Cauchy type boundary condition*. 080002. https://doi.org/10.1063/5.0199585

Smith, L., & Freeze, R. A. (1979). Stochastic analysis of steady state groundwater flow in a bounded domain: 1. One-dimensional simulations. *Water Resources Research*, *15*(3), 521–528. https://doi.org/10.1029/WR015i003p00521

Sobol', I. M. (1993). Sensitivity estimates for nonlinear mathematical models. *Math. Model. Comput. Exp.*, *1*, 407–414.

Sobol′, I. M. (2001). Global sensitivity indices for nonlinear mathematical models and their Monte Carlo estimates. *Mathematics and Computers in Simulation*, *55*(1–3), 271–280. https://doi.org/10.1016/S0378-4754(00)00270-6

Solo-Gabriele, H. M., Jones, A. S., Lindstrom, A. B., & Lang, J. R. (2020). Waste type, incineration, and aeration are associated with per- and polyfluoroalkyl levels in landfill leachates. *Waste Management*, *107*, 191–200. https://doi.org/10.1016/j.wasman.2020.03.034

Sörengård, M., Östblom, E., Köhler, S., & Ahrens, L. (2020). Adsorption behavior of per- and polyfluoralkyl substances (PFASs) to 44 inorganic and organic sorbents and use of dyes as proxies for PFAS sorption. *Journal of Environmental Chemical Engineering*, *8*(3), 103744. https://doi.org/10.1016/j.jece.2020.103744

Srivastava, S. K., & Ramanathan, A. (2018). Assessment of landfills vulnerability on the groundwater quality located near floodplain of the perennial river and simulation of contaminant transport. *Modeling Earth Systems and Environment*, *4*(2), 729–752. https://doi.org/10.1007/s40808-018-0464-7

Sudret, B. (2008). Global sensitivity analysis using polynomial chaos expansions. *Reliability Engineering & System Safety*, *93*(7), 964–979. https://doi.org/10.1016/j.ress.2007.04.002

Tang, D. H., & Pinder, G. F. (1977). Simulation of groundwater flow and mass transport under uncertainty. *Advances in Water Resources*, *1*(1), 25–30. https://doi.org/10.1016/0309-1708(77)90005-7

Tartakovsky, D. M. (2007). Probabilistic risk analysis in subsurface hydrology. *Geophysical Research Letters*, *34*(5), 2007GL029245. https://doi.org/10.1029/2007GL029245

Touze-Foltz, N., Barroso, M., Cartaud, F. (2006). Experimental investigation of flow rates through composite liners at the metric scale. *In: Kuwano, J., Koseki, J. (Eds.), Proceedings of the 8th International Conference on Geosynthetics (8ICG). IOS Press, Amsterdam, the Netherlands*, 305–308.

Touze-Foltz, N., Lupo, J., & Barroso, M. (2008). Geoenvironmental applications of geosynthetics. Keynote Lecture. *Proceedings Eurogeo 4, 98 the 4th European Conference on Geosynthetics, Edinburgh, Scotland, UK*.

Touze-Foltz, N., Rowe, R. K., & Duquennoi, C. (1999). Liquid Flow Through Composite Liners due to Geomembrane Defects: Analytical Solutions for Axi-Symmetric and Two-Dimensional Problems. *Geosynthetics International*, *6*(6), 455–479. https://doi.org/10.1680/gein.6.0160

Touze-Foltz, N., Xie, H., & Stoltz, G. (2021). Performance issues of barrier systems for landfills: A review. *Geotextiles and Geomembranes*, *49*(2), 475–488. https://doi.org/10.1016/j.geotexmem.2020.10.016

Uma Shankar, M., & Muthukumar, M. (2017). Comprehensive review of geosynthetic clay liner and compacted clay liner. *IOP Conference Series: Materials Science and Engineering*, *263*, 032026. https://doi.org/10.1088/1757-899X/263/3/032026

Umeh, A. C., Naidu, R., Shilpi, S., Boateng, E. B., Rahman, A., Cousins, I. T., Chadalavada, S., Lamb, D., & Bowman, M. (2021). Sorption of PFOS in 114 Well-Characterized Tropical and Temperate Soils: Application of Multivariate and Artificial Neural Network Analyses. *Environmental Science & Technology*, *55*(3), 1779–1789. https://doi.org/10.1021/acs.est.0c07202

UNEP. (2019a). *Stockholm Convention on Persistent Organic Pollutants (POPs)*. Secretariat of the Stockholm Convention, United Nations Environment Programme (UNEP). https://www.pops.int/TheConvention/Overview/TextoftheConvention/tabid/2232/Default.aspx

UNEP. (2019b). *Basel Convention on the Control of Transboundary Movements of Hazardous Wastes and their Disposal*. Secretariat of the Basel Convention, UNEP. https://www.basel.int/TheConvention/Overview/TextoftheConvention/tabid/1275/Default.aspx

USEPA. (2000). *EPA and 3M ANNOUNCE PHASE OUT OF PFOS*. https://www.epa.gov/archive/epapages/newsroom_archive/newsreleases/33aa946e6cb11f35852568e1005246b4.html

USEPA. (2023). *Proposed PFAS National Primary Drinking Water Regulation*. https://www.epa.gov/sdwa/and-polyfluoroalkyl-substances-pfas

Vaalgamaa, S., Vähätalo, A. V., Perkola, N., & Huhtala, S. (2011). Photochemical reactivity of perfluorooctanoic acid (PFOA) in conditions representing surface water. *Science of The Total Environment*, *409*(16), 3043–3048. https://doi.org/10.1016/j.scitotenv.2011.04.036

Van Genuchten, M. Th. (1981). Analytical solutions for chemical transport with simultaneous adsorption, zero-order production and first-order decay. *Journal of Hydrology*, *49*(3–4), 213–233. https://doi.org/10.1016/0022-1694(81)90214-6

Van Glubt, S. (2020). *Processes Contributing to the Retention and Transport of Per and Polyfluoroalkyl Substances (PFAS) in Soils and Groundwater*. ProQuest Dissertations Publishing.

Varank, G., Demir, A., Top, S., Sekman, E., Akkaya, E., Yetilmezsoy, K., & Bilgili, M. S. (2011). Migration behavior of landfill leachate contaminants through alternative composite liners. *Science of The Total Environment*, *409*(17), 3183–3196. https://doi.org/10.1016/j.scitotenv.2011.04.044

Venkatesan, A. K., & Halden, R. U. (2013). National inventory of perfluoroalkyl substances in archived U.S. biosolids from the 2001 EPA National Sewage Sludge Survey. *Journal of Hazardous Materials*, *252–253*, 413–418. https://doi.org/10.1016/j.jhazmat.2013.03.016

Vestergren, R., Herzke, D., Wang, T., & Cousins, I. T. (2015). Are imported consumer products an important diffuse source of PFASs to the Norwegian environment? *Environmental Pollution*, *198*, 223–230. https://doi.org/10.1016/j.envpol.2014.12.034

Vierke, L., Staude, C., Biegel-Engler, A., Drost, W., & Schulte, C. (2012). Perfluorooctanoic acid (PFOA)—Main concerns and regulatory developments in Europe from an environmental point of view. *Environmental Sciences Europe*, *24*(1), 16. https://doi.org/10.1186/2190-4715-24-16

Vishnupriya, A., & Rajagopalan, V. (2022). Comparative Performance of Compacted Clay Liner (CCL) and Geosynthetic Clay Liner (GCL). *J Bioanal Methods Tech*, *2*(1), 103.

Wan, X., & Karniadakis, G. E. (2005). An adaptive multi-element generalized polynomial chaos method for stochastic differential equations. *Journal of Computational Physics*, *209*(2), 617–642. https://doi.org/10.1016/j.jcp.2005.03.023

Wan, X., & Karniadakis, G. E. (2006). Multi-Element Generalized Polynomial Chaos for Arbitrary Probability Measures. *SIAM Journal on Scientific Computing*, *28*(3), 901–928. https://doi.org/10.1137/050627630

Wang, F., & Shih, K. (2011). Adsorption of perfluorooctanesulfonate (PFOS) and perfluorooctanoate (PFOA) on alumina: Influence of solution pH and cations. *Water Research*, *45*(9), 2925–2930. https://doi.org/10.1016/j.watres.2011.03.007

Wang, Z., Buser, A. M., Cousins, I. T., Demattio, S., Drost, W., Johansson, O., Ohno, K., Patlewicz, G., Richard, A. M., Walker, G. W., White, G. S., & Leinala, E. (2021). A New OECD Definition for Per- and Polyfluoroalkyl Substances. *Environmental Science & Technology*, *55*(23), 15575–15578. https://doi.org/10.1021/acs.est.1c06896

Wang, Z., Cousins, I. T., Scheringer, M., Buck, R. C., & Hungerbühler, K. (2014). Global emission inventories for C4–C14 perfluoroalkyl carboxylic acid (PFCA) homologues from 1951 to 2030, Part I: Production and emissions from quantifiable sources. *Environment International*, *70*, 62–75. https://doi.org/10.1016/j.envint.2014.04.013

Warren, J. E., & Price, H. S. (1961). Flow in Heterogeneous Porous Media. *Society of Petroleum Engineers Journal*, *1*(03), 153–169. https://doi.org/10.2118/1579-G

Wee, S. Y., & Aris, A. Z. (2023). Environmental impacts, exposure pathways, and health effects of PFOA and PFOS. *Ecotoxicology and Environmental Safety*, *267*, 115663. https://doi.org/10.1016/j.ecoenv.2023.115663

Wiener, N. (1938). The Homogeneous Chaos. *American Journal of Mathematics*, *60*(4), 897. https://doi.org/10.2307/2371268

Winter, C. L., & Tartakovsky, D. M. (2008). A reduced complexity model for probabilistic risk assessment of groundwater contamination. *Water Resources Research*, *44*(6), 2007WR006599. https://doi.org/10.1029/2007WR006599

Wu, Q., & Wang, J. (2020). A Thermo-Hydro-Mechanical Coupling Analysis for the Contaminant Transport in a Bentonite Barrier with Variable Saturation. *Water*, *12*(11), 3114. https://doi.org/10.3390/w12113114

Wu, R., Li, X., Sun, Y., Szymczak, P., & Jiao, W. (2023). Second-order accurate implicit finite volume method for two-dimensional modeling of PFAS transport in unsaturated porous media with variable surface tension. *Advances in Water Resources*, *178*, 104490. https://doi.org/10.1016/j.advwatres.2023.104490

Xie, H., Cai, P., Yan, H., Ding, H., & Li, C. (2025). Analytical Model for Contaminant Transport in Composite Liners Considering the Longevity of Barrier Components. *Water, Air, & Soil Pollution*, *236*(1), 32. https://doi.org/10.1007/s11270-024-07634-z

Xie, H., Chen, Y., Ke, H., Tang, X., & Chen, R. (2009). Analysis of diffusion-adsorption equivalency of landfill liner systems for organic contaminants. *Journal of Environmental Sciences*, *21*(4), 552–560. https://doi.org/10.1016/S1001-0742(08)62307-4

Xie, H., Chen, Y., & Lou, Z. (2010). An analytical solution to contaminant transport through composite liners with geomembrane defects. *Science China Technological Sciences*, *53*(5), 1424–1433. https://doi.org/10.1007/s11431-010-0111-7

Xie, H., Ding, H., Yan, H., Yang, D., Lou, Z., Qiu, Z., & Chen, Y. (2022). A semi-analytical solution to organic contaminants transport through composite liners considering a single crack in CCL. *Environmental Science and Pollution Research*, *29*(27), 40768–40780. https://doi.org/10.1007/s11356-021-18171-1

Xie, H., Lou, Z., Chen, Y., Jin, A., Zhan, T. L., & Tang, X. (2013). An analytical solution to organic contaminant diffusion through composite liners considering the effect of degradation. *Geotextiles and Geomembranes*, *36*, 10–18. https://doi.org/10.1016/j.geotexmem.2012.10.007

Xie, H., Yan, H., Feng, S., Wang, Q., & Chen, P. (2016). An analytical model for contaminant transport in landfill composite liners considering coupled effect of consolidation, diffusion, and degradation. *Environmental Science and Pollution Research*, *23*(19), 19362–19375. https://doi.org/10.1007/s11356-016-7147-6

Xie, H., Zhang, C., Feng, S., Wang, Q., & Yan, H. (2018). Analytical Model for Degradable Organic Contaminant Transport through a GMB/GCL/AL System. *Journal of Environmental Engineering*, *144*(3), 04018006. https://doi.org/10.1061/(ASCE)EE.1943-7870.0001338

Xiu, D., & Karniadakis, G. E. (2002). The Wiener—Askey Polynomial Chaos for Stochastic Differential Equations. *SIAM Journal on Scientific Computing*, *24*(2), 619–644. https://doi.org/10.1137/S1064827501387826

Xiu, D., & Karniadakis, G. E. (2003). Modeling uncertainty in flow simulations via generalized polynomial chaos. *Journal of Computational Physics*, *187*(1), 137–167. https://doi.org/10.1016/S0021-9991(03)00092-5

Xu, C., Liu, Z., Song, X., Ding, X., & Ding, D. (2021). Legacy and emerging per- and polyfluoroalkyl substances (PFASs) in multi-media around a landfill in China: Implications for the usage of PFASs alternatives. *Science of The Total Environment*, *751*, 141767. https://doi.org/10.1016/j.scitotenv.2020.141767

Yadav, R. R., & Roy, J. (2022). Analytical solutions of one-dimensional scale dependent advection-dispersion equations for finite domain solute transport. *Groundwater for Sustainable Development*, *16*, 100712. https://doi.org/10.1016/j.gsd.2021.100712

Yan, H., Cousins, I. T., Zhang, C., & Zhou, Q. (2015). Perfluoroalkyl acids in municipal landfill leachates from China: Occurrence, fate during leachate treatment and potential impact on groundwater. *Science of The Total Environment*, *524–525*, 23–31. https://doi.org/10.1016/j.scitotenv.2015.03.111

Yan, H., Xie, H., Wu, J., Ding, H., Qiu, Z., & Sun, Z. (2021a). Analytical model for transient coupled consolidation and contaminant transport in landfill liner system. *Computers and Geotechnics*, *138*, 104345. https://doi.org/10.1016/j.compgeo.2021.104345

Yan, H., Sedighi, M., Ding, H., Sun, Z., & Xie, H. (2021b). Analytical model for non-isothermal diffusion of contaminants in unsaturated composite liner. *Journal of Hydrology*, *603*, 126848. https://doi.org/10.1016/j.jhydrol.2021.126848

Yeh, G., & Tripathi, V. S. (1991). A Model for Simulating Transport of Reactive Multispecies Components: Model Development and Demonstration. *Water Resources Research*, *27*(12), 3075–3094. https://doi.org/10.1029/91WR02028

Yin, K., Viana, P. Z., & Rockne, K. J. (2018). Modeling Organic Contaminant Transport through Reactive Media. *Journal of Environmental Engineering*, *144*(9), 04018084. https://doi.org/10.1061/(ASCE)EE.1943-7870.0001429

Yin, T., Chen, H., Reinhard, M., Yi, X., He, Y., & Gin, K. Y.-H. (2017). Perfluoroalkyl and polyfluoroalkyl substances removal in a full-scale tropical constructed wetland system treating landfill leachate. *Water Research*, *125*, 418–426. https://doi.org/10.1016/j.watres.2017.08.071

Yu, Q., Zhang, R., Deng, S., Huang, J., & Yu, G. (2009). Sorption of perfluorooctane sulfonate and perfluorooctanoate on activated carbons and resin: Kinetic and isotherm study. *Water Research*, *43*(4), 1150–1158. https://doi.org/10.1016/j.watres.2008.12.001

Yu Tan, Craig H. Benson, Mehmet Yilmaz, Sabrina L. Bradshaw, & Tuncer Edil. (2022). Hydraulic Conductivity of Compacted Clay Liners to Landfill Leachates Containing PFAS. *ISSMGE*. https://doi.org/10.53243/ICEG2023-73

Yu, Y., Hu, W., & Rowe, R. K. (2025). Complementary use of analytical equations and numerical models for composite liner designs. *Geosynthetics International*, *32*(3), 394–409. https://doi.org/10.1680/jgein.24.00070

Yu, Y., & Zhao, N. (2024). Deterministic and Probabilistic Assessment of Compacted Clay Liners in Municipal Solid Waste Landfills. In S. Wang, R. Huang, R. Azzam, & V. P. Marinos (Eds.), *Engineering Geology for a Habitable Earth:*

IAEG XIV Congress 2023 Proceedings, Chengdu, China (pp. 219–227). Springer Nature Singapore. https://doi.org/10.1007/978-981-99-9065-8_15

Zech, A., Attinger, S., Bellin, A., Cvetkovic, V., Dagan, G., Dietrich, P., Fiori, A., & Teutsch, G. (2023). Evidence Based Estimation of Macrodispersivity for Groundwater Transport Applications. *Groundwater*, *61*(3), 346–362. https://doi.org/10.1111/gwat.13252

Zech, A., Attinger, S., Bellin, A., Cvetkovic, V., Dietrich, P., Fiori, A., Teutsch, G., & Dagan, G. (2019). A Critical Analysis of Transverse Dispersivity Field Data. *Groundwater*, *57*(4), 632–639. https://doi.org/10.1111/gwat.12838

Zerenduoji, D., & Yu, Y. (2024). Evaluation of a Landfill Composite Liner System Using Different Contaminants. In S. Wang, R. Huang, R. Azzam, & V. P. Marinos (Eds.), *Engineering Geology for a Habitable Earth: IAEG XIV Congress 2023 Proceedings, Chengdu, China* (pp. 239–248). Springer Nature Singapore. https://doi.org/10.1007/978-981-99-9065-8_17

Zhai, H., & Benson, C. H. (2006). The log-normal distribution for hydraulic conductivity of compacted clays: Two or three parameters? *Geotechnical and Geological Engineering*, *24*(5), 1149–1162. https://doi.org/10.1007/s10706-005-1135-9

Zhan, L., Chen, C., Bouazza, A., & Chen, Y. (2018). Evaluating leakages through GMB/GCL composite liners considering random hole distributions in wrinkle networks. *Geotextiles and Geomembranes*, *46*(2), 131–145. https://doi.org/10.1016/j.geotexmem.2017.11.001

Zhan, L., Chen, C., Wang, Y., & Chen, Y. (2017). Failure probability assessment and parameter sensitivity analysis of a contaminant's transit time through a compacted clay liner. *Computers and Geotechnics*, *86*, 230–242. https://doi.org/10.1016/j.compgeo.2017.01.014

Zhang, H. J., Jeng, D.-S., Seymour, B. R., Barry, D. A., & Li, L. (2012). Solute transport in partially-saturated deformable porous media: Application to a landfill clay liner. *Advances in Water Resources*, *40*, 1–10. https://doi.org/10.1016/j.advwatres.2012.01.007

Zhang, K., Achari, G., & Li, H. (2009). A comparison of numerical solutions of partial differential equations with probabilistic and possibilistic parameters for the quantification of uncertainty in subsurface solute transport. *Journal of Contaminant Hydrology*, *110*(1–2), 45–59. https://doi.org/10.1016/j.jconhyd.2009.08.005

Zhang, M., Zhao, X., Zhao, D., Soong, T.-Y., & Tian, S. (2023). Poly- and Perfluoroalkyl Substances (PFAS) in Landfills: Occurrence, Transformation and Treatment. *Waste Management*, *155*, 162–178. https://doi.org/10.1016/j.wasman.2022.10.028

Zhao, S., Sun, B., & Su, X. (2024). Sustainable Management of Pollutant Transport in Defective Composite Liners of Landfills: A Semi-Analytical Model. *Sustainability*, *16*(24), 10954. https://doi.org/10.3390/su162410954

Zhao, Z., Li, J., Zhang, X., Wang, L., Wang, J., & Lin, T. (2022). Perfluoroalkyl and polyfluoroalkyl substances (PFASs) in groundwater: Current understandings

and challenges to overcome. *Environmental Science and Pollution Research*, *29*(33), 49513–49533. https://doi.org/10.1007/s11356-022-20755-4

Zheng, C., & Bennett, G. D. (1995). *Applied contaminant transport modeling: Theory and practice*. Van Nostrand Reinhold.

Zhi, Y. (2017). *Sorption of Perfluoroalkyl and Polyfluoroalkyl Substances (PFASs) by Natural and Anthropogenic Carbonaceous Sorbents*. ProQuest Dissertations Publishing.